A SPECTROSCOPIC STUDY OF THE AGGREGATION OF REACTIVE DYES

NEIL M SPEIRS

PhD THESIS
SEPTEMBER 2002
THE UNIVERSITY OF EDINBURGH

In Loving Memory Of

My Dearest Grandad

Martin Lardner

1912 – 2001

A true scientist is an artist as well, for he presents not just the truth of things but the beauty of things.

Anon.

ABSTRACT

This thesis is concerned primarily with the use of fluorescence spectroscopy and UV-Vis absorption spectroscopy to study the aggregation of phthalocyanine and ortho-hydroxyazo textile dyes in solution. A preliminary investigation of the use of laser irradiation to induce fading of dyed textiles, as a possible method of assessing light fastness of dyes, is also reported.

Fluorescence and UV-Vis spectroscopy have been used to investigate the aggregation of a commercial reactive textile dye, a sulphonated copper phthalocyanine dye, known here as turquoise~1. With very few exceptions, phthalocyanine dimers are found to be non-fluorescent. This thesis reports on the observation of a fluorescent dimer of turquoise~1 in ethanol and water. Fluorescence excitation and emission spectra at room temperature and 77K are presented. These are consistent with the conventional model of exciton coupling in a cofacial dimer. The fluorescence arises from a dimer with a particular geometry, while the majority of dimer species present in solution, which give rise to the characteristic hypsochromically shifted absorption spectrum, are non-fluorescent. Theoretical modelling of extinction co-efficients obtained from aqueous solution of turquoise~1 shows that, in salt-free solutions, aggregates higher than dimers exist. However, in solutions containing high salt concentrations the tendency to form the higher aggregates dramatically decreases.

The fluorescence spectra of the monomer and dimer species of a typical ortho-hydroxyazo dye, known here as red~1, are shown to be clearly distinguishable, while their absorption spectra overlap strongly and cannot be resolved. Thus, the aggregation of this dye in aqueous and ethanolic solution is not readily apparent from the absorption spectrum, but is revealed by fluorescence spectroscopy. Fluorescence excitation spectra and emission spectra in water and ethanol, at room temperature and 77K are reported. The effect of increasing the temperature of the dye solution on the extent of aggregation has also been investigated. A number of ortho-hyroxyazo reactive dyes related structurally to red~1have also been investigated. These systems

show similar behaviour to red~1 and fluorescence spectroscopy is again shown to be a valuable probe of aggregation.

Initial studies show that laser irradiation of dyed textile fabrics can be used to induce fading of the dye without damage to the textile fibre. The time taken for laser-induced fading of standard samples of blue-dyed wool is consistent with their light fastness values defined by the international dyestuffs industry. The effect of dye strength on laser-induced fading times is in line with results from conventional light fastness measurements.

DECLARATION

I hereby declare the work presented in this thesis is my own work unless otherwise stated by reference.

N M Speirs
September 2002

CONTENTS

COURSES ATTENDED

Lecture courses attended; Ultra-Fast Molecular Processes

Advanced Organic Synthesis

Lasers I and II

Industrial Inorganic Chemistry.

Presented a poster at the House of Commons, representing The University of Edinburgh as part of SET 2000.

Attended Departmental Colloquia.

Attended physical chemistry sectional meetings, giving a presentation every year.

Made a number of presentations to members of staff at Dystar UK Ltd.

ACKNOWLEDEMENTS

CHAPTER 1 - INTRODUCTION

The aggregation of dye molecules is of interest to the dyestuffs industry because it influences the effectiveness of the dyeing process. The aggregation of a dye in the dyebath prior to fixation has an impact on the fixation process and properties of the dye thereafter. Factors affected include;

1/ The affinity of the dye for the fibre

2/ The properties of the dye on the fibre

3/ The mobility of the dye migrating into and around the fibre

4/ The photostability of the dye

Aggregation affects the value of a dyestuffs associated absorption co-efficient; the absorption co-efficient is a measure of the colour strength of the dye per mole. A pure dye monomer will have an associated absorption co-efficient, if the dye aggregates then this will not be the case and the monomer and dimer will have their own specific absorption co-efficients. Thus, aggregation effects the colour strength of a dye.

Thus, characterisation of dimerisation or aggregation is important in the development of new dyestuffs. This thesis reports on the use of absorption and fluorescence spectroscopy to investigate aggregation in examples of commercial reactive textile dyes. Two types of reactive dyes were employed; phthalocyanine and ortho-hydroxyazo dyes. Conventionally, aggregation of dyes in solution is often studied using only UV-Vis absorption spectroscopy. However, the addition of fluorescence spectroscopy offers a potentially more sensitive method for detecting dye aggregation, particularly in systems such as the ortho-hydroxyazo dyes studied here, where there is very close overlap between the dimer and monomer absorption bands.

In this thesis, dimer defines the association of two monomer units, while aggregate defines the association of three or more monomers.

CHAPTER 2 – BACKGROUND THEORY

2.1 – The Interaction of Light with Matter

2.1.1 – The Nature of Light

The work carried out by Isaac Newton [1,2] on the dispersion of white light into its constituent colours using prisms led him to conclude that light was corpuscular, or particulate, in nature. Not until 1867 following work by Thomas Young and Michael Faraday did James Clerk Maxwell publish his electromagnetic theory of light. Maxwell indicated that electromagnetic radiation propagates as a wave motion. Between 1905 and 1906 Einstein used work by Planck to explain the photoelectric effect, and concluded that radiation energy was localised in discrete packets. In 1926 it was G N Lewis that called these packets of energy photons. It is now clear that electromagnetic radiation should be interpreted to consist of quantum wave particles, which are called photons [3]. The connection between the photon frequency, υ, and the energy that may be imparted to a molecule by absorption of a photon of light is given by equation 2.1.

$$E = h\upsilon \qquad \text{Equation 2.1}$$

This equation makes it clear that radiation with a frequency υ, can be absorbed by a molecule only in discrete quantities [4]. In 1924 Louis de Broglie suggested that any moving body possess an associated wave like property, characterised by a wavelength, as given in equation 2.2.

$$\lambda = h / p \qquad \text{Equation 2.2}$$

The dual wave particle nature of the electron drove the need for the way in which the behaviour of electrons in atoms and molecules was viewed to be changed. The

classical Rutherford-Bohr model of electrons moving with high velocity in fixed orbits around the nucleus was replaced with a model that includes the electron's wave like properties.

2.1.2 – Molecules and Radiation

A molecule may interact with electromagnetic radiation in a variety of different ways [5]. In the strongest of the different types of transitions that a molecule may experience under the influence of radiation, the electric component of the radiation interacts with the electric dipole moment of the molecule. Consider a molecule that posses two quantum states, characterised by the molecular wavefunction Ψ_m, with energy E_m and Ψ_n, energy E_n, with $E_m < E_n$. The transition, shown in figure 2.1, involves promotion of the molecule from the lower to the upper energy state, which is an absorption transition.

$$\Psi_n, E_n$$

$$\Psi_m, E_m$$
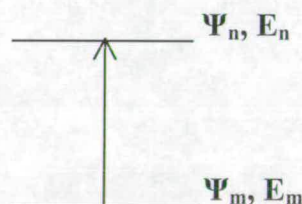
Figure 2.1 – Absorption transition between two quantum states

Before the radiation field is applied, the molecule is in state Ψ_m. Some time after the application of the field, the molecule may be presumed to be in state Ψ_n. If one considers the transition process, here the molecule is in both states with probabilities varying over time. So the molecule may be assumed to be in the superposition of states given in equation 2.3.

$$\Psi = a_m \Psi_m + a_n \Psi_n \qquad \text{Equation 2.3}$$

3

Before the transition occurs then $a_m = 1$, $a_n = 0$ and $\Psi = \Psi_m$ and after the transition $a_m = 0$, $a_n = 1$ and $\Psi = \Psi_n$. A measure of the progression of the transition is given by the probability that the molecule is in state Ψ_n. This probability is denoted as P_n and is described as in equation 2.4.

$$P_n = \left| a_n \right|^2 \qquad \textbf{Equation 2.4}$$

2.1.3 – Einstein Co-Efficients

The separation between molecular electronic energy levels corresponds to the energy of photons in the ultraviolet, visible and infrared regions of the electromagnetic spectrum. Absorption of a photon of equivalent energy to this separation will excite an electron from a lower to a higher energy level, producing an excited state of the molecule. The probability that the absorption transition will occur is defined by the Einstein B coefficient. The rate of transition of molecules from a ground state m to an excited state n due to the absorption of radiation is given by equation 2.5;

$$-(d/dt)\, N_m = N_m\, B_{m\text{->}n}\, \rho\, (\nu_{m\text{->}n}) \qquad \textbf{Equation 2.5}$$

where N_m is the number of molecules in state m, $\nu_{m \to n}$ is the frequency of the radiation and ρ is the radiation energy density. The probability of spontaneous emission is defined by the Einstein A coefficient, with the rate of transition of molecules from state n to m given by equation 2.6;

$$-(d/dt)\, N_n = N_n\, [A_{n\text{->}m} + B_{n\text{->}m}\, \rho\, (\nu_{n\text{->}m})] \qquad \textbf{Equation 2.6}$$

where N_n is the number of molecules in state n and, $B_{n\text{->}m} = B_{m\text{->}n}$; $\nu_{m\text{->}n} = \nu_{n\text{->}m}$.

$A_{n \to m}$ is related to the radiative lifetime τ_r^* through equation 2.7;

$$(1/ A_{n \to m}) = \tau_r^*$$ <div style="text-align:right">**Equation 2.7**</div>

2.1.4 - Transition Moments

For a molecule to be able to interact with the electromagnetic field and absorb or create a photon of frequency υ, it must possess, at least transiently, a dipole oscillating at that frequency. This transient dipole is expressed quantum mechanically in terms of the transition dipole moment, μ_{nm}, between states m and n.

$$\mu_{nm} = \langle \Psi_n | \mu | \Psi_m \rangle$$ <div style="text-align:right">**Equation 2.8**</div>

Where μ, is the electric dipole moment operator. The size of the transition dipole can be regarded as a measure of the charge redistribution that accompanies a transition; a transition will be active, and generate or absorb photons, only if the accompanying charge redistribution is dipolar. The co-efficient of stimulated absorption and emission, and therefore the intensity of the transition, is proportional to the square of the transition dipole moment. Only if the transition moment, μ_{nm}, is non-zero does the transition contribute to the spectrum

2.1.5 - The Franck-Condon Principle

The electronic transition, or promotion of an electron which has been excited by electromagnetic radiation, occurs rapidly compared to nuclear motion. This is often referred to as the Franck-Condon principle, while the Born-Opennheimer approximation refers to the separability of the electronic and nuclear wavefunctions. Thus the nuclei remain essentially frozen at the equilibrium configuration of the ground state molecule during the transition. Since the electronically excited state thus generated is likely to have very different structural properties compared to the

ground state, it is expected that some changes in the nuclear configuration take place after the transition has occurred. It is possible to illustrate the principle for a generalised diatomic as shown in figure 2.2. The potential curve for the electronically excited state is shown to be displaced to larger equilibrium internuclear separation compared to that of the ground state. This is consistent with a weakening of the bond strength due to excitation of an electron into some antibonding orbital. The electronic transition is represented by a vertical upward arrow, conveying the idea that the electron is excited to the upper state before the nuclei have had a chance to respond to the new electronic structure. It is therefore expected that the excited state is produced with some additional vibrational and rotational excitation since the transition intercepts the upper state curve at a position above that of the lowest, vibrationless level.
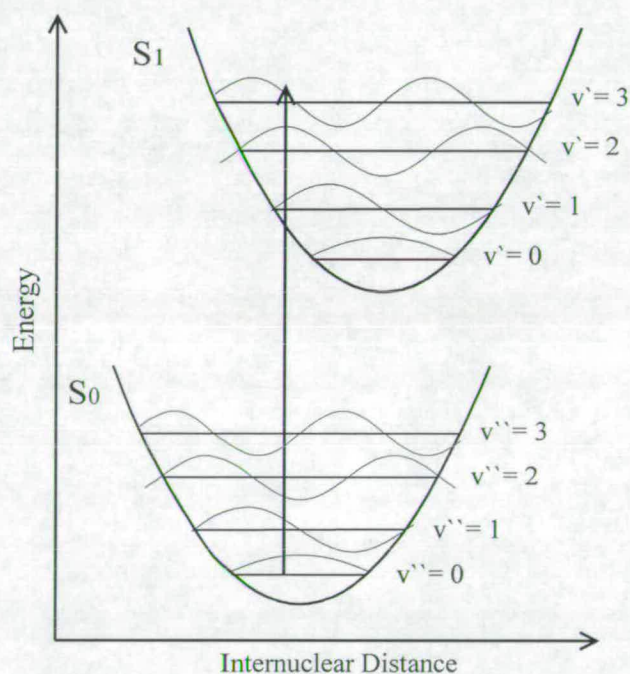
Figure 2.2 – Illustration of the Franck-Condon principle.

For polyatomic molecules the situation is more complicated due to the fact that the potential energy surfaces of their ground and excited states have many dimensions. In addition, many vibrational motions are anharmonic and their vibrational

wavefunctions are therefore not represented by the functions shown in figure 2.2. The consequences of having many vibrational motions which may be involved in the transition is that they become overlapped in the spectrum to form a featureless absorption profile. Since the overall shape of the absorption profile is still controlled by the Franck-Condon principle, it is often referred to as the Franck-Condon envelope.

2.2 – De-Excitation of Electronically Excited Molecules

The absorption of electromagnetic radiation resulting in the excitation of an electron from a lower to a higher molecular quantum state is the first step towards some final photochemical product. The electronically excited molecule is obviously energetically unstable with respect to the ground state. If the molecule does not re-arrange or fragment, it will find some way of losing its excitation energy in order to return to the ground state. There are a number of different possible physical de-excitation pathways; they can be grouped into three broad categories.

2.2.1 – The Jablonski Diagram

The various different types of radiative and non-radiative transitions can be summarised by a modified Jablonski diagram [6], named after Alexander Jablonski (1898-1980) born in Voskresenovka, Ukraine.
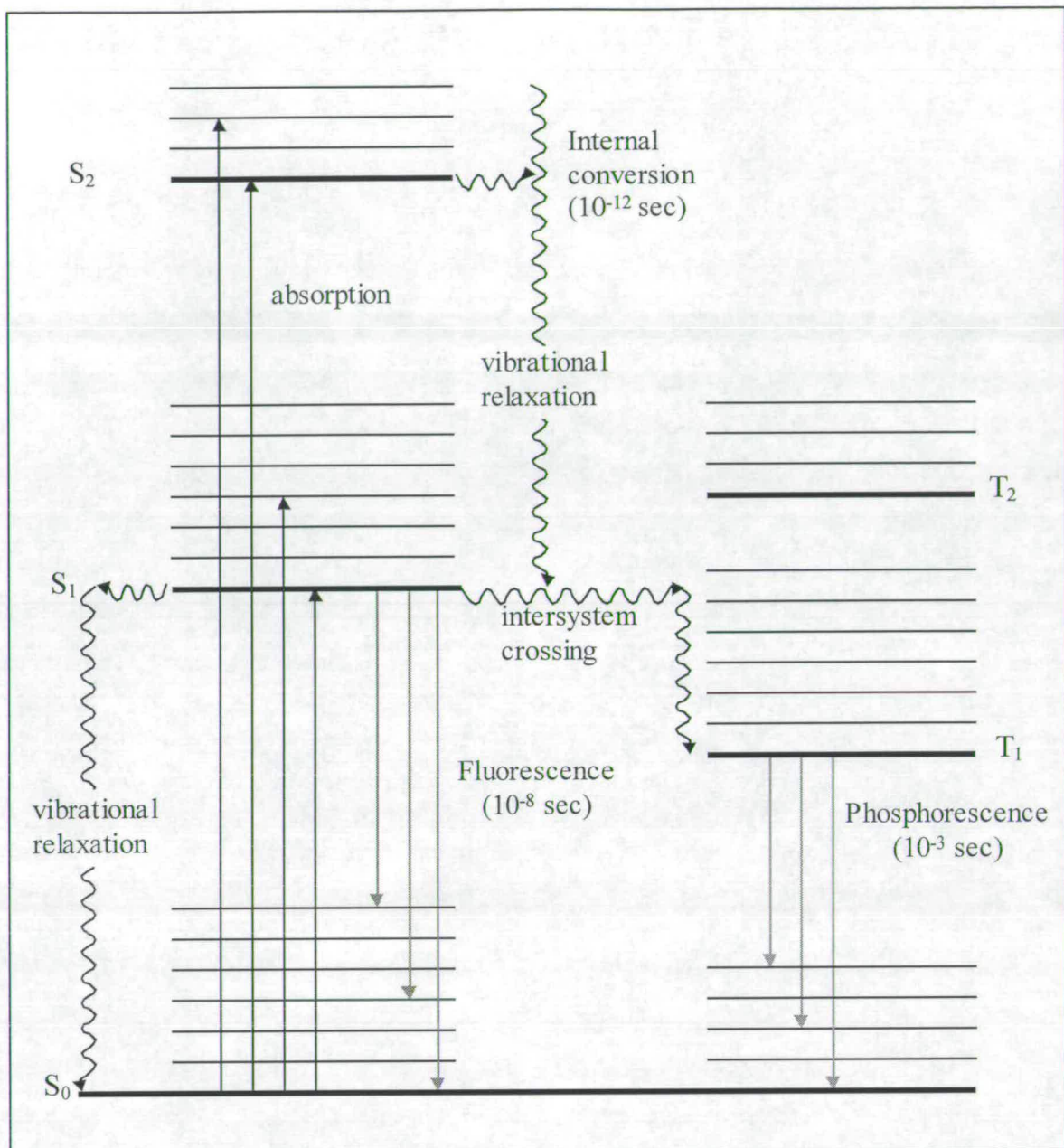
Figure 2.3 – The modified Jablonski diagram.

2.2.2 – Radiative Processes

It is possible to distinguish between two different types of radiative transition, fluorescence and phosphorescence. Fluorescence is the radiative emission from an excited singlet state to the ground singlet state, this is spin allowed and occurs rapidly with the emission of a photon. The rate constants of fluorescence are typically 10^8 s^{-1}. Phosphorescence is emission from triplet excited states to the ground singlet state. This transition is formally forbidden, and rate constants are slow, typically 10^3 to 10^0 s^{-1}.

Fluorescence measurements can be broadly classified into two types of measurements, steady-state and time-resolved [7]. Steady-state measurements are performed with constant illumination and observation, this is the most common type of measurement. The sample is illuminated with a continuous beam of light, and the intensity of the emission is recorded. Examination of the Jablonski diagram in figure 1.3 shows that the energy of the emission is typically less than that of absorption. Consequently fluorescence typically occurs at lower energies or longer wavelengths. G. G. Stokes first observed this phenomenon in 1852 [8]. A fluorescence emission spectrum is a plot of intensity versus emission wavelength, while a fluorescence excitation spectrum is a plot of intensity versus excitation wavelength. The emission spectrum is typically a mirror image of the absorption spectrum of the S_0 --> S_1 transition. This similarity occurs because electronic excitation does not greatly alter the nuclear geometry. Hence, the spacing of the vibrational energy levels of the excited states is similar to that of the ground state. As a result, the vibrational structures seen in the absorption and the emission spectra are similar.

Another general property of fluorescence is that the same fluorescence emission spectrum is generally observed irrespective of the excitation wavelength. This is known as Kasha's rule [9], upon excitation into higher electronic and vibrational levels, the excess energy is quickly dissipated, leaving the fluorophore in the lowest vibrational level of S_1. Because of this rapid relaxation, emission spectra are usually independent of the excitation wavelength.

2.2.3 – Non-Radiative and Quenching Processes

A non-radiative process is one in which the population in the initially excited quantum states are transferred to others without any accompanying emission. Internal conversion involves the transfer of population between electronic states of the same spin multiplicity, while intersystem crossing involves the transfer of population between states of different spin multiplicity. Quenching processes involve bi- or termolecular mechanisms that result in the transfer of energy by some means from the initially excited molecule to other molecules that are in collision with it.

2.3 – THE BEER-LAMBERT LAW

2.3.1 – Absorption and Concentration

The experimentally determined absorption spectrum consists of a number of spectral features, of primary importance is the wavelength of maximum absorption and the related intensity. An experimental measurement of absorption intensity is provided by the Beer-Lambert Law, as in equation 2.9.

$$\log (I / I_o) = -\varepsilon cl \qquad \qquad \textbf{Equation 2.9}$$

Where I_o is the incident intensity, I is the intensity after passage through a sample of length l, that is the path length of the cell in cm, and c is the molar concentration in $molL^{-1}$. The quantity ε is the molar absorption co-efficient of the species at the frequency of the incident radiation, with units $Lmol^{-1}cm^{-1}$.

$$A = \varepsilon cl \qquad \qquad \textbf{Equation 2.10}$$

Equation 2.10 shows the relationship that involves A, the absorbance, and is a unitless quantity, and was formally known as the optical density [10]. The molar

absorption co-efficient is a function of the radiation frequency; this functional dependence provides a useful connection between experimental molecular electronic spectroscopy and quantum mechanics. A good measure of the transition intensity is obtained by integrating ε over the whole of the absorption feature, to give the integrated absorption co-efficient, A, defined in equation 2.11.

$$A = \int \varepsilon d\bar{v}$$
         Equation 2.11

The integrated absorption co-efficient provides a connection between the experimental spectrum and a theoretical quantity known as the oscillator strength of the transition. The oscillator strength is a measure of the strength of an electric dipole transition compared with that of a free electron oscillating in three dimensions.

2.3.2 – Aggregation Studies

Many dyes aggregate under certain conditions in aqueous solution. The main factors influencing aggregation are dye concentration, electrolyte concentration and temperature. Increases in the first two and a decrease in the third promote aggregation. There are many techniques employed to study the degree of aggregation of dyes including conductivity, light scattering, diffusion and spectrophotometry amongst others. It is possible to use UV-Vis spectroscopy with the aid of Beer's law to investigate aggregation. When the degree of aggregation of a dye changes with concentration, the system shows an apparent deviation from Beer's law, that is a plot of absorption versus concentration will not be linear passing through the origin. It is also appropriate at this point to note that comparison of absorption spectra at varying concentration or temperature for example may present an isosbestic point. This implies that the two absorbing species are present, monomer and dimer, or, monomer and aggregate [11, 12].

2.4 – BIBLIOGRAPHY

1 H. Leicester, *The Historical Background of Chemistry,* Dover Publications New York New York., **1971**.

2 The Norton Anthology of English Literature Sixth Edition Volume 2, edited by M .H. Abrams, Published by W. W. Norton and Co. New York, **1993**.

3 A. Gilbert & J. Baggott, *Essentials of Molecular Photochemistry,* Blackwell Science Ltd, **1995.**

4 P. W. Atkins, *Concepts in Physical Chemistry,* Oxford University Press, **1995.**

5 C. E. Wayne & R. P. Wayne, *Photochemistry,* Oxford Science Publications, **1996**.

6 A. Jablonski, *Z. Phys.,* 94, 1935, 38-46.

7 J. R. Lakowicz, *Principles of Fluorescence Spectroscopy Second Edition,* Kluwer Academic/Plenum Publishers New York, **1991**.

8 G. G. Stokes, *Phil. Trans. R. Soc.,* 142, **1852**, 463-562.

9 M. Kasha, *Disc. Faraday Soc.,* 9, **1950**, 14-19.

10 R. A. Alberty & R. J. Silbey, *Physical Chemistry,* John Wiley and Sons Inc., **1997**.

11 D. Pugh, C. H. Giles and D. G. Duff, *J. Chem. Soc. Faraday Trans.,* 67, **1971**, 563-73.

12 D. S. E. Campbell, D. Cathcart, C. H. Glies and S. M. K. Rahman, *Trans. Faraday Soc.,* 55, **1959**, 1631.

CHAPTER 3 – DYES AND AGGREGATION

3.1 – The Natural Dyes

At the beginning of the 19th century natural dyes dominated the world market. Only a fraction of a percent of the market was taken by a synthetic dye, it was called picric acid, and was discovered by Woulfe in 1771. The yellow dyes comprised the largest group of natural dyes, but were technically inferior to the reds, blues and blacks. They had poor light fastness properties and low tinctorial strength. Natural yellow dyes were based on flavones, chalcones and polyenes, while the reds and blues were based on anthraquinone and indigoid, respectively. The structures of these dyes are shown in figures 3.1 and 3.2 [1].

Flavone

Chalcone

$$RO_2 C\text{--}(\text{--}CH=CR\text{--})\text{--}CO_2R$$

Polyene
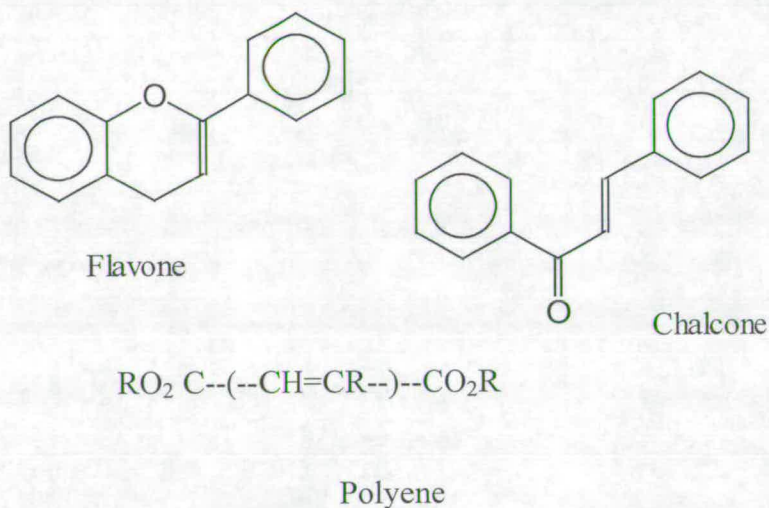
Figure 3.1 - Basic units of natural yellow dyes.

Anthraquinone

Indigoid
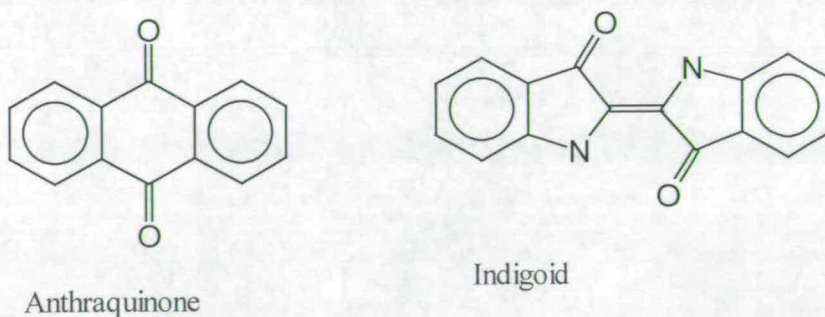
Figure 3.2 - Basic units of natural red and blue dyes.

All the natural yellow dyes were obtained from vegetable sources. The most important yellow dye of the middle ages was weld, which originated from the plant *reseda luteula* L. This dye used in conjunction with the blue dye woad produced a dye made famous by Robin Hood called Lincoln green.

In contrast to the yellow dyes three of the four natural red dyes were derived from insects rather than plants [2]. They were kermes, cochineal and lac. The most important red dye called madder or alizarin was of vegetable source, the outfits worn by the English 'red coats' were tunics dyed with madder. Madder comes from the roots of the plant *rubia tinctorum*, root was known as alizari hence alizarin. There are two natural blue dyes indigo and woad, these derive from the leaves of the indigo plant *indigofera tinctoria* L. Indigo is one of the only natural dyes still used today, the other is logwood. The later is the only important black dye; its colouring matter is haematein, shown in figure 3.3, and is actually red in colour.
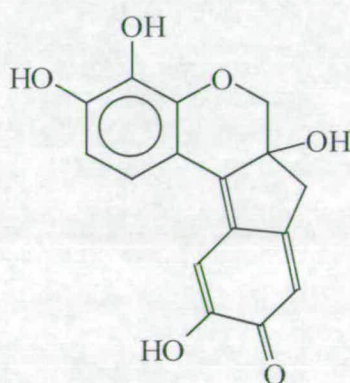
Figure 3.3 – The structure of Haematein.

Combining this red colour with a source of chromium gives a black shade, and it is for this that logwood has become renowned. The majority of black shades today are obtained by mixing two or more dyes, due to the lack of synthetic black dyes. It is a measure of logwood's success that it is still used for dyeing silk and leather.

3.2 – Perkin and Beyond

In 1856 while attempting to prepare quinine the antimalarial drug, W. H. Perkin [1] synthesised a purple crystalline compound, that would later be called mauveine, figure 3.4, but was originally named aniline purple.
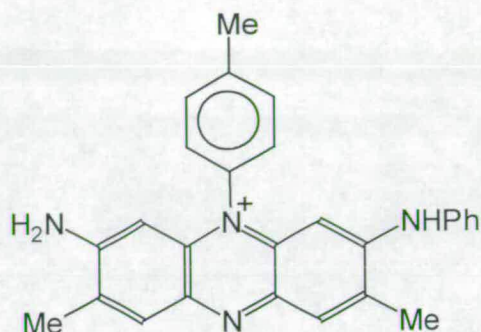
Figure 3.4 – The structure of mauveine

For many years the structure of mauveine was reported incorrectly, but after analytical investigation of an original sample of the dye was it found that the dye is a mixture, with the principal component illustrated in figure 3.5. [2]
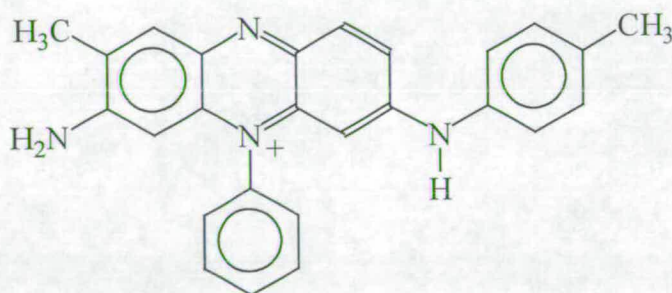
Figure 3.5 – The principal component in mauveine.

After large scale synthesis had been achieved, Perkin's dye increased greatly in importance when he developed a method for dyeing wool with mauveine using tannic acid. Perkin's achievements have since earned him the title 'Founder of the Dyestuffs Industry'. Much work was carried out in the nine years that followed

15

Perkin's discovery, including the discovery of the diazotisation reaction by Peter Griess [3]. This is the singularly most important reaction carried out in the dyestuffs industry It involves treating an aromatic amine with a nitrosating agent to obtain a diazonium salt. This salt then reacts with a phenol or aromatic amine to give an azo compound. This is represented in figure 3.6.
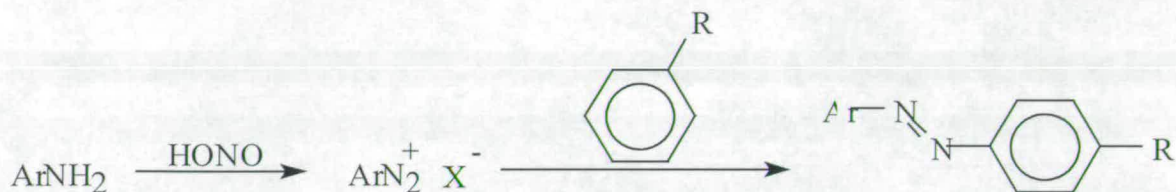
Figure 3.6 – Diazotisation followed by coupling with a phenol or aromatic amine, R = OH or NR^1R^2.

The first commercially successful azo dye was bismarck brown, discovered by Martius in 1863. The work that was carried out over this time was done without any knowledge of the structures of the aromatic amines involved, hence the rationalisation of chemical reactions was almost impossible and so research was somewhat hit and miss. It was though largely due to Kekulé that this situation was resolved. In the period 1857-1858, he published a series of papers on the quadrivalency of carbon and the idea that carbon could form multiple bonds with itself and other elements. In 1865 Kekulé [4] made possibly his single most memorable contribution to chemistry with a paper on the structure of benzene. The solution of the structure of benzene made a tremendous impact on both organic chemistry and the dyestuffs industry, in that now many of the conspicuous enigmas were seen in a new light. Much of the chemistry that had gone before could now be accounted for, indeed, systematic and strategic research was at last possible.

Following Perkin's discovery of mauveine it was Britain that dominated the research and development of synthetic dyestuffs; nevertheless, by 1875 many of the leading German chemists like Caro had returned to their home land and Germany became the leader. In the forty years that followed, Germany built up a strong and powerful dyestuffs industry, while British industry remained stagnant. By 1914, Germany

produced 90% of the world's dyes and supplied 80% of the dyes used in the British market. As the First World War started, all trade between Britain and Germany ceased and Britain was cut off from its main supplier of dyes. This reached crisis point when Britain had no dye to colour their soldiers uniforms and ended up buying the essential dyes from Germany. This crisis forced the British dyestuffs industry to rejuvenate itself [1].

The period after the First World War saw the dyestuffs industry grow worldwide, with USA and Japan now major players for a slice of the enormous market. The direction of research has been more towards optimisation and development of available dyes as opposed to discovery of new ones. This is not to say that there has been no work in finding new chromophores; for example the discovery of copper phthalocyanine. During large-scale preparation of phthalimide at the Grangemouth plant of Scottish Dyes Ltd., the glass-lined vessel cracked exposing the outer steel casing to reaction. A coloured impurity was found and later identified as iron phthalocyanine. Further research by ICI, who now owned Scottish Dyes Ltd., in the 1930's found that the Cu^{2+} derivative was a superb pigment and was later marketed under the name monastral blue. This is illustrated in figure 3.7.
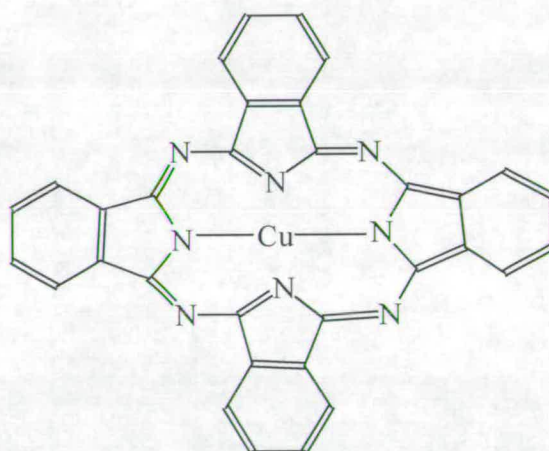

Figure 3.7 – Structure of copper (II) phthalocyanine.

The phthalocyanines represent one of the very few new chromophores to have been found since the nineteenth century. Once the methods of preparation and the structure had been established by Linstead [5] and then Robertson [6], it became

apparent that metal free phthalocyanine had already been prepared by Braun and Tcherniak in 1907 [7] and that von der Weid and de Diesbach [8] had prepared a copper derivative in 1927. Neither of these groups had further investigated their newly synthesised compounds in order to achieve structural information. The rise of the dyestuffs industry paralleled the early advances in organic chemistry, indeed it is doubtful that either would be as advanced today without the close relationship between them, especially in the early years. Just as Perkin is recognised as the father of the dyestuffs industry, so the very same dyestuffs industry itself could be called the mother of the modern organic chemical industry.

3.3 – Types of Dyes

The classes of dyes studied in this project are ortho-hydroxyazo and phthalocyanine dyes; they are discussed in detail in chapters 5,6 and 7. Dyes are classified either by their use or by their chemical structure. To ensure that it is the chemistry of the dyes that is emphasised, a system that catalogues dyes by chemical structure is employed. Although, not comprehensive, the following outline gives reference to those dyes other than azo or phthalocyanine that are of greatest chemical and economical significance. The anthraquinone dyes, second only to azo dyes in terms of commercial importance are widely used. Vat dyes, which are dyes of any chemical class that are applied by a vatting process, are also important. The vatting process involves treating the insoluble colourant with a reducing agent in an alkaline medium to give the reduced or leuco form. After application of the leuco form of the dye to the fibre, the process is reversed and the coloured dye is generated by oxidation. Indigoid dyes are often treated separately from other vat dyes because of their importance as representatives of a discrete class of coloured compounds, exclusive from the rest of the vat dyes. Di and tri-aryl carbonium dyes comprise the oldest class of synthetic dye; in fact mauveine belongs to this group. The nitro dyes are important historically since picric acid was the first synthetic compound to be used commercially for colouring substrates. Finally there are the sulphur and polymethine dyes [9].

3.4 – Reactive Dyes

There are five broad categories of dye-fibre interactions; these include physical adsorption, solid solutions, insoluble aggregates with the fibre, ionic bonding and covalent bonding. The dyes studied in this project are reactive dyes, the covalent bonds that these reactive dyes form with the fibre are discussed here.

3.4.1 – Covalent Bonds

Dyes such as polyazo, azoic and vat were used to dye cellulosic fibres, but due to their dull shades and poor wet fastness properties there was a drive for improved dyes for cellulosic fibres. The idea of a dye that would link covalently to a fibre was popular; this would overcome the problems with the weak physical forces that were involved with the dye-fibre binding in for example polyazo dyes. The first practical success was in 1954 when Rattee and Stephen working for ICI found that dyes carrying a dichlorotriazinyl group reacted with cellulose under gentle alkaline conditions. In 1956, some one hundred years after Perkin's discovery of mauveine, ICI introduced the first reactive dyes for cotton. Other dye manufacturers were quick to follow suit and today all major dye manufacturers sell an extensive range of reactive dyes for cotton. The bulk of reactive dyes use the nucleophilic displacement reaction depicted below in fig 3.8, while chemists working for Hoechst contrived a different working reactive system: a vinyl sulphone group, which reacts with the cellulose by Michael addition. This is shown in fig 3.9.

Dye—N(H)—triazine(Cl, Cl) + cellulose--OH $\longrightarrow$ Dye—N(H)—triazine(O--Cellulose, Cl) + HCl
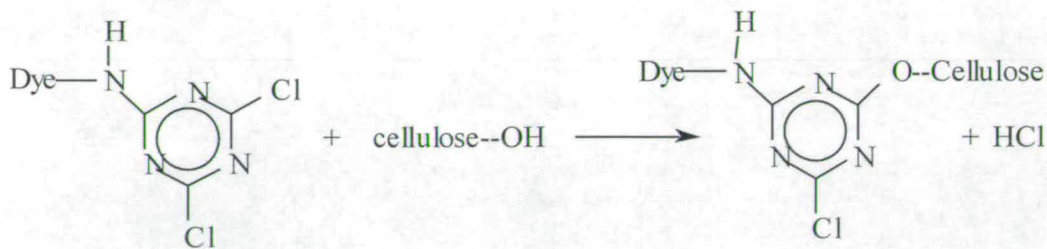
Figure 3.8 – Outline of reaction of cellulose with dichlorotriazinyl group.

$$Dye-SO_2CH_2CH_2OSO_3H \xrightarrow{OH^-} Dye-SO_2CH=CH_2$$

$$\downarrow cellulose\text{--}OH$$

$$Dye-SO\ CH_2CH_2O_2-cellulose \longleftarrow$$
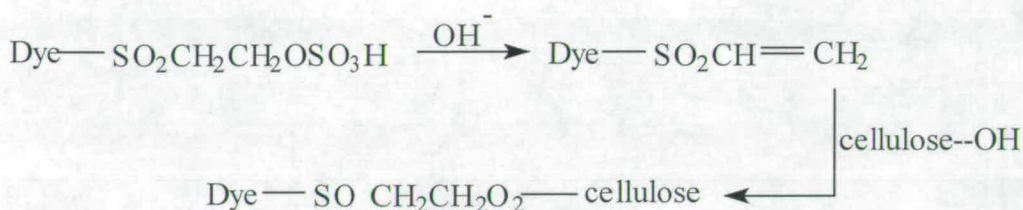
Figure 3.9 – Outline of vinyl sulphone group reacting with cellulose.

Not all of the dyestuff reacts with the cellulose, indeed a competing hydrolysis reaction that involves the dye reacting with the water in the dyebath transpires. The amount of fixation of the dye varies immensely and thus a substantial effort is being made towards achieving 100% fixation.

3.5 – The Photostability of Dyes

A successful dye must satisfy many conditions, and photostability or light fastness is considered amongst the most important of these. Generally, a dye with low light fastness is acceptable if the product is used for dyeing paper, as the life-times of such products are relatively short. That is, of course, if the dye itself is inexpensive. Likewise, a dye used to dye curtains or furnishings would be required to have excellent light fastness, since the product is expected to last for many years. Dyes for apparel fall in between these two extremes. Substantial efforts have been made in studying the photo-fading processes, not only from the scientific point of view but also from a commercial angle.

Once a molecule has absorbed a photon of light energy it is raised to an excited level. The excited molecule may react with another molecule before it has time to return to the ground state. Such a reaction is termed a bimolecular photochemical reaction, of equal importance is the unimolecular photochemical reaction, when there is no second molecule. Several factors may effect the ultimate photostability to reaction of a dye and amongst these are;

a) the nature of the light source
b) the absorption characteristics of the dye
c) the lifetime of the S_1 and T_1 states.
d) The efficiency of intersystem crossing
e) The nature of the solvent or substrate
f) The presence or absence of air or moisture

The idea is, that the longer the molecule spends in the excited states, then the more chance it has to be involved in photochemical processes. Oxidation and reduction are the two most important pathways for the fading of dyes. These reactions can be directly photochemical or indirect and caused by another photoexcited molecule. The major influence on the reaction mechanism is the nature of the fibre [1]. There are two distinct fibre types that determine whether a dye is oxidised or reduced. These fibre types are:

a) proteins such as wool or silk which advance through a reductive mechanism,
b) non-proteins such as cellulose and polyester which advance through an oxidative mechanism.

The aggregation of the dye has a crucial bearing on the rate of fading of dyed fibres. It has been suggested [1] that the more aggregated a dye is then the higher its light fastness is, consequently the nearer to the monomeric state the lower the light fastness. The reasons for the effect that aggregation has on the light fastness of a dye are far from understood. However, a highly aggregated dye should dissipate the

energy from the excited dye molecule before it has the opportunity to react, that is the lifetime of the excited state is reduced.

It is possible to reduce the light fastness of a dye through exposure to moisture. The water has an effect that is as yet not completely understood, but believed to be chemical in nature. Also, water plays a part in oxidative fading, because it may facilitate the generation of hydrogen peroxide, which is present during photooxidation. Catalytic fading is the term used to refer to the enhanced rate of fading of one component in dye mixtures. A mechanism is shown below:

a) transfer of energy from excited triplet state of dye A to dye B in the ground state.

Dye A (T_1) + Dye B (S_0) $\longrightarrow$ Dye A (S_0) + Dye B (T_1)

3.5.2 – Defects

While factors such as oxidation and aggregation can effect the photostability of a dye, these are not considered defects in the dye or of the fibre. Examples of defects in dyes will now be discussed. In phototendering the dye causes a change in the fibre substrate, the effect usually will manifest itself as a change in the physical properties of the fibre. This is seen to a greater extent in cellulosic fibres dyed with vat dyes. It is important to note that azo dyes do not cause phototendering. Some dyes will change colour upon exposure to light, this effect is known as photochromism, or phototropism, and is considered a defect in textile dyes. For example isomerisation produces reversible colour changes, known as photochromism, and is of particular relevance to azobenzene dyes, since the azo link is extremely susceptible to *cis-trans* isomerisation. Also considered to be a defect is metamerism, where illumination by different light sources causes the colour of the dye to appear different. Although not actually a defect, but an important concept to give reference to is solvatochromism. This is the effect that a solvent has upon the colour of a dye. Positive solvatochromism is when a dye undergoes a bathochromic shift with increasing solvent polarity.

3.5.3 – Light Fastness Standards

The most common form of calibration for light fastness testing is the blue wool scale (International Standards Organisation, 1992). The scale consists of a series of eight woollen samples; each dyed with a specific dye. The dyed woollen samples are selected to fade in a controlled way on exposure to light. The scale is geometric, that is each standard takes twice as long to fade as the next in succession, 1 is low light fastness and 8 is high light fastness. The dyes used fall into two categories, light fastness 1 to 6 are all acid dyes and 7 and 8 are solubilised vat dyes. The dyes used for the scale are as follows; acid blue 104 (blue wool 1), acid blue 109 (blue wool 2), acid blue 83 (blue wool 3), acid blue 121 (blue wool 4), acid blue 47 (blue wool 5), acid blue 23 (blue wool 6), solubilised vat blue 5 (blue wool 7) and solubilised vat blue 8 (blue wool 8). The international standards organisation test methods for assessing the light fastness of textiles involves the samples being mounted on card along with the appropriate blue wool standards. The card is then placed is a holder in the exposure chamber, or fadometer, and is then exposed to the light source. The samples are checked periodically until a contrast equivalent to that of grey scale 4 is achieved. This sample is then compared with the blue wool standards; the sample is said to have the light fastness that corresponds to the blue wool standard with the same degree of fading.

3.6 - Bibliography

1 P. F. Gordon & P. Gregory, *Organic Chemistry in Colour,* Springer-Verlag, **1987**

2   R. M. Christie, *Colour Chemistry,* RSC Paperbacks, **2001**.P. Griess, *Ann.,* **1858**, 160, 123

3   H. Zollinger, *Azo and Diazo Chemistry*, Interscience Publishers, **1961**

4. F. R. Japp, *J. Chem. Soc., Trans.* **1898**, 100

5 R. P. Linstead, *J. Chem. Soc.,* **1934**, 1016, 1017, 1022, 1027, 1027, 1031.

6 J. M. Robertson, *J. Chem. Soc.,* **1935**, 615; **1936**, 1195, 1736; **1937**, 219.

7 R. L. M. Allen, *Colour Chemistry*, Pitman Press, **1971**.

8 H. de Diesbach, E. van der Weid, *Helv. Chim. Acta,* **1927**, 10, 886.

9   ICI Dyestuffs Division, *An Outline of the Chemistry & Technology of the Dyestuffs Industry,* Kynoch Press, **1968**.

CHAPTER 4 – EXPERIMENTAL

In this chapter the experimental techniques used during the course of this project are outlined. These include UV-VIS spectroscopy, steady state fluorescence spectroscopy at room temperature and at low temperature (77K), and use of laser irradiation to induce fading of dyed fabrics such as cotton and wool.

4.1 – Chemicals

All dyes used in the course of this project were kindly supplied by Dystar UK Limited. They include turquoise~1 – a phthalocyanine dye, red~1, red~2, base~1 and trioxa~1 – all of which are o-hydroxyazo dyes. These are commercial dyestuffs whose structures are shown below; full patents are owned by Dystar UK Ltd. Before using the dyes they were recrystallised from deionised water, to remove any synthetic precursors. The solvents used were deionised water and ethanol (Acros spectrophotometric grade); both were tested for extraneous fluorescence before use. All solutions were prepared in a fume hood because the dyes are suspected respiratory sensitisers.
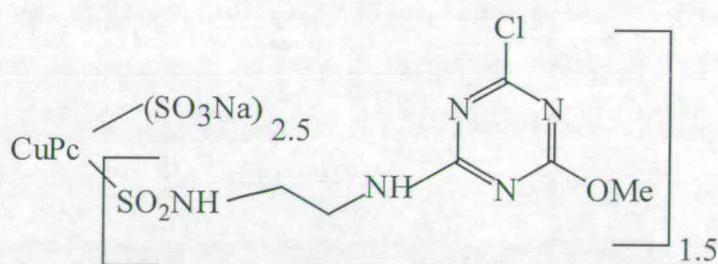
Figure 4.1 – The structure of turquoise~1.
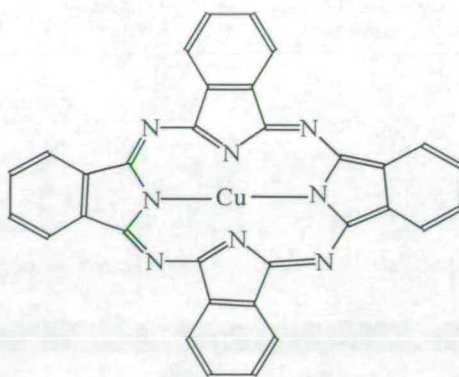
Figure 4.2 – The structure of CuPc, copper phthalocyanine.
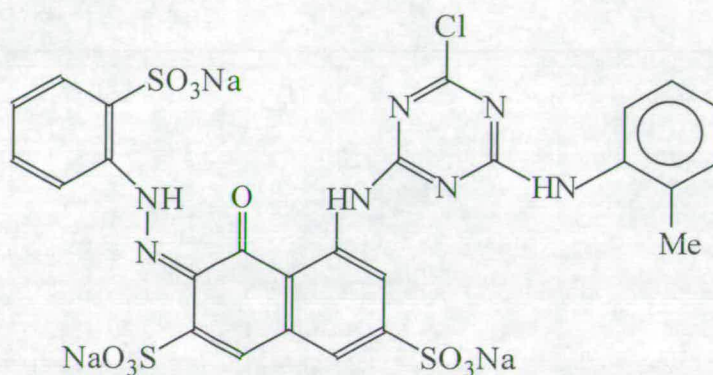
Figure 4.3 – The structure of red~1.
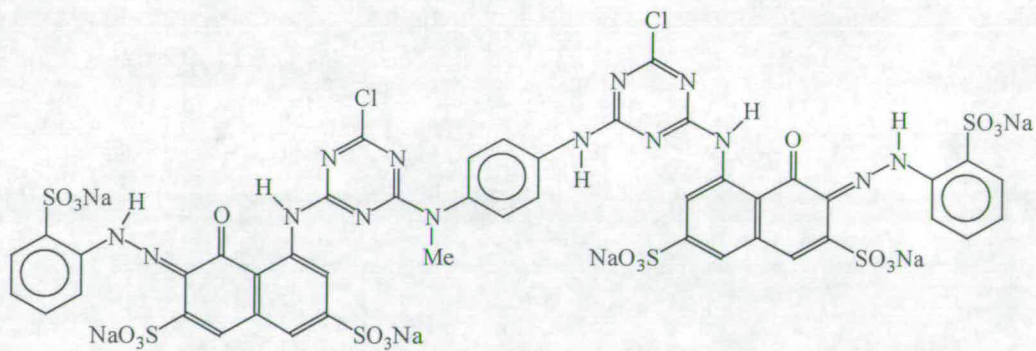
Figure 4.4 – The structure of red~2.
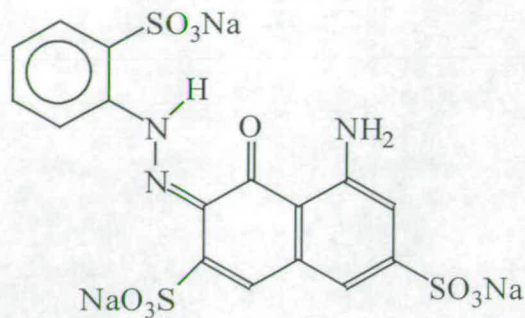
Figure 4.5 – The structure of base~1.
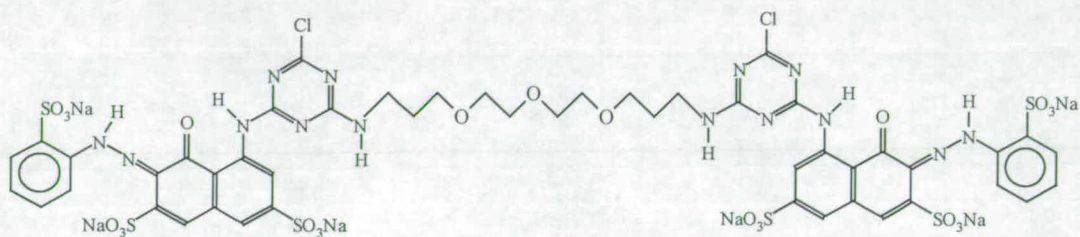
Figure 4.6 – The structure of trioxa~1

4.2 – Synthesis

The following is an outline of the synthesis of base~1 and trioxa~1, all synthetic work was carried out at the Dystar UK Limited labs in Cheadle Hulme, Cheshire. All reagents were of Analar grade or equivalent and used as received unless otherwise stated.

4.2.1 - Methodology for Base~1

A total of 39.6g 2-aminobenzenesulphonic acid was dissolved in 400ml of water. The pH of the solution was adjusted to 6.0 with the addition of concentrated NaOH. 2M $NaNO_2$ (110ml 0.22mol) was added to the solution and stirred. This $NaNO_2$/2-aminobenzenesulphonic acid solution was added to concentrated HCl (56ml) and ice

with continuous stirring over approximately 30mins, this was carried out in an ice bath in order to keep temp < 5C. The pH was monitored using congo red, which showed pH was < 4. Then 109.7g of 1-acetylamino-8-napthol-3,6-disulphonic acid was added to 600ml of water, the pH was kept at 6 with addition of concentrated NaOH. This 1-acetylamino-8-napthol-3,6-disulphonic acid solution was added to the reaction mixture making it a deep red colour. The reaction mixture was allowed to stir. Erlich's reagent, a test for primary amines, was negative indicating there was no starting amine present. Starch iodide paper went from white to a dark blue colour, indicating there was oxidising agent present i.e. HONO; sulphone indicator also suggested this. A 10% solution of sulphamic acid was added to destroy the HONO;

$$NH_2SO_3H + HONO \longrightarrow N_2 + H_2SO_4$$

The reaction mixture was allowed to stir. HPLC was used to monitor the reaction progress; the reaction mixture contained 80% product, the reaction mixture was left to stir for a further 1.5 hours. HPLC was used again; this time products were 100%. Then 112g of NaOH pellets were added to give the 1400ml solution a concentration of 2M. The solution was then heated to 65°C, and allowed to stir at this temperature for an hour. The pH was 13.5 but fell to 12.75 due to liberation of HO-CO-Me (acidic) when pH was stable, i.e. there was no more acid liberated, the reaction was complete. To confirm this TLC was used, the reaction mixture was left to cool overnight. The reaction mixture was heated to 60°C and allowed to cool to 40°C, then 275ml of concentrated HCl was added, making the pH 6.86. The reaction was allowed to stir for 1.5hours. The reaction mixture was then filtered and washed with approximately 100ml of acetone, left overnight to dry in an oven and then crushed into a powder; HPLC showed one product.

4.2.2 – Methodology for Trioxa~1

Base~1, 10g, was dissolved in 500ml of water, and stirred at pH 6.5 and 0°C. Then 3.32g of cyanuric chloride in 50ml of acetone was added to base~1 and stirred at pH

6.5 and 0°C. One hour and twenty five minutes later HPLC was used to show that the reaction was complete, the mixture was screened and the liquor was kept. This was stirred at room temperature for 1 hour at pH 6.5. The total volume at this point was 610ml which is equivalent to 0.016mol, so 381ml is equivalent to 0.01mol. A total of 1.1g (0.005mol MI 220.31) of 4, 7, 10-trioxa-1, 13-tridecanediamine was added to the 381ml of liquor stirred at room temperature and pH 10. HPLC was used immediately and showed the reaction had begun; the reaction mixture was stirred at room temperature and pH 10 for 1 hour. Then 42ml of base~1 was added to balance the reaction. 2M HCl was added to reduce the pH to 6.8. There was difficulty in using methylated spirits to precipitate out, so the reaction mixture was put on a rotary evaporator to reduce the volume to one third of its initial volume. Three times the volume of the reaction mixture of methylated spirits was added to precipitate out the product, which was filtered and dried overnight.

4.3 – Steady State Fluorescence Spectroscopy

4.3.1 – Practical Considerations

The apparent fluorescence intensity and spectral distribution is dependent upon the optical density of the sample and the precise geometry of sample illumination in the spectrometer. The most common geometry used for fluorescence measurements is right angle observation of the centre of a centrally illuminated cuvette, as shown in figure 4.7. This geometrical set up was used in the present work.
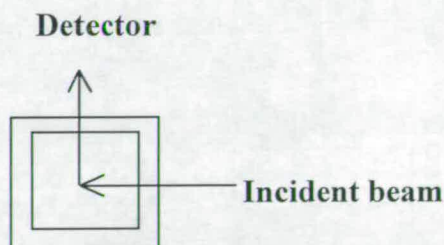

Figure 4.7 – Representation of typical right angle observation geometry.

There are two potential practical problems to consider; the inner filter effect and fluorescence re-absorption. Both of these effects can arise when the solution of sample under investigation is too concentrated. The inner filter effect is illustrated in figure 4.8, and shows how the incident excitation beam is absorbed in a short path length as it enters a concentrated sample solution. The excited species in this volume of the solution can then emit radiation, but this emission is not detected because it is outside the field of view of the detection optics. The inner filter effect causes distortion of the fluorescence excitation spectrum.

Detector

Emission

Incident beam
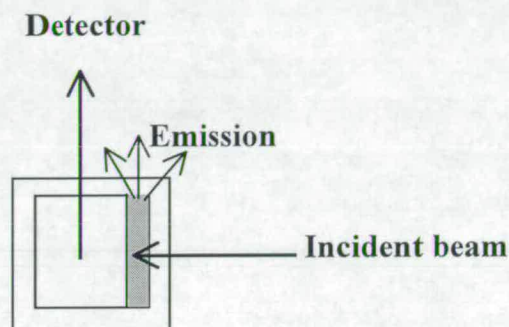
Figure 4.8 – The inner filter effect.

Fluorescence re-absorption is when a photon of fluorescence is emitted and then absorbed by another molecule in solution. This occurs when a highly concentrated sample is used and there is overlap between the fluorescence emission and excitation spectra. The result is the distortion of the fluorescence emission spectrum at those wavelengths where there is overlap between the emission and excitation spectra, at the blue edge of the emission spectrum. To avoid the distortion of spectra by these two effects, sample concentrations of less than or equal to 10^{-5}M were used.

4.3.2 – The Spectrometer

All steady state fluorescence measurements were carried out on a Jobin Yvon Spex Fluoromax spectrofluorimeter, Instruments S.A. group. The electronic and optical layouts of the spectrometer are shown in figures 4.9 and 4.10, respectively. Data were acquired and manipulated using Instruments S.A. Datamax software. The

excitation source is a 150W continuous ozone-free xenon lamp. There are modified Czerny-Turner spectrometers in both the emission and excitation positions; gratings allow light dispersion from 200nm to 900nm. A photon counting detection system was used, the detector was a PMT Hamatsu R928. Two types of experiment can be run. If the excitation wavelength is held constant and the emission spectrometer scanned, then the result is an emission spectrum. If the emission spectrometer is held at a constant wavelength and the excitation wavelength scanned, then an excitation spectrum results. The typical bandwidth for excitation and emission slits was 5nm, with one second integration time and a 1nm data interval.
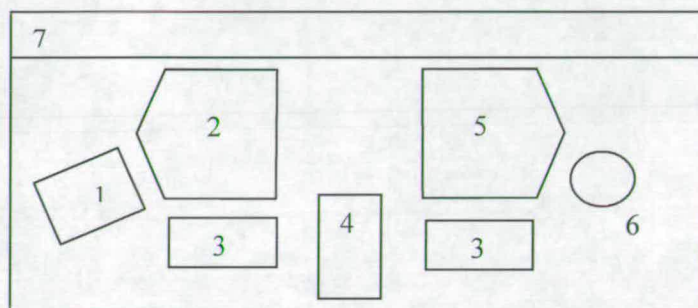
1. Illuminator
2.Excitation spectrometer
3.Sample compartment coupling optics
4.Sample compartment
5. Emission spectrometer
6. Emission detector
7. Electronic components

Figure 4.9 – Schematic diagram of the components of the fluorescence spectrometer.
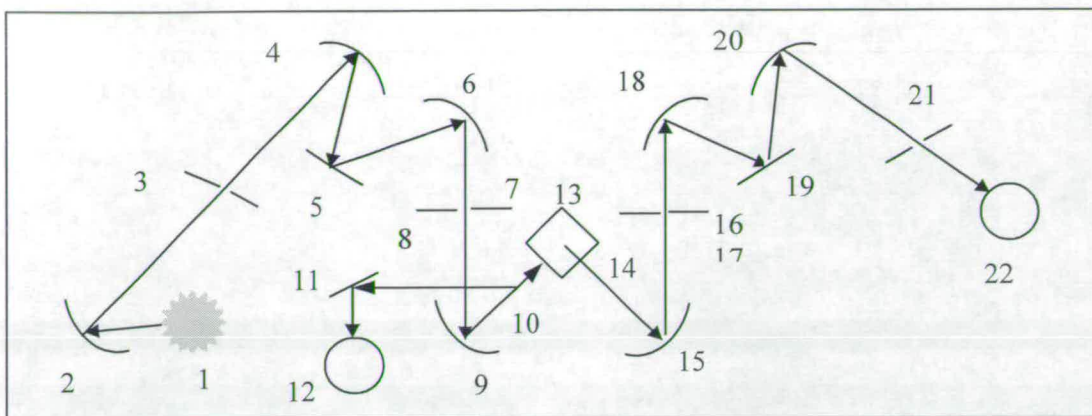
1. 150W ozone free lamp
2. Collection mirror (excitation spectrometer)
3. Entrance slit (excitation spectrometer)
4. Collection mirror (excitation spectrometer)
5. Grating
6. Focussing mirror (excitation spectrometer)
7. Excitation slit (emission spectrometer)
8. Excitation shutter
9. Collection mirror (excitation spectrometer)
10. Beam splitter
11. Deflection mirror
12. Photodiode reference collector
13. Sample position
14. Window
15. Sample collection mirror
16. Emission shutter
17. Entrance slit
18. Collection mirror
19. Grating (1200 gr./mm)
20. Focussing mirror.
21. Exit slit (emission spectrometer)
22. Emission detector

Figure 4.10 – Schematic diagram of the optical layout of the fluorescence spectrometer.

4.3.3 – Room Temperature Experiments

All room temperature fluorescence measurements were carried out using disposable poly(methyl methacrylate), (PMMA) cuvettes with path length 10mm (Fisons 4.5ml).

4.3.4 – Low Temperature Experiments

All low temperature experiments were carried out using fused silica sample tubes that were constructed within the department. Samples were cooled to 77K by immersion in liquid nitrogen contained in a fused silica dewar, (Instruments S.A.).

The only suitable solvent for the low temperature work was ethanol; which freezes to form a clear glass without cracking, giving good transmission of the excitation light without excessive scattering.

4.4 – UV-Vis Spectroscopy

Absorption spectra were recorded on a UNICAM UV2 UV-Vis spectrometer, using matched pairs of fused silica cuvettes, with a path length of 10mm. Shorter path lengths of 5mm, 2mm and 1mm were used for solutions of concentration greater than 10^{-4}M, while a path length of 100mm was used for low concentration solutions ($< 10^{-6}$M). The sources in the spectrometer used were a tungsten lamp and a deuterium lamp, the wavelength range is from 190-900nm and the bandwidth was fixed at 2nm.

4.5 – Laser-Induced Fading of Textiles

A Q-switched Nd:YAG laser, JK Lasers HY 750, with output at 532nm, a repetition rate of 10Hz and a pulse length of 10ns was used to irradiate various dyed textile samples. The time for a particular sample to just begin to fade, as judged by eye, was recorded at varying power densities. The 532nm output was chosen as the dyestuffs on the fabric samples absorbed at this wavelength. The experimental set-up was simple; the unfocused laser beam was incident at the sample, giving an irradiation area of 3mm^2, and peak power densities in the range 2.5 x 10^6 Wmm^{-2} to 1.2 x 10^7 Wmm^{-2}. The experimental arrangement is represented in figure 4.11.
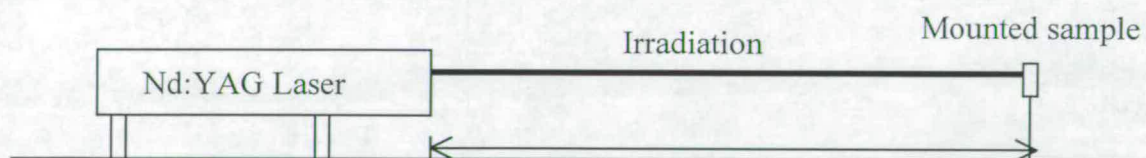
Figure 4.11 – Schematic diagram of the set up used to fade textiles.

CHAPTER 5 – STUDY OF A PHTHALOCYANINE DYE

5.1 – The Importance of Phthalocyanine Dyes

This chapter deals with the study of the copper phthalocyanine dye turquoise~1, its structure is shown in figure 5.1.
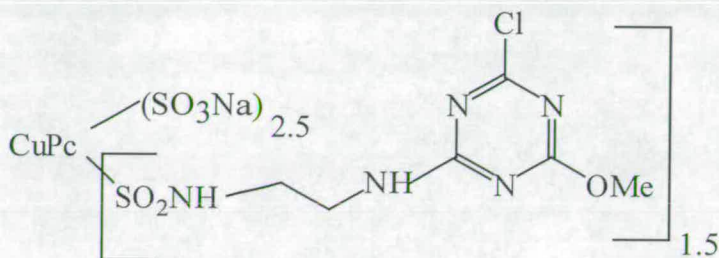
Figure 5.1 – The structure of turquoise~1

The major commercial impact of phthalocyanines is based on three factors:

a) the attractive bright blue to green shades and high tinctorial strengths;

b) the remarkable chemical stability, eg copper phthalocyanine sublimes at 580°C and dissolves in concentrated sulphuric acid in its protonated form;

c) the excellent light fastness or photostability.

This combination of properties is extremely difficult to obtain in other dyestuffs. It is true that many metal derivatives of phthalocyanines have been prepared, yet the copper derivative is by far the most commercially significant. Copper phthalocyanines are used as both pigments and dyes, with the pigments having a greater turnover worldwide.

Dyes and pigments are distinguished on the basis of their solubility characteristics. Dyes are almost invariably applied to fibres through an aqueous medium, so they are generally required to dissolve in water. Pigments [1], in contrast, are required to be completely insoluble in the medium into which they are introduced. A pigment is introduced into a medium by a dispersion process, which reduces the clusters of solid particles into a more finely divided form. The pigment is not dissolved in the medium but rather it is held in place mechanically, usually in a matrix of solid polymer. Like most phthalocyanine pigments, copper phthalocyanine exhibits polymorphism, that is can exist in more than one crystalline form. The two major polymorphs are called the α-form and the more stable β-form, which is greener in colour. Copper phthalocyanine dyes are used almost entirely for dyeing the cellulosic substrates cotton and paper. The size of the copper phthalocyanine molecule is primarily responsible for the lesser importance of the phthalocyanine dyes compared to phthalocyanine pigments. It is too large to dye the synthetic fibres, polyester and polyacrylonitrile, and is only of use on a limited scale for nylon. It is consequently, used almost exclusively for dyeing the cellulosic substrates, cotton and paper. The first commercial phthalocyanine dye was CI Direct Blue 86. The study of the phthalocyanines and the related porphyrins is widely documented in the literature, as are their aggregation properties and the resultant effects on the absorption spectra.

5.2 – Previous Studies of Dimerisation and Aggregation

In 1944 Sheppard and Geddes [2] noted that there existed the possibility of two contrasting types of oriented aggregates of dyestuffs. Ionic aggregates bonded via hydrophilic groups and H_2O molecules, which show no major effects on the absorption spectra, and organic aggregates bonded via essential resonance circuits of aliphatic or cyclic systems of double bonds, that lead to very notable effects on the absorption spectra. The authors conclude their report with the idea that the observed new bands in the absorption spectra of various dyestuffs, including phthalocyanines,

that develop with changing concentration need not derive from the dimer. This is in contrast to Scheibe [3] who attributed the new bands to dimers.

In 1971 Monahan *et al* [4] published a paper that dealt with the dimerisation of copper (II) phthalocyanine in CCl_4 and C_6H_6. The authors discuss the idea that aggregation of a dye is diminished in solvents yielding the greatest dye solubility, and in general the largest dielectric constant. They go on to reason that to form a dimer, dye-dye interactions must be stronger than any other forces available such as solvation, and hence non-polar solvents are preferred. The exception would be water, in which solvent-solvent interactions would exclude the dye molecules from solution, causing them to aggregate. They found that the absorption spectrum of the dimer lay to the blue of the monomer species, yet neglected to discuss this point in detail. Yang *et al* [5] carried out experiments in 1985 that showed that a sulphonated Co (II) phthalocyanine in water yielded a positive entropy for dimerisation. They postulated, with assistance from a paper by Ohling [6], that water participates in dimer formation but is released into bulk solvent when the dimer forms and is not incorporated into the dimer.

The book 'Phthalocyanines Properties and Applications' published in 1989 contains a chapter by Stillman and Nyokong [7] that discusses the absorption spectra of phthalocyanines; of particular interest is the section that deals with the interpretation of the spectral effects of dimerisation. They note that the spectral changes expected following dimerisation of phthalocyanines include a blue shift of the Q and B bands. That is, a dimer will exhibit Q and B bands to the blue of the monomer bands. This contradicts earlier work done by Sheppard and Geddes [2], who had stated that the new bands they had observed were not peculiar to the dimer. It is accepted now that in fact these new bands or blue shifted bands are peculiar to the dimer; transitions that give rise to these bands only occur in the dimer. The spectral effects of dimerisation are explained by exciton coupling. Several authors have given theoretical treatments for exciton interactions between molecules in solution and in the solid state and the effect of the interaction on absorption and emission spectra [8-14]. The spectral effects of dimerisation can be explained in terms of exciton coupling between the two monomer chromophores. For a phthalocyanine dimer with

overall D_{4h} symmetry, that is a centrosymmetric dimer with the two rings lying parallel, the Q and B states of the monomer (both ^1E_u) are each split into two states, an upper state of ^1E_u symmetry and a lower state of ^1E_g symmetry. The transition from the dimer ground state to the lower ^1E_g is forbidden. The observed transition to the ^1E_u state lies at higher energy than the corresponding monomer transition. This is illustrated in figure 5.2a. The monomer transition, E_m in figure 5.2a, is of lower energy than the allowed dimer absorption transition, E_+. This explains why the dimer Q-band is blue shifted compared to the monomer.

In discussing the spectroscopic effects of aggregation, we will assume that the electronic excitation energy of the monomer is perturbed by interaction with one other neighbouring molecule, i.e. dimerisation, and will neglect interaction with two or more neighbouring molecules. That is not to assume that higher aggregates are not present, since pairs of interacting molecules may occur as isolated dimers or within larger aggregates. As illustrated in Figure 5.2a, the excitation energy of the two excitonic components of the electronic origin of a dimer (M_2) is given by:

$$E_\pm = E_M + \Delta I \pm X \qquad \textbf{Equation 5.1}$$

where E_M is the excitation energy of the isolated monomer; ΔI is the change in intermolecular interaction energy on excitation of M in the dimer ($I^I - I^{II}$ in figure 5.2a); and X is the half-exciton splitting due to the excitation exchange interaction between the two identical chromophores in the dimer [18-20].
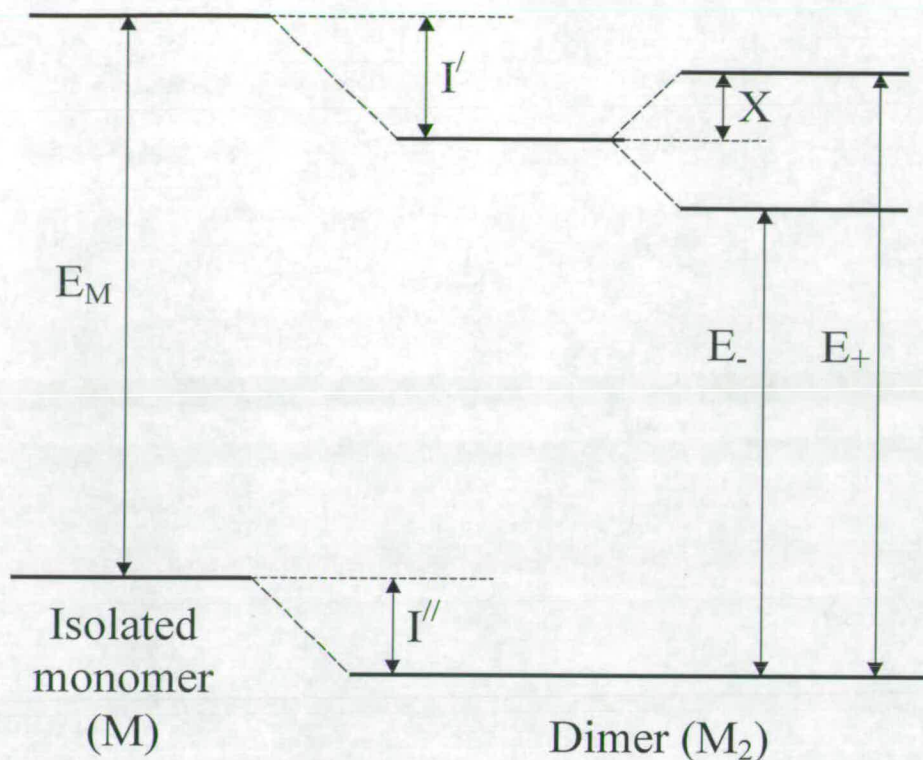
Figure 5.2a – Energy level diagram representing the relationship between monomer and dimer excitation energies.

Kasha's paper [52] entitled; 'The Exciton Model in Molecular Spectroscopy' provides a general diagram similar to that in figure 5.2a. Considering the two co-facial monomers that form the dimer species the energy diagram in figure 5.2c [52] charts the monomer units as they become associated end to end as in figure 5.2b. The variables, R and angle A are shown in figure 5.2b.
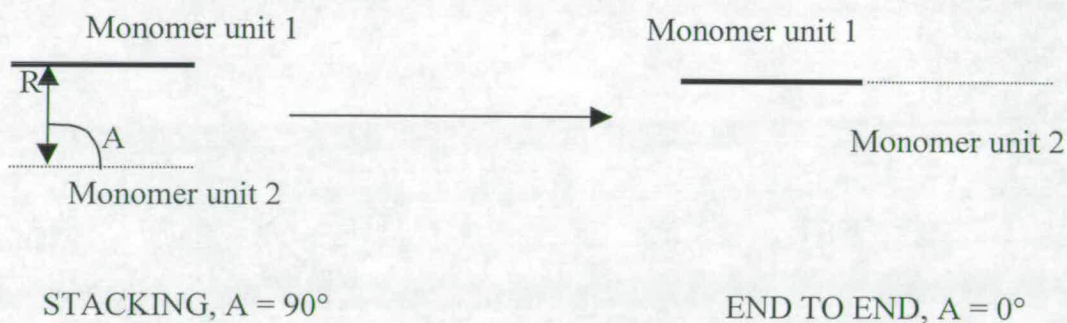
Figure 5.2b – Transition from co-facial to slipped end to end association of monomers in the phthalocyanine dimer.
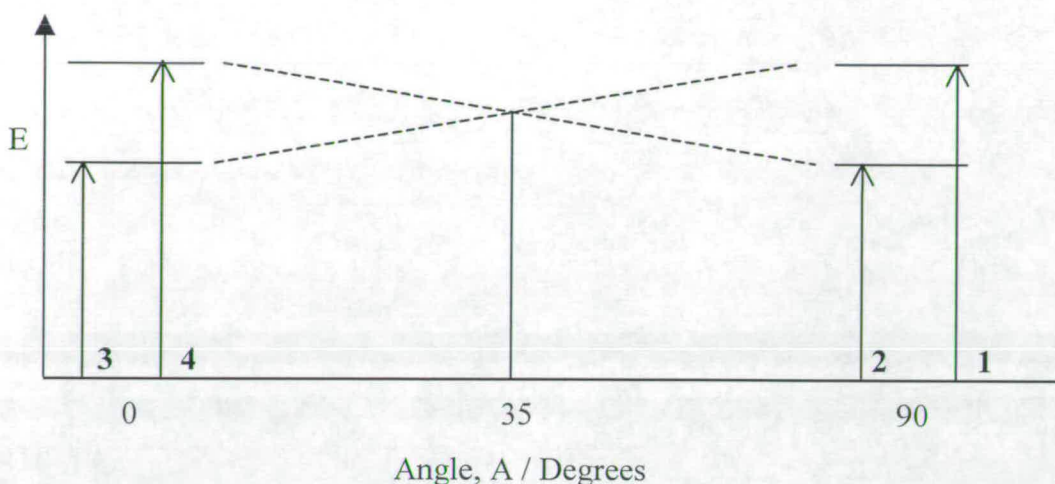
Figure 5.2c – Energy diagram to show the change in the relative energy levels of the exciton split Q-band. Transitions 1 and 3 are allowed, transitions 2 and 4 are formally forbidden.

Figure 5.2c shows that as the two monomers that constitute the dimer move to end to end association the allowed absorption labelled 1 in figure 5.2c becomes the lower energy absorption, labelled 3. Thus the dimer band is no longer shifted to the blue with respect to the monomer but is now shifted to the red. In contrast, the formally forbidden absorption, labelled 2 in figure 5.2c, becomes the higher energy transition, labelled 4.

The effect of many variables on the aggregation of phthalocyanines has been studied widely, including temperature, solvent and different ligands. Gruen [41] studied a number of phthalocyanine dyes by varying firstly the concentration and noting that aggregation increases with increasing concentration. Gruen also investigated pH, ionic strength, solvent and temperature, finding that aggregation was a function of each variable. Aggregation increased with a decrease in temperature, an increase in ionic strength and with the hydrophilicity of the solvent. A similar study by Martin *et al* [42] some twenty years later studied these same variables while investigating a different phthalocyanine dye. The conclusion of the authors was that these same

variables do of course vary the extent to which a particular dye species aggregates. Other studies have specifically looked at the effect of pH on aggregation [15, 16] or the effect halogenation or quinone substitution of the ring system has on aggregation [17-19 and 20].

At the beginning of the 1970's Pugh and co workers [20] showed that changing amount of aggregation of a dye results in a deviation from Beer's Law. Many authors use the phrase 'deviation from Beer's law' to show evidence that a dye species is aggregating, and the literature holds many examples [22-24].

X-ray crystallography has been used to determine the number of dye molecules in an aggregate structure [25-27]; the paper by Shimode et al [28] is a nice example. The authors report that Reactive Blue 19 exists at its highest form of aggregation in dimeric form, with the two rings some 5 Angstroms apart. The addition of salt increases the extent of aggregation as the aggregates now hold 5 monomer units, with each phthalocyanine ring now 7 Angstroms apart.

Although a number of phthalocyanines, for example free base, zinc and aluminium derivatives, show intense fluorescence from the monomer the dimers are generally non-fluorescent. The lack of fluorescence emission from the dimer is often attributed to an increase in the rate of internal conversion from the first excited singlet state. Any observed dimer fluorescence emission is a result of an emissive transition from the lower exciton split energy level in figure 5.2. This transition is formally forbidden but can be induced through vibronic coupling. Spikes and Bommer [31] have reported that the dimer of $ZnPcS_4$ displayed no fluorescence emission, and Negri *et al* [32] have determined that the dimer of the diamide of zinc tetracarboxyphthalocyanine also doesn't fluoresce. Indeed the evidence for non-fluorescent dimers continues [33-35]. Fluorescence from phthalocyanine dimers is not completely unknown though. Oddos-Marcel et al reported weak fluorescence from an oxygen-bridged silicon phthalocyanine dimer [36]. The absorption bands of the lower and upper exciton states were observed, lying bathochromic and hypsochromic to the monomer band, respectively, with an exciton splitting of $\sim 3800 cm^{-1}$. The emission spectrum of the lower exciton state was in the range 8000-

12000cm^{-1}, with its short wavelength tail overlapping the long wavelength edge of the absorption spectrum. The fluorescence quantum yield of the dimer was ~10^{-3} that of the monomer. Similar absorption spectra and weak near-infrared emission were reported for Si-O-Ge and Si-O-Sn dimers [37]. The first observation of sulphonated aluminium phthalocyanine dimer fluorescence was reported by Yoon et al [29] in 1993. They observed a red shifted Q band in the absorption spectrum, which is contrary to the blue shift that has been observed previously with other sulphonated metallo phthalocyanines. The emission that they ascribed to dimers was red shifted with respect to the monomer emission; the authors failed though to excite at 685nm where they observed dimer absorption. If they had excited at 685nm and then observed emission then clearly little doubt would exist that dimer fluorescence had been observed. The authors also point out that in contrast to other sulphonated metallo phthalocyanines water plays an important role in preventing aggregation in the sulphonated aluminium phthalocyanine studied, but aggregation is promoted by aqueous alcoholic solution. In a paper by Rumbles et al [30] the following year, the problem of the inner filter effect distorting fluorescence spectra from sulphonated aluminium phthalocyanine is discussed. The paper contradicts the earlier work done by Yoon et al [29] by concluding that the distortions in their spectra, red shifted emission, could be attributed to re-absorption, and not the presence of dimers. The authors stress the fact that re-absorption and the inner filter effect is often overlooked despite being discussed in the literature. Also, the authors agree that the red shifted absorption band is due to dimers, but direct excitation of the dimer absorption band yielded no fluorescence. In a study carried out 3 years after Yoon et al, Kaneko et al [38] observed formation of fluorescent dimer of zinc(II) tetrasuphonatophthalocyanine in aqueous acetonitrile. The absorption and emission spectra of the dimer were red-shifted relative to the monomer spectra. The assignment of fluorescence to the dimer was confirmed by its excitation spectrum which was consistent with the absorption spectrum. The Stokes shift between the dimer absorption and emission spectra was very small, as for the monomer. In pure water, a 'normal' dimer was observed: this was non-fluorescent, with a blue-shifted absorption band and it was assumed to have an eclipsed cofacial geometry. The

formation of a fluorescent dimer in aqueous acetronitrile was attributed to a solvent-induced change in geometry to a slipped or tilted conformation. The removal of D_{4h} symmetry allows the strictly forbidden emissive transition to occur.

The current driving force for studying sulphonated phthalocyanines, primarily aluminium and zinc, lies in their application to photodynamic therapy, (PDT) of tumours. This application to PDT is discussed by Beeby, Phillips *et al* [39]. Fluorescence spectroscopic studies were carried out on aluminium phthalocyanines with defined numbers of sulphonate groups: mono, di, tri, tetra. The absorption spectra indicated the occurrence of aggregation, most notably for AlS_4Pc which exhibits dimer absorption near 640nm. For AlS_2Pc, and to a lesser extent AlS_3Pc an underlying broad absorption band from 600-800nm is present. The fluorescence lifetime experiments that were carried out showed single exponential fits, indicating that aggregates of sulphonated phthalocyanines are generally non-fluorescent. The authors conclude that the presence of sulphonate ligands on AlPc has very little effect on the photophysical properties of the monomer unit. Two recent papers by Beeby et al [46, 47] report on the protonation of the phthalocyanine ring, leading to a red shift in the fluorescence emission and a large decrease in fluorescence quantum yeild. The red shifted absorption and fluorescence emission reported by Kaneko et al [38] and attributed to the dimer was investigated. Beeby et al showed that it is the protonation of the phthalocyanine ring at the azomethine nitrogens that is responsible for Kaneko's results and not a dimer. In a subsequent paper Beeby et al [48] have reported dimer fluorescence. The authors used two similar zinc phthalocyanines, one with a 1,3-dioxolane ring system substituent and another without. On cooling from 293K to 77K only the phthalocyanine with the ring system as a substituent experiences an increase in the extent of aggregation and dimer fluorescence is observed. The authors suggest that these results are due to the peripheral substituent forcing the macrocycles into a conformation that allows dimer emission. Zinc phthalocyanines usually form slipped cofacial, non-fluorescent dimers.

5.3 – Observation of a Fluorescent Phthalocyanine Dimer

5.3.1 – UV-Vis Spectroscopy

The Q-band region of the electronic absorption spectra of turquoise~1 in aqueous solution is shown in figure 5.3, for concentrations from 10^{-7}M to 10^{-4}M. At low concentrations the narrow Q-band of the monomer at 665nm is distinct. As the concentration increases, the spectrum broadens and the band on the short wavelength side of the Q-band, peaking at 626nm, increase in intensity. These observations are typical of the well known spectral effects of dimerisation of phthalocyanines. The hypsochromically shifted absorption band indicates the presence of dimers of turquoise~1. Figure 5.4 shows the absorption profile of turquoise~1 in ethanol, the monomer Q-band appears to be at 668nm and the dimer Q-band at 603nm. The evidence from the absorption profiles thus indicates that over a concentration range turquoise~1 aggregates to form a dimer species in ethanol.
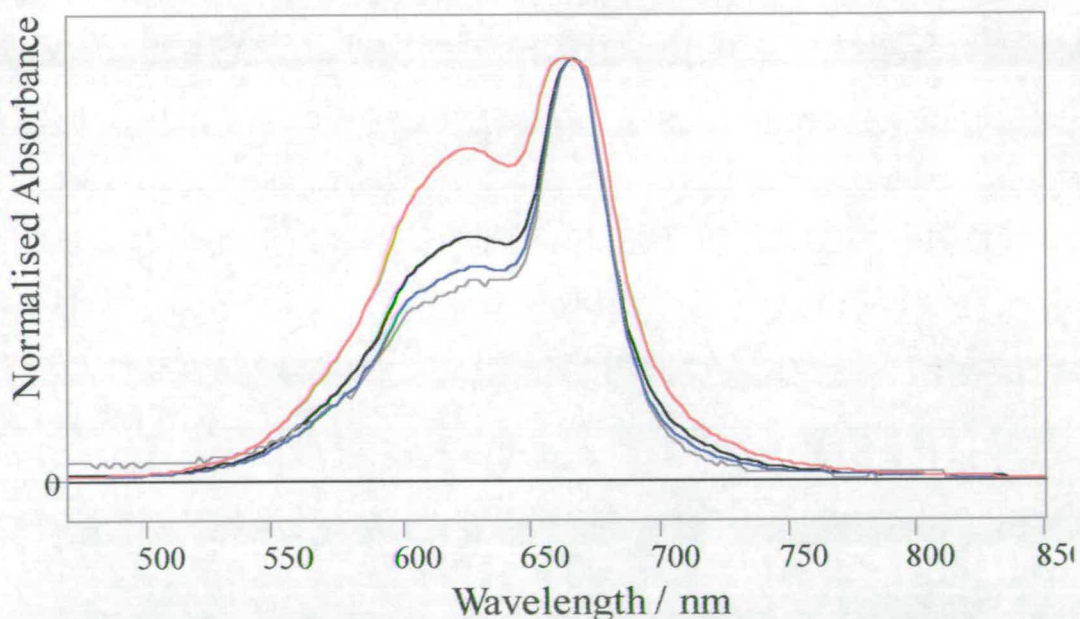

Figure 5.3 – Turquoise~1 absorption spectra in water at room temperature, red at 10^{-4} M (max absorbance 3.252), black 10^{-5} M (0.505), blue 10^{-6} M (0.055) and grey 10^{-7} M (0.006).
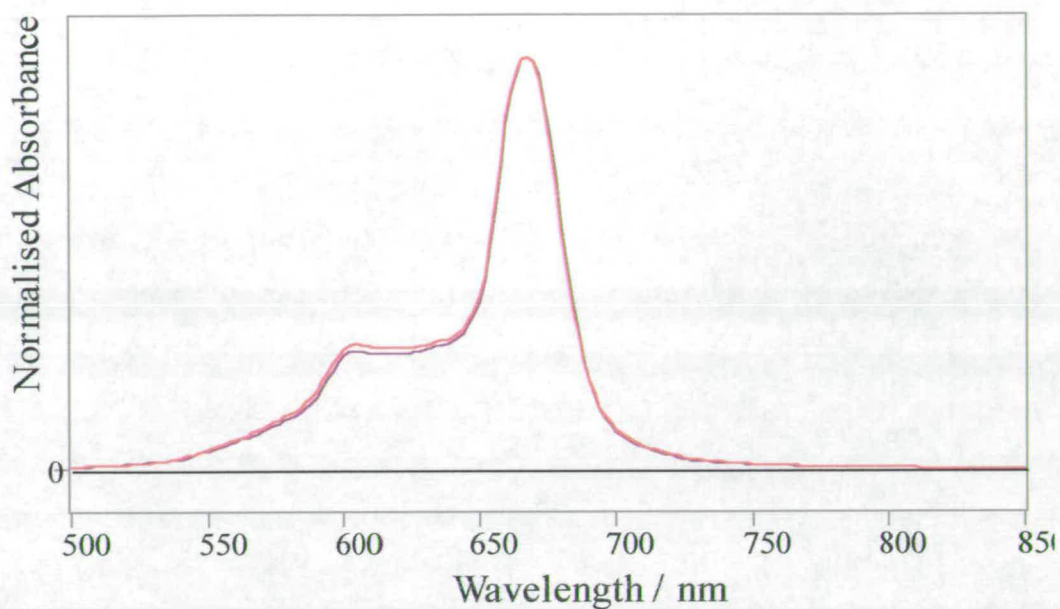
Figure 5.4 – The absorption spectrum of a 10^{-4} M (red, max absorption 1.482) and 10^{-5} M (purple, 0.824) sample of turquoise~1 in ethanol at room temperature.

5.3.2 – Steady State Fluorescence Spectroscopy

Although the fluorescence of turquoise~1 is not intense, it is easily detectable. The fluorescence spectra of a 10^{-5}M aqueous solution, at excitation wavelengths across the absorption envelope, are shown in figure 5.5. The fluorescence emission is dependent on the excitation wavelength, which is contrary to Kasha's rule. This implies that there is more than one species present in the sample. It has already been established that turquoise~1 aggregates from the analysis of UV-Vis spectra. By exciting across the absorption envelope the fluorescence emission narrows. That is, as the excitation wavelength increases towards that of the monomer Q-band the emission spectra narrow. This indicates that the dimer of turquoise~1 is fluorescent, as when the dimer band is excited directly fluorescence emission is broad, while direct excitation of the monomer Q-band reveals a narrow fluorescence emission.
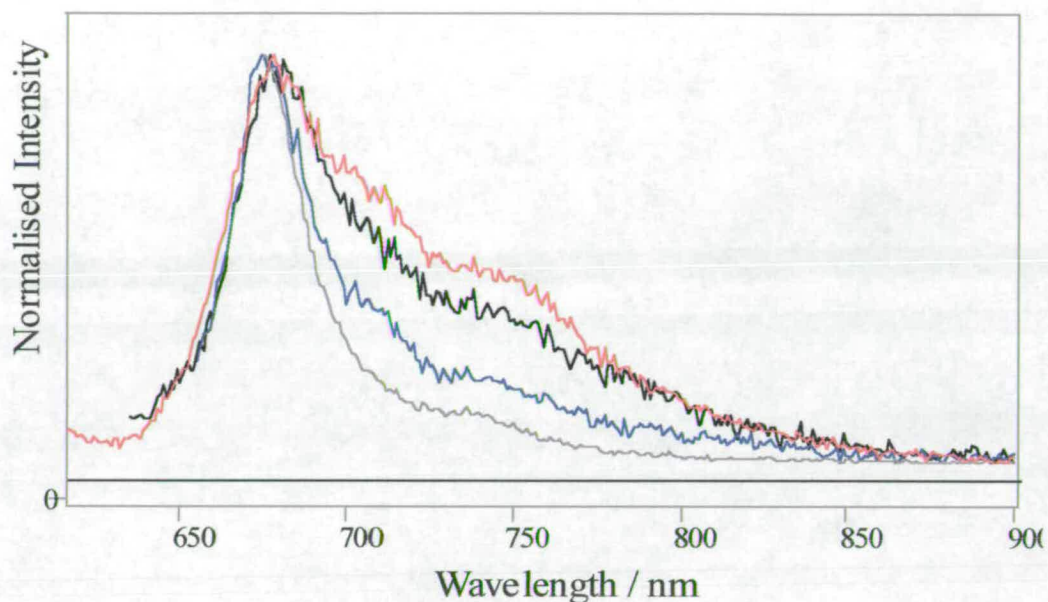
Figure 5.5 – Fluorescence emission spectra for a 10^{-5} M sample of turquoise~1 in water at room temperature at excitation wavelengths of 600nm red (max intensity 11164cps), 620nm black (7068cps), 640nm blue (7996cps) and 660nm grey (19359cps).

The fluorescence excitation spectra in figure 5.6 show that by starting with an emission wavelength to the blue of the emission maximum and working towards the emission maximum the monomer Q-band dominates the spectrum, the red spectrum in figure 5.6. Continuing towards an emission wavelength corresponding to the broader dimer emission one obtains excitation spectra that are dominated by the dimer Q-band, the grey spectrum in figure 5.6 for example. It is evident that the absorption spectrum of turquoise~1 shows blue shifted absorption of the dimer with respect to the monomer, while the fluorescence emission spectra show the dimer with red shifted emission.
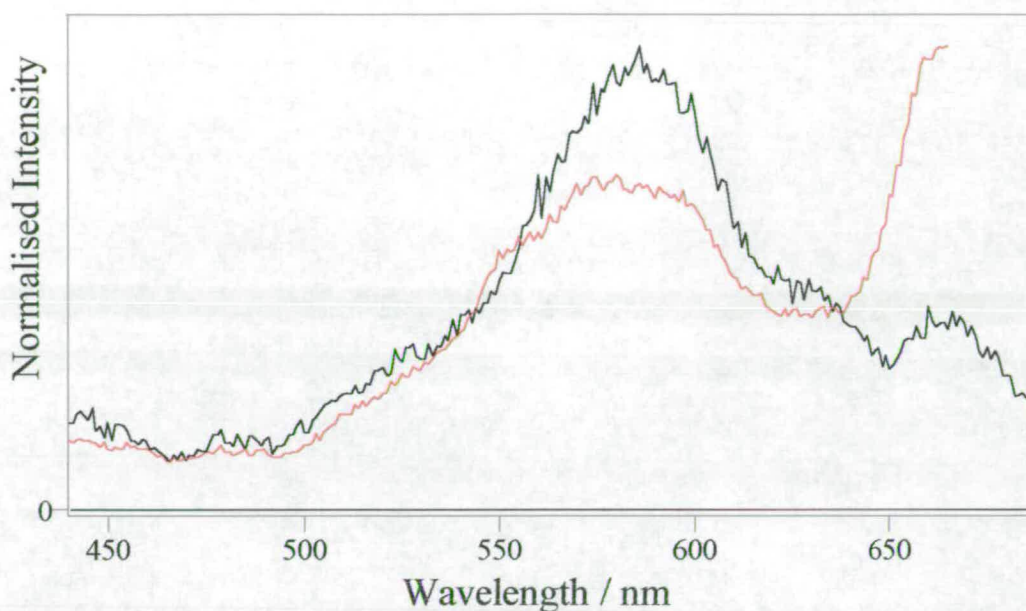
Figure 5.6 – Excitation spectra of turquoise~1 in water, 10^{-5} M, at room temperature at emission wavelengths of 680nm red (max intensity 18717cps) and 740nm black (18674cps).

The spectral effects of dimerisation are explained in terms of exciton coupling between the two monomer chromophores [8-14]. The presence of a fluorescent dimer in ethanol has also been detected. The absorption spectra in Figure 5.4 illustrate the presence of a dimer of turquoise~1 in ethanol. The emission spectra, obtained by exciting across the absorption envelope, are shown in figure 5.7; one can note the dependence of the emission on excitation wavelength. The primary focus here is the different emission spectra obtained when exciting the monomer and dimer absorption bands. This indicates that not only does the turquoise~1 monomer fluoresce in ethanol, but as in the aqueous environment the turquoise~1 dimer fluoresces as well. The fluorescence excitation spectra shown in figure 5.8, confirm the presence of a fluorescent dimer. A long emission wavelength, positioned at the broad red shifted dimer emission, results in a fluorescence excitation spectrum dominated by the dimer Q-band. A shorter emission wavelength, positioned at the

narrow monomer emission, results in the excitation spectrum being dominated by the monomer Q-band.

Figure 5.7 – Fluorescence emission spectra of turquoise~1, 10^{-5} M, in EtOH at room temperature at excitation wavelengths of black 600nm (max intensity 21017cps), grey 620nm (12183cps) and red 650nm (17944cps).

Figure 5.8 – Fluorescence excitation spectra of turquoise~1, 10^{-5} M, in EtOH at room temperature at excitation wavelengths of black 720nm (max intensity 11261cps), grey 700nm (17345cps) and red 680nm (32149cps).

The dependence of the emission spectrum on excitation wavelength in ethanol glass at 77K is shown in figure 5.9. Excitation at 640nm gives the fluorescence spectrum of the free monomer, with a characteristic intense, narrow 0-0 band at 673nm and two relatively weak vibronic bands, with a vibronic interval of ~700cm^{-1}. When the excitation wavelength is decreased to 600nm, a shoulder appears to the blue of the monomer 0-0 transition and another to the red. Exciting at 580nm, these shoulders become clearly defined bands at 658 and 688nm, with another weaker band apparent at about 720nm. These new bands constitute the spectrum of the perturbed monomer chromophore in the dimer, with the 0-0 transition at 658nm shifted ~300cm^{-1} to the blue of the free monomer 0-0.
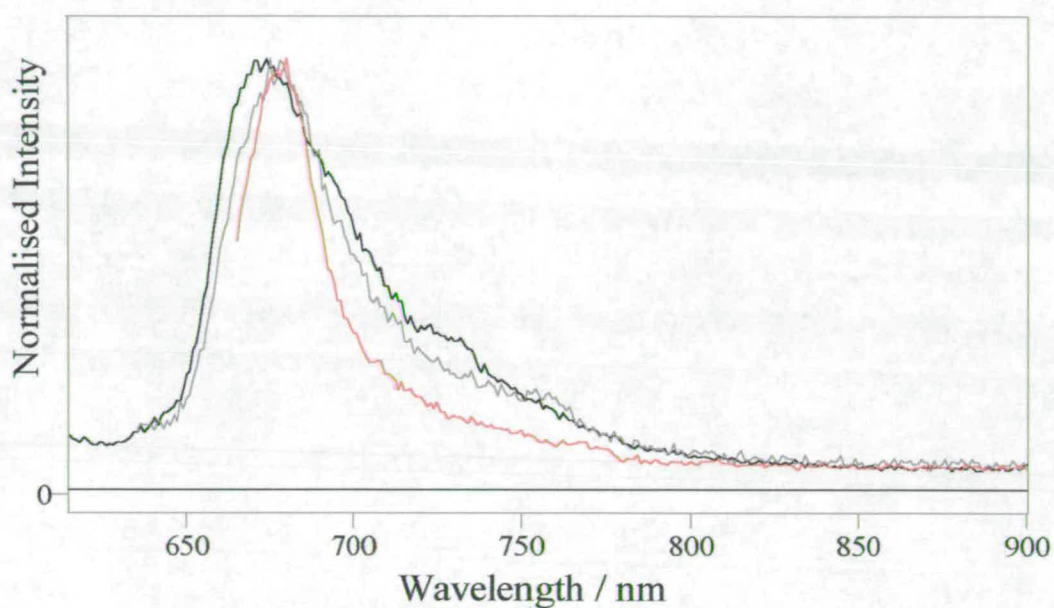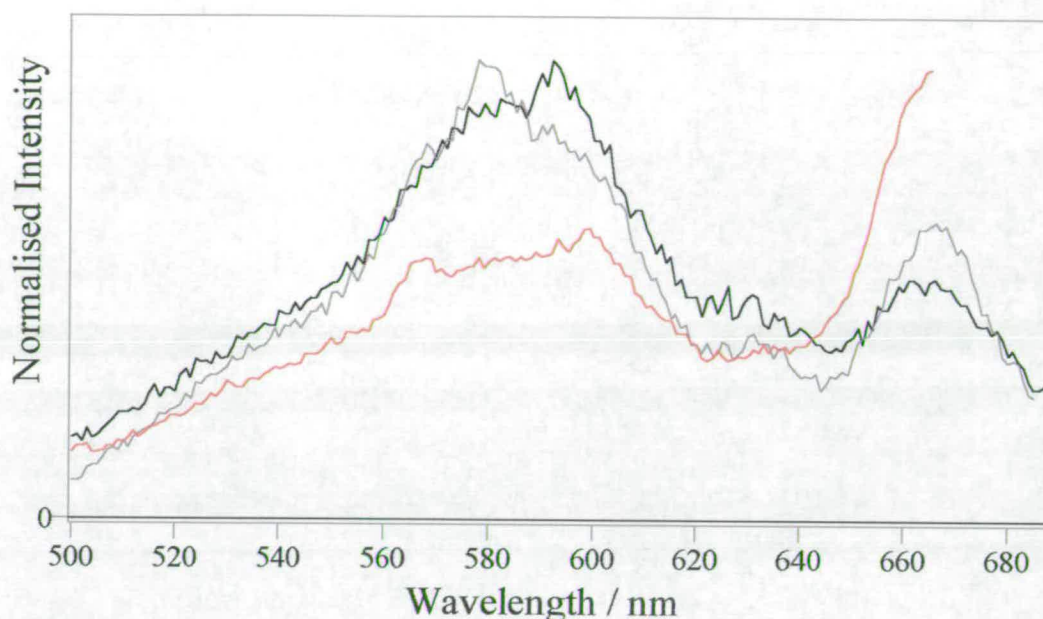
Figure 5.9 – Fluorescence emission spectra of turquoise~1, 10^{-5} M, in EtOH / 77K at excitation wavelengths of black 580nm (max intensity 107504cps), grey 600nm (145614cps) and red 640nm (124637cps).

The excitation spectrum detected at 680nm, shown in Figure 5.10, is characteristic of the free monomer. Detection at 687nm and 720nm, corresponding to the dimer vibronic bands, gives a broad excitation band to the blue of the monomer 0-0 (Figure 5.10 emission at 720nm and 687nm), very similar to the dimer excitation spectrum seen at room temperature, figure 5.6. The large shift between the dimer excitation and emission spectra is consistent with the accepted model of exciton coupling in a cofacial phthalocyanine dimer in which the monomer transition moments are parallel, i.e an upper allowed exciton state and a lower forbidden state. There will be rapid radiationless relaxation from the initially excited upper state to the lower state, from which emission will occur. Although the fluorescence transition from the lower state is formally forbidden, it can be induced by vibronic coupling. Alternatively, the monomer subunits may be twisted or tilted from a perfectly parallel alignment, giving the lower exciton state a finite transition moment. A weak absorption to the lower exciton state would be concealed under the monomer absorption band.
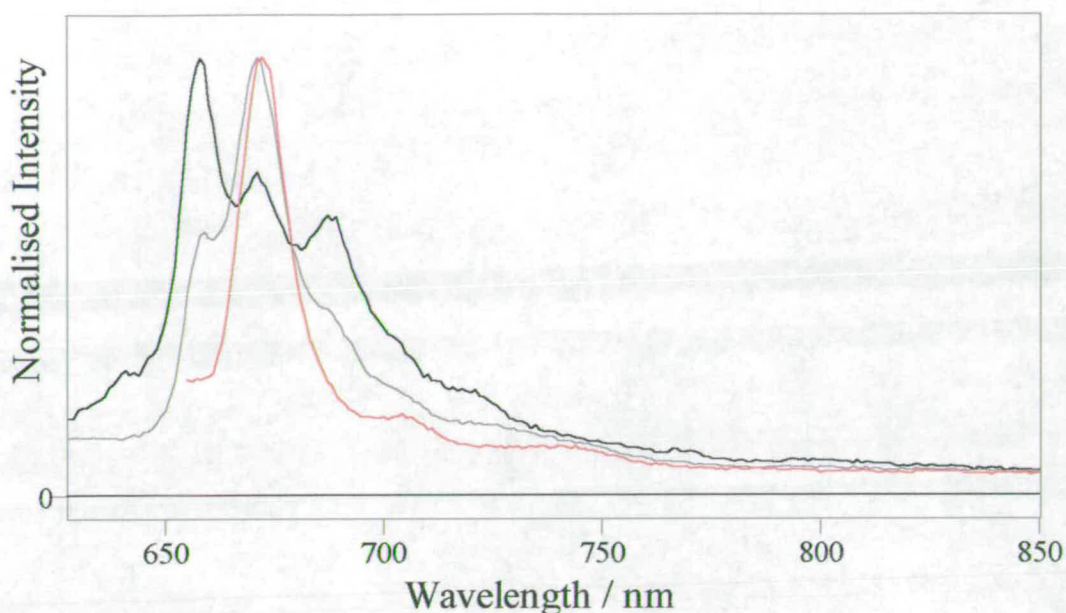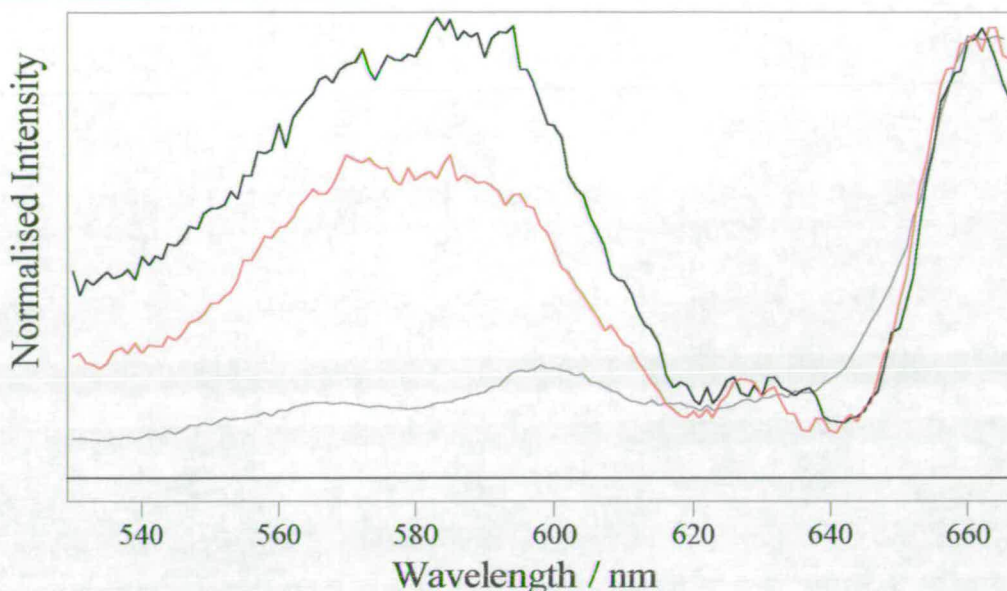
Figure 5.10 – Fluorescence excitation spectra of turquoise~1, 10^{-5} M, in EtOH / 77K at emission wavelengths of black 720nm (max intensity 26779cps), red 687nm (82326cps) and grey 680nm (228191cps).

The observation of this large shift between excitation and emission spectra in frozen ethanol at 77K rules out the possibility that it is due to solvent relaxation about the initially excited state or rearrangement of the structure of the Franck-Condon excited state. From the separation (~1300cm^{-1}) between the rising edge of the excitation band and the emission 0-0 band, and assuming that the Stokes shift of the dimer fluorescence is the same as that of that of the monomer (250cm^{-1}), the exciton splitting (2X in equation 5.1) is estimated to be at least 1000cm^{-1}. The lower exciton level lies 300cm^{-1} above the monomer S_1 state indicating a decrease in binding energy of the dimer on excitation of at least 800cm^{-1}.

The narrow vibronic structure of the dimer emission spectrum at 77K indicates that the fluorescence arises from a single dimer structure, or a narrow distribution of structures. However, the dimer excitation spectrum at 77K is broad, resembling that at room temperature, indicating absorption by dimers with a variety of geometries in which the monomer experiences different intermolecular interactions and exciton splitting. There may be efficient energy transfer from the multiple absorbing dimer

species to the single emitting species, implying that the different species exist in close proximity as constituents of larger aggregates. Comparison of the dimer excitation and absorption spectra shows that the majority of the intensity in the excitation spectrum is due to species which absorb in the short wavelength tail of the absorption spectrum and contribute relatively little to the total absorption intensity. The fluorescence arises from excitation of the minority of the dimers, with the majority being non-fluorescent themselves and unable to transfer their excitation energy to the higher energy emitting species.

5.4 – Aggregation Studies of Turquoise~1

During the dyeing process, such variables as concentration of dye, temperature of the dyebath and ionic strength are important. The importance of these variables lies in the fact that each variable effects the extent to which the dye is aggregating. The following section of work looks at the ability to vary the extent of aggregation through the variation of each of these variables.

5.4.1 – Concentration and the Aggregation of Turquoise~1

Section 5.2 referred to the fact that when the amount of aggregation increases with increasing concentration, the system shows an apparent deviation from Beer's law [45]. A plot of absorbance versus concentration should yield a straight line through the origin, as stated by Beer's law, so any deviation from this would be further evidence for aggregation. Figure 5.11 shows how the absorbance of a 10^{-5}M solution of turquoise~1 varies with concentration. The data points show a clear deviation from the Beer's law straight-line behaviour. This adds to the evidence that turquoise~1 aggregates. The deviation from Beer's law indicates that the extinction co-efficient, the gradient of the plot, for the sample of 10^{-5}M solution is not constant. The plot clearly deviates from the behaviour of Beer's law. If one assumes that that the extinction co-efficient at 10^{-7}M is that of the monomer then a linear Beer plot can

be drawn. It is the case though that at 10^{-7}M the dye solution indeed does aggregate, so the true extinction co-efficient of the monomer would be greater in magnitude. Thus the slope of the Beer plot would be greater, if the experimental data deviates from the approximation in place here then the data will clearly deviate from the exact case.
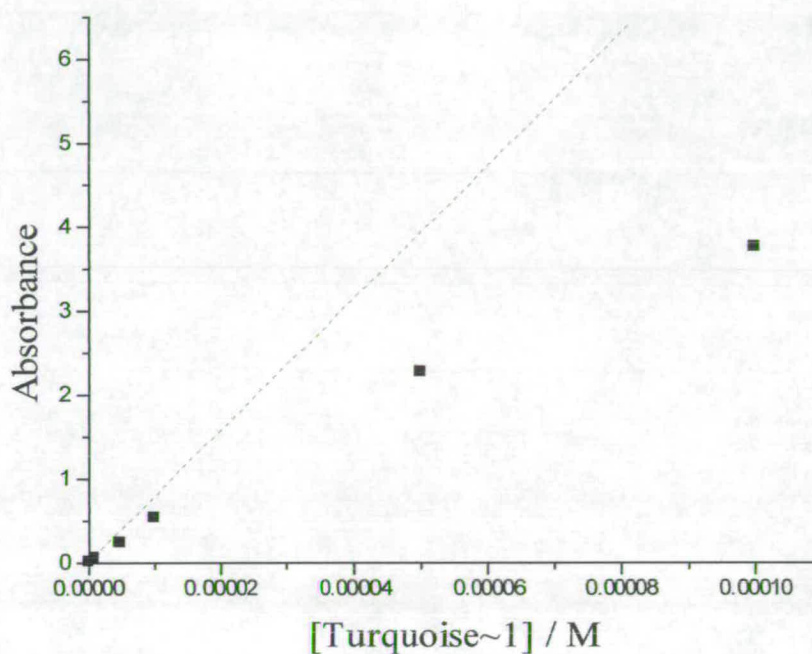
Figure 5.11 – Deviation from Beer's law plot for a 10^{-5} M solution of turquoise~1 in water at room temperature. Absorbance measured at 603nm.

Figure 5.12 illustrates how the extinction co-efficient varies with concentration, the extinction co-efficient being at its greatest at low concentration. This is where the solution is approaching a composition of monomer only, but still contains dimer, even at 10^{-7}M the absorption profile shows clear evidence of dimers being present.
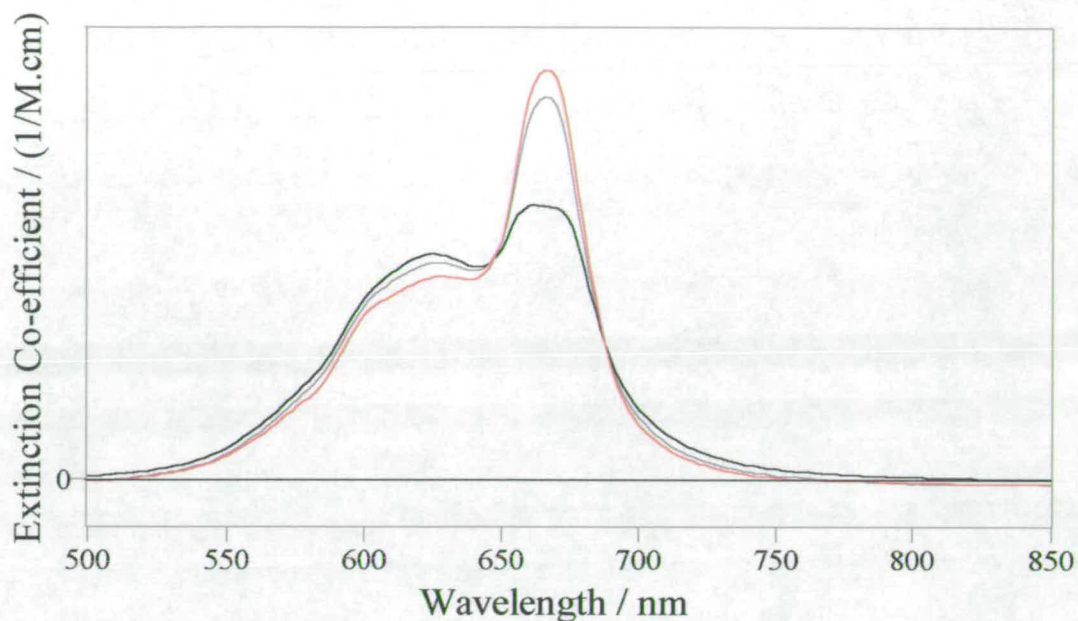
Figure 5.12– Comparison of extinction co-efficient of turquoise~1 in water at room temperature at varying concentrations, red 10^{-6} M (max value 56064 $M^{-1}cm^{-1}$), grey 10^{-5} M (52300 $M^{-1}cm^{-1}$) and black 10^{-4} M (37570 $M^{-1}cm^{-1}$).

Figure 5.13 – Plot of extinction co-efficient, versus the logarithm of concentration for a sample of turquoise~1 at room temperature fitted at 665nm.

Figure 5.13 shows how the extinction co-efficient of turquoise~1 varies with the logarithm of the concentration, the extinction co-efficient is measured at the monomer Q-band, 665nm. Examples of authors that suggest theoretical fits of data such as that in figure 5.13 are K. Hamada et al [49] and B. Neumann et al [50]. The data that these authors collected do not span the same large range of concentrations that the d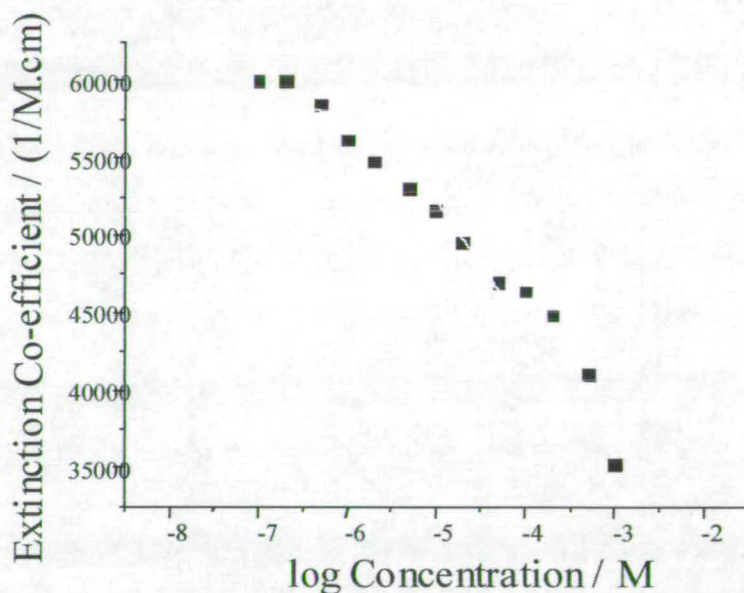ata collected for this project does. This data used in this project extends over four orders of magnitude. The theoretical fits used by such authors as Hamada and Neumann are based on monomer-dimer equilibrium only, the authors do not detect any polyaggregates over the limited concentration range employed. A model [51] for the data in figure 5.13 has been developed by Philip Camp, it involves making the assumption that there are only three types of molecule in solution. These are described as free monomers, external molecules and internal molecules. This is illustrated in figure 5.14.
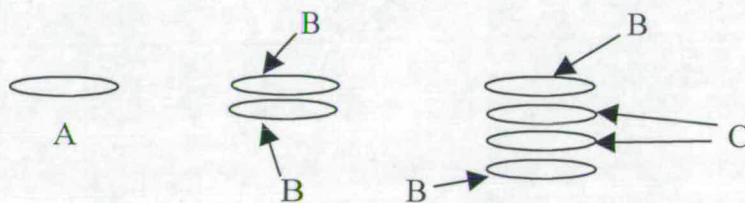
Figure 5.14 – Diagram showing A-free monomers, B-external molecules and C-internal molecules.

One can now define the extinction co-efficient in terms of the extinction co-efficient of the monomer, ε_1, that of the external molecules, ε_{ex} and that of the internal molecules, ε_{in}. The same definition is given to the mole fraction of the three types of molecule; x_1, x_{ex} and x_{in}. These mole fractions are of course a function of the concentration of the sample, c. So the extinction co-efficient, ε, can be defined as in equation 5.2;

$$\varepsilon = \varepsilon_1 x_1(c) + \varepsilon_{ex} x_{ex}(c) + \varepsilon_{in}(1 - x_{1(c)} - x_{ex}(c)) \qquad \textbf{Equation 5.2}$$

If, as assumed previously, only monomers and dimers exist in equilibrium then $x_{in} = 0$, the partition co-efficient q_{ex} can be defined as in equation 5.3. This initial assumption is not implicit in the model but is dealt with in order to allow comparison with the final model.

$$q_{ex} = [dimers] / [monomers]^2 = \frac{1}{2} [external\ mols] / [internal\ mols]^2$$

$$q_{ex} = (c-[monomers]) / 2[monomers]^2 \qquad \textbf{Equation 5.3}$$

and the mole fraction of monomers, x_1;

$$x_1 = [monomers] / c = (-1 + \sqrt{(1 + 8q_{ex}c)}) / 4q_{ex}c \qquad \textbf{Equation 5.4}$$

Now, one can fit the extinction co-efficient, ε, using the parameters q_{ex}, ε_1 and ε_{ex}. This fit is compared with the experimental data, from figure 5.13, and is shown in figure 5.15;

Figure 5.15 – Illustration of how the monomer-dimer approximation fit, solid line, is in poor agreement with the experimental data, represented by the data points, fitted at 665nm.
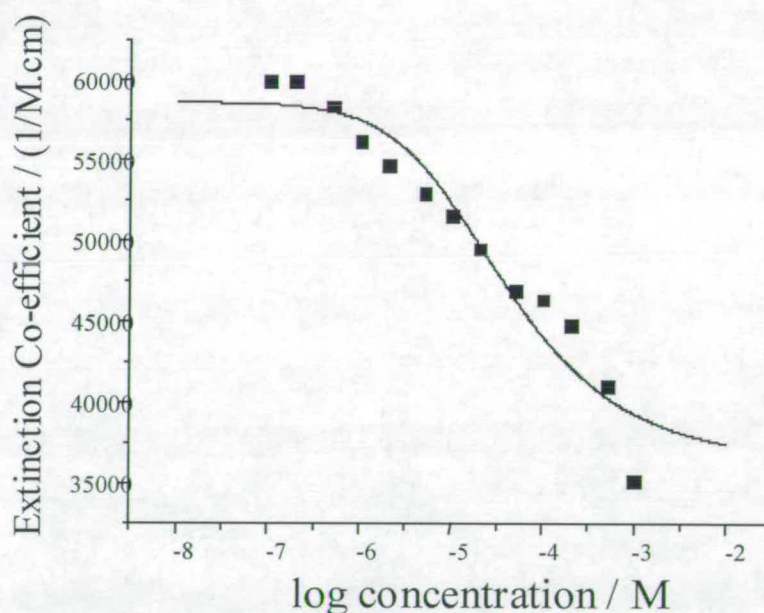
Figure 5.15 shows how the monomer-dimer model does not allow for a satisfactory agreement with the experimental data. This implies that the monomer-dimer model is insufficient. The next stage of the approximation involves allowing for infinite aggregation, that is aggregates higher than simply the dimer species, but assuming only one partition co-efficient, q_{ex}. Essentially one has the equilibrium in equation 5.6, with the equilibrium constant q_{ex} independent of n;

$$\text{n-mer} + \text{monomer} \underset{}{\overset{q_{ex}}{\rightleftharpoons}} (n+1)\text{-mer} \qquad \textbf{Equation 5.6}$$
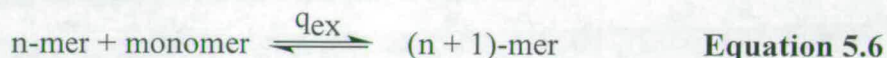
The mole fractions for the free monomer, the external molecules and the internal molecules are defined as follows;

$$x_1 = (1/q_{ex}) + (1/2(q_{ex}c)^2) \, (1-(\surd\, 1 - 4q_{ex}c)) \qquad \textbf{Equation 5.7}$$

$$x_{ex} = 2q_{ex}cx_1^2 \, / \, 1-q_{ex}cx_1 \qquad \textbf{Equation 5.8}$$

$$x_{in} = 1-x_1-x_{ex} \qquad \textbf{Equation 5.9}$$

The fit obtained from this method is compared to the experimental data, from figure 5.13, in figure 5.16. This shows that there is no improvement in the agreement between the theoretical model and the experimental data when compared with the simple monomer dimer model from figure 5.15. The model shown in figure 5.16, like that in figure 5.15, is insufficient.

The final approach involves having unlimited aggregation but not simply one partition co-efficient. If one considers two equilibrium systems;

$$\text{n-mer} + \text{monomer} \underset{}{\overset{K}{\rightleftharpoons}} (n+1)\text{-mer} \qquad \textbf{Equation 5.10}$$
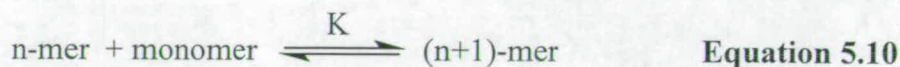
The equilibrium constant K can be written as in equation 5.11,

$$K = q_{ex}^2 q_{in}^{(n+1-2)} / q_{ex}^2 q_{in}^{n-2} = q_{in} \qquad \text{Equation 5.11}$$
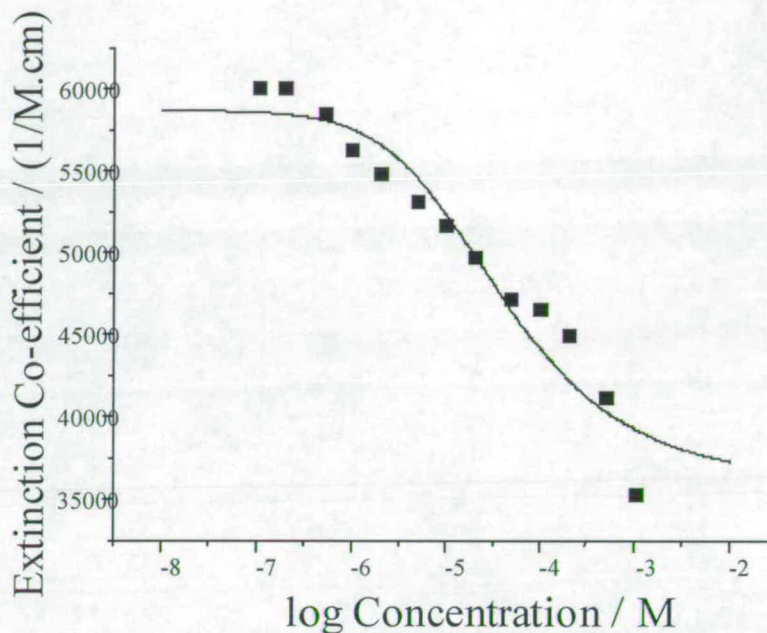
Figure 5.16 - Illustration of how the unlimited aggregation with only one equilibrium constant approximation fit, solid line, is in poor agreement with the experimental data, represented by the data points, fitted at 665nm.

The equilibrium constant for the equilibrium set up in equation 5.12 is q_{ex}.

$$2 \text{ monomers} \xrightleftharpoons{q_{ex}} \text{dimer} \qquad \text{Equation 5.12}$$

Figure 5.17 illustrates the processes that are occurring and the associated partition co-efficients, q;

Plus one external molecule

Plus one internal molecule   Plus one internal molecule
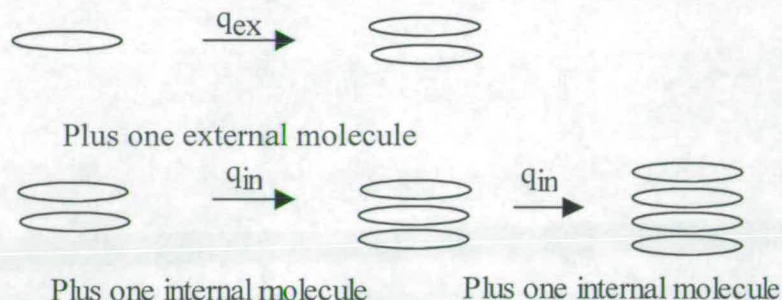
Figure 5.17 – Illustration of the partition co-efficients associated with the progressive increase in aggregation, from monomer through dimer to tetramer and higher.

Figure 5.18 shows how the model that accounts for unlimited aggregation, but with more than just one partition co-efficient, gives a very good fit to the experimental data from figure 5.13.
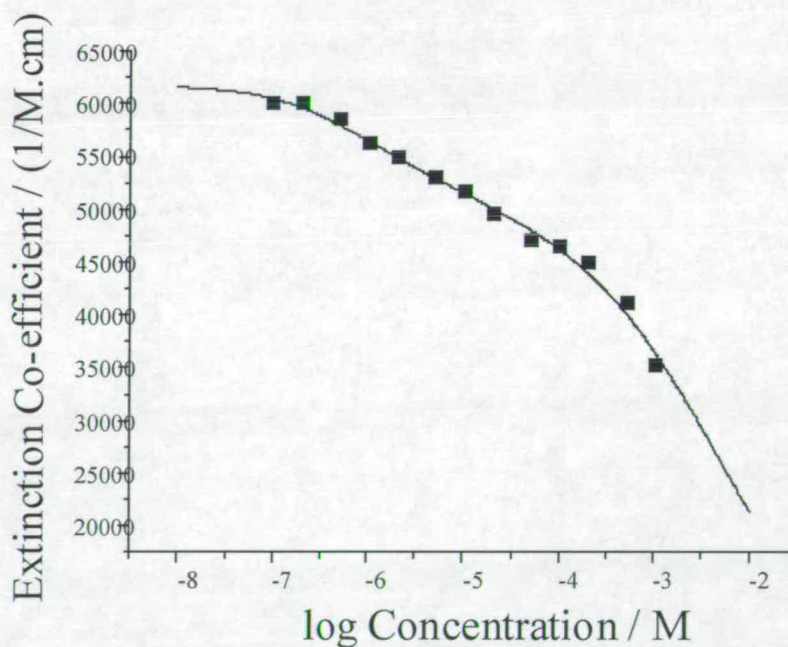
Figure 5.18 - Illustration of how the unlimited aggregation model with more than one partition co-efficient approximation, solid line, is in good agreement with the experimental data, represented by the data points, fitted at 665nm.

The fact that the unlimited aggregation model is the theoretical best fit to the experimental data implies that that the dye solution does contain higher aggregates. The solution does not only contain monomer and dimer but higher aggregates such as trimer and tetramer, this is illustrated in figure 5.19. The figure shows how the fraction of aggregates containing n molecules over the concentration range 10^{-8} M to 10^{-2} M changes with the increase in higher aggregates with increasing concentration.
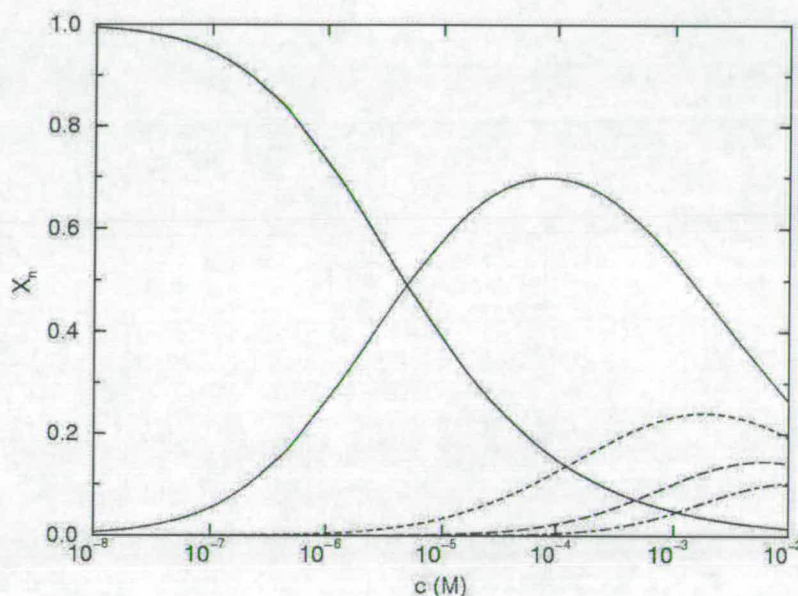
Figure 5.19 –Fractions of aggregates containing n molecules as functions of turquoise~1 concentration in water from the unlimited aggregation model in figure 5.18; n=1 (solid line), n=2 (dotted line), n=3 (dashed line), n=4 (long dashed line) and n=5 (dot-dashed line).

5.4.2 – Ionic Strength and the Aggregation of Turquoise~1

It is well known that the addition of an electrolyte such as sodium chloride will increase the degree to which a species is aggregating [40, 41]. The effect of adding such an electrolyte to a dye solution is explained by considering that the ionic strength of the solution is increased. This suggests that the repulsion between like

charges on the dye are screened by the higher ionic strength on the solution. Figures 5.20 and 5.21 show how on addition of salt to a solution of turquoise~1 the dimer Q-band increases in intensity. Comparison of the two figures show how increasing the salt concentration from $20gL^{-1}$ to $240gL^{-1}$ increases the amount of aggregation. This is, as one would expect, as the ionic strength of the solution is greater when the salt loading is greater.

Figure 5.20 – Comparison of absorption spectra of 10^{-5} M solutions of turquoise~1 in water at room temperature, with 0.2g NaCl per 10ml of solution, red, (max absorption 0.405) and without salt, black (0.523).

By plotting absorption profiles at varying salt loading it is possible to look for an isosbestic point. The discovery of such a point would infer that only two absorbing species are present in the solution as discussed by Gruen [41] and Gouterman et al [42]. Figure 5.22 shows absorption plots at six varying salt concentrations and a clear isosbestic point at 693nm. The isosbestic point indicates the presence of monomers and dimers only, this is contrary to the theoretical predictions that allow for trimers and higher aggregates. The theoretical modelling describes the system

free of salt, the observed isosbestic point is in a system that includes salt. Thus salt appears to decrease the formation of higher aggregates than dimers. This does not mean that these higher aggregates do not exist, but that there are far fewer of them than in a system free of salt. Figures 5.23 to 5.25 illustrate the effect that increasing salt loading has on the formation of higher aggregates. The extinction co-efficient in figures 5.23 to 5.25 were measured at the monomer Q-band, 665nm.
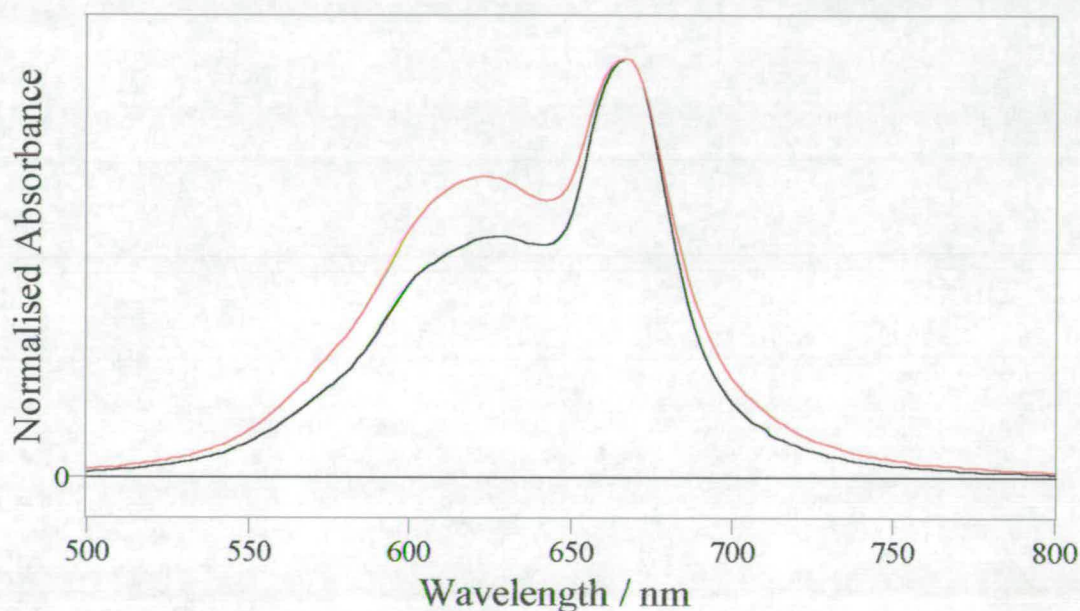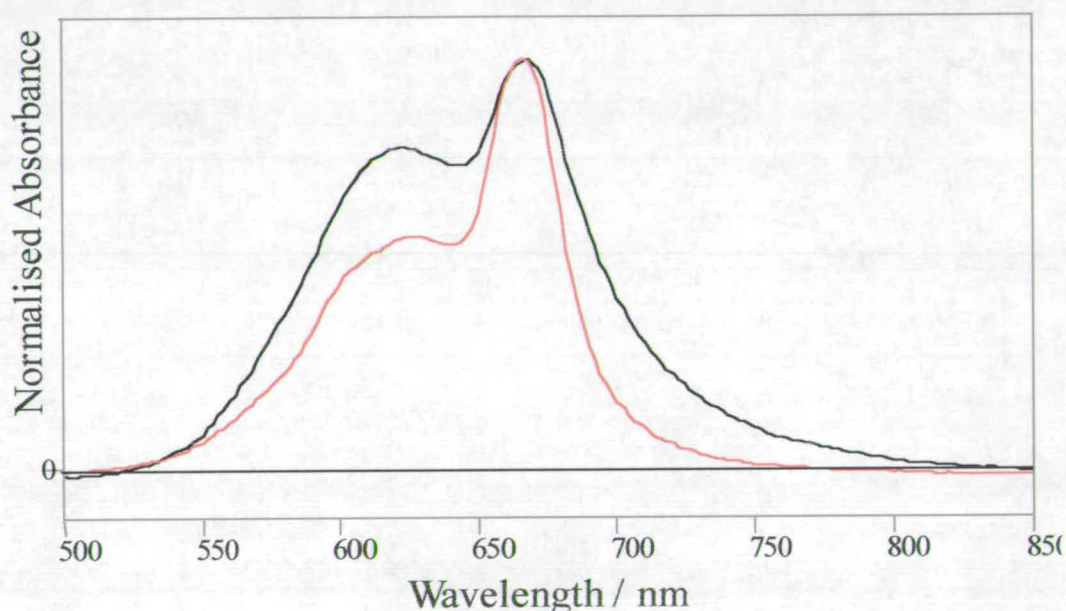

Figure 5.21 – Comparison of absorption spectra of 10^{-5} M solutions of turquoise~1 in water at room temperature, with 2.4g NaCl per 10ml of solution, black (max absorbance 0.252), and without salt, red (0.523).

They show the complete theoretical model including higher aggregates, solid line, experimental data and monomer-dimer equilibrium fit, dotted line. The three figures, 5.23 to 5.25, represent an increasing concentration of salt, and that as the salt loading increases the monomer-dimer equilibrium model becomes the actual dominant physical equilibrium. The presence of higher aggregates is negligible at these salt concentrations. The belief that an increase in ionic strength increases the amount of aggregation is shown not to be strictly true.
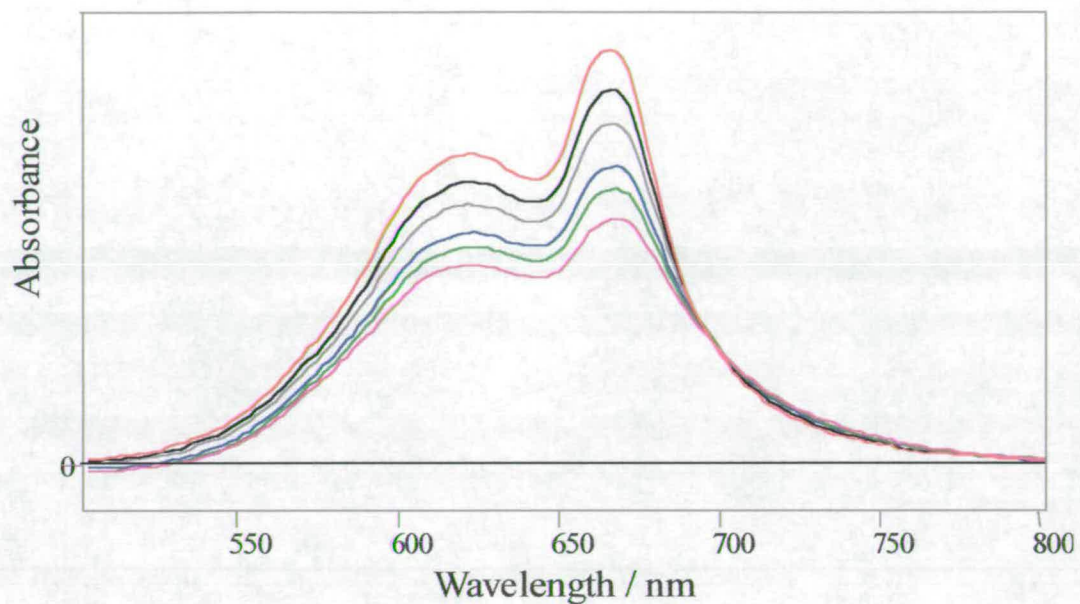
Figure 5.22 – Comparison of absorption spectra of 10^{-5} M solutions of turquoise~1 in water at room temperature, with various NaCl loading per 10ml of solution, red 0.6g (max absorbance 0.350), black 1g (0.320), grey 1.4g (0.297), blue 2g (0.268), green 2.4g (0.252) and pink 3g (0.229).
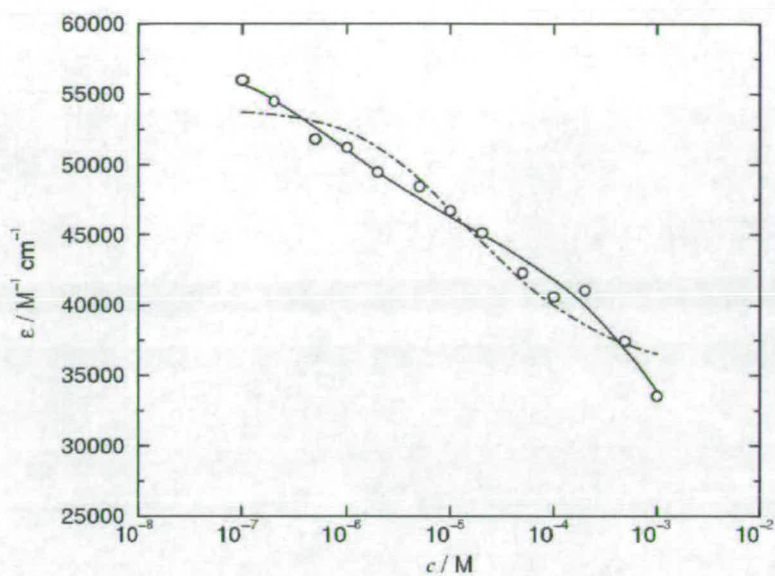
Figure 5.23 – Comparison of fit, in dotted line, of monomer-dimer equilibrium versus full theory including higher aggregates. Salt concentration of 0.01M, plot shows extinction co-efficient versus dye concentration.
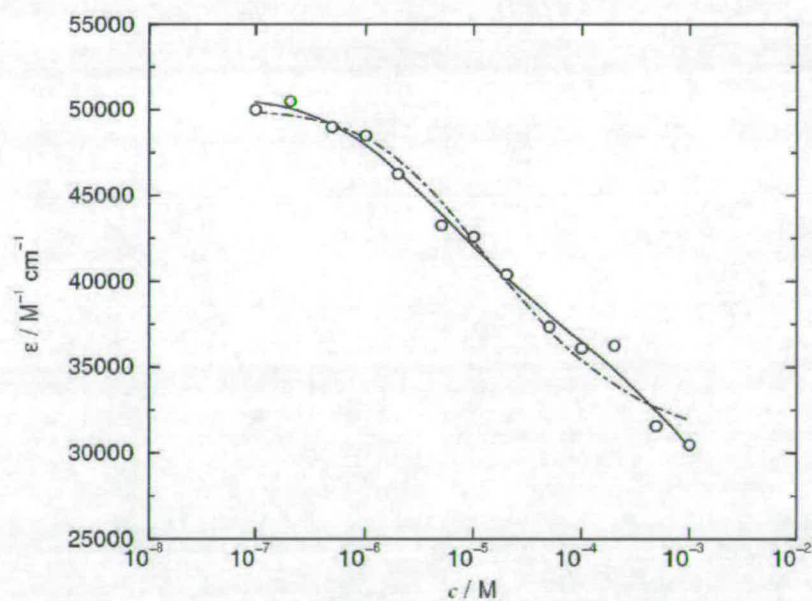
Figure 5.24 – Comparison of fit, in dotted line, of monomer-dimer equilibrium versus full theory including higher aggregates. Salt concentration of 0.1M, plot shows extinction co-efficient versus dye concentration.

The formation of the higher aggregates, in such high salt loading systems as that of the observed isosbestic point, is less favoured now. The monomer has become more favoured, than the aggregates higher than dimer, than in the salt free system. On comparison of a salt free sample and a sample of same concentration with salt, aggregation would of course have increased. The presence of higher aggregate though would not, only that of dimers. The high salt loading systems have little contribution from higher aggregates while the salt free system has an appreciable contribution.
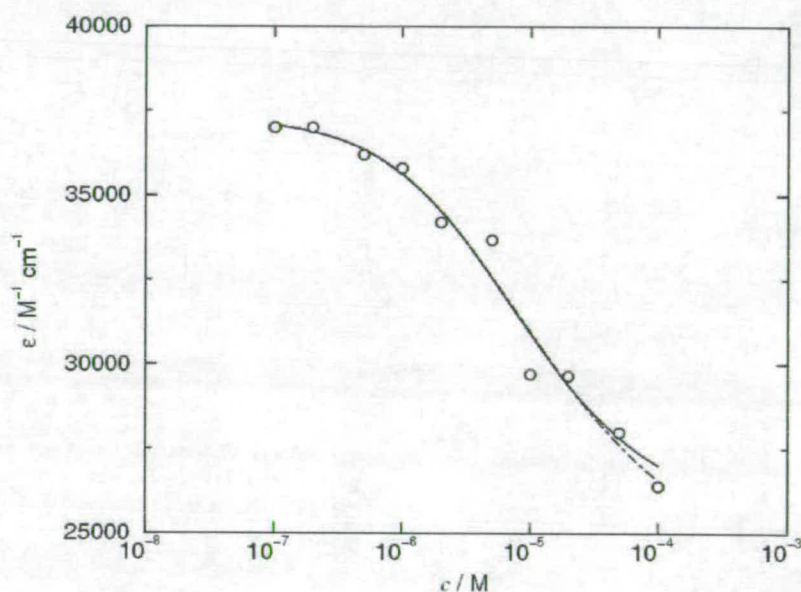
Figure 5.25 – Comparison of fit, in dotted line, of monomer-dimer equilibrium versus full theory including higher aggregates. Salt concentration of 2.0M, plot shows extinction co-efficient versus dye concentration.

The extinction co-efficient of turquoise~1 can be varied over a concentration range. It is also possible to vary the extinction co-efficient, and hence the amount of aggregation, of a solution of constant concentration by varying the salt loading of that solution. This is illustrated in figure 5.26, where a solution of 10^{-5}M has a increasing salt loading. This increases the amount of aggregation, thus leading to a

reduced extinction co-efficient as the composition moves further and further away from monomer only. An increasing load of salt was added to a sample of 10^{-5}M turquoise~1, the extinction co-efficient of the monomer Q-band was monitored as a function of the increasing salt loading and plotted in figure 5.27. The result was an exponential type decay of the extinction co-efficient as the salt loading increased. As the salt loading increased the relative amount of aggregation increased, although not higher aggregates, thus the extinction co-efficient decayed from its value with no added salt. The value at zero salt though is not the extinction co-efficient of the monomer, as here a 10^{-5}M solution is being investigated and its absorption profile clearly shows the existence of dimers at this concentration.
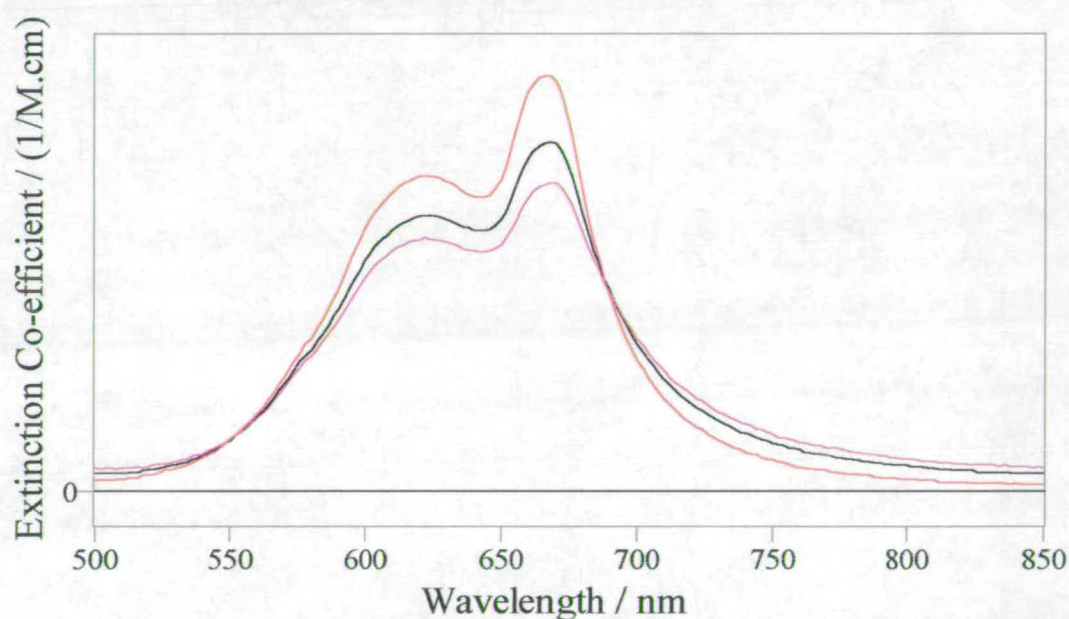
Figure 5.26 – Comparison of extinction co-efficient of 10^{-5} M solution of turquoise~1 in water at room temperature at varying salt loadings g/10ml of solution, red 1g (max value 31906 $M^{-1}cm^{-1}$), black 2g (26800 $M^{-1}cm^{-1}$) and pink 2.8g (23600 $M^{-1}cm^{-1}$).
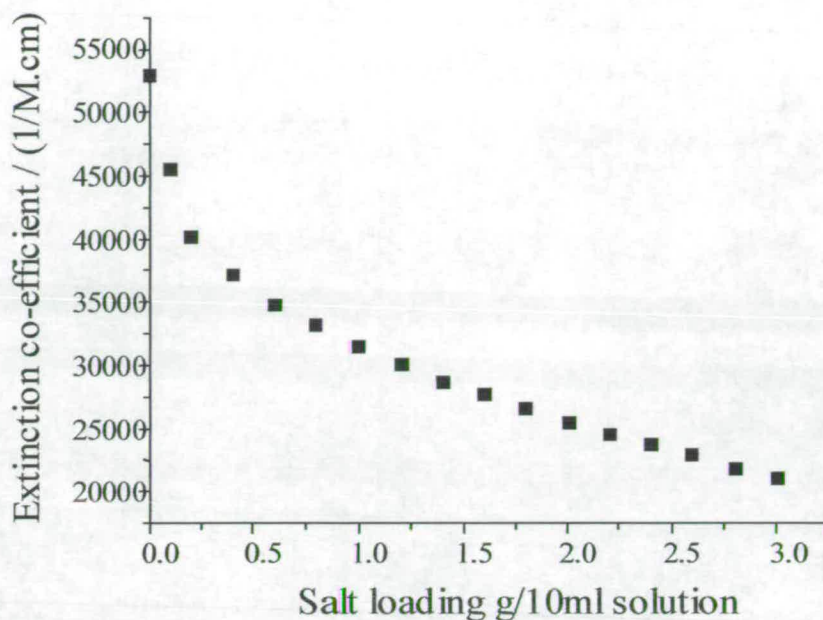
Figure 5.27 – Plot of extinction co-efficient versus salt loading for a 10^{-5} M sample of turquoise~1 in water at room temperature.

5.4.3 – Temperature and the Aggregation of Turquoise~1

The effect of temperature on the absorption profile of turquoise~1 was investigated. Previous studies [41, 43 and 44] indicated that as the temperature is increased the relative amount of monomer to aggregate increases. Part of this disaggregation effect has been attributed to the reduction of the dielectric constant [45] of water at higher temperatures, but also the provision of energy to overcome the intermolecular forces that hold the aggregates together. The correlation between the increasing amount of monomer with the decreasing dielectric constant was specifically looked at by Gruen [41]. Figure 5.28, for aqueous solution, shows how the amount of monomer increases as the temperature is increased to 80°C and also the decrease in the amount of dimer at 30°C. This implies a degree of control within the dyebath on the state of aggregation. Figure 5.29, for ethanolic solution, shows how the relative amount of monomer is increased as the temperature of the solution is increased. Thus a certain amount of control of the degree of aggregation is attainable when using ethanol as a solvent.
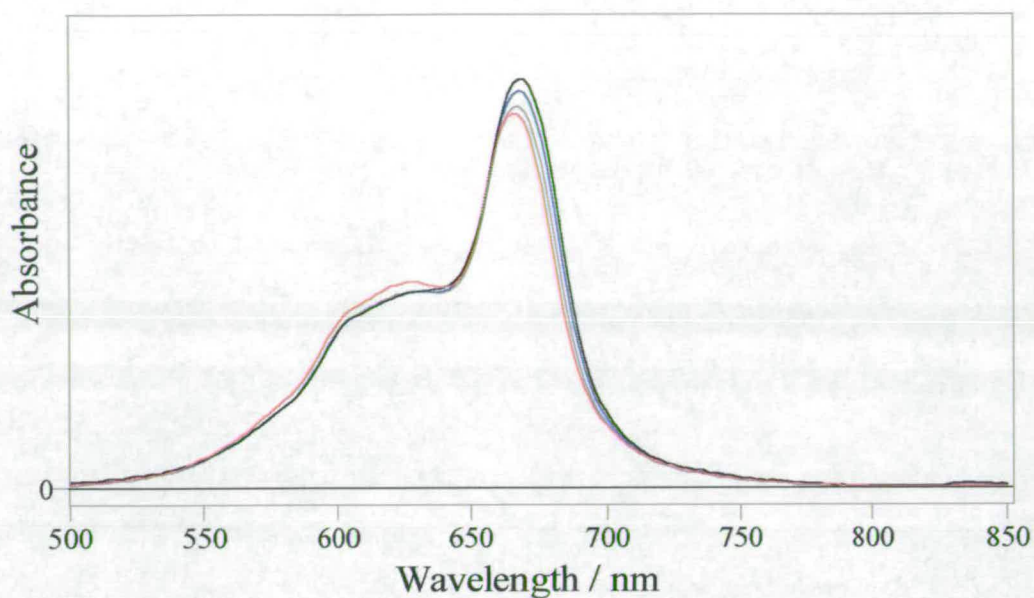
Figure 5.28 – Comparison of absorption spectra of 10^{-5} M solutions of turquoise~1 in water at varying temperature, black 80°C (max absorbance 0.600), blue 70°C (0.572), grey 50°C (0.542) and red 30°C (0.519).
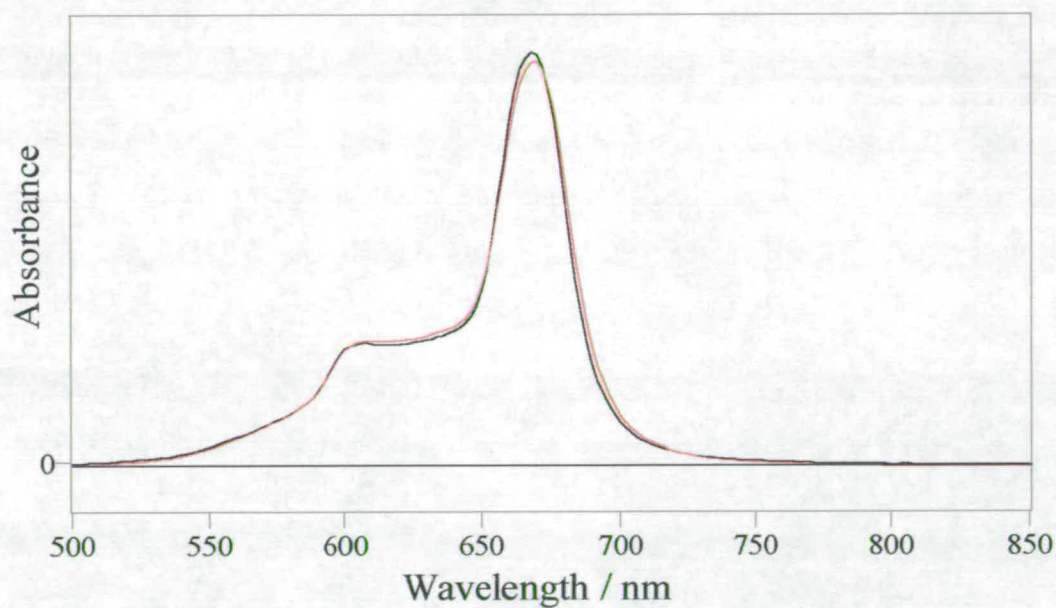
Figure 5.29 – Comparison of absorption spectra of a 10^{-5} M sample of turquoise~1 in ethanol at different temperatures, black 70°C (max absorbance 0.778) and red 40°C (0.760).

5.4.4 – Comparison of the Aqueous and Ethanolic Systems

Because ethanol has a lower dielectric constant than water, see figure 5.30 one would expect that in ethanol the extent of aggregation would be less than that in water. As already noted the increase in temperature that induces a decrease in dielectric constant results in an increase in the amount of monomer in solution. Thus if a solvent such as ethanol is used, which has a lower dielectric constant than water, one would expect that the extent of aggregation would be greater in water.

Substance	Dielectric Constant / κ
Water (20°C)	80.4
Water (25°C)	78.5
Ethanol	25

Figure 5.30 – The values of the dielectric constant of solvents of interest. For a vacuum, κ = unity.
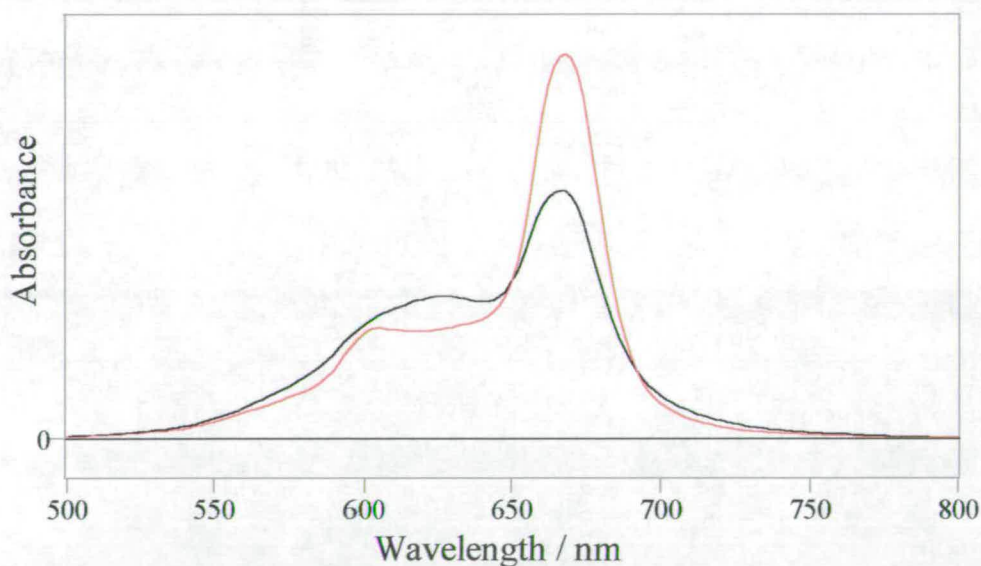
Figure 5.31 - Comparison of absorption spectra of turquoise~1 in EtOH, red (max absorbance 0.821) and in water, black (0.522) at room temperature, 10^{-5} M solutions.

The interesting feature of figure 5.31 is the relative intensities of the monomer and dimer Q-bands. It is quite clear that in both solvent systems the monomer Q-band appears to have a greater relative intensity than the dimer does. This though is extremely clear in the ethanolic system where the monomer Q-band almost dwarfs that of the dimer, although the region corresponding to dimer absorption appears to be broader than that of the monomer. This can be attributed to the fact that as one is using a solvent system with lower dielectric constant then the result is that although aggregation is occurring, it is not happening to the same extent.

5.5 – Conclusions

Excitation of the monomer and dimer absorption bands of turquoise~1 result in different fluorescence emission spectra. With the assistance of the excitation spectra as well as the emission, the evidence clearly points to the observation of a fluorescent phthalocyanine dimer in both the aqueous and ethanolic environment. This is indeed a very rare observation. The absorption profiles at varying concentration show that as concentration of the sample is increased so too is the relative amount of dimer present. This is seen in the increase in the relative intensity of the dimer Q-band. The aggregation of turquoise~1 is clearly confirmed by its deviation from Beer's law. The theoretical modelling of the variation of the monomer absorption band with concentration clearly indicates that it is insufficient to claim merely a monomer and dimer equilibrium in water. The interesting conclusion that can be made from the successful theoretical model is that although the monomer-dimer equilibrium exists so to do dimer-trimer, trimer-tetramer and so on. A plot of a number of absorption profiles at fixed dye concentration but with varying salt loading show an isosbestic point, which is a good indication that two absorbing species are present in solution. However, this is contrary to the theoretical modelling that indicates the presence of higher aggregates along with monomer and dimer. This can be explained if the higher aggregates that the theoretical model accounts for are present in a salt free system, while in a system with salt the formation of higher aggregates is not as strongly favoured. Although these higher aggregates may exist in salt containing

systems, their concentration is minimal in comparison with dimer species. Consequently, the amount of dimers can be increased by the addition of a simple electrolyte such as salt; this is seen by the increase in relative intensity of the dimer Q-band. It is also possible to decrease the relative amount of aggregation by controlling the temperature of the sample. By increasing the temperature of the solution the relative amount of monomer increases, this is viewed by the increase in the relative intensity of the monomer Q-band. This has in part been attributed to the decrease in the dielectric constant of the water. It is also possible to suppose that as the temperature of the solution is increased, any intermolecular forces that exist between monomers in order to create dimers will be overcome, leading to a shift in equilibrium in favour of the monomer.

5.6 - Bibliography

1 R. R. Mather, *J. Porphyrins Phthalocyanines*, 3, **1999**, 643-646.

2 S.E. Sheppard, A.L. Geddes, *J. Amer. Chem. Soc.*, 66, **1944**, 1995-2002

3 G. Scheibe, *Kolloid-Z*, **82**, 1938.

4 A. R. Monahan, J. A. Brado, A. F. DeLuca, *J. Phys. Chem.*, 76, **1972**,446-449.

5 Y. C. Yang, J. R. Ward, R. P. Seiders, *Inorg. Chem.*, 24, **1985**, 1765-1769.

6 W. Ohling, *Ber. Bunsen-Ges Phys. Chem.*, 88, **1984**, 109-115.

7 *Phthalocyanines Properties and Applications*, C. C. Leznoff & A. B. P. Lever, VCH Publishers Inc, **1989**.

8 M. R. Philpott, *J. Chem. Phys.*, 53, **1970**, 968.

9 M. Nastasi, R. W. Yep, V. L. Seligy, A. G. Szabo and R. E. Williams, *Nature*, 249, **1974**, 248.

10 M. Gouterman, D. Holten and E. Lieberman, *Chem. Phys.*, 25, **1977**, 139-153.

11 E. S. Dodsworth, A. B. P. Lever, P. Seymour and C. C. Leznoff, *J. Phys. Chem.*, 89, **1985**, 5698-5705.

12 O. Ohno, Y. Kaizu, H. Kobayashi, *J. Chem. Phys.*, 82, **1985**, 1779.

13 O. Ohno, N. Ishikawa, H. Matsuzawa, Y. Kaizu and H. Kobayashi, *J. Phys. Chem.*, 93, **1989**, 1713-18.

14 Z. Gasyna, N. Kobayashi and M. J. Stillman, *J. Chem. Soc. Dalton Trans.*, **1989**, 2397-2405.

15 L. C. Gruen *Aust. J. Chem.*, 25, **1972**, 1661-7.

16 P. C. Martin, M. Gouterman, B. V. Pepich, G. E. Renzoni and D. C. Schindele, *Inorg. Chem.*, 30, **1991**, 3305-9.

17 R. B. Ostler, A. D. Scully, A. G. Taylor, I. R. Gould, T. A. Smith, A. Waite and D. Phillips, *PhotoChem. PhotoBiol.*, 71(4), **2000**, 397-404.

18 A. P. Savitsky, K. V. Lopatin, N. A. Golubeva, M. Poroshina Yu, E. B. Chernyaeva, N. V. Stepanova, L. I Solovieva and E. A. Lukyanets, *J. Photochem. Photobiol. B: Biol.*, 13, **1992**, 327-333.

19 Xian-Fu Zhang and Hui-Jun Xu, *J. Chem. Soc. Faraday Trans.*, 89(18), **1993**, 3347-3351.

20 N. Kobayashi, Y. Nishiyama, T. Ohya and M. Sato, *J. Chem. Soc. Chem. Commum.*, **1987**, 390-392.

21 D. Pugh, C. H. Giles and D. G. Duff, *J. Chem. Soc. Faraday Trans.*, 67, **1971**, 563-73.

22 D. A. Fernandez, J. Awruch and L. E. Dicelio, *Photochem. Photobiol.*, 63(6), **1996**, 784-92.

23 S. Dhami and D. Phillips, *J. Photochem. Photobiol. A:Chemistry*, 100, **1996**, 77.

24 Yu-Chu Yang, *Inorg. Chem.*, 24, **1985**, 1765-69.

25 O. Kratky, H. Ledwinka and I. Pilz, *Ber. Bunsengsel.*, 70, **1966**, 904.

26 O. Kratky, H. Ledwinka and I. Pilz, *Markromol. Chem.*, 105, **1967**, 171.

27 W. E. Bennett, D. E. Broberg and N. C. Baenziger, *Inorg. Chem.*, 12, **1973**, 930.

28 M. Shimode, H. Urakawa, S. Yomanaka, H. Hoshino, N. Harada and K. Kajiwara, *Sen-I-Gakkaishi*, 52, **1996**, 293-300.

29 Yoon, M., Y. Cheon and D. Kim, *Photochem.Photobiol.*,58, **1993**, 31-36.

30 S. Dhami, A.J. DeMello, G. Rumbles, S.M. Bishop, D. Phillips, and A. Beeby, *Photochem.Photobiol.*, 61, **1995**, 341-346.

31 J. D. Spikes & J. C. Bommer, *Int. J. Radiat. Biol.*, 50, **1986**, 41-45.

32 R. M. Negri, A. Zalts, E. A. San Roman, P. F. Aramendia & S. E. Braslavski, *Photochem. Photobiol.,* 53, **1991**, 317-322.

33 D.A. Fernandez, J. Awruch and L.E. Dicelio, Photochem. Photobiol., 63, 1996, 784-792

34 M.G. Lagorio, L.E. Dicelio and E.San Roman, J. Photochem Photobiol., 72, 1993, 153-161

35 A. Ferencz, D. Neher, M. Schulze, G. Wegner, L. Viane and F.C. De Schryver, Chem Phys Lett 245, 1995, 23-29.

36 L. Oddos-Marcel, F. Madeore, A. Bock, D. Neher, A. Ferencz, H. Rengel, G. Wegner, C. Kryschi and H.P. Trommsdorf, J. Phys. Chem., 1996, 100, 11850-11856

37 A.P. Pelliccioli, K. Henbest, G. Kwag, T.R. Carvagno, M.E. Kenney and M.A.J. Rodgers, J. Phys. Chem. A, 2001, 105, 1757-1766.

38 Y. Kaneko, T. Arai, K. Tokumaru, D. Matsunaga and H. Sakuragi, *Chem. Lett.,* **1996**, 345

39 M. Ambroz, A. Beeby, A.J. MacRobert, M. S. C. Simpson, R. K. Svensen, and D. Phillips, *J. Photochem. Photobiol. B: Biol.,* 9, **1991**, 87-95.

40 M. Shimode, H. Urakawa, S. Yamanaka, H Hoshino, N. Harada, K.Kajiwara, *Sen-I-Gakkaishi,* 52, **1996**, 293-300.

41 L. C. Gruen *Aust. J. Chem.,* 25, **1972**, 1661-7.

42 P. C. Martin, M. Gouterman, B. V. Pepich, G. E. Renzoni and D. C. Schindele, *Inorg. Chem.,* 30, **1991**, 3305-9.

43 J. C. Wang, *Advances in Colour Science and Technology,* 3, **2000**, 20-31.

44 L. Peters, *The Theory of Colouration of Textiles,* Ed. C. L. Bird and W. S. Boston, Dyers Company Publications Trust, SDC, Bradford, **1975**.

45 Thanks to Mr. R. K. Neely for his help.

46 A. Beeby, S. FitzGerald and C. F. Stanley, *J. Chem. Soc.Perkin Trans.,* 2, **2001**, 1978-1982.

47 A. Beeby, S. FitzGerald and C. F. Stanley, *Photochem. and Photobiol.,* 74(4), **2001**, 566-569.

48 C. Farren, S. FitzGerald, A. Beeby and M. R. Bryce, *Chem. Commun.,* **2002**, 572.

49 K. Hamada, K. Yamada, M. Mitsuishi, M. Ohira and K. Mesuda, *J. Chem. Soc. Faraday Trans.*, 91(11), **1995**, 1601-05.

50 B. Neumann, K. Huber and P. Pollmann, *Phys. Chem. Chem. Phys.*, 2, **2000**, 3687-3695.

51 P. J Camp, A. C. Jones, N. K. Neely and N. M. Speirs, *J. Phys. Chem. A*, 106, **2002**, 10725-10732.

52 M. Kasha, H. R. Rawls and M. Ashraf El-Bayoumi, *Pure Appl. Chem.*, 11, **1965**, 371-392.

CHAPTER 6 – STUDY OF AN *O*-HYDROXYAZO DYE

6.1 – Overview

Although the dyes studied in this project were of the ortho-hydroxyazo type, it is important to first introduce the azo dyes. Figure 6.1 is a simple representation of an azo dye. All azo dyes contain one, but more usually two, aromatic residues attached to the azo group. They exist in the more stable *trans* form as shown in figure 6.1 as opposed to the *cis* form.

$$R-N=N-R'$$
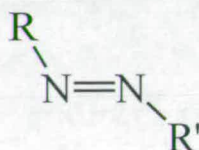
Figure 6.1 – Representation of an azo dye.

Trans-azobenzene, shown in figure 6.3, the basic azo chromogen, is essentially planar in both the solid state and the solution phase, though it is non-planar in the vapour phase. Bond length determinations indicate some contribution from resonance forms, so that the carbon-nitrogen bond lengths are slightly shorter than expected and the nitrogen-nitrogen bond length slightly longer. Also, both phenyl rings show some quinonoid character. Electron donor groups in one ring and electron acceptor groups in the other, especially when they are conjugated to the azo linkage, enhance such resonance contributions. The principal photoreactions of azo compounds are *cis-trans* isomerisation and elimination of nitrogen, giving radicals. These two competing processes are illustrated in figure 6.2.

(A) Isomerisation

Trans ⇌ Cis

(B) Elimination

N_2 + 2R·
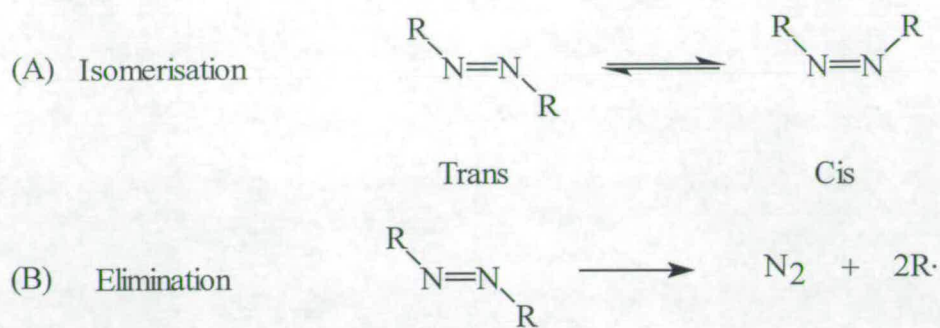
Figure 6.2 – Isomerisation and elimination processes.

The photo-isomerisation of azobenzene, is reversible and is thought to be one of the cleanest photo-reactions known [1-3]. The structures of *cis* and *trans* isomers of azobenzene are shown in Figure 6.3.

trans azobenzene   cis azobenzene
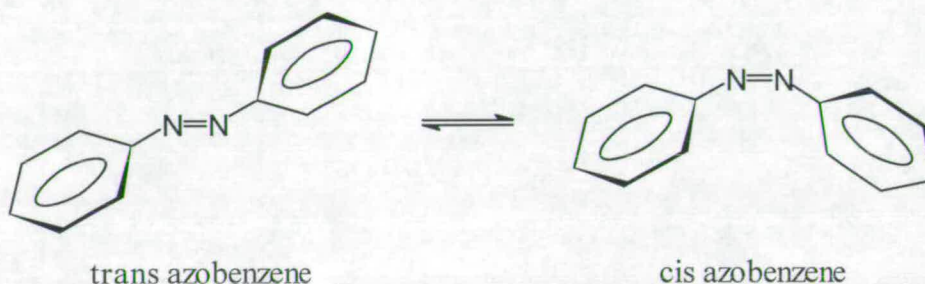
Figure 6.3 – The structure of *cis* and *trans* azobenzene.

Under normal conditions, azobenzene exists almost exclusively as the *trans* isomer since the *trans* isomer is energetically more stable than the *cis* isomer. Isomerisation can be induced by light in the *cis – trans* and in the *trans – cis* directions and by heat in the *cis – trans* direction. Upon photo-excitation, the excited state of, for example the *trans* isomer, decays non-radiatively to the ground state of either the *trans* or the *cis* isomer. Similarly, the excited state of the *cis* isomer may decay non-radiatively to the ground state of the *trans* or *cis* isomer. In this way, a photo-equilibrium, more aptly described as the Photostationary State (PSS) is attained [4]. The percentage composition of each isomer at the PSS depends on the extinction coefficients of each

isomer at the wavelength of irradiation, and the efficiencies (or quantum yields), of the forward and reverse photochemical processes. Concentration may only influence the PSS if inter-molecular processes are involved. Geometrical isomerisation is an entirely intra-molecular process, and so the only controllable factor influencing the PSS, is the wavelength of irradiation used. The proportion of the *cis* isomer at the PSS will increase if the wavelength of light used is not absorbed strongly by the *cis* isomer [5]. For azobenzene, photostationary states are thought to reach between 15 and 40 % *cis* azobenzene [6]. Photoelimination of nitrogen and the formation of radical pairs is a common process occurring from the excited singlet state of azo compounds. There is debate [7] concerning whether the extrusion of nitrogen is a concerted reaction or whether it involves an initial C-N bond fission. While the latter process of α-cleavage followed by nitrogen elimination has been established in some cases in which the diazenyl radical may have enhanced stability, conclusive evidence is lacking for a more general stepwise process.

Azo dyes can also exist as disazos and trisazos, i.e. with more than a single azo group, they may also exist as hydroxyazo dyes. In 1884 Zincke and Bindewald suggested a mobile equilibrium existed between tautomeric forms of a hydroxyazo dye, as shown in figure 6.4.

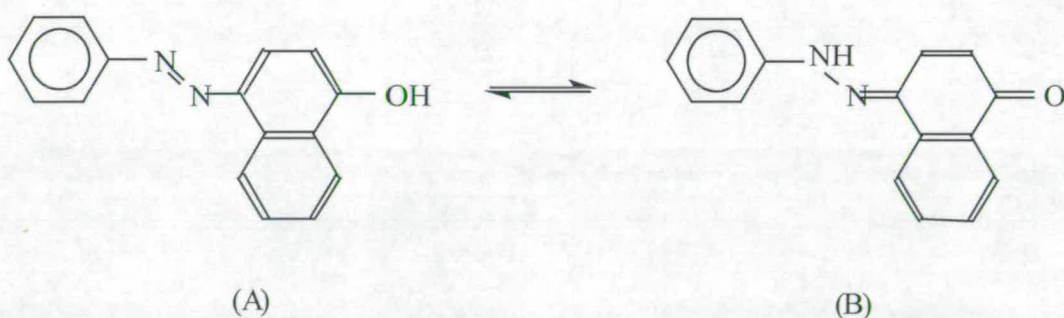(A)   (B)

Figure 6.4 – The equilibrium between (A) azo and (B) hydrazone tautomers of a hydroxyazo dye.

The azo and hydrazone tautomers have different colours and different properties such as light fastness. In order for this equilibrium to exist, the hydroxyl group must be conjugated with the azo group, hence if the hydroxy group is ortho or para to the azo

group the tautomerisation may occur. Intramolecular hydrogen bonding is not usually encountered in para-hydroxyazo dyes, but this is very important in ortho-hydroxyazo dyes. In such a system, the predominance of the hydrazone tautomer is such that the effect of substituents and solvent on the tautomeric equilibrium is negligible. The dominance of the hydrazone form is due to the intramolecular hydrogen bonding being stronger in that form than in the azo form. The existence of the ortho-hydroxyazo dyes in the tinctorially stronger hydrazone form, plus their pH and solvent insensitivity, make them ideal colourants, and they have found extensive use in most dyestuff classes.

Studies of azo, ortho-hydroxyazo and derivatives of azo dyes is plentiful in the literature. In contrast to the phthalocyanines there are no specific spectral effects of aggregation that one can immediately identify. Thus the use of UV-Vis spectroscopy alone is insufficient to reveal aggregation, and fluorescence spectroscopy becomes a very significant tool.

6.2 – Literature Survey

The azo dyes, and particularly their aggregation [8-15], have been examined as extensively in the literature as the phthalocyanines, due to their usage in photography and the dyestuffs industry, to name two examples. Hamada [16] et al analysed an azo dye in aqueous solution using UV-Vis spectroscopy and ^{19}F NMR in their paper from 1986. They were able to deduce that a peak at 483nm in the UV-Vis derived from a monomer species while a shoulder at 500nm derived from an aggregate species. The latter species was then calculated to be a dimer. The authors noted that the addition of salt seemed only to facilitate aggregate formation, leading not to a change of the equilibrium system, but to an increased aggregation constant. Another paper published 5 years later by Hamada et al [17], points out that the number of sulphonate groups affects not only the aggregation constant but also the structure of the aggregates. They continue by specifying that sulphonate groups are the key to elucidating the aggregation process. The two azo dyes studied in [17] are similar to that studied in [16], in that they are sulphonic acid azo dyes. At approximately

510nm a peak in the UV-Vis is observed, deduced to derive from a dimer. A shoulder at approximately 550nm, deriving from the monomer, decreased in relative intensity with increasing concentration. The K_{AGG} value calculated for the first dye was less than that for the second; this is incompatible with the notion that electrostatic repulsion is enhanced with an increase in the number of sulphonate groups, as the first dye contains a greater number of these groups. Hamada [18] also looked at the effect of position of a trifluoromethyl group, with respect to the azo linkage, on aggregation of a dye. The estimated aggregation number was 2, and the decreasing aggregation constant with increasing temperature suggested that the aggregation process was exothermic. Hamada followed up this paper in 1995 [19] by using UV-Vis spectroscopy to calculate aggregation constants and the temperature dependence of the UV-Vis to determine thermodynamic parameters. He concluded that the substituents, methyl and trifluoromethyl, affected entropically the aggregation process. He also concluded that over the concentration range studied that there existed a monomer and dimer equilibrium, this was deduced due to the presence of isosbestic points and the calculation of the aggregation number to be two. Navarro and Sanz [20] evaluated CI direct red 1 in 1998, but this study was concerned more with the effect of pH and temperature on aggregation rather than dye concentration. Their UV-Vis results were difficult to interpret, but the electrochemical technique, DC polarography, allowed the average aggregation number in aqueous solution to be calculated. The aggregation number was found to be greater at lower pH. In 1997 Szawowski and Niewiadomski [21] investigated the effect of temperature on the aggregation and deaggregation of monoazo dyes containing imidazolone residues, under conditions that were similar to those used in a conventional dye bath. The authors conclude that imidazolone azo dyes are deaggregated mostly at elevated temperatues, then they diffuse into the fibres, as monomers. After being cooled to a minimum of 60°C the dye reaggregates, and only in this form is the dye durably bound to the fibre. The location of the imidazolone residue in the dye is of importance, as if this group is conjugated with the chromophore the affinity of the dye for the cellulose is increased, whereas if the

imidazolone group is not conjugated to the chromophore, then the increase in affinity for the cellulose is minimal.

The ortho ortho' – dihydroxyazo dye, HCAN was investigated by Dakiky *et al* in 1999 [22]. The UV-Vis results indicated that the dye does aggregate. As concentration increases a shoulder at 527nm decreases in intensity and the peak at 495nm, deriving from the aggregate, dominates. A mechanism of H-bonding was proposed as the intermolecular driving force behind formation of the aggregate. On dilution this H-bonding undergoes gradual stretching. This results in monomerisation due to the severing of the intermolecular H-bonding. The postulate of H-bonding being responsible for aggregation was also made by Monahan et al [23]. The effect of solvent on the position of the monomer-dimer equilibrium was also investigated. Dakiky *et al* and Dan *et al* [22, 25] looked at the effect of surfactants on the aggregation properties of dyes. Dan *et al* particularly noted that while electrolytes induce aggregation, surfactant micelles cause dis-aggregation. Neumann *et al* [26] reported on a ^{19}F NMR, UV-Vis and static light scattering study of the azo dye acid red 266. The techniques used were similar to those used by Hamada *et al* [16, 19], mentioned earlier. The subsequent paper by Neumann [27] also discussed acid red 266 and the analysis of these results is pertinent to the work in this project. Deviation from Beer's law, plots of extinction co-efficient versus dye concentration and the addition of an electrolyte to increase aggregation were all discussed, in the same way as Bredereck *et al* [28] and El-Taher *et al* [29]. Also pointed out was that the occurrence of an isosbestic point infers only an equilibrium between two different absorbing species which could be monomers and aggregates of various sizes, not necessarily a monomer and dimer only. Hamlin *et al* [30] published work that invloved that study of dyestuffs that have similar absorption envelopes to those studied in the present work. The two maxima of the UV-Vis were assigned as monomer and dimer. The use of fluorescence spectroscopy or even a concentration range study of the UV-Vis would help in the confirmation of this analysis, but the authors failed to do this. An important point that emerges from the present project is, that UV-Vis alone may not be enough to understand the system and that fluorescence spectroscopy is a very valuable tool, that complements the UV-

Vis results. Mandal and Par [31] reported in 2000 that they expected that higher aggregates of 3,3'-diethylthiacyanine iodide, THIA, would be weakly fluorescent. However, the fluorescence of higher aggregates of THIA in the presence of aerosol-OT was dramatically enhanced with widely separated dual peaks at 494nm and 601nm, when excited at the strong absorbance peak of the higher aggregate, instead of being excited at the monomer peak. The work by Mandal and Par is a good example of the use of fluorescence spectroscopy in aggregation studies. The review of the aggregation of dyes by Wang from 2000 [32] is useful, bringing together a number of important observations. Factors that effect aggregation such as hydrogen bonding and the hydrophobic effect and methods for studying dye aggregation like UV-Vis spectroscopy and NMR spectroscopy are discussed. The interesting point is made that aggregation is a property that is difficult to control. Therefore, it is difficult to repeat experiments and get reproducible aggregation numbers or particle size distribution.

In 1982 Ball and Nicholls [33] published a review paper concerning azo-hydrazone tautomerisation of hydroxyazo compounds. The authors discuss how Kuhn and Bar [34] proved the existence of a rapidly formed tautomeric equilibrium between azo and hydrazone forms. This equilibrium is influenced by structural factors within the molecule and by the nature of the medium surrounding the molecule. Studies on 2-phenylazo-1-napthol have indicated that strong internal hydrogen bonds in ortho derivatives favour the hydrazone tautomer and stabilise the equilibrium against external influences such as a change of solvent.

6.3 – Detecting Aggregation of Red~1

This section of works aims to illustrate how the use of UV-Vis spectroscopy alone may be insufficient to detect the aggregation of a dye. The addition of fluorescence spectroscopy as a sensitive probe of aggregation is of enormous help. Red~1 is an o-hydroxyazo dye, its structure is shown in section 4.1.

6.3.1 – The Use of UV-Vis Spectroscopy

An absorption spectrum obtained from a 10^{-5}M solution of red~1 in water is shown in figure 6.5. The important feature to note is the presence of two maxima, one at 509nm and a second at 534nm. Figure 6.6 compares the absorption profiles of a 10^{-4} M solution and a 10^{-6}M solution of red~1 in water. As is apparent, there is no change in the absorption profile over this concentration range. This is contrary to expectation, if one of the maxima corresponds to an aggregate and the other a monomer. In a similar sense to the phthalocyanine case, chapter 5, one would expect to observe some changes in relative intensity. Thus it is not possible from inspection of the UV-Vis spectrum to infer the occurrence of aggregation. However, a plot of absorbance at 534nm, versus concentration reveals a deviation from Beer's Law as shown in figure 6.7. This plot is not a straight line; it curves away from the ideal behaviour of Beer's Law. The straight line representing Beer's Law is obtained by assuming that the extinction co-efficient at 10^{-7}M is that of the monomer, and extrapolating to higher concentration. The deviation from Beer's Law, shown in figure 6.7, indicates red~1 aggregates in water. Figure 6.8 shows the absorption profile of red~1 in ethanol. The two absorption maxima are at 511nm and 540nm. Figure 6.9 clearly shows that red~1 in ethanol deviates from Beer's Law indicating that in ethanol red~1 aggregates.
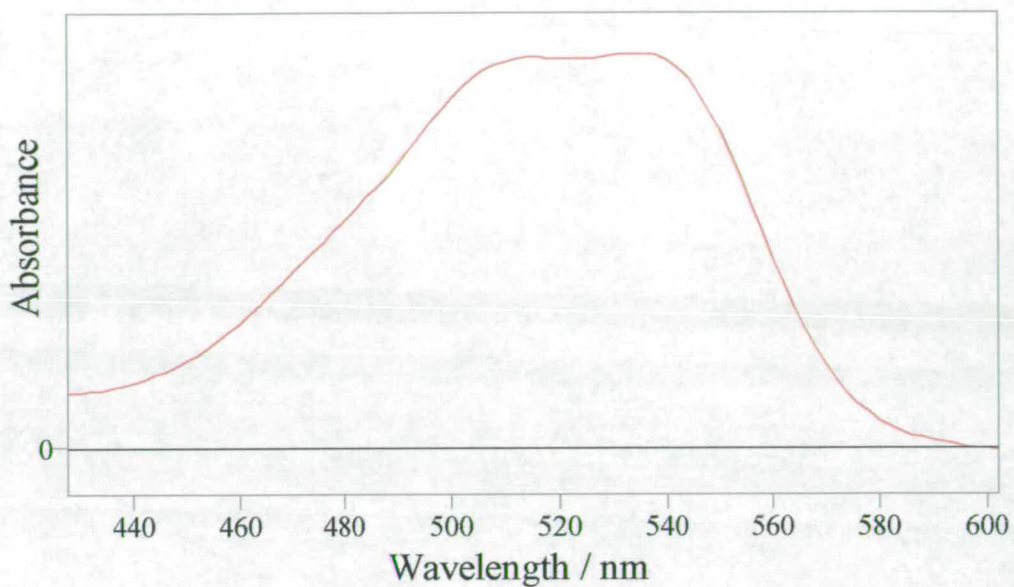
Figure 6.5 – Absorption spectrum of 10^{-5} M solution of red~1 in water at room temperature. Max absorbance at 534nm 0.245.
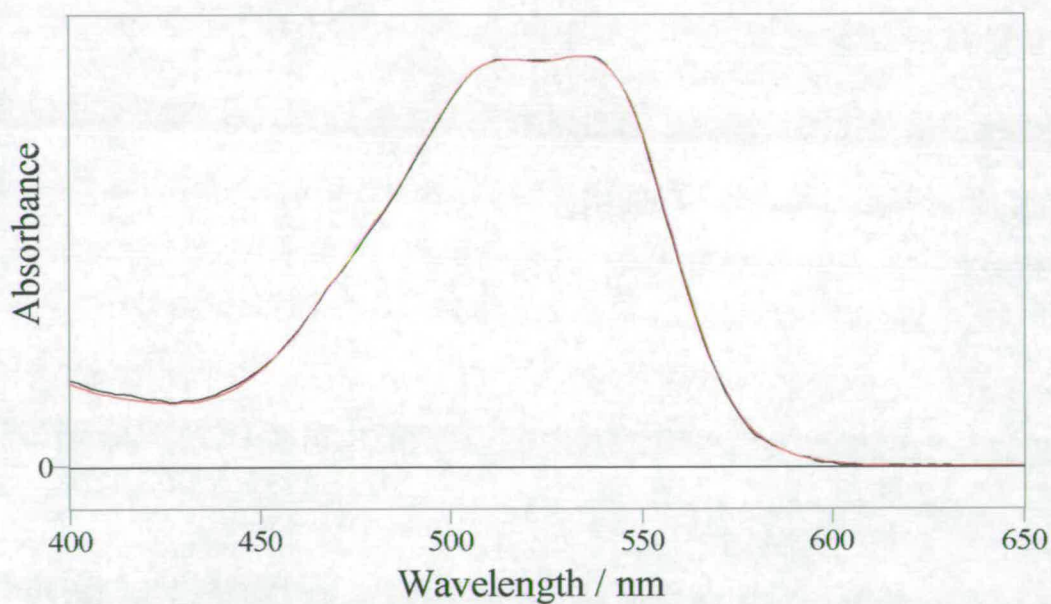
Figure 6.6 – Comparison of absorption spectra of red~1 in water, obtained at 10^{-6} M black (max absorbance 0.024 at 534nm) and 10^{-4} M red (2.874), at room temperature.
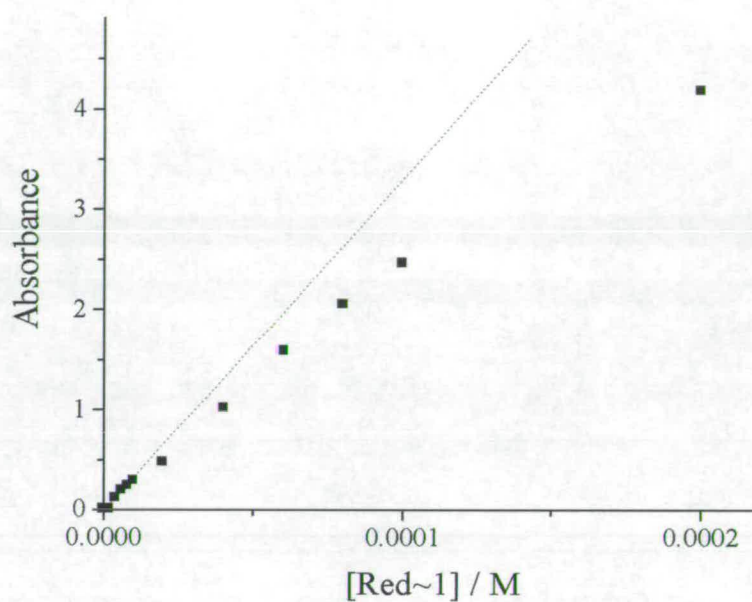
Figure 6.7 – Plot of absorbance at 534nm versus concentration for a sample of red~1 in water at room temperature. The straight line represents the prediction of Beer's Law.
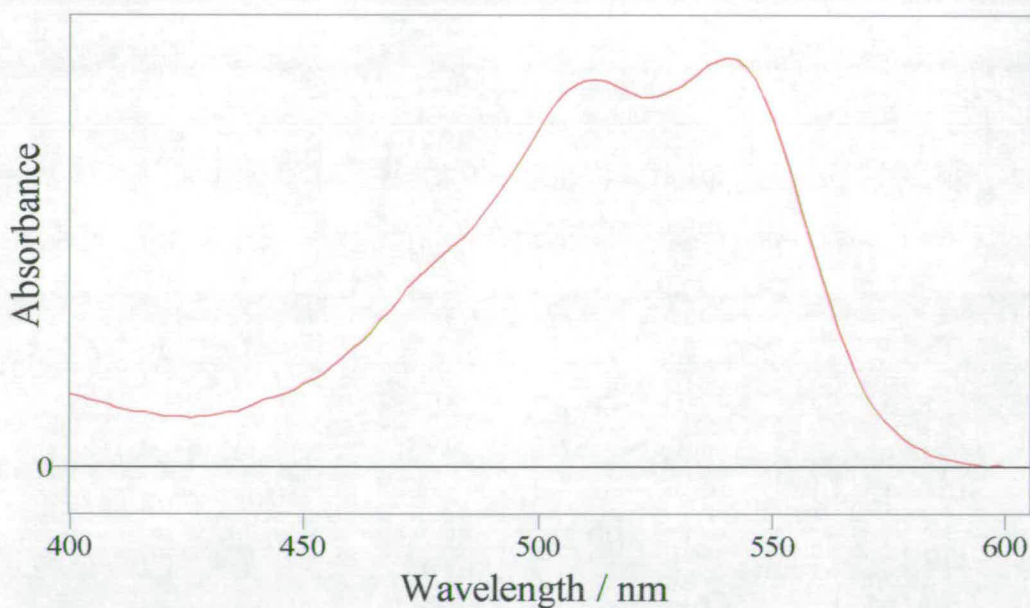
Figure 6.8 – Absorption profile of a 10^{-5} M sample of red~1 in ethanol at room temperature. Max absorbance at 540nm 0.206.
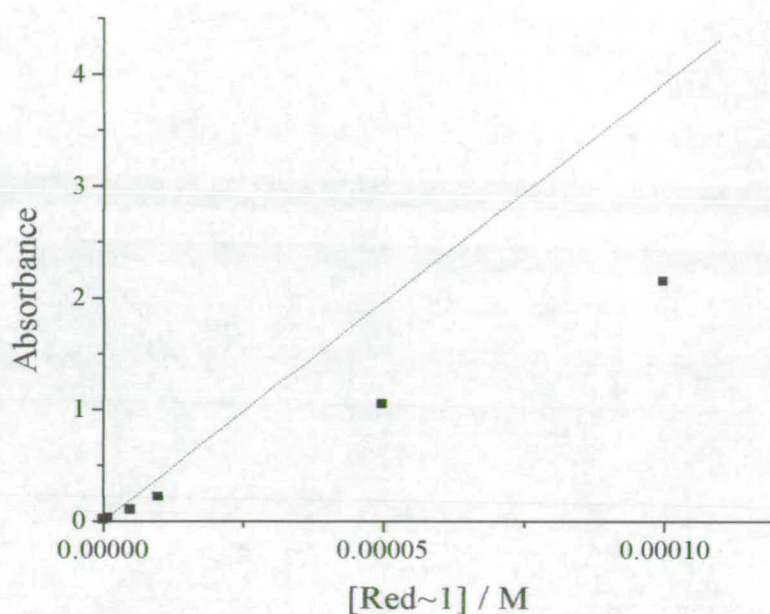
Figure 6.9 – Plot of absorbance at 540nm versus concentration of a sample of red~1 in ethanol .

Although it has been established that red~1 aggregates in both the aqueous and ethanolic environments, it is still not clear how to interpret the double maxima of the absorption profiles in the two solvent systems.

6.3.2 – The Use of Steady State Fluorescence Spectroscopy

While UV-Vis spectroscopy has successfully shown that red~1 does aggregate, the complete understanding of the absorption profile is assisted by the use of fluorescence spectroscopy. Red~1 is indeed fluorescent and significantly figure 6.10 shows that the fluorescence emission spectrum is dependent on the excitation wavelength. As the excitation wavelength is increased from 500nm the fluorescence emission spectrum begins to narrow until an excitation wavelength of 560nm (that is to the red of the longer wavelength maximum of the UV-Vis spectrum) is reached. This is where the fluorescence emission spectrum is at its narrowest.
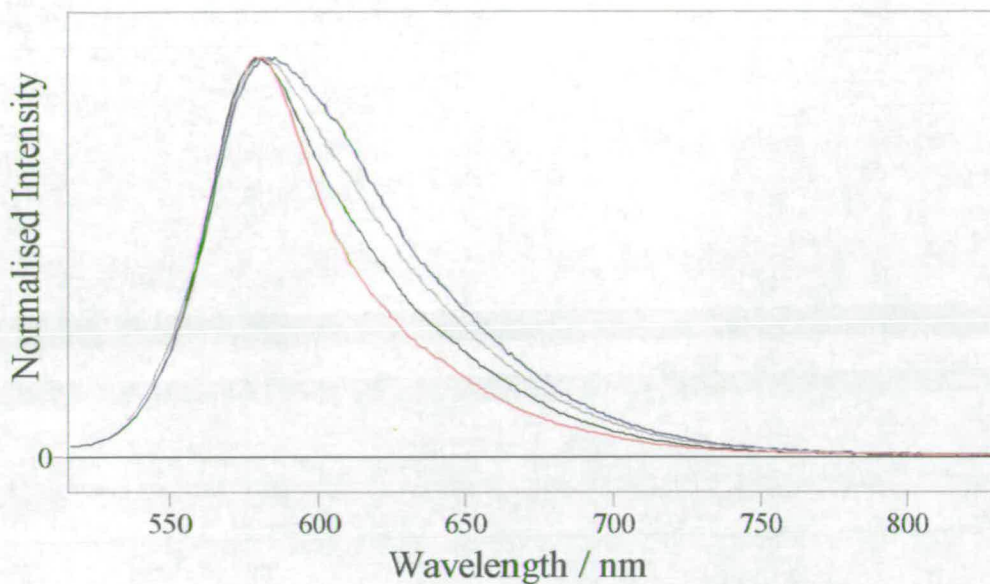
Figure 6.10 – Fluorescence emission spectra of a 10^{-5} M sample of red~1 in water at room temperature, at excitation wavelengths of blue 500nm (max intensity 257996cps), grey 520nm (330373), black 540nm (453381cps) and red 560nm (501559cps).
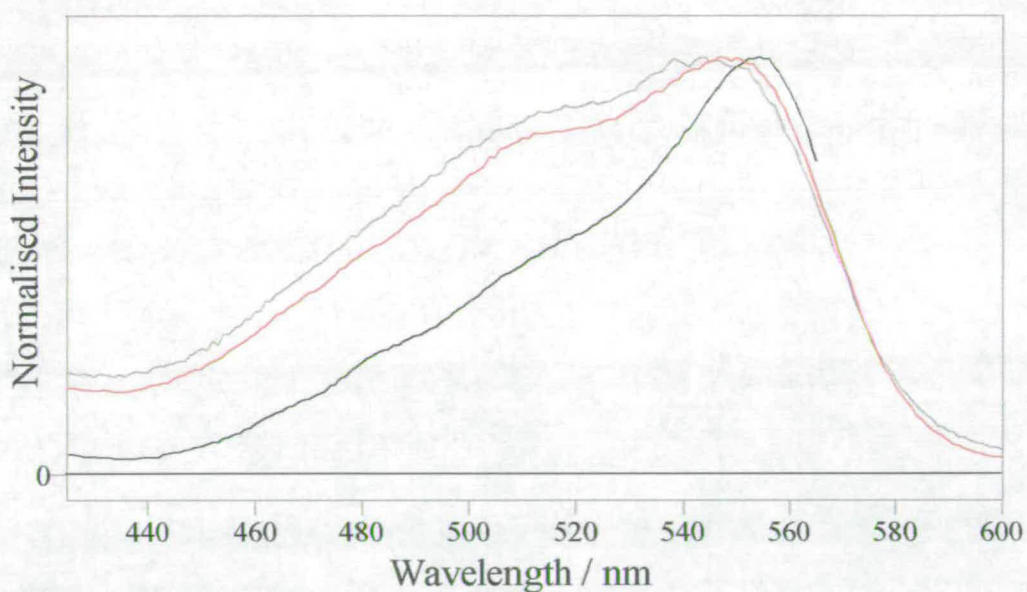
Figure 6.11 – Fluorescence excitation spectra of red~1, 10^{-5} M, in water at room temperature, at emission wavelengths of black 580nm (max intensity 548581cps), red 620nm (235267cps) and grey 660nm (95307cps).

Figure 6.11 shows the dependence of the fluorescence excitation spectrum on emission wavelength. Excitation spectra recorded at shorter emission wavelengths are narrow, while those at longer emission wavelengths exhibit the growth of a clear shoulder at approximately 510nm. The spectra at longer emission wavelengths begin to resemble the absorption profile of red~1.

The broad red shifted fluorescence emission is attributed to aggregates of red~1, while the narrower shorter wavelength emission is due to the monomer. Exciting across the absorption envelope, broad fluorescence is observed due to the aggregate, until excitation to the red of the 534nm peak where narrow monomer emission is observed. The fluorescence excitation spectra agree with this. Looking at emission wavelengths that correspond to the monomer for example 580nm as in figure 6.11, one obtains the monomer excitation spectrum. Emission wavelengths that correspond to the aggregate, for example 660nm in figure 6.11, result in a broader profile, one that resembles the UV-Vis spectrum of red~1. It is clear, then, that the absorption spectrum of red~1 is primarily due to the aggregate; thus on changing the concentration of the sample we see no change in the absorption profile. The monomer excitation spectrum lies to the red of the double maxima of the aggregate, at 553nm, as shown in figure 6.12. There is a considerable overlap between the aggregate and the monomer spectra under the UV-Vis envelope. So, one can not excite exclusively the monomer or the aggregate, although it is possible to some extent to detect selectively the monomer, as for example in the excitation spectrum at an emission wavelength of 580nm.

When dissolved in ethanol the fluorescence spectrum of red~1 is also dependent on the excitation wavelength, as shown in figure 6.13. At short excitation wavelengths, less than 520nm, the emission spectrum is broad. At longer emission wavelengths in the range 520-530nm the spectrum narrows and at excitation wavelengths greater than 530nm the spectrum is broad again.
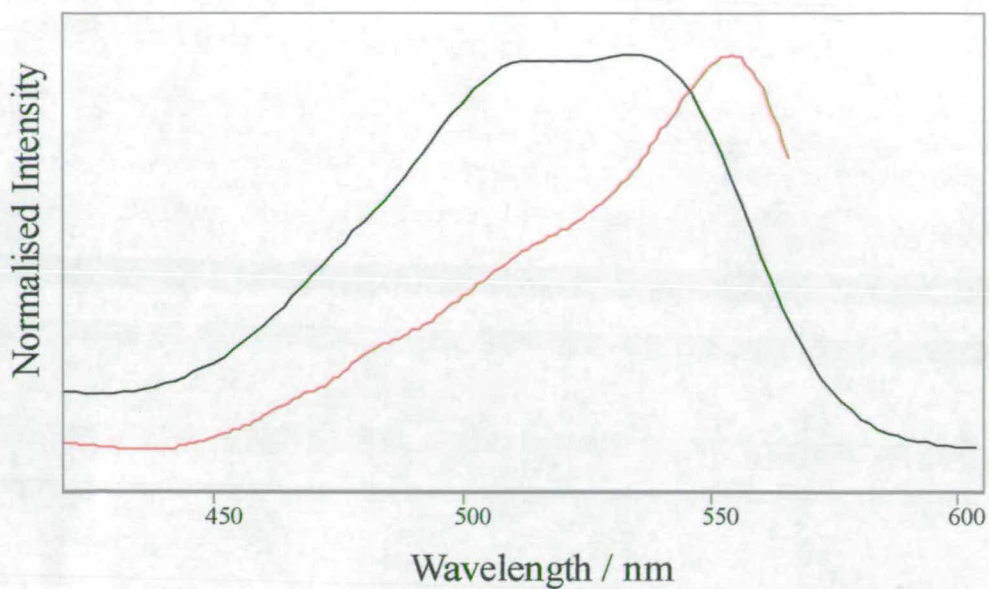
Figure 6.12 – **Comparison of fluorescence excitation spectrum-red obtained with emission wavelength of 580nm and absorption spectrum-black, of 10^{-5} M red~1 in water at room temperature.**

**Figure 6.13** – **Comparison of fluorescence emission spectra of a 10^{-5} M sample of red~1 in ethanol at varying excitation wavelengths: red 520nm (max intensity 786042cps), black 530nm (915291cps) and grey 540nm (628866cps).**
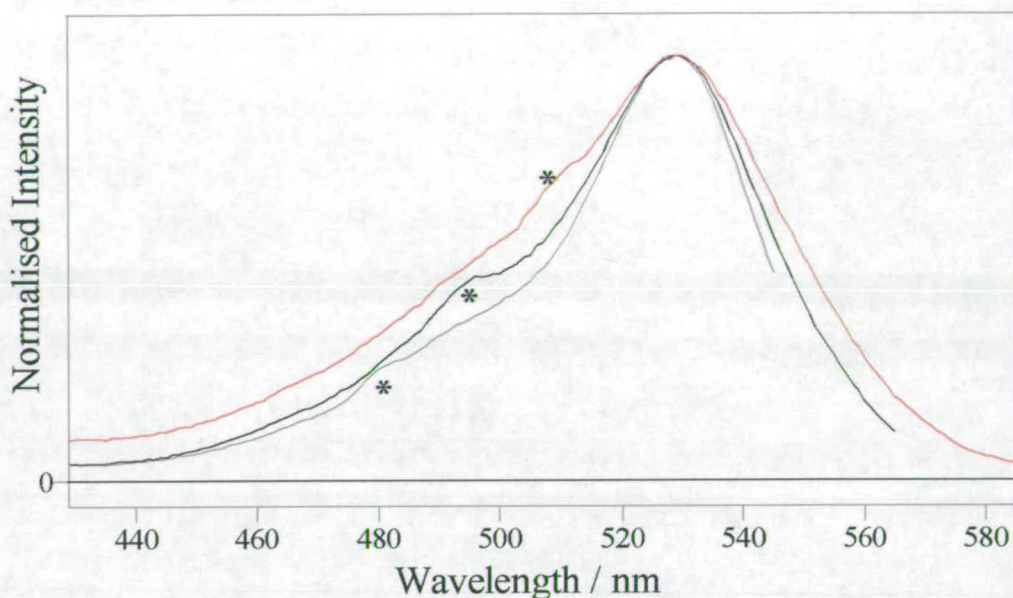
Figure 6.14 – Comparison of fluorescence excitation spectra of a 10^{-5} M sample of red~1 at emission wavelengths of: grey-560nm (max intensity 888738cps), black 580nm (510375cps) and red 600nm (308619cps). * indicates Raman scattering peaks.

The trend is that on moving from short excitation wavelengths toward the absorption maxima the spectra narrow and shift to the blue. On further increasing the excitation wavelength, the spectra broaden again and shift to the red. The initial broad emission is attributed to aggregate fluorescence, the narrow emission results from the monomer and then the return to broad emission is a return to aggregate fluorescence. As can be seen in figure 6.14 the fluorescence excitation spectra vary with the emission wavelength. At short emission wavelengths, 560nm, the spectra are relatively narrow while at longer emission wavelengths the spectra begin to broaden to the red and to the blue of the maximum. This broadening is a result of absorption by the aggregate, while the narrow spectrum is that of the monomer. Figure 6.15 shows the relationship between the monomer excitation and the overall absorption profile. It can be seen that the monomer absorption maximum lies between the two maxima of the absorption envelope. There is complete overlap between monomer and aggregate spectra beneath the absorption envelope, with the aggregate spectrum

extending to the red and the blue of the monomer spectrum. The absorption profile in ethanol, as in the aqueous environment, is dominated by the aggregate.
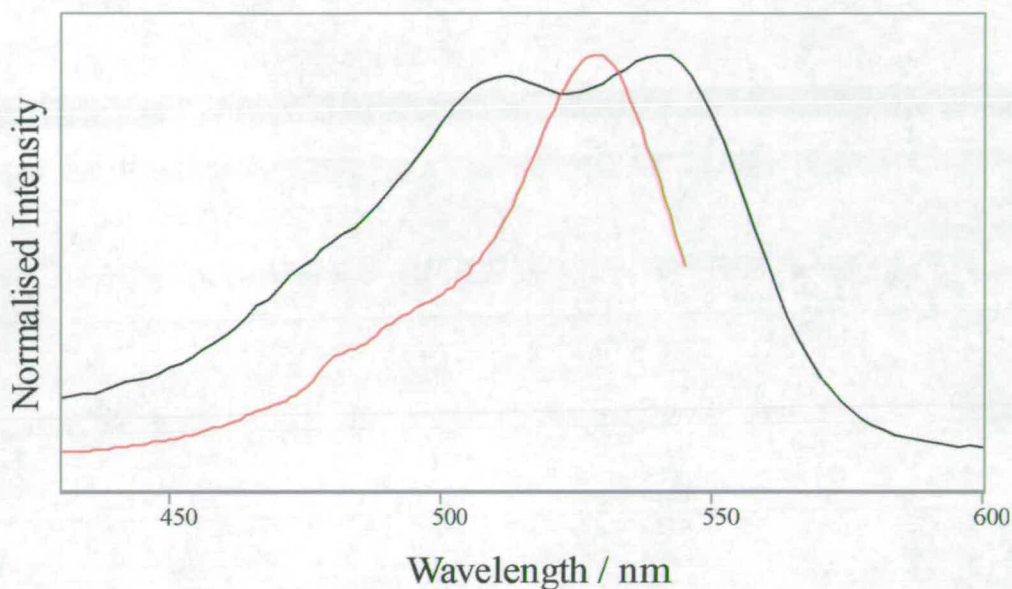
Figure 6.15 – Comparison of the absorption profile and fluorescence excitation spectrum resulting from emission wavelength of 560nm, of a 10^{-5} M sample of red~1 in ethanol.

Figures 6.16 and 6.17 show the fluorescence emission and excitation spectra, respectively, of red~1 in ethanol at 77K. The monomer and dimer spectra remain overlapped over most of the excitation and emission wavelength range. The monomer can be selectively excited at the short wavelength edge of the excitation spectrum, giving the emission spectrum resulting from an excitation wavelength of 440nm, as shown in figure 6.16. The partial excitation spectrum of the monomer, as shown in figure 6.17 was obtained by detecting emission on the extreme blue edge of the emission spectrum at an emission wavelength of 540nm. Similarly, red edge excitation and detection, respectively, gave the dimer emission spectrum (exciting at 560nm) and excitation spectrum (emission at 620nm). These are shown in figures 6.16 and 6.17, respectively.
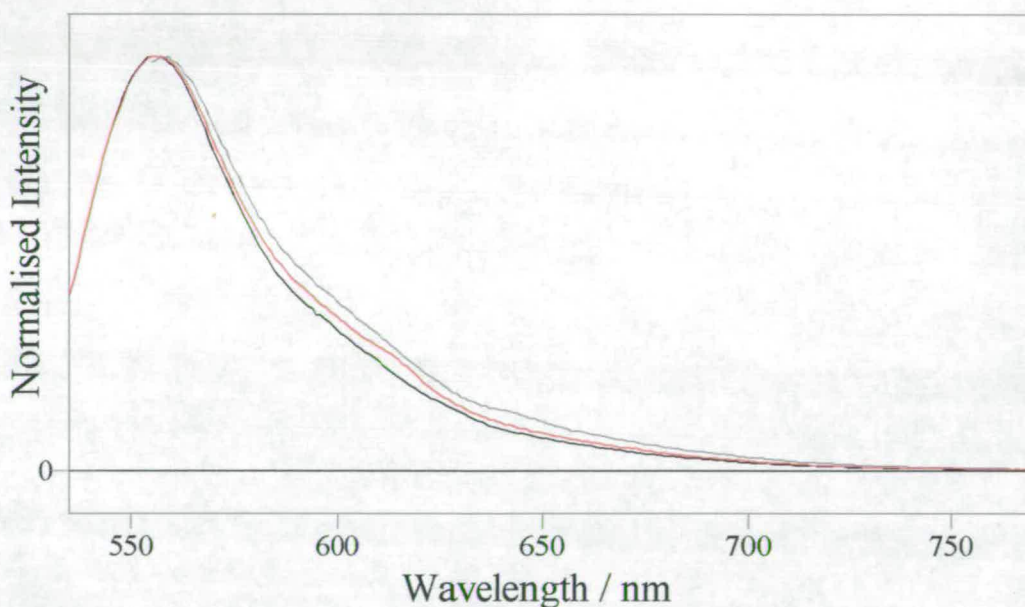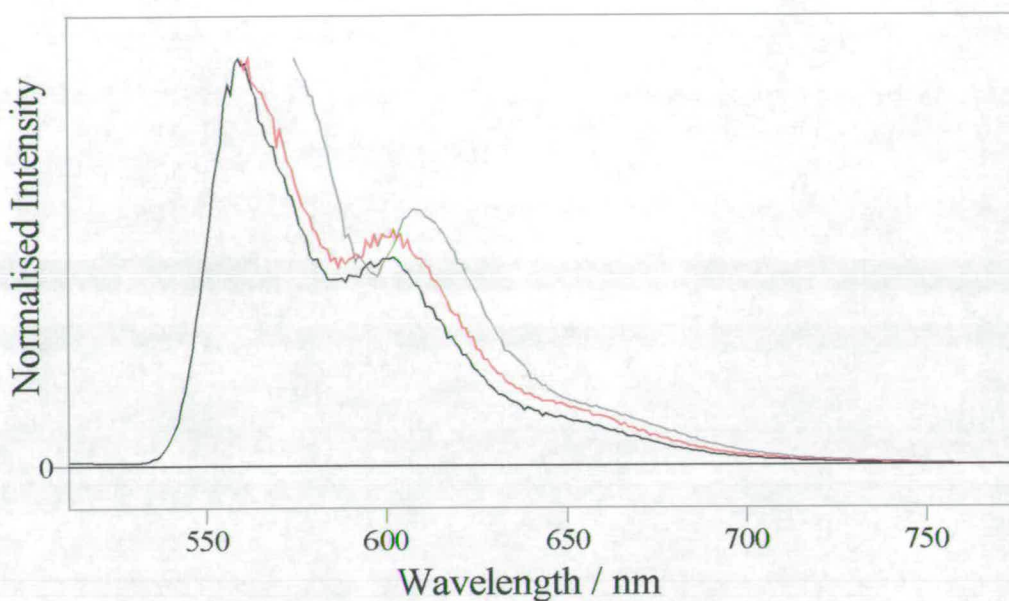
Figure 6.16 – Comparison of fluorescence emission spectra of a 10^{-5} M sample of red~1 in ethanol at 77K at excitation wavelengths of black 440nm (max intensity 17×10^6 cps), red 545nm (12×10^7 cps) and grey 560nm (28×10^6 cps).
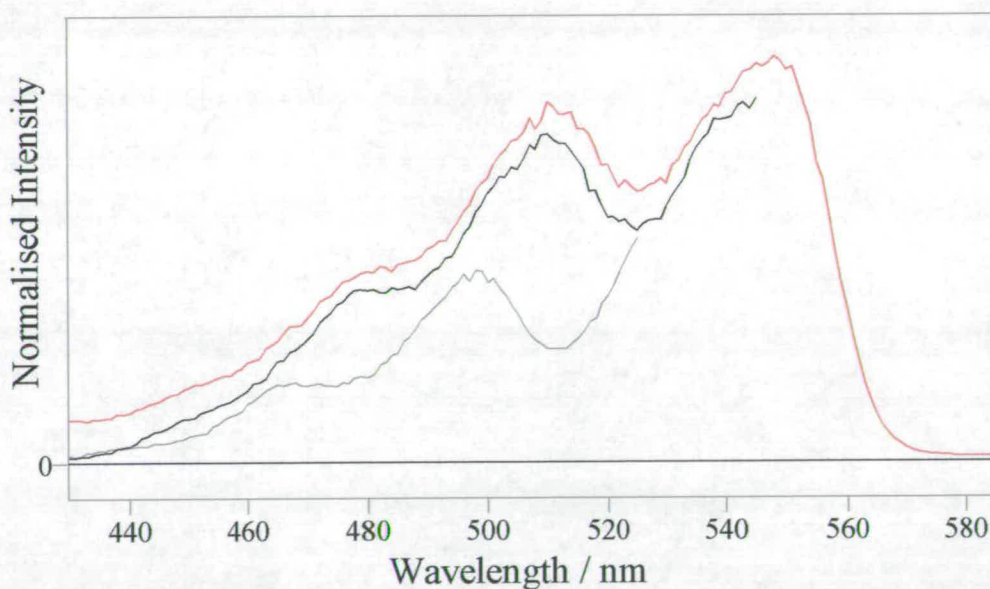
Figure 6.17 – Comparison of fluorescence excitation spectra of a 10^{-5} M sample of red~1 in ethanol at 77K at emission wavelengths of grey 540nm (max intensity 64×10^5 cps), black 560nm (11×10^7 cps) and red 620nm (46×10^6 cps).

In figure 6.18, the difference spectrum, figure 6.18(a), between the 620nm-excitation spectrum and 580-nm (predominantly monomer) excitation spectrum, at room temperature, is compared with the dimer excitation spectrum at 77K. The difference spectrum clearly corresponds to the excitation spectrum of the dimer, the vibronic structure of which extends to either side of the monomer spectrum. Comparison of the absorption spectrum in ethanol (Figure 6.18(c)) with the dimer excitation spectrum (Figure 6.18(b)) and the monomer excitation spectrum (Figure 6.15) shows that the absorption spectrum is a superposition of monomer and dimer spectra. The characteristic dual maxima of the absorption profile appear to arise from the dimer vibronic structure.
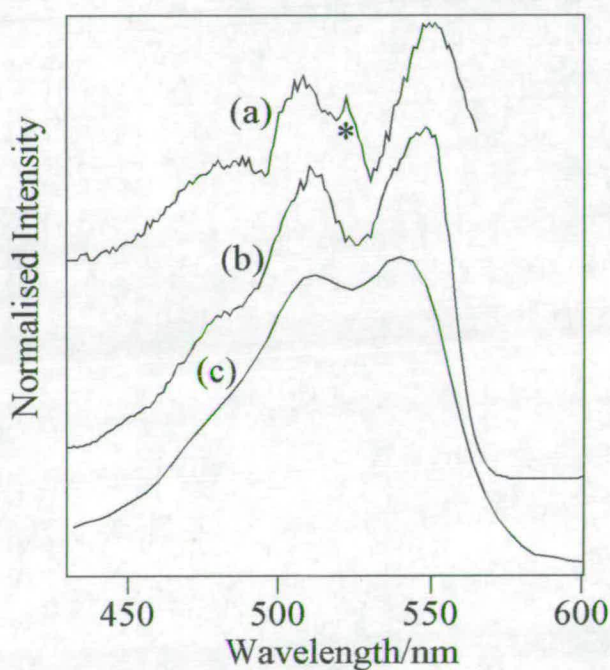
Figure 6.18 - (a) The difference spectrum between the 620nm-excitation spectrum and 580nm-excitation spectrum of red~1 in ethanol at room temperature. (* indicates the position of a solvent Raman band). (b) The excitation spectrum of red~1 dimer at 77K; (c) The absorption spectrum of red~1 in ethanol at room temperature. The spectra are offset for comparison.

6.3.3 – Comparison of the Aqueous and Ethanolic Environment

An interesting comparison to be made between the aqueous and ethanolic solvent systems, is the position of the monomer excitation spectrum with relation to the absorption profile. Figure 6.19 shows how in water the monomer excitation spectrum is on the red edge of the UV-Vis profile, the aggregate essentially being responsible for the shape of the absorption profile. In ethanol the monomer excitation spectrum shifts to the blue and lies in between the two maxima of the absorption spectrum. This then leads to different behaviour of the fluorescence emission spectra in ethanol compared to the case in aqueous media. Exciting across the absorption envelope in ethanol gives us progression from aggregate emission to monomer and back to aggregate again. The case in water is from aggregate emission to narrow monomer emission as one excites across the UV-Vis spectrum.
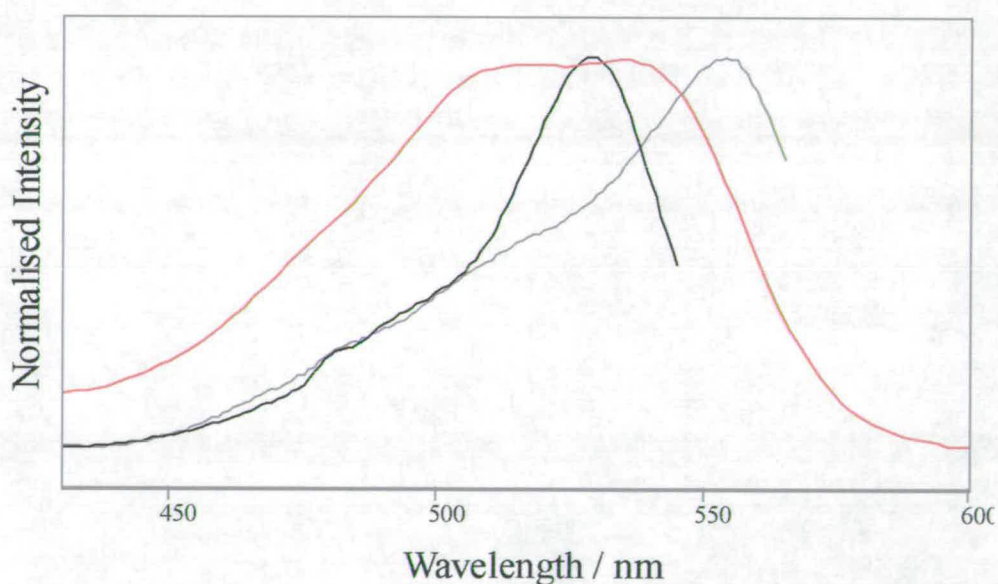
Figure 6.19 – Comparison of the UV-Vis spectrum in water (red), the fluorescence excitation spectrum of the monomer in water (grey) and the fluorescence excitation spectra of the monomer in ethanol (black). 10^{-5} M sample of red~1.

In water, the excitation energy of the monomer is decreased by some 900cm^{-1} compared with ethanol. This may be due to a specific hydrogen bonding interaction between the red~1 molecule, which contains a number of proton-accepting groups, and water. In contrast, the absorption spectra in the two solvents are almost identical. Thus, the absorption spectra must be dominated by the dimer which is not subject to the same solvent interaction as the monomer. Hydrogen bonding with water may be sterically inhibited in the dimer, particularly if the dimer is in fact a larger aggregate. In water, the dimer excitation spectrum lies to the blue of the monomer spectrum, but the dimer emission is red-shifted relative to the monomer. That is to say the Stokes shift of the dimer fluorescence, is much larger than that of the monomer: $\sim1600\text{cm}^{-1}$ for the dimer compared with $\sim900\text{cm}^{-1}$ for the monomer. This is not attributed to exciton splitting because it is clear from the similarity of the absorption spectra in ethanol and water that the same dimer species is being excited in both solvents and the 77K spectra in ethanol show no detectable exciton splitting. The large Stokes shift of the dimer fluorescence in water must be due to solvent relaxation or structural relaxation of the Franck-Condon excited state prior to emission.

6.4 – Aggregation Studies of Red~1

Given that it has been established that red~1 aggregates, this section of work aims to study the dependence of aggregation on variables such as solvent, electrolyte concentration and temperature of the dye solution. These variables are important in the dyebath during the dyeing of textiles.

6.4.1 – Electrolyte Concentration and the Aggregation of Red~1

The extent of aggregation can be increased by the addition of an electrolyte such as sodium chloride. Figure 6.20 illustrates what happens to the extinction co-efficient of a 10^{-5}M sample of red~1 when the salt concentration of the dye solution is increased.
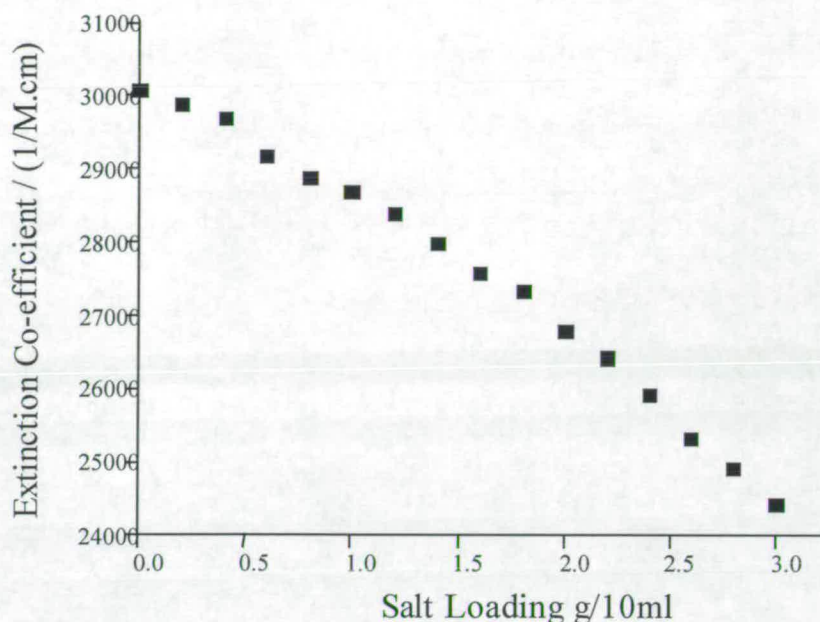
Figure 6.20 – Plot of apparent extinction co-efficient at 534nm versus salt loading of a 10^{-5} M sample of red~1 in water at room temperature.

The presence of a simple electrolyte, like salt, in solution with red~1 increases the ionic strength of the solution. This leads to an increase in the relative amount of aggregation as the salt loading is increased. Thus in turn the absorption co-efficient decreases as the measure of aggregation increases due to the increased salt loading. This is discussed in more detail in section 5.4.

The presence of an isosbestic point at 560nm in figure 6.21 indicates the presence of two species in solution. This implies the presence of monomer and dimer only. The addition of salt increases the relative amount of aggregation, but the isosbestic point indicates that this corresponds to an increase in dimer concentration, not the formation of higher aggregates. These findings are similar to those for turquoise~1 in chapter 5, where in salt free solution higher aggregates were present but in a high salt concentration solution only the dimer and monomer were present in appreciable amounts.
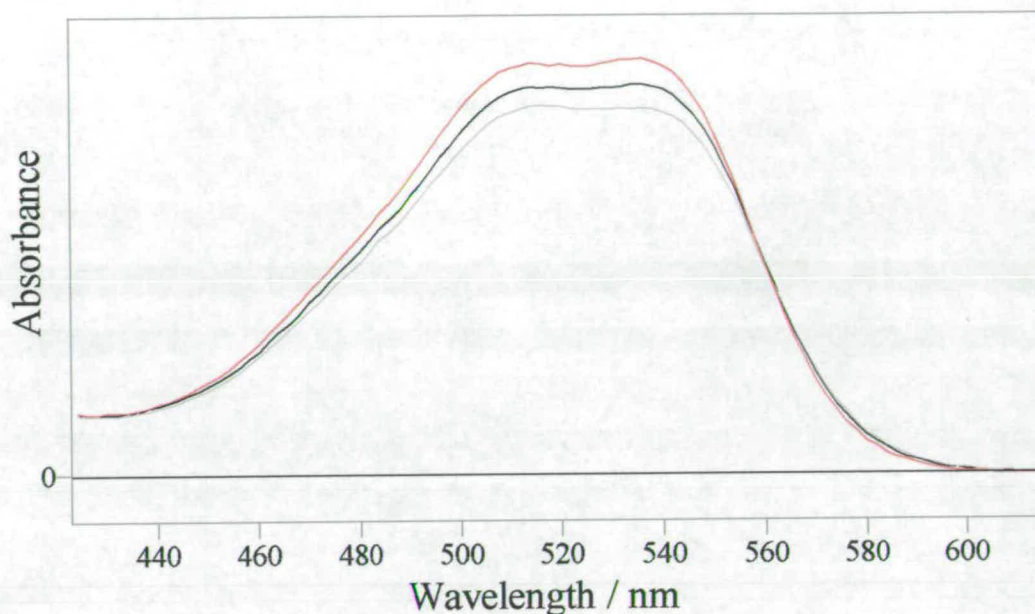
Figure 6.21 - Comparison of absorption spectra of a 10^{-5} M sample of red~1 in water with various salt loadings of red 0.4g/10ml (max absorbance at 534nm 0.294) , black 1.6g/10ml (0.275), and grey 2.4g/10ml (0.258) showing isosbestic point at 560nm. Results were obtained at room temperature.

The increase in aggregation of a solution of red~1 by adding salt, can also be viewed through fluorescence emission and excitation spectra as shown in figures 6.22, 6.23 and 6.24. Figure 6.22 shows a comparison of fluorescence emission spectra, in the presence and absence of salt both at an excitation wavelength of 520nm. It is clear that the spectrum of the sample with added salt has increased red shifted emission, compared to the spectrum of the sample without salt. This supports the assertion that the red shifted emission results from the aggregate.
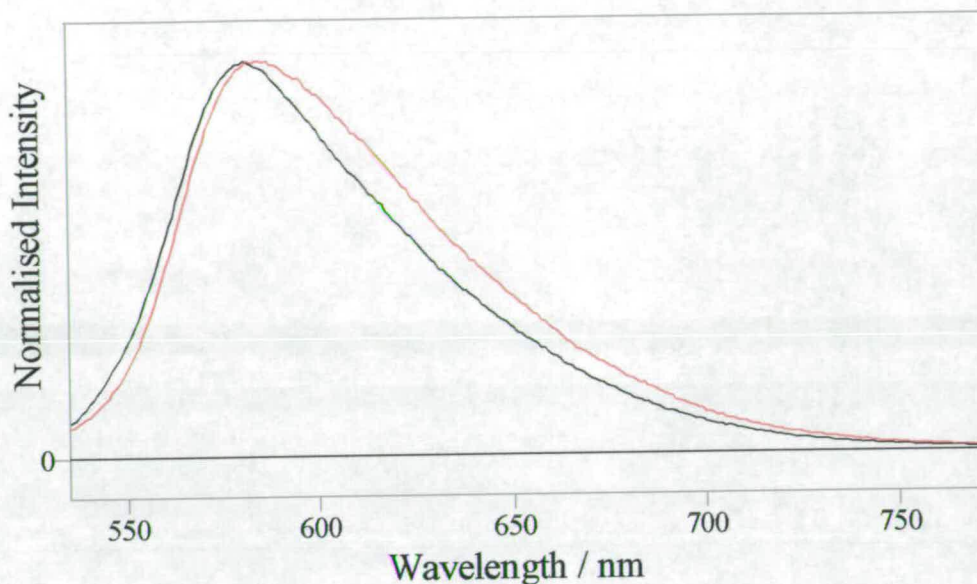
Figure 6.22 – Comparison of fluorescence emission spectra obtained with an excitation wavelength of 520nm for 10^{-5} M red~1 in water at room temperature, red with added salt (max intensity 280042cps) and black without salt (329364cps).
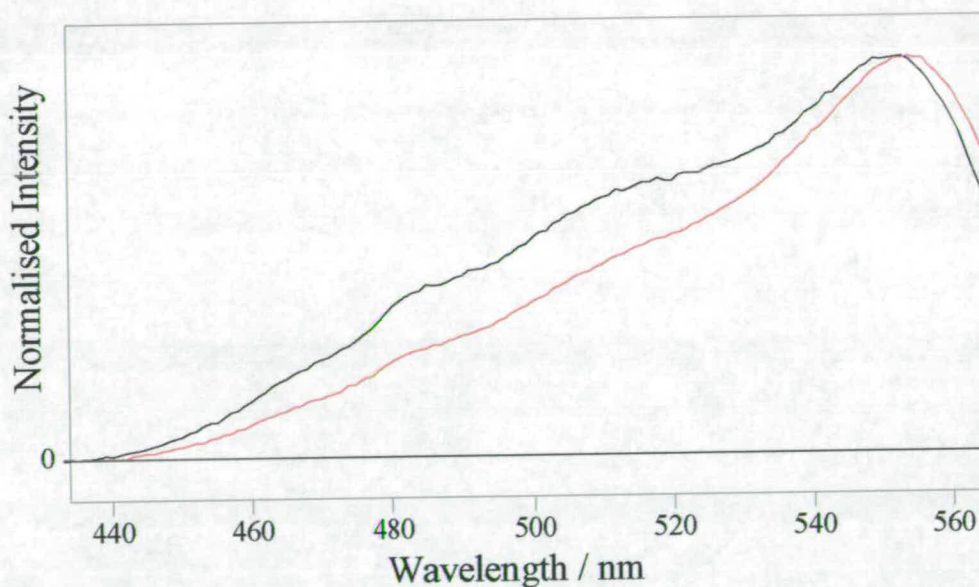
Figure 6.23 – Fluorescence excitation spectra of red~1, 10^{-5} M, in water at room temperature, at an emission wavelength of 580nm, with added salt black (max intensity 340267cps) and without red (545391cps).
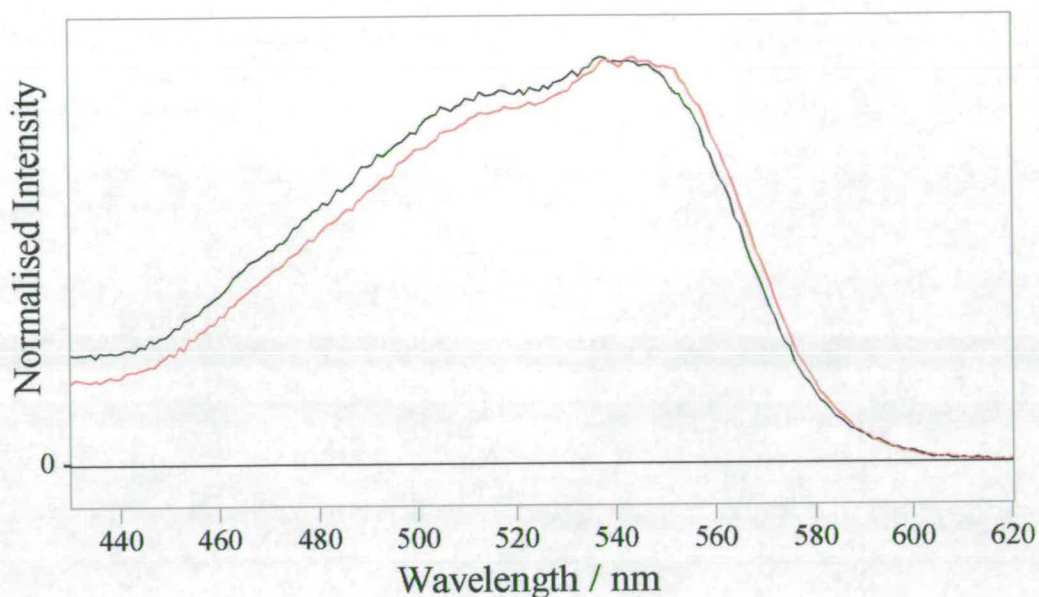
Figure 6.24 – Comparison of fluorescence excitation spectra of red~1, 10^{-5} M, in water at room temperature, with emission wavelength 660nm, with added salt black (max intensity 85938cps) and without red (93354cps).

Figure 6.23 shows the effect of salt on the fluorescence excitation spectrum at short emission wavelength (predominately monomer). It is clear that the relative amount of aggregate has increased as identified by the greater presence of the shoulder to the blue of the maxima. In the excitation spectrum obtained with emission wavelength at 660nm, (predominately aggregate) the effect of increased aggregation can also be seen as an increase of the shoulder to the blue of the maximum, and a shift to the blue of the spectrum compared with the sample with no salt.

In addition to a 10^{-5}M sample, a 10^{-4}M sample was also analysed. Figure 6.25 shows how the plot of extinction co-efficient versus concentration differs; the plot begins similarly to the 10^{-5}M concentration sample then at a critical salt loading the extinction co-efficient drops rapidly before continuing as the lower concentration plot.
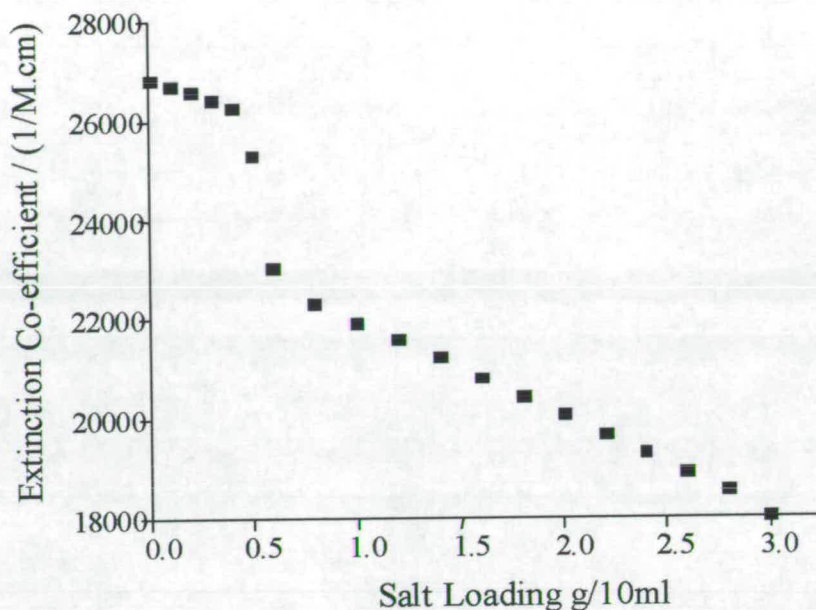
Figure 6.25 – Plot of apparent extinction co-efficient at 534nm versus salt loading g per 10ml of solution, of 10^{-4} M red~1 in water at room temperature.

This rapid decrease in extinction co-efficient means that there is an accompanying rapid increase in aggregation. This could be interpreted as the formation of a higher aggregate, or a change in the geometry of the aggregate already present that in turn favours an increase in aggregation.

6.4.2 – Temperature and the Aggregation of Red~1

Aggregation can be decreased by increasing the temperature of the sample, as shown for red~1 in ethanol in figures 6.26 and 6.27. When the temperature is increased from room temperature to 40°C there is an increase in the intensity in the trough between the two maxima in the absorption spectrum. A similar effect is observed when the temperature of the sample is increased further to 70°C as shown in figure 6.27. The variation in temperature thus gives an observable change in the UV-Vis envelope. Overlaying spectra obtained at 40°C, 50°C and 60°C, figure 6.28, shows the presence of isosbestic point at 547nm, evidence for the presence of two absorbing species, namely monomer and dimer. The presence of only monomer and dimer in

appreciable quantities at elevated temperatures indicates that as the monomer is becoming increasingly dominant only the dimer aggregate is present. The probability of higher aggregates being present is decreased as the equilibrium shifts in favour of the monomer.
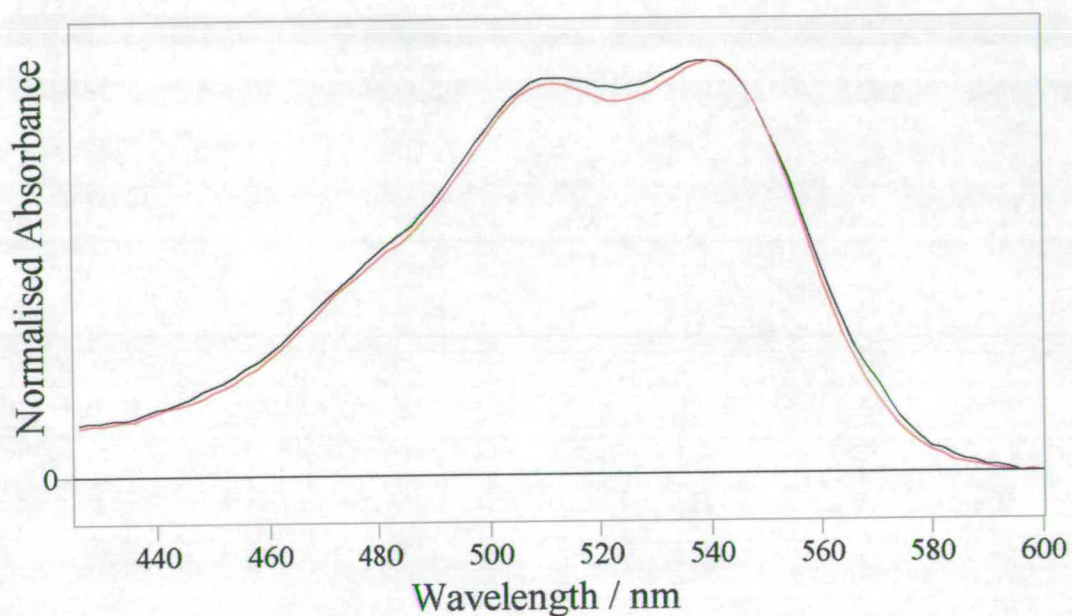
Figure 6.26 – Comparison of absorption spectra of a 10^{-5} M sample of red~1 in ethanol at varying temperatures, room temperature red (max absorbance 0.205) and 40°C black (0.188).
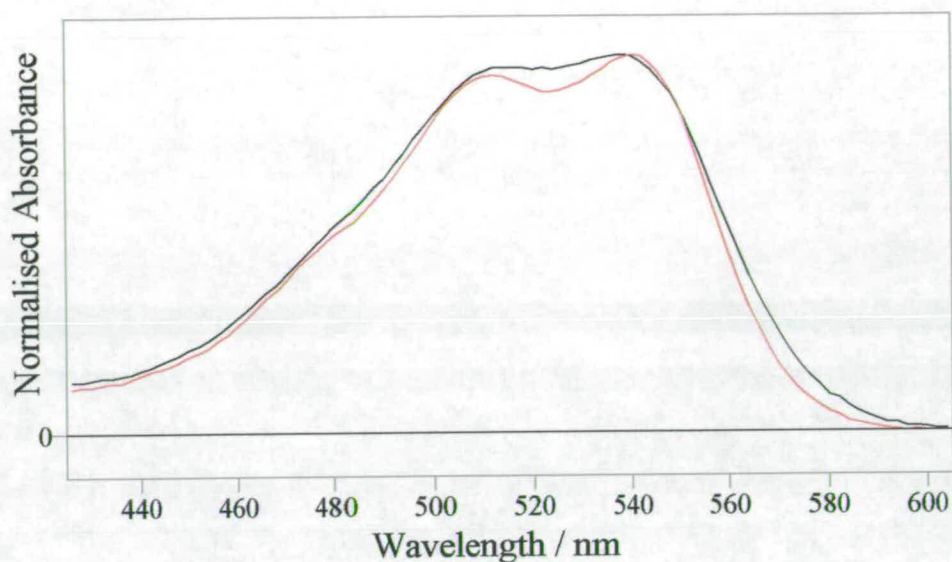
Figure 6.27 – Comparison of absorption spectra of a 10^{-5} M sample of red~1 in ethanol at varying temperatures, room temperature red (max absorbance 0.205) and 70°C black (0.195).
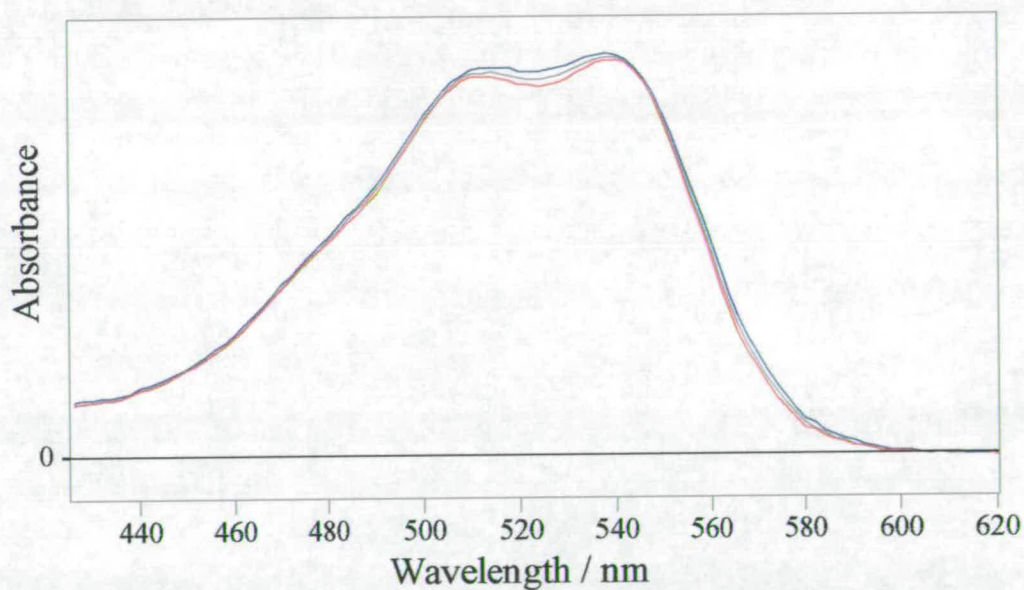
Figure 6.28 – Comparison of absorption spectra of a 10^{-5} M sample of red~1 in ethanol at varying temperatures, 60°C blue (max absorbance at 540nm 0.192), 50°C grey (0.191) and 40°C red (0.190), they show the presence of an isosbestic point at 547nm.

It is now possible to understand the effect that the increase in temperature has on the absorption profile. Figure 6.29 shows the relationship between the monomer excitation spectrum, the UV-Vis spectrum at room temperature and the UV-Vis spectrum at elevated temperature. It is clear that the increase in intensity between the two maxima, as the temperature is increased, is consistent with an increase in monomer absorbance as disaggregation occurs.
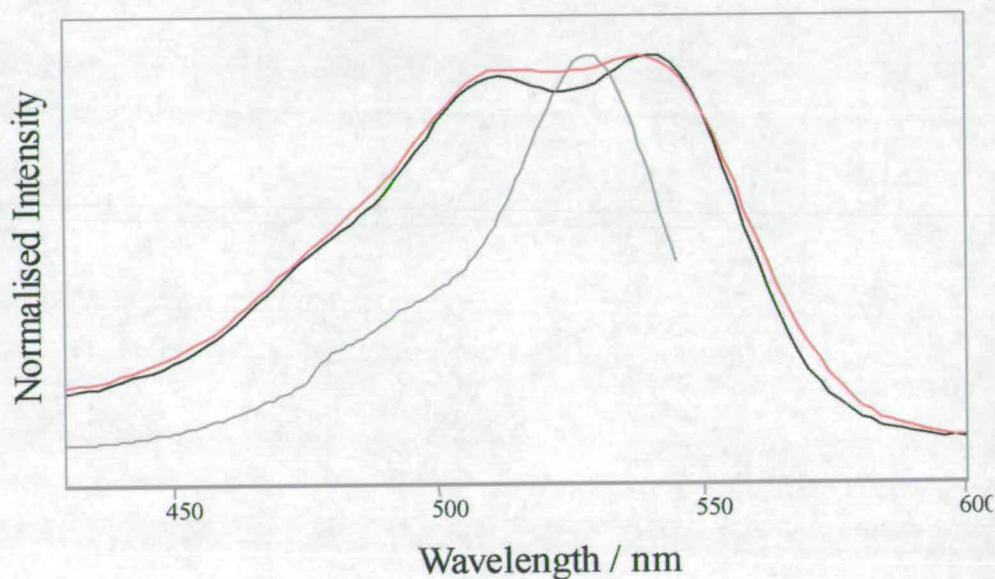
Figure 6.29 – Comparison of absorption profile at room temperature (black), absorption profile at 60°C (red) and fluorescence excitation spectrum obtained at emission wavelength of 560nm (grey), for a 10^{-5} M sample of red~1 in ethanol.

6.4.3 – DMSO Solvent System

The solvent DMSO and the additive to other solvents, urea, will reduce aggregation [35]; this section concentrates on a comparison of the aqueous and DMSO solvent systems. Figure 6.30 shows the absorption spectrum of red~1 in DMSO. Figure 6.31 shows how the spectrum in DMSO is shifted towards the monomer excitation spectrum. There is of course, as in water and ethanol considerable overlap of the monomer and aggregate spectra. Nevertheless, there is a clear shift of the UV-Vis

spectrum in DMSO to the red compared with that in water, i.e. a shift towards the monomer.
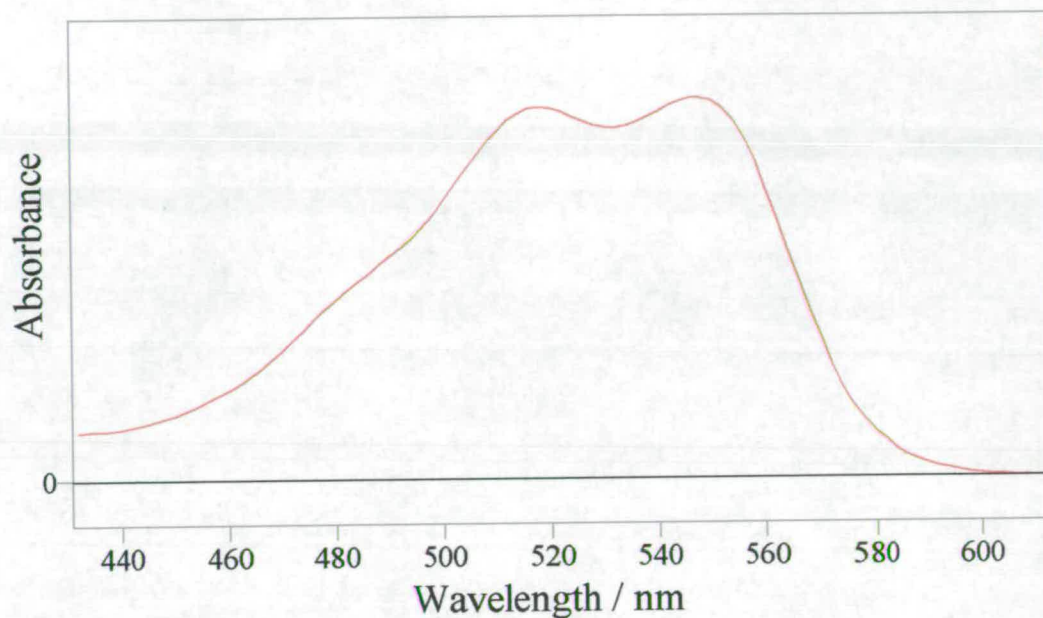
Figure 6.30 – Absorption profile of a 10^{-5} M sample of red~1 in DMSO at room temperature, max absorbance at 547nm 2.377.
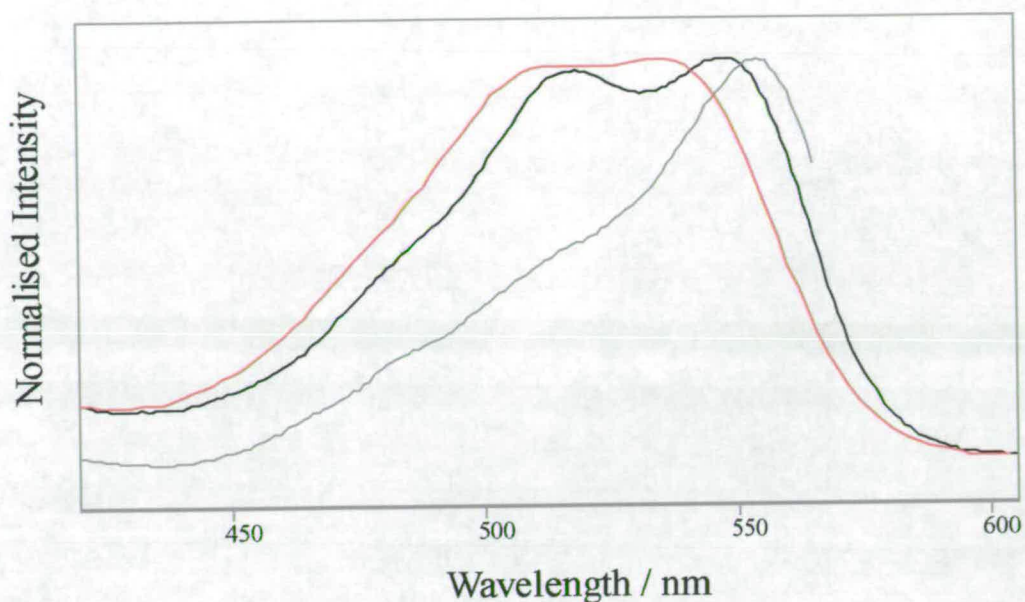
Figure 6.31 – Comparison of UV-Vis spectrum in DMSO (black), and water (red) and fluorescence excitation spectrum of the monomer in water (grey). A 10^{-5} M sample of red~1 was used at room temperature.
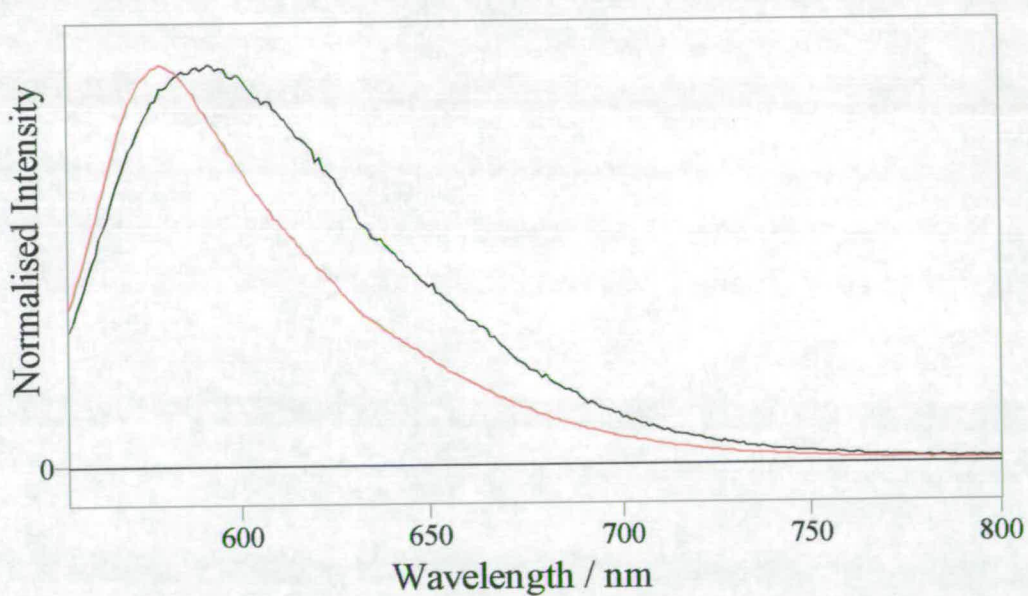
Figure 6.32 – Comparison of two fluorescence emission spectra obtained with excitation wavelength of 540nm, of a 10-5M sample of red~1 in water black (max intensity 338901cps) and in DMSO red (453456cps) at room temperature.

The fluorescence emission spectra, figure 6.32, show a hypsochromic shift when red~1 is dissolved in DMSO. The shifting of the fluorescence emission to the blue has been associated with an increased contribution of monomer emission when in water and ethanol. This would suggest that in DMSO red~1 is aggregating to a lesser extent than in water. As shown in figure 6.33, a plot of absorbance versus concentration shows a deviation from Beer's law, indicating that red~1 does aggregate to some extent in DMSO, albeit to a lesser extent than in aqueous solution.
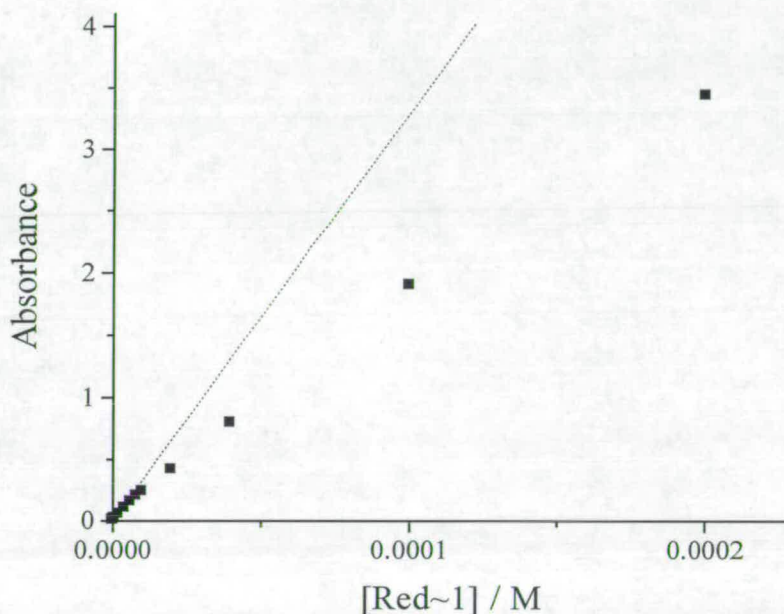
Figure 6.33 – Plot of absorbance at 547nm versus concentration for a sample of 10^{-5} M red~1 in DMSO at room temperature.

6.5 - Conclusions

The aggregation of red~1 in water and ethanol has been revealed through the use of UV-Vis spectroscopy and steady state fluorescence spectroscopy. Aggregation is not evident from the absorption profile alone over the concentration range 10^{-7} M to 10^{-4} M, but deviation from Beer's law shows the presence of aggregates in solution. Fluorescence spectroscopy confirmed the presence of monomers and dimers (aggregates) and the monomer and dimer excitation spectra of the two species could

be distinguished. The characteristic double maxima of the UV-Vis was shown to be due to vibronic structure of the dimer. The position of the monomer excitation spectrum, relative to that of the dimer, differs in water and ethanol. In water the monomer is to the red of the double maxima absorption profile, in ethanol the monomer lies in between the double maxima of the absorption profile. The extent of aggregation was shown to depend on electrolyte concentration, temperature and the nature of the solvent. Similarly to turquoise~1, the addition of salt increased the extent of aggregation, but the presence of an isosbestic point implied only monomer and dimer were present in high salt concentration solutions. The increase of the dye solution temperature above room temperature, caused the equilibrium to shift in favour of the monomer. The presence of an isosbestic point again indicated the presence of monomer and dimer only. The use of DMSO as solvent appears from qualitative examination of the spectra to reduce aggregation in comparison to the aqueous solvent system.

6.6 – Bibliography

1   J. Rabek, CRC Press, Boca Raton, **1990**, vol 2, chpt 4.

2   P. P. Birnbaum, *Trans.Faraday Soc.*, 49, **1953**, 735.

3   J. Griffiths, *Chem. Soc. Rev.*, 1, **1972**, 481.

4   J. Coyle, *Introduction to Organic Photochemistry*, John Wiley & Sons, **1986**.

5   H. Rau, *Angew. Chem. Int. Ed. Engl.*, 12, **1973**, 274.

6   S. Malkin, S., *J. Am. Chem. Soc.*, 66, **1962**, 2482.

7   A. Gilbert and J. Baggot, *Essentials of Molecular Photochemistry,* Blackwell Science, **1995**, p443.

8   R. T. Buwalda, J. M. Jonker and J. B. F. N. Engberts, *Langmuir,* 15, **1999**, 1083.

9   M. Levitus, G. Zepeda, H. Dang, C. Godinez, T-A. V. Khuong, K. Schmieder and M. A. Garcia-Garibay, *J. Org. Chem.*, 66, **2001**, 3188-3195.

10 S. E. Ingles, A. Katzenstein, W. Schlenker and K. Huber, *Langmuir,* 16, **2000,** 3010-3018.

11 S. Lenher and J. E. Smith, *J. Phys. Chem.*, 40, **1936**, 1005.

12 E. Coates, *J. Soc. Dyers Colourists,* 85, **1969**, 355.

13 R. S. Asquith, W. F. Kwok and M. S. Otterburn, *JSDC,* 95, **1979**, 21

14 A. G. Tull, *J. Soc. Dyers Colourists,* 89, **1973**, 133.

15 K. Hamada, M. Mitsuishi, *Dyes and Pigments*, 19, **1992**, 161-168.

16 K. Hamada, S. Take, T. Iijima, *J. Chem. Soc. Faraday Trans. 1, 82, **1986**, 3141-3148.

17 K. Hamada, H. Nonogaki, Y. Fukushima, B. Munkhbat, M. Mitsuishi, *Dyes and Pigments,* 16, **1991**, 111-118.

18 K. Hamada, M Mitshuishi, M Ohira and K. Miyazaki, *J. Phys. Chem.* **1993**, 97, 4926-4929.

19 K. Hamada, K. Yamada, M. Mitsuishi, M. Ohira and K. Mesuda, *J. Chem. Soc. Faraday Trans.,* 91(11), **1995**, 1601-05.

20 A. Navarro, F. Sanz, *Dyes and Pigments,* 40, **1991**, 131-139.

21 J. Szadowski, Z. Niewiadomski, *Dyes and Pigments,* 33, **1997**, 97-105.

22 M. Dakiky, I. Nemcova, *Dyes and Pigments,* 40, **1999**, 141-150.

23 A. R. Monahan and D. F. Blossey, *J. Phys. Chem.,* 74, **1970**, 4014.

24 M. Dakiky and I. Nemcova, *Dyes and Pigments,* 44, **2000**, 181-193.

25 P. Dan, I. Willner, N. S. Dixit and A. Mackay, *J. Chem. Soc. Perkin Trans. II,* **1984**, 455-459.

26 B. Neumann, K. Huber and P. Pollmann, *Phys. Chem. Chem. Phys.,* 2, **2000**, 3687-3695.

27 B. Neumann, *Langmuir*, 17, **2001**, 2675-2682.

28 K. Bredereck and C. Schumacher, *Dyes and Pigments*, 21, **1993**, 45-66.

29 M. A. El-Taher, M. T. El-Haty and A. A. Montaser, *Mikrochim. Acta,* 129, **1998**, 133-138.

30 J. D. Hamlin, D. A. S. Phillips and A. Whiting, *Dyes and Pigments,* 41, **1999**, 137-142.

31 A. K. Mandal and M. K. Pal, *Chem. Phys.*, 253, **2000**, 115-124.

32 J. C. Wang, *Adv. Colour Sci. and Tech.*, 3, **2000**, 20-31.

33 P. Ball, C. H. Nicholls, *Dyes and Pigments*, 3, **1982**, 5-26.

34 R. Kuhn and F.Bar, *Annalen*, 516, **1935**, 143-155.

35 L. C. Gruen *Aust. J. Chem.,* 25, **1972**, 1661-7.

CHAPTER 7 – A STUDY OF DYES RELATED TO RED~1

This chapter concentrates on the analysis of three o-hydroxyazo dyes structurally related to red~1. These dyes are: base~1, red~2 and trioxa~1. The UV-Vis spectra and fluorescence spectra of the dyes was investigated and will be compared to that of red~1.

7.1 – A Study of Base~1

Base~1 is a common starting point for making many o-hydroxyazo red dyes, for example red~1, trioxa~1 and red~2. It is of interest to consider briefly how base~1 is synthetically prepared. The methodology is described in chapter 4. The symbol $ refers to a SO₃Na group.

7.1.1 – Preparation of Base~1

A - Synthetic Scheme

$ NH₂ + HONO + OH NHCOMe $ $ pH 6 →

N=N OH HN–C(=O)–Me $ $ ⁻OH →

N=N OH NH₂ $ $ S

108
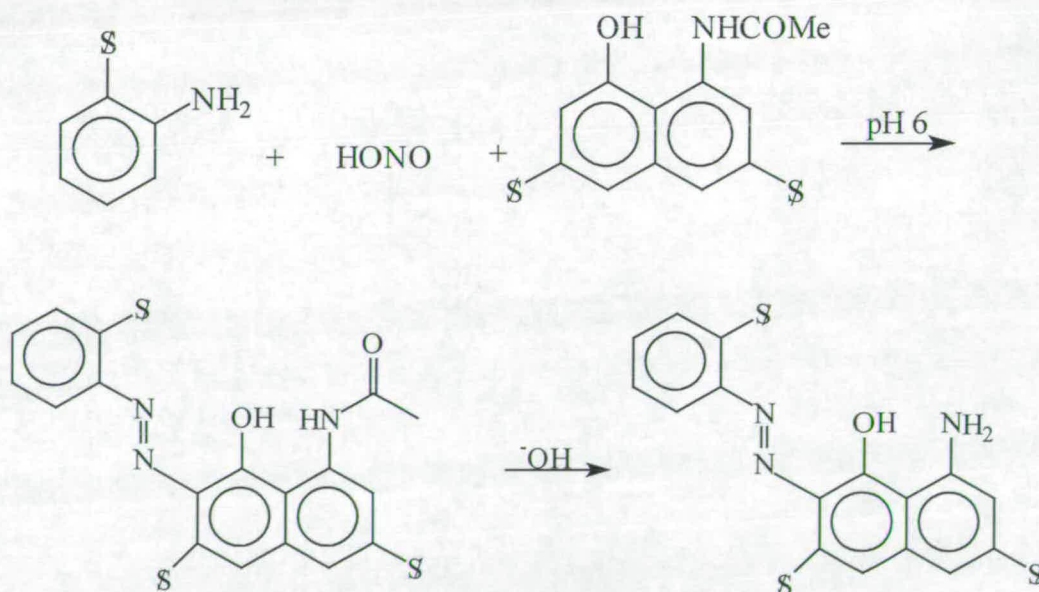
B - Mechanistic Outline

a) Generation of HONO and Diazotisation

$$NaNO_2 \ + \ H_3O^{\oplus} \ \longrightarrow \ HONO \ + \ H_2O \ + \ Na^{\oplus}$$
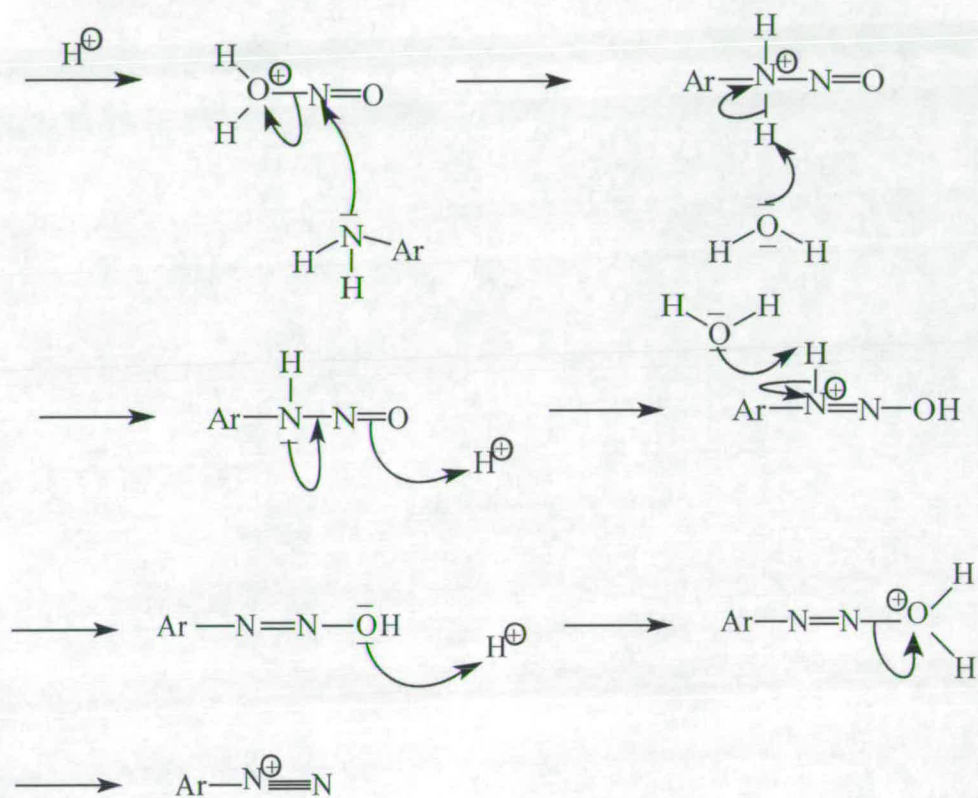
b) Coupling via Electrophilic Aromatic Substitution $S_E Ar$

$H^{\oplus}$ →

(structure: Ar—N=N— naphthalene with OH and NHCOMe, S substituents)
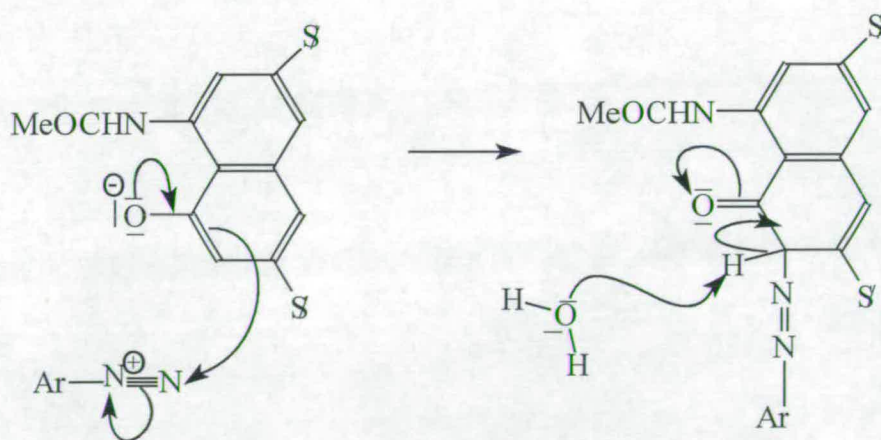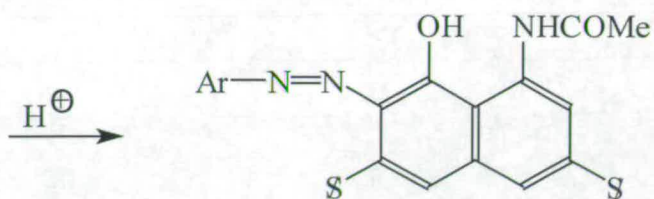
c) Site of Coupling

The hydroxyl group directs to 1 and 2, as shown below, while an NH_2 group would direct to 3 and 4. The NH_2 group though is protected as an amide, thus directing much less strongly to positions 3 and 4. Hence the choice of coupling site is 1 or 2, and as 2 is sterically hindered position 1 is favoured.

(structure: naphthalene with OH and NHCOMe, positions 1, 2, 3, 4 and S substituents)
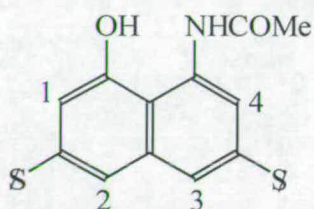
d) Base Hydrolysis of Amide

(reaction scheme)

$$Me\text{—C(O)—N(H)(R)} + \overline{O}H^{\ominus} \longrightarrow Me\text{—C}(\overline{O}^{\ominus})(OH)(NHR)$$

$$\longrightarrow Me\text{—C(O)—OH} + HRN^{\ominus} \longrightarrow Me\text{—C(O)—O}^{\ominus} + H_2RN$$

$R =$ Ar—N=N— (naphthalene with OH and S substituents)

110
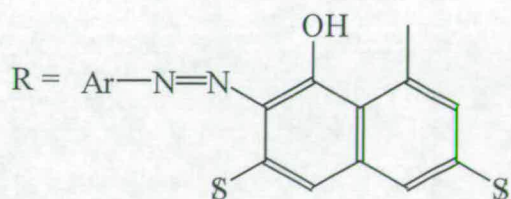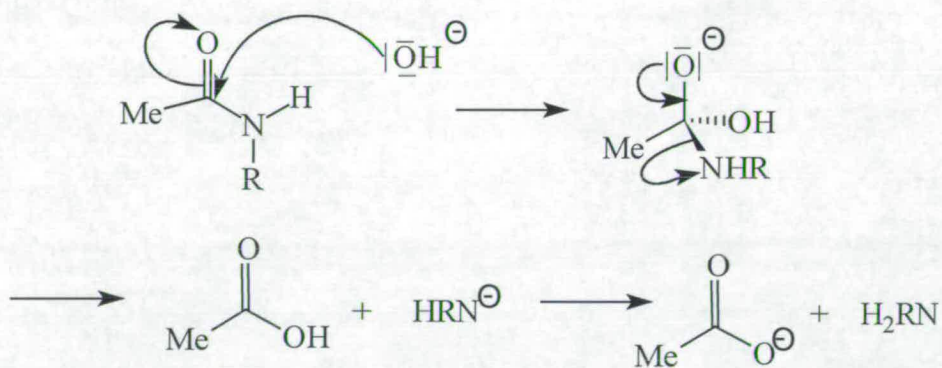
The main structural difference with base~1 when compared with red~1 is the absence of the triazinyl group. It is of interest to observe any differences in the behaviour of the absorption spectrum and fluorescence spectra when compared to red~1.

7.1.2 – Detecting Aggregation of Base~1

The results in chapter 5 and 6 and references therein show how organic solvents like ethanol will start to reduce the relative amount of aggregation of a dye. The extent of aggregation of base~1 in water was so great that the ability to distinguish monomer and aggregate fluorescence emission and excitation spectra was difficult. The results that follow are those obtained in ethanol where the extent of aggregation is reduced.

7.1.2.1 – UV-Vis Spectroscopy

Over the concentration range 10^{-7} M to 10^{-4} M the profile of the UV-Vis spectrum of base~1 does not change in ethanol. Figure 7.1 shows the UV-Vis spectrum of base~1 in ethanol. From the UV-Vis spectra alone, aggregation in ethanol cannot be inferred, but a plot of absorbance versus base~1 concentration, figure 7.2, shows deviation from Beer's law indicating that base~1 aggregates in ethanol.
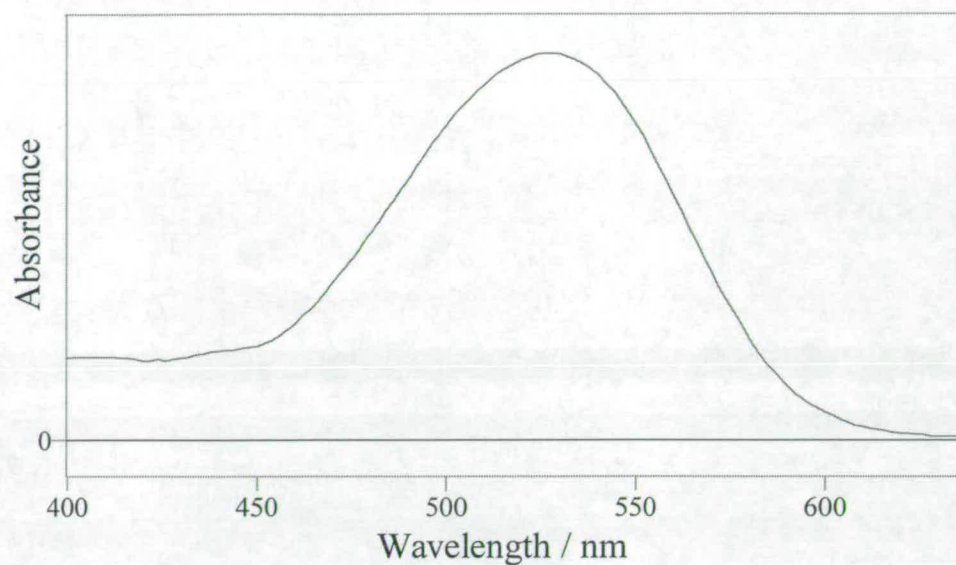
Figure 7.1 – The UV-Vis spectrum of a 10^{-5} M sample of base~1 in ethanol at room temperature. Max absorbance 0.292.
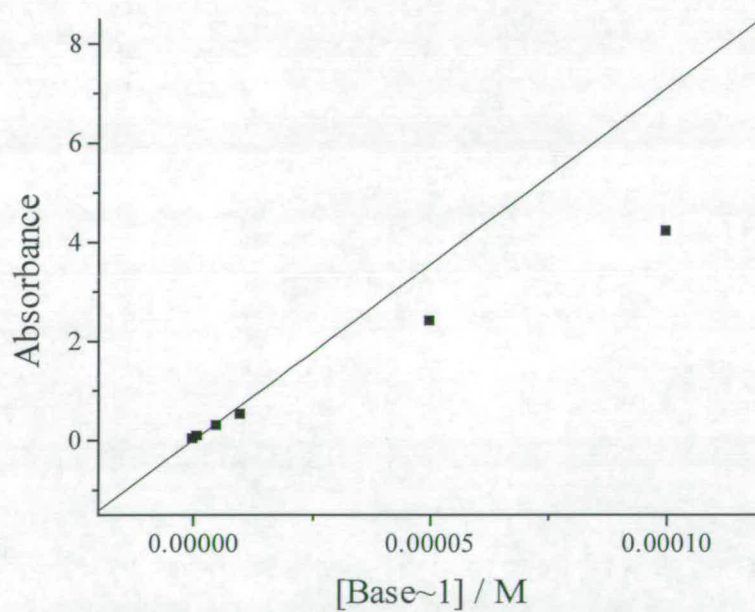
Figure 7.2 – Plot of experimental absorbance, at absorbance max, versus concentration of base~1 (black data points), indicating deviation from Beer's law.

7.1.2.2 – Fluorescence Spectroscopy

The fluorescence emission spectra in ethanol are shown in figure 7.3. The spectra illustrate that the emission is dependent upon the excitation wavelength. As a longer excitation wavelength is chosen the spectra begin to shift to the red. This trend continues in figure 7.4 where the excitation wavelengths continue to increase while the emission spectra continue to shift bathochromically.
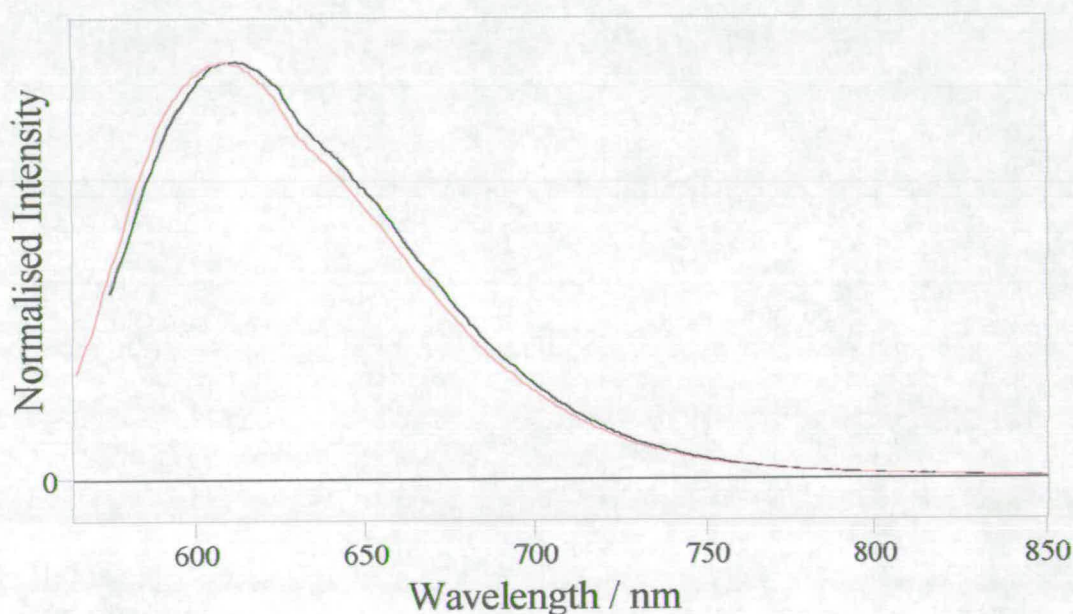
Figure 7.3 – Fluorescence emission spectra of a 10^{-5} M sample of base~1 in ethanol at room temperature, excitation wavelengths of: red 500nm (max intensity 12×10^{5}cps) and black 560nm (10×10^{5}cps).

The red shift in the emission spectrum with increasing excitation wavelength suggests increasing contribution from aggregate emission with increased excitation wavelength. However, unlike the case of red~1 there is no observation of a distinct narrow emission spectrum characteristic of the monomer. The excitation spectrum, figure 7.5, recorded on the blue edge of the emission spectrum (560nm) appears narrower than the excitation spectra at longer emission wavelengths, suggesting a

113

greater contribution of monomer emission at short wavelengths. But, again the excitation spectrum is broad compared with the equivalent excitation spectrum of
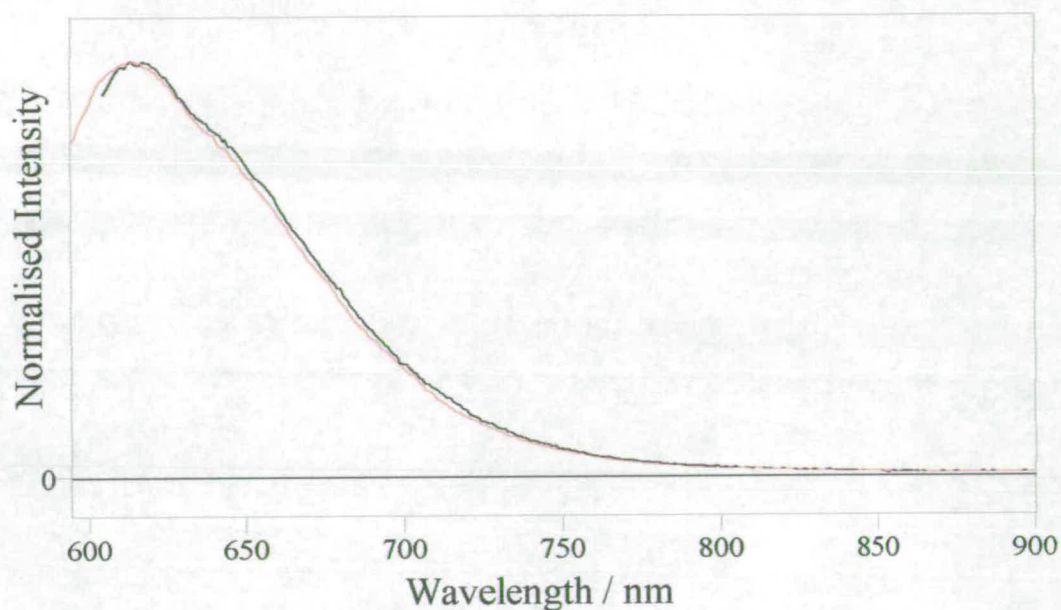
Figure 7.4 – Fluorescence emission spectra of a 10^{-5} M sample of base~1 in ethanol at room temperature, excitation wavelengths of: red 580nm (max intensity 446380cps) and black 590nm (224001cps).

red~1, as in figure 7.10. Decreasing the concentration from 10^{-5} M to 10^{-6} M results in a blue shift in the emission spectrum, as shown in figure 7.6, this is consistent with a predominance of monomer emission at shorter wavelength. Figures 7.7 and 7.8 show the fluorescence emission and excitation spectra, respectively, of base~1 in ethanol at 77K. The monomer and dimer spectra remain overlapped over most of the excitation and emission wavelength range, but the monomer can be selectively excited at the short wavelength edge of the excitation spectrum, (460nm) as shown in figure 7.7. The partial excitation spectrum of the monomer, as shown in figure 7.8 was obtained by detecting emission on the extreme blue edge of the emission spectrum at 570nm. Similarly, red edge excitation and detection, respectively, gave the dimer emission spectrum (exciting at 560nm) and excitation spectrum (emission

at 700nm). The emission from the aggregate is characterised by broadening to the red with the development of a shoulder at ~625nm. The excitation spectrum of the monomer is indeed blue-shifted relative to that of the aggregate, as suggested by the room temperature spectra.
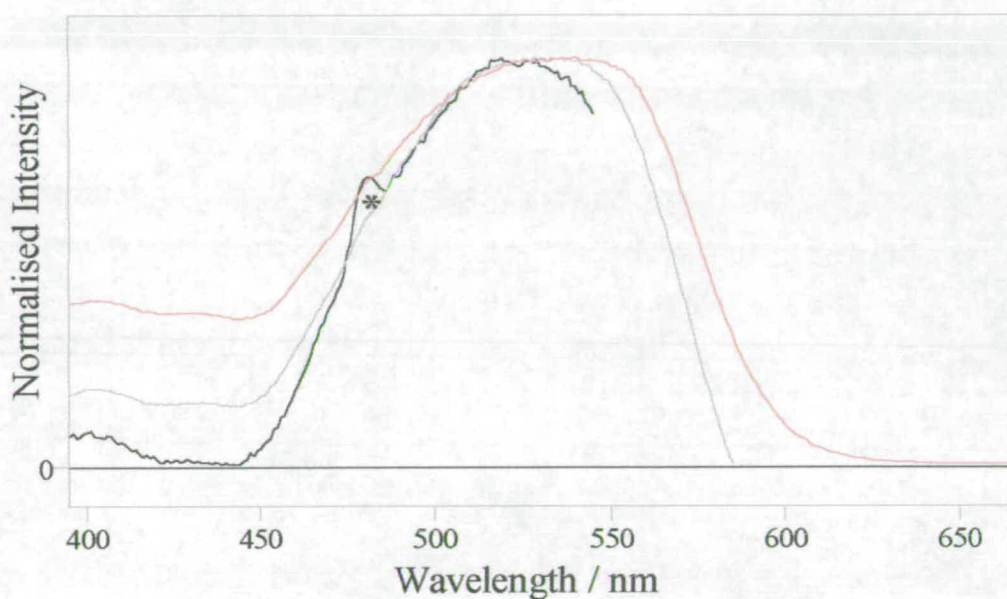
Figure 7.5 – Fluorescence excitation spectra of a 10^{-5} M sample of base~1 in ethanol at room temperature at emission wavelengths of: black 560nm (max intensity 194993cps), grey 600nm (11×10^{-5}cps) and red 680nm (529360cps). The * indicates a Raman solvent peak.
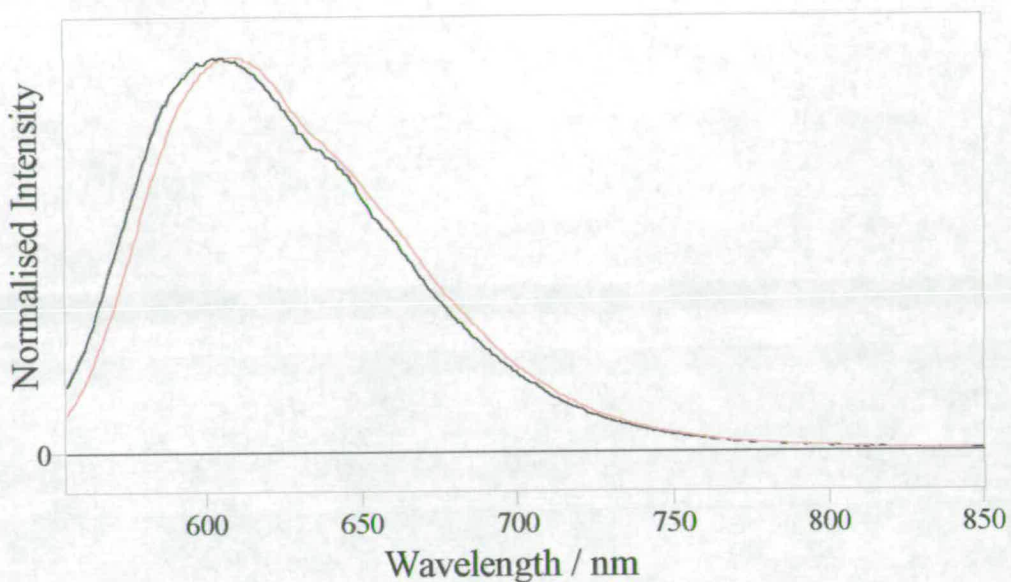
Figure 7.6 – Comparison of fluorescence emission spectra of a sample of base~1 in ethanol at room temperature with excitation wavelength of 540nm at: black 10^{-6} M (max intensity 267753cps) and red 10^{-5} M (12×10^{5}cps).
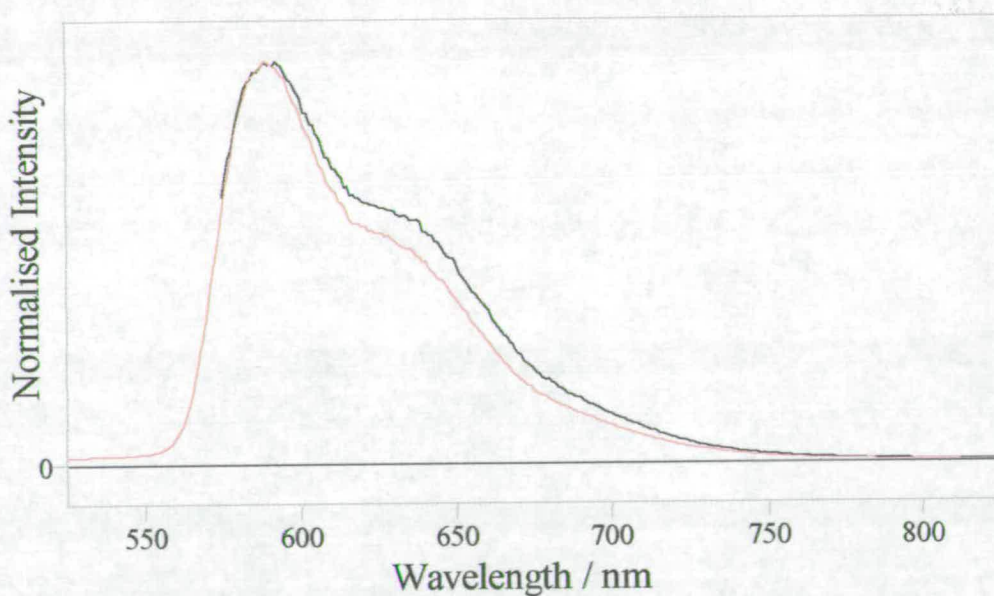
Figure 7.7 – Comparison of fluorescence emission spectra of a 10^{-5} M sample of base~1 at 77K in ethanol at excitation wavelengths of 460nm red (max intensity 22×10^{6}cps) and 560nm black (64×10^{6}cps).
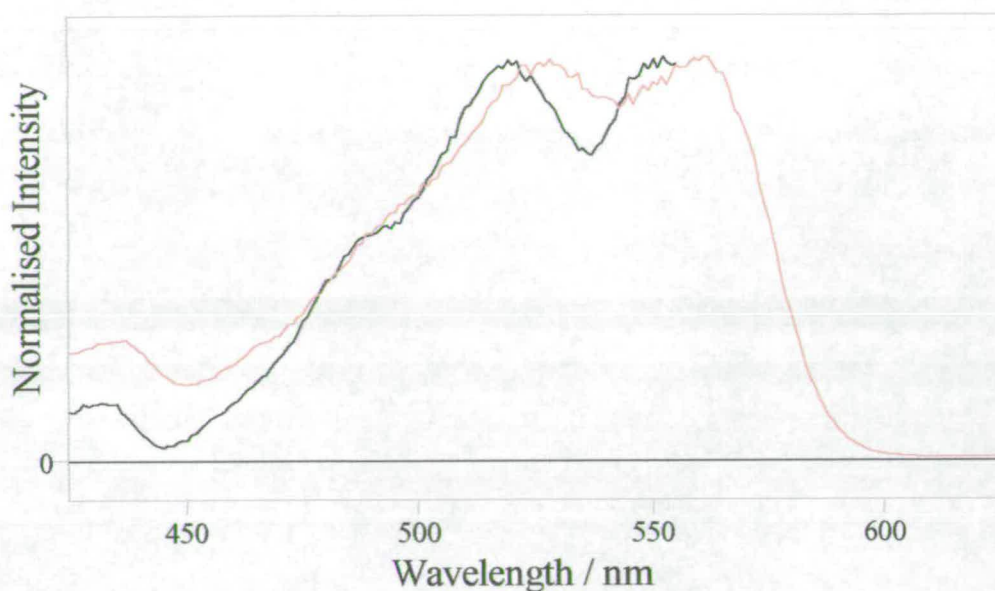
Figure 7.8 – Comparison of fluorescence excitation spectra of a 10^{-5} M sample of base~1 at 77K in ethanol at emission wavelengths of 570nm black (max intensity 28×10^{6}cps) and 700nm red (78×10^{5}cps) .

7.1.3 – Comparison of Base~1 with Red~1

Figure 7.9 shows a comparison of the absorption spectra of base~1 and red~1 in ethanol. The absorption spectrum of base~1 appears to be broader than that of red~1, particularly at wavelengths greater than 550nm. Both species absorb over the region ~450nm to 600nm.
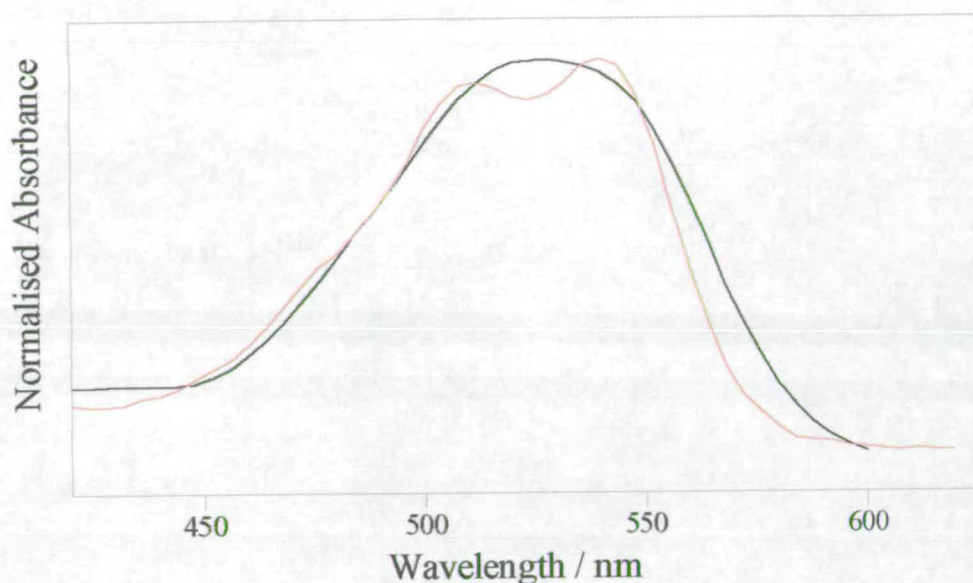
Figure 7.9 – Comparison of UV-Vis spectrum of base~1 (black) and red~1 (red) in ethanol at room temperature, 10^{-5} M samples.

In figure 7.10 the excitation spectrum of blue edge emission (where the monomer predominates) is compared with the absorption spectrum for each dye. The fact that the blue-edge excitation spectrum for base~1 is broader than that of red~1 suggests that base~1 aggregates to a greater extent than red~1. Consequently, the overlap between monomer and aggregate under the emission envelope of base~1 precludes the selective detection of the monomer excitation spectrum. The lower tendency for aggregation of red~1 may be due to the presence of the triazinyl group, figure 7.11, which could sterically hinder the interaction of monomer molecules.
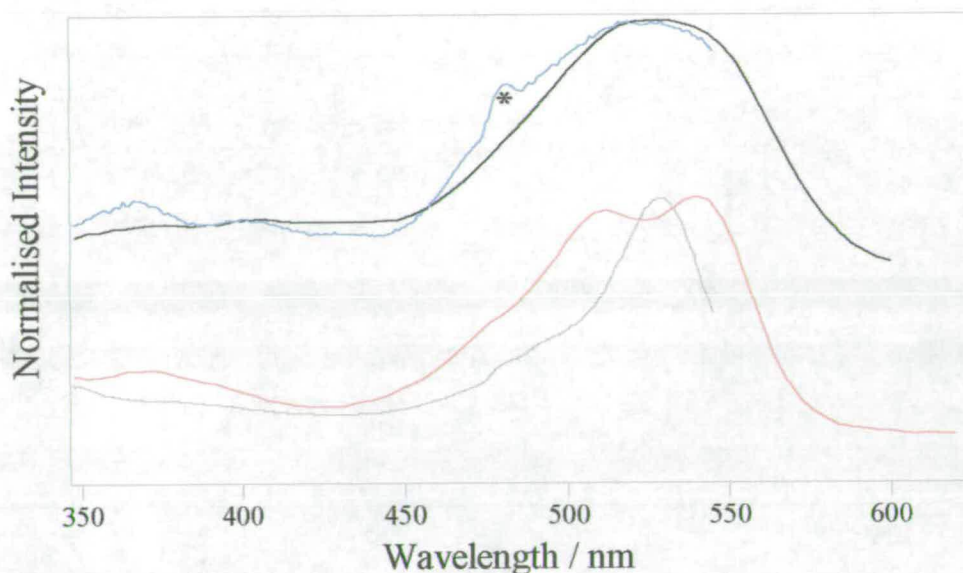
Figure 7.10 – Comparison of absorption spectrum (black) and monomer excitation spectrum, emission at 560nm, (blue) of base~1 with the absorption spectrum (red) and monomer excitation spectrum, emission at 560nm, (grey) of red~1. All spectra were taken at room temperature in ethanol and using sample concentration of 10^{-5} M.
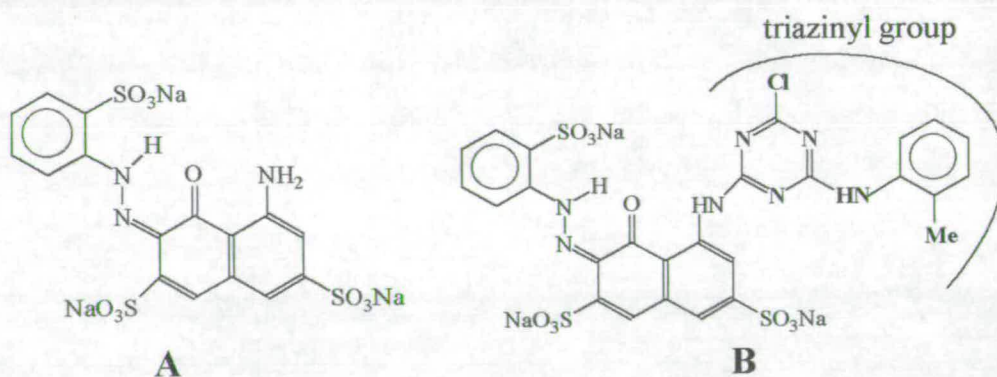
Figure 7.11 – Comparison of the structure of (A) base~1 and (B) red~1, showing area of possible steric hindrance in red~1.

7.2 – A Study of Red~2

Red~2 essentially consists of 2 red~1 chromophores joined through a linking group, as shown in figure 7.12.

Figure 7.12 – The structure of red~2.

7.2.1 – Detecting Aggregation of Red~2

7.2.1.1 – UV-Vis Spectroscopy

The UV-Vis profile of red~2 is shown in figure 7.13. The two maxima occur at 514nm and 535nm. The profile resembles that of red~1, but the wavelengths of the maxima of the latter are different, at 509nm and 534nm. Over the concentration range of 10^{-7} to 10^{-4} M the shape of the spectral envelope does not change, but the occurrence of aggregation is revealed by a deviation from Beer's Law. This again is similar to the behaviour of red~1, figure 7.14.

Figure 7.13 – Absorption profile of a 10^{-5} M sample of red~2 in water at room temperature. Max absorbance at 535nm 0.351.
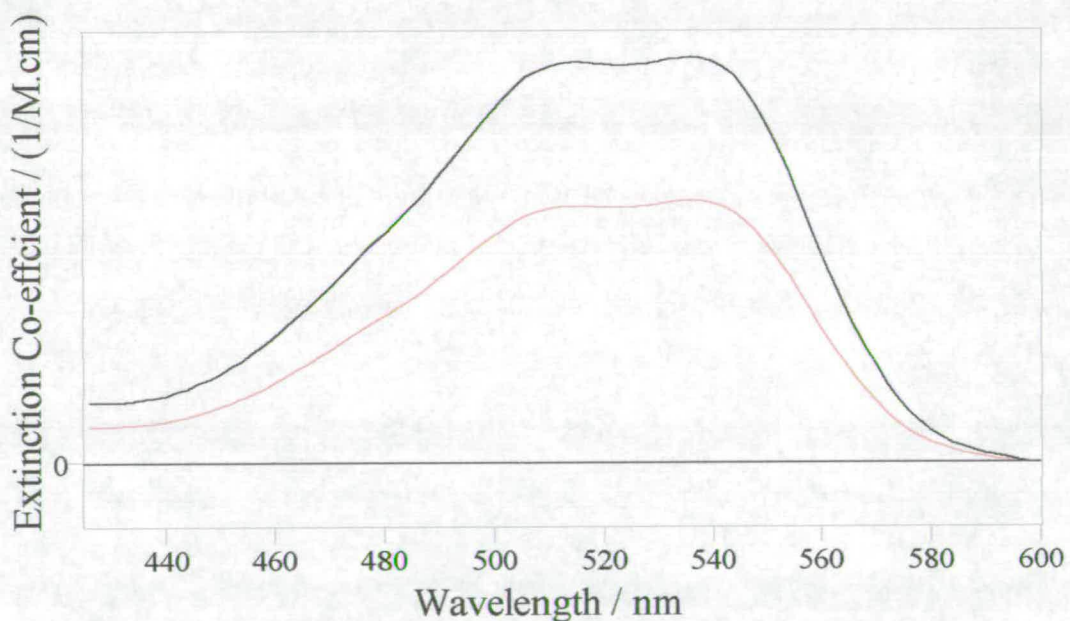
Figure 7.14 – Plot of extinction co-efficient versus wavelength for a sample of red~2 in water at room temperature black 8×10^{-7} M (max value at 535nm 50592$M^{-1}cm^{-1}$) and red 2×10^{-5} M (33550 $M^{-1}cm^{-1}$).

7.2.1.2 – Fluorescence Spectroscopy

Exciting across the absorption envelope of red~2, varying fluorescence emission is observed as shown in figure 7.15. Moving from 500nm-excitation wavelength to 530nm the emission spectra shift to the blue, figure 7.15. But as shown in figure 7.16 when moving to longer excitation wavelengths the spectra now shift to the red. If the emission observed when exciting at 500nm results from an aggregate, then the blue shifted emission most likely results predominately from the monomer. Finally, the red shifted emission observed with an excitation wavelength of 550nm, results from the aggregate. As the emission wavelength is increased, the excitation spectra in figure 7.17 broaden to the red and the blue of the maximum. This broadening is attributed to the aggregate, while the spectrum obtained at emission wavelength of 560nm is a result of the monomer.
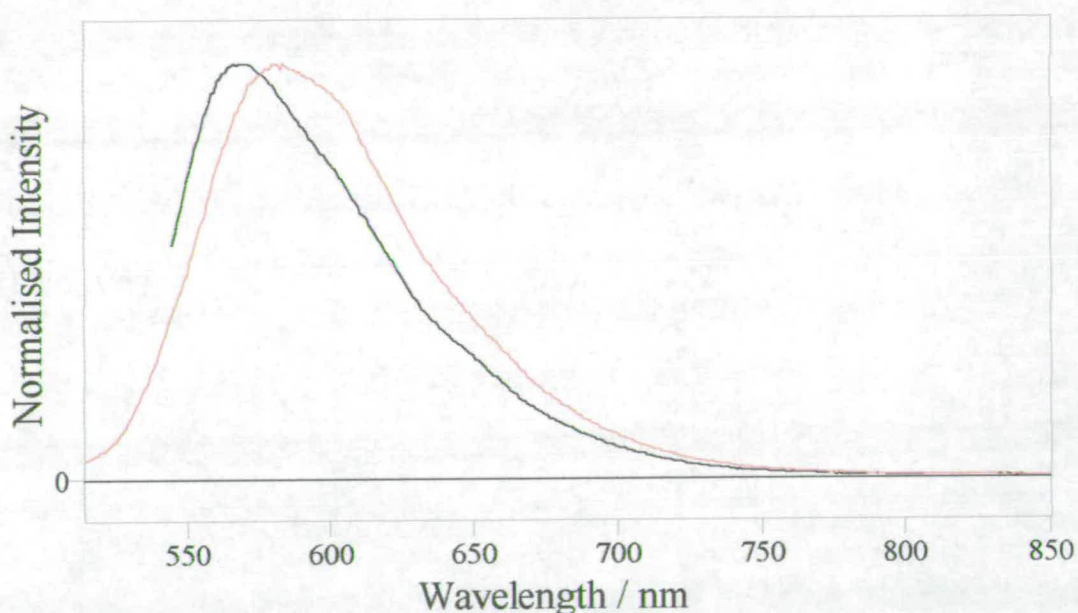
Figure 7.15 – Fluorescence emission spectra of a 10^{-5} M sample of red~2 in water at room temperature, excitation wavelengths are red 500nm (max intensity 241075cps) and black 530nm (343235cps).
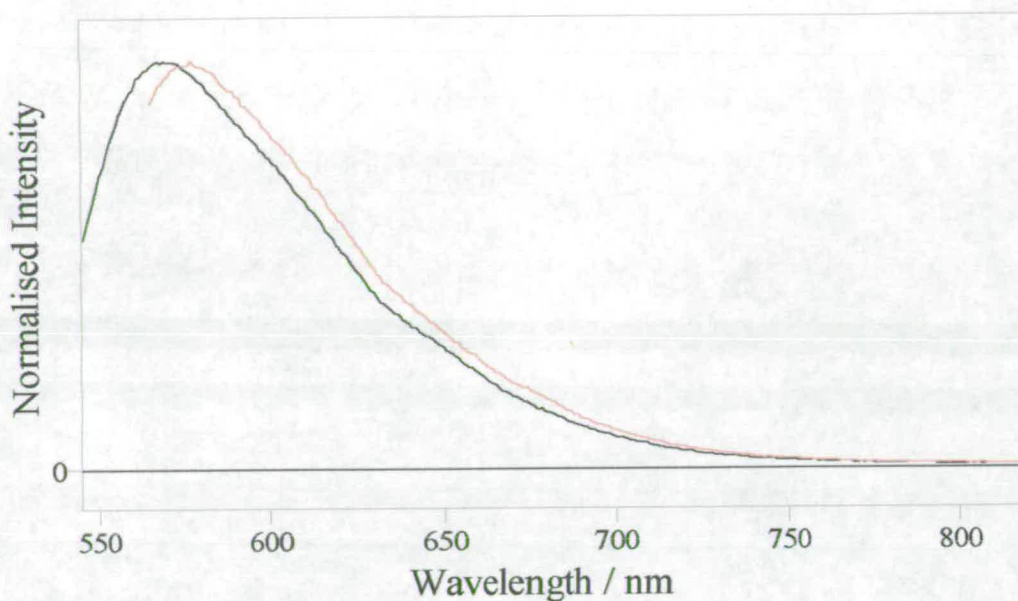
Figure 7.16 – Fluorescence emission spectra of a 10^{-5} M sample of red~2 in water at room temperature, excitation wavelengths are red 550nm (max intensity 277039cps) and black 530nm (343235cps).

As observed previously for red~1, there is a large amount of overlap between monomer and aggregate spectra beneath the absorption envelope, preventing exclusive excitation of monomer or dimer species, but some selectivity can be achieved.
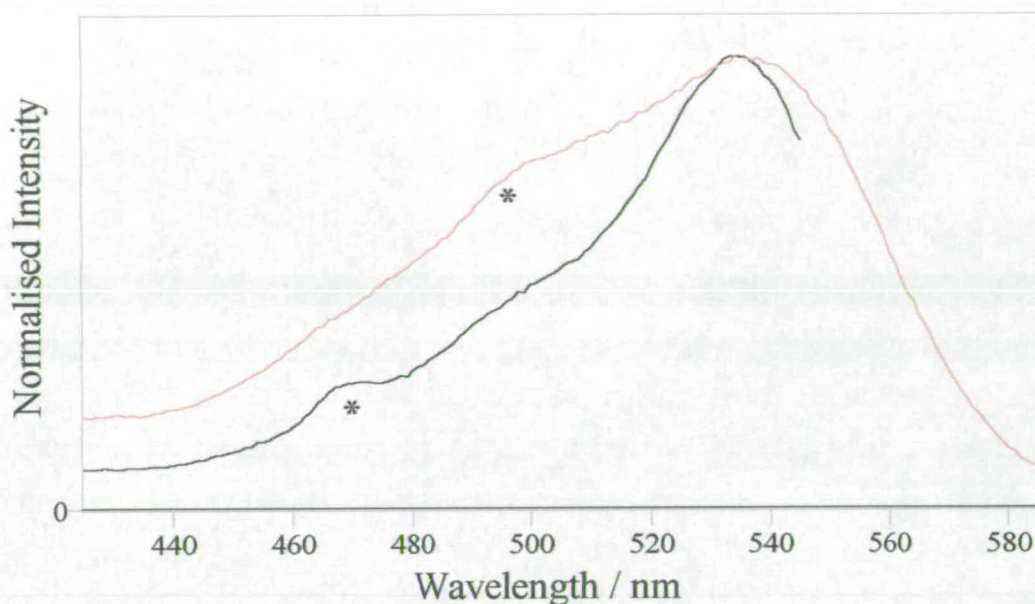
Figure 7.17 – Fluorescence excitation spectra of a 10^{-5} M sample of red~2 at room temperature in water; emission wavelengths are black 560nm (max intensity 336993cps) and red 600nm (265055cps). The * represents solvent Raman peaks.

7.2.2 – Comparison of Red~2 with Red~1

The position of the monomer excitation spectrum of red~2, relative to the dimer, is different to that of red~1 in water as shown in figure 7.18. In the case of red~1 the monomer was located to the red of the maxima of the absorption profile. The monomer excitation spectrum of red~2 resides under its absorption envelope. The excitation wavelength dependence of the fluorescence emission is different when compared with red~1 as a result of the position of the monomer excitation spectrum. With red~1 there was a narrowing of the emission spectrum as the wavelength of excitation was increased, moving towards monomer excitation wavelengths. In the case of red~2 there is an initial narrowing, with increasing excitation wavelength, moving towards narrow excitation maximum, and then a broadening as one returns to

exciting the aggregate again. The shift to the blue of the monomer excitation spectrum of red~2 in comparison with red~1 is comparable to the shift in the monomer excitation spectrum of red~1 in ethanol compared with red~1 in water, section 6.3.2. This was a solvent effect. It is possible that the shift illustrated in figure 7.18 is a result of the bis-chromophore system of red~2 existing in a different solvent environment compared to the mono-chromophore system of red~1.
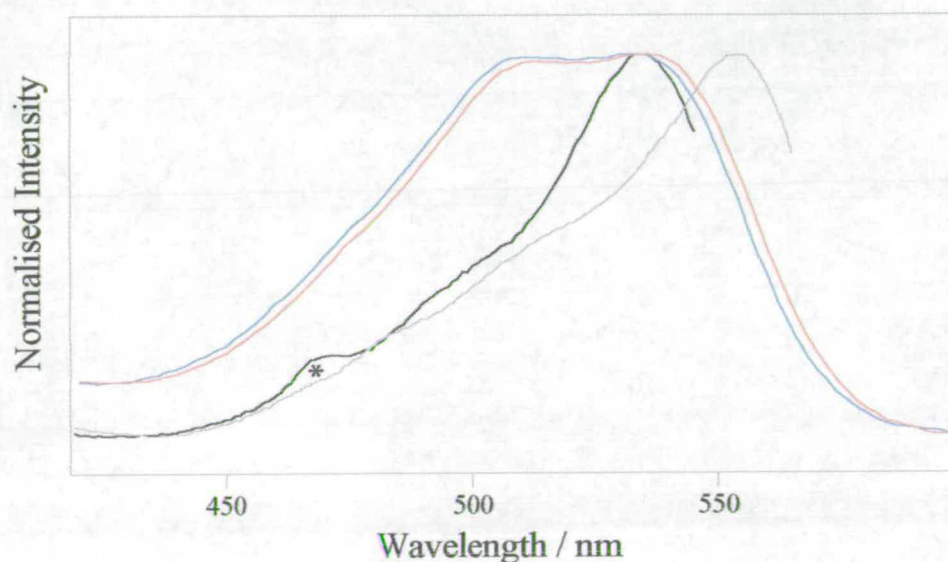
Figure 7.18 – Comparison of absorption spectrum (blue) and monomer excitation spectrum, emission at 580nm, (grey) of 10^{-5} M sample of red~1 in water with of absorption spectrum (red) and monomer excitation spectrum, emission at 560nm, (black) of 10^{-5} M sample of red~2 in water.

7.2.3 – Aggregation Studies of Red~2

As noted when discussing turquoise~1 and red~1 it is possible to change the extent to which a particular dye solution is aggregating in the dyebath, by increasing the temperature of the sample or by adding an electrolyte such as sodium chloride. The effect of these factors on aggregation of red~2 has also been investigated.

7.2.3.1 – Ionic Strength and the Aggregation of Red~2

Figure 7.19 shows how the addition of salt to the dye solution increases the relative amount of aggregation. Figure 7.19 also importantly shows the presence of an isosbestic point at 560nm, indicating that there are two species in equilibrium; monomer and aggregate. The presence of an isosbestic point was noted in chapter five with turquoise~1, at high salt concentrations such as those being used here with red~2. It was shown that the aggregate that existed in solution was in fact a dimer, with any other aggregates in solution having negligible concentration. At the salt concentrations that are used in figure 7.19 essentially only monomer and dimer exist in equilibrium. The relative intensity of the two maxima of the absorption profile change with the addition of electrolyte. The observation of a decrease in relative intensity of the 535nm absorption maxima with increased salt concentration is consistent with a decrease in concentration of monomer, since the fluorescence excitation spectrum shows that the peak of the monomer absorption spectrum occurs in this wavelength region. As salt concentration is increased the contribution of the monomer species to the absorption spectrum decreases. The extent of the change in the absorption profile shown in figure 7.19 is not observed in the case of red~1. The change in the absorption envelope of red~2 with the addition of salt implies that the salt has a greater effect on the state of aggregation of red~2 than red~1.
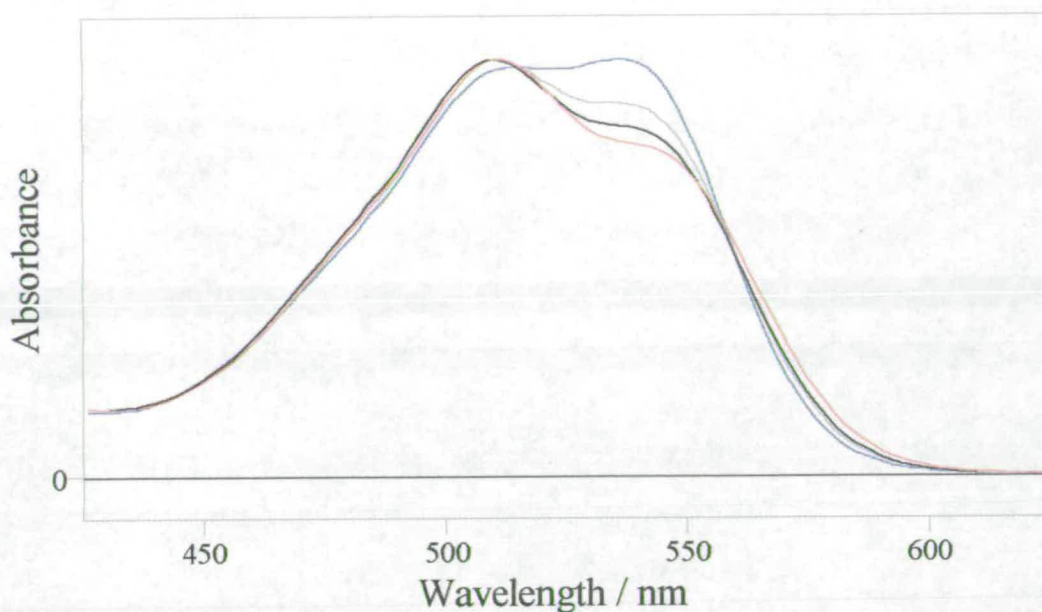
Figure 7.19 – Absorption spectra of a 10^{-5} M sample of red~2 in water at room temperature, with various salt loadings in g per 10ml of solution; blue zero (max absorbance at 535nm 2.527), grey 0.2 (2.148), black 0.4 (2.016) and red 1.0 (1.879).

7.2.3.2 – Temperature and the Aggregation of Red~2

When the temperature of a solution of red~2 in ethanol is increased the relative amount of monomer is expected to increase. The effect of increasing temperature on the spectral profile is shown in figure 7.20. In a similar way to the behaviour of red~1 in ethanol the trough between the two maxima becomes less distinct with increasing temperature. For red~1, this effect was due to the monomer excitation spectrum being positioned in that region. It is assumed, then, that this is also the case with red~2 in ethanol. Figure 7.20 also shows the presence of an isosbestic point at 555nm. This is evidence that there are two absorbing species in solution, the monomer and a single aggregate species, probably dimer.
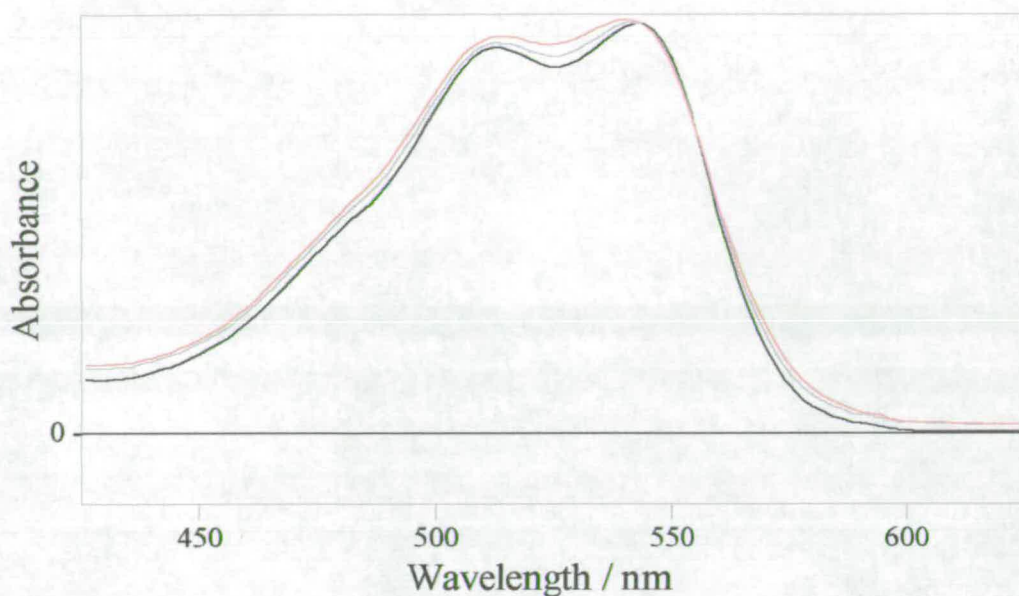
Figure 7.20 – Comparison of absorption spectra of a 10^{-5} M sample of red~2 in ethanol at varying temperatures to show an isosbestic point at 555nm; black 30°C (max absorbance at 535nm 0.969), grey 50°C (0.968) and red 70°C (0.972).

7.2.4 – Red~2 on Cotton

The ability to analyse fluorescence and absorption spectra of dyestuffs in solution gives information about the state of aggregation of these dyes in the dyebath prior to dyeing. Therefore, the capacity to obtain fluorescence spectra of a dye when on a substrate such as cotton would be of considerable value. Fluorescence emission spectra were obtained for red~2 on cotton. Figure 7.21 shows a comparison of the fluorescence emission spectrum at the same wavelength of excitation for red~2 in the aqueous environment and on a cotton substrate. The fluorescence emission spectra from red~2 on cotton do not change with excitation wavelength. This lack of dependence of the emission with the excitation wavelength infers that there is only one emitting species. Comparison of emission spectra in figure 7.21 shows that the emission from the dye on cotton is clearly red shifted when compared with emission from the dye in aqueous solution. The un-dyed cotton was tested, and found to have no fluorescence emission, confirming that the fluorescence observed comes from the

dye and not the cotton. Since, in solution, red-shifted emission is attributed to aggregate emission, a possible interpretation is that red~2 on cotton is in a state of greater aggregation than in aqueous solution. However, the environment of the dye molecules will also influence the emission spectrum, so the observation of red-shifted emission is not unequivocal evidence of increased aggregation
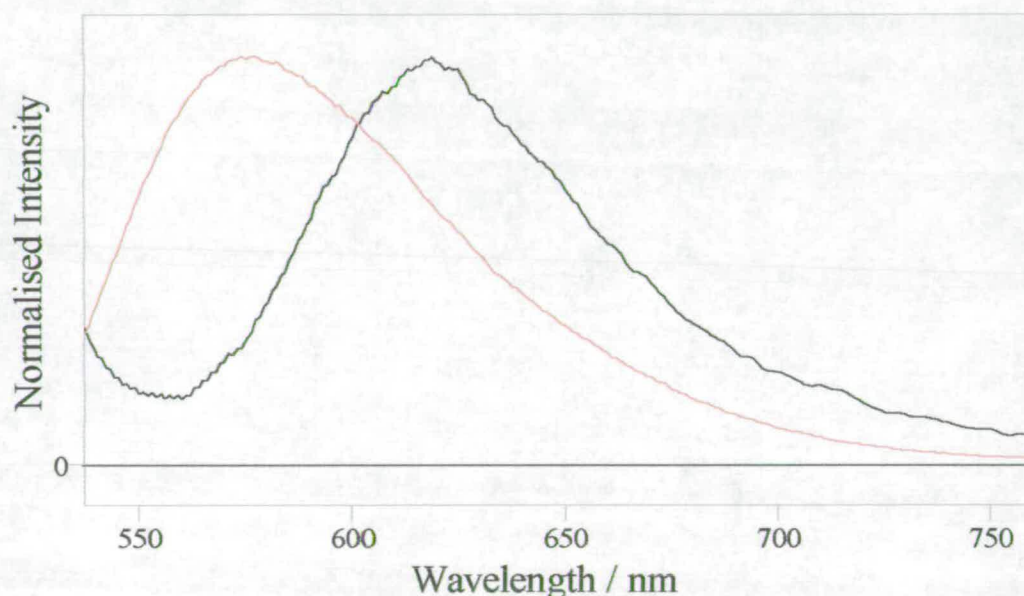
Figure 7.21 – Comparison of fluorescence emission spectra of red~2 at excitation wavelength of 520nm, in water at room temperature red (max intensity 302077cps) and on cotton substrate at room temperature black (77437cps).

7.3 – A Study of Trioxa~1

7.3.1 – Preparation of Trioxa~1

Trioxa~1 is similar to red~2 in that it contains two identical chromophores joined by a linker, the difference in structure between red~2 and trioxa~1 is in the nature of the linker. It is of interest to consider briefly how trioxa~1 was synthetically prepared.

A - Synthetic Scheme

i) generation of intermediate
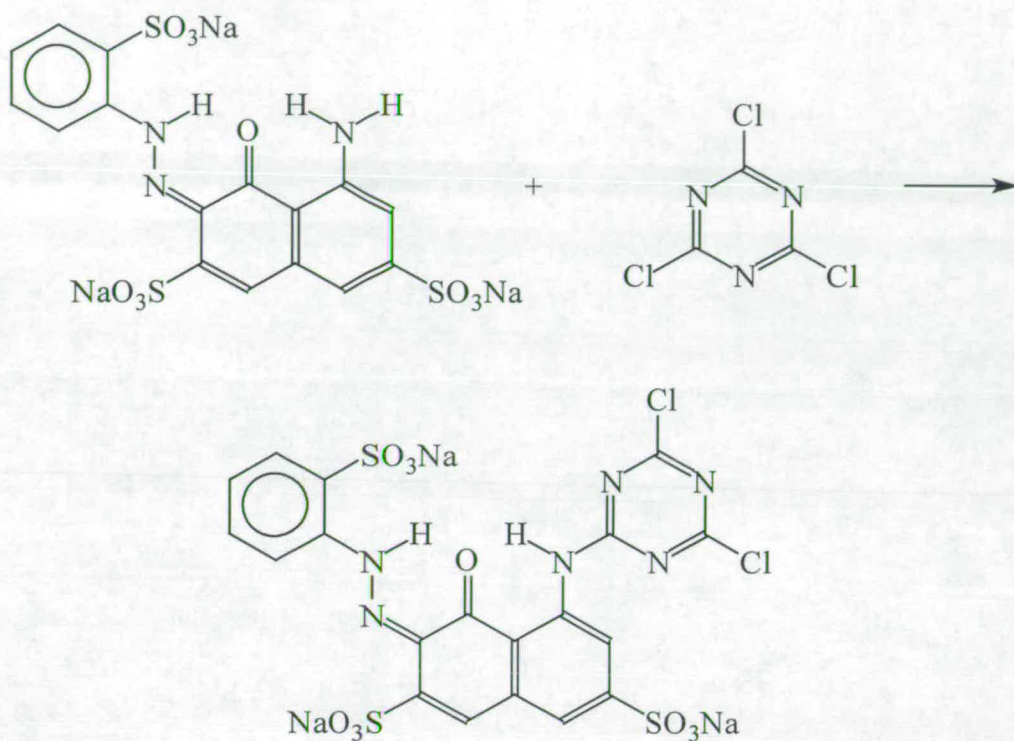
ii) generation of product
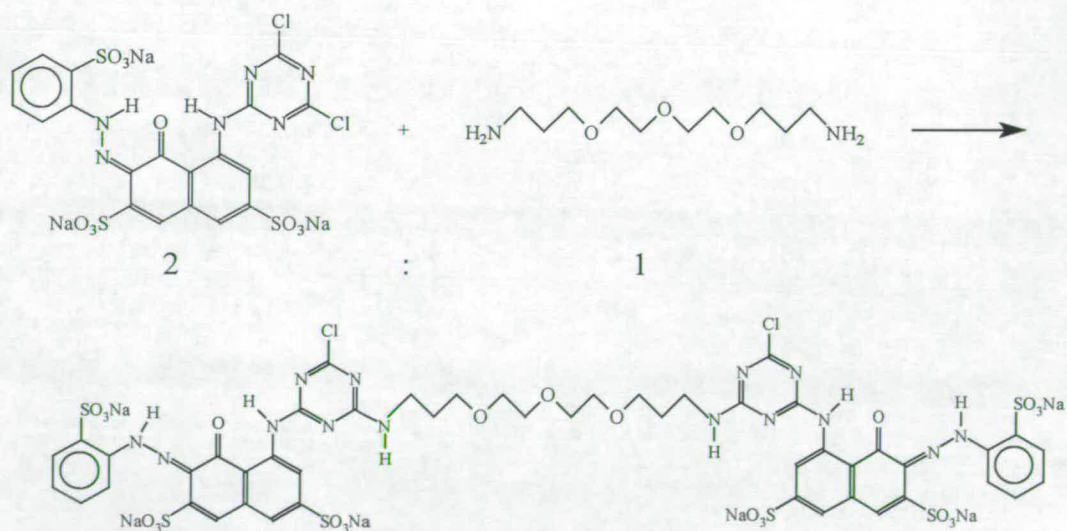
B – Mechanistic Outline

a) Synthesis of intermediate via aromatic nucleophilic substitution, S$_N$Ar.

Meisenheimer Complex
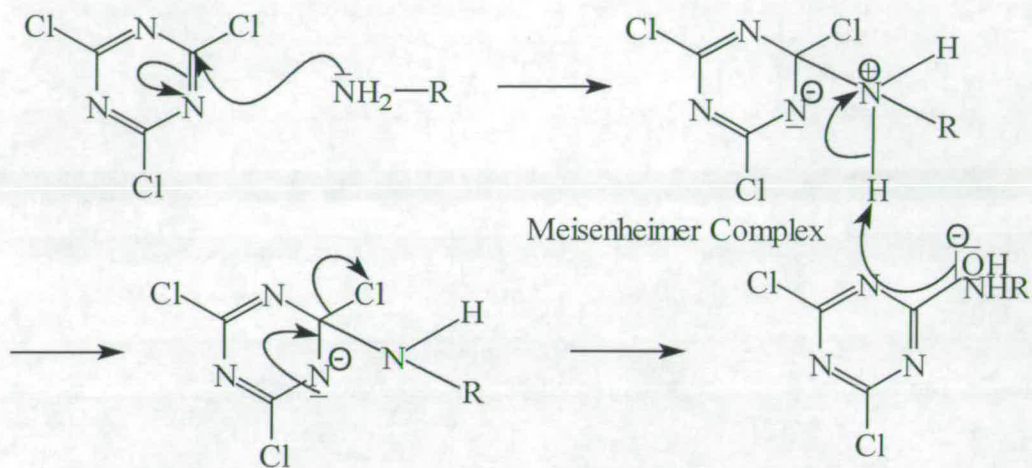
RNH$_2$ is base~1

b) Synthesis of troxa~1 via S$_N$Ar
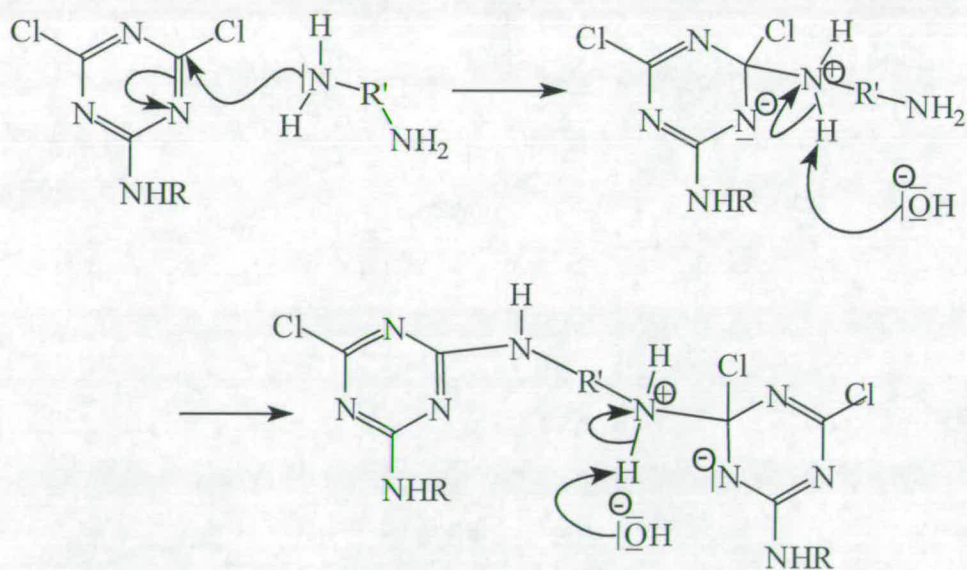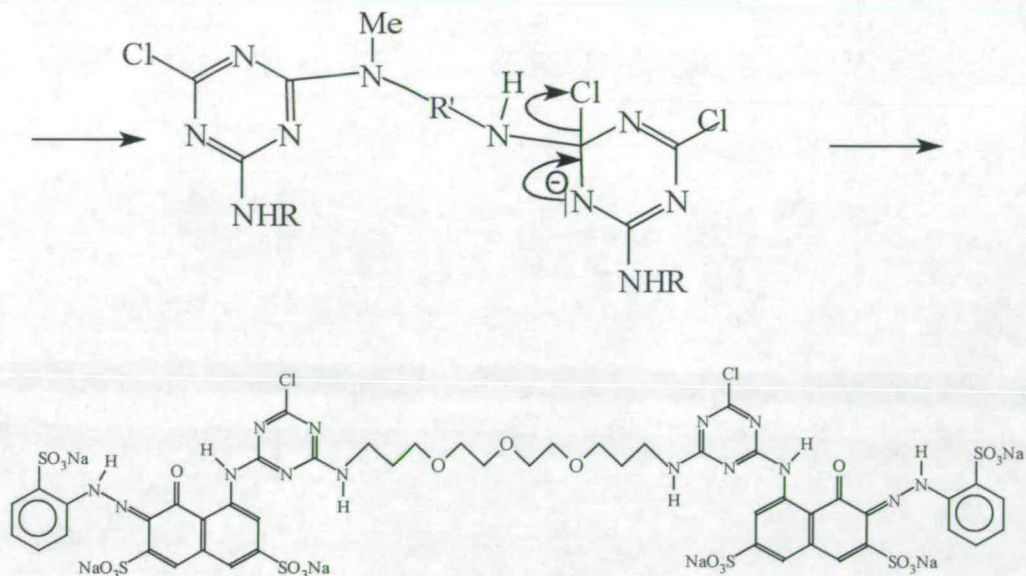
7.3.2 – Detecting Aggregation of Trioxa~1

7.3.2.1 – UV-Vis Spectroscopy

The absorption profile of trioxa~1 in ethanol is shown in figure 7.22, it shows the characteristic double maxima that most of the red *o*-hydroxyazo dyes have exhibited. The maxima appear at 542nm and 515nm. Over the concentration range 10^{-7} M to 10^{-4} M there is no change in the profile of the UV-Vis spectrum of trioxa~1.
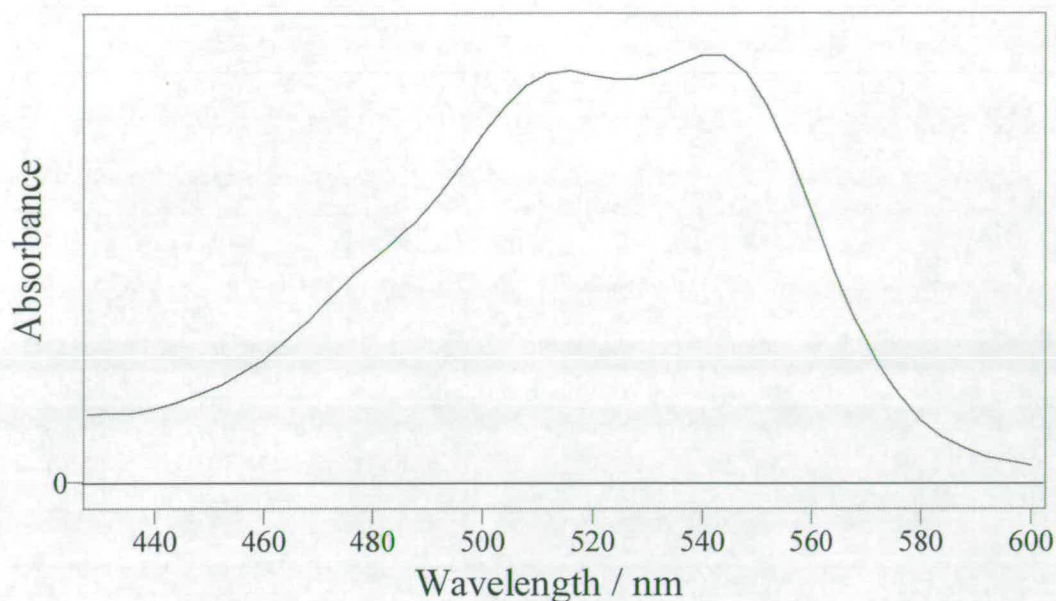
Figure 7.22 – The absorption spectrum for a 10^{-5} M sample of trioxa~1 in ethanol at room temperature. Max absorbance at 542nm 0.539.

7.3.2.2 – Fluorescence Spectroscopy

Excitation across the absorption spectrum of trioxa~1 reveals that the dye fluoresces and that the emission is dependent upon the excitation wavelength. Figure 7.23 illustrates how the emission shifts to the blue as the excitation wavelength is increased from 500nm to 530nm. Figure 7.24 shows how on increasing the excitation wavelength further towards 560nm the emission shifts to the red. The initial emission resulting from excitation at 500nm, figure 7.23, results from an aggregate. The blue shifted emission results from the monomer, and the return to red shifted emission, figure 7.24, is a return to emission from the aggregate.
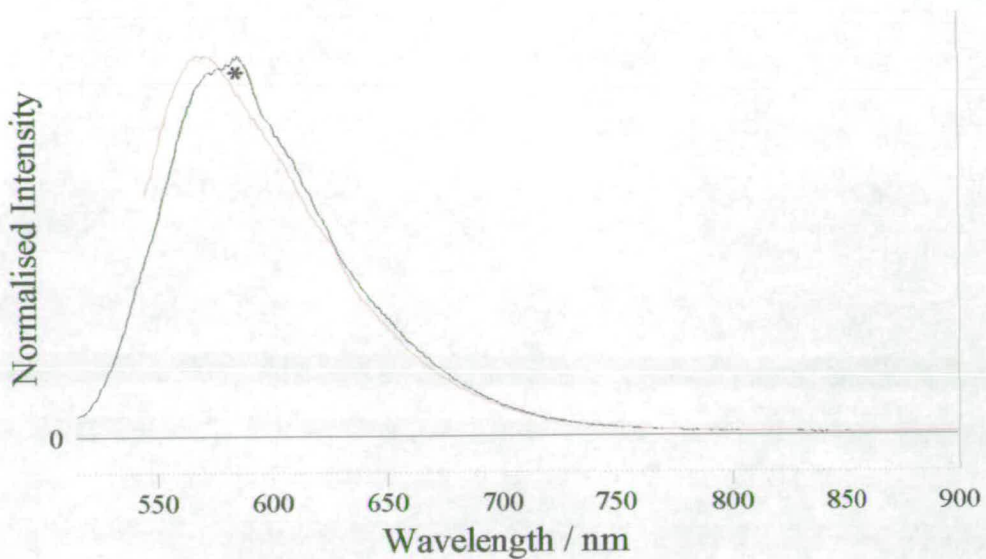
Figure 7.23 – Comparison of fluorescence emission spectra of a 10^{-5} M sample of trioxa~1 in ethanol at room temperature, excitation at 500nm black (max intensity 190373cps) and 530nm red (261565cps). The * represents a solvent Raman peak.
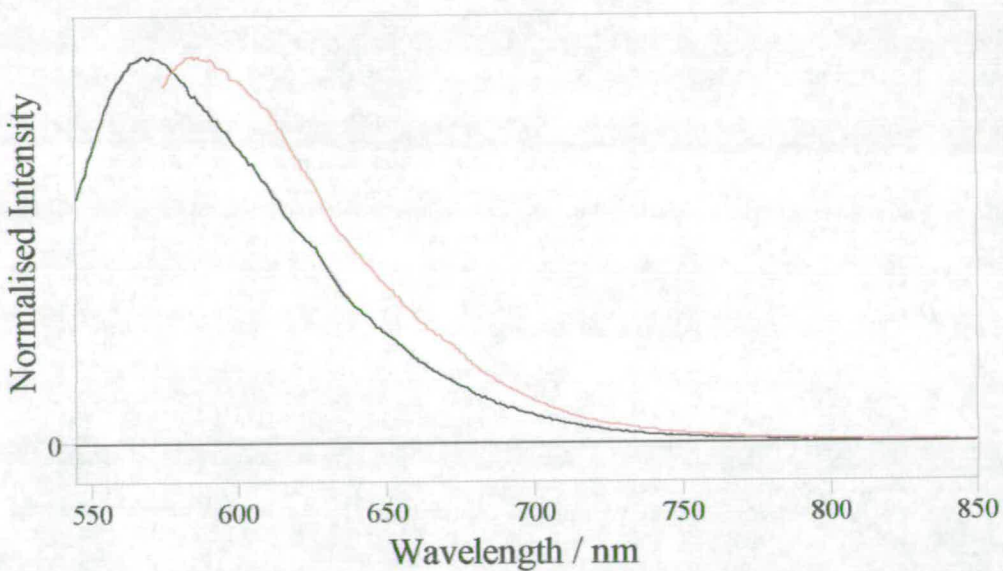
Figure 7.24 - Comparison of fluorescence emission spectra of a 10^{-5} M sample of trioxa~1 in ethanol at room temperature, excitation at 530nm black (max intensity 261565cps) and 560nm red (283513cps) .

The fluorescence excitation spectra are presented in figure 7.25. They show the monomer excitation spectrum resulting from an emission wavelength of 560nm, the monomer emission maximum, figure 7.23. An increase in the emission wavelength results in the spectrum broadening to the red and blue of the maxima. This is due to the aggregate. At an emission wavelength of 640nm the excitation spectrum resemble the UV-Vis. This implies that the absorption profile is dominated by the aggregate. There is a large amount of overlap between the monomer and aggregate under the absorption profile, but the double maxima is attributed to the aggregate in a similar way to red~1, chapter 6. Figure 7.26 shows two fluorescence emission spectra obtained from an excitation wavelength of 530nm, one from 10^{-5} M and the other at 10^{-6} M solutions. This clearly illustrates the increase in the intensity of red-shifted aggregation fluorescence with increased concentration, even at this excitation wavelength which favours the monomer.
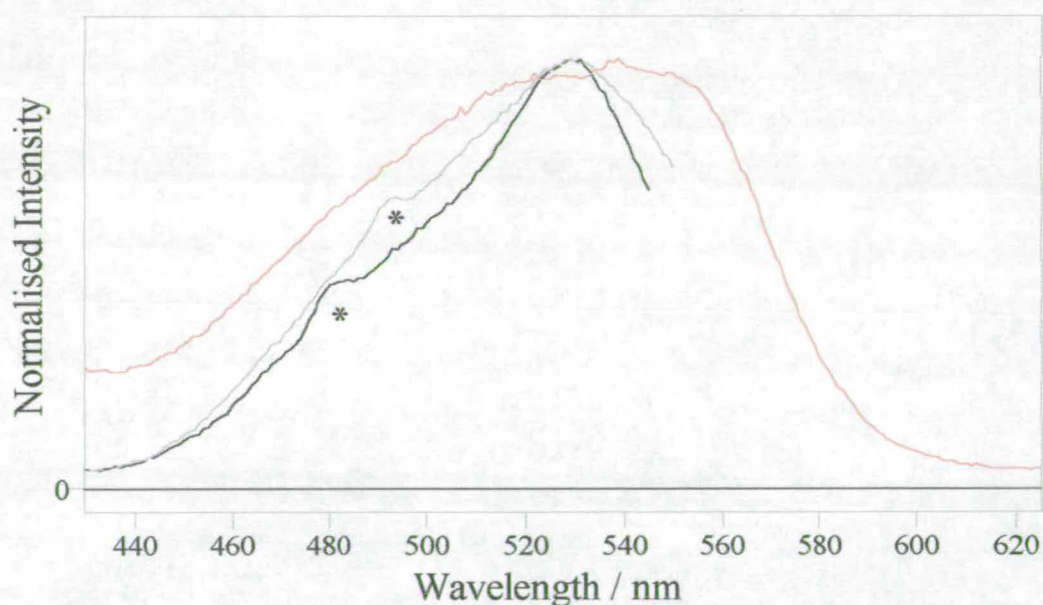
Figure 7.25 – Fluorescence excitation spectra of a 10-5 M sample of trioxa~1 in ethanol at room temperature, at emission wavelengths of black 560nm (max intensity 297686cps), grey 575nm (359238cps) and red 640nm (136494cps). The * represents solvent Raman peaks.
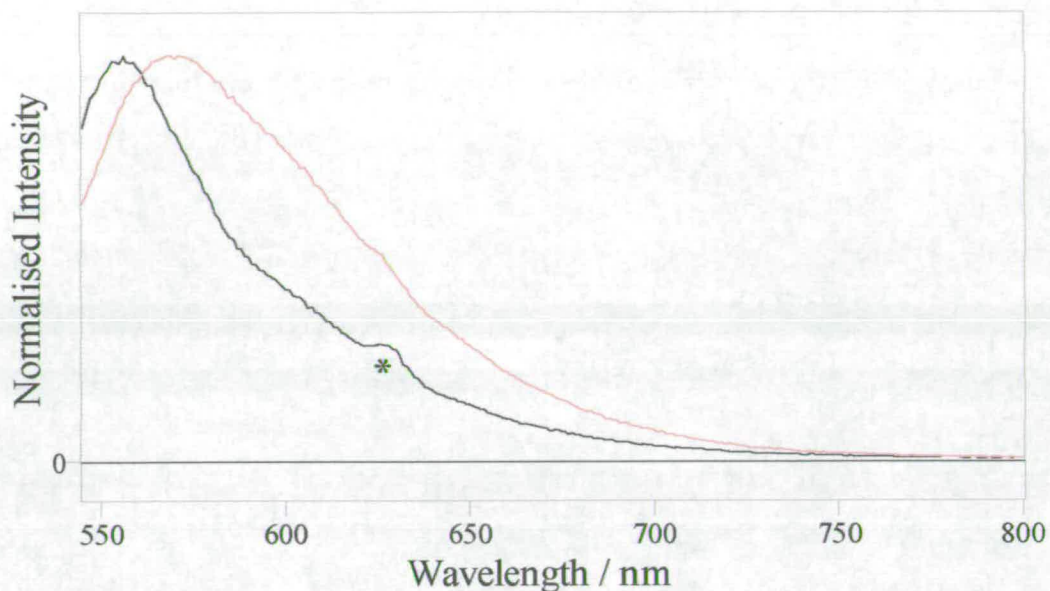
Figure 7.26 – Comparison of fluorescence emission spectra at excitation wavelength of 530nm for a sample of trioxa~1 at room temperature in ethanol at 10^{-6} M black (max intensity 164881cps) and 10^{-5} M red (261565cps). The $*$ represents a solvent Raman peak.

7.3.3 – Comparison of Trioxa~1 with Red~1

Figure 7.27 shows how the monomer excitation spectrum of trioxa~1 lies at the trough between the two maxima of the absorption spectrum, very similar to the situation for red~1, figure 7.28. The behaviour of the fluorescence excitation and emission spectrum of red~1 and trioxa~1 in ethanol is very similar. Both dyes exhibit the same trends with respect to variation of spectra with emission and excitation wavelengths.
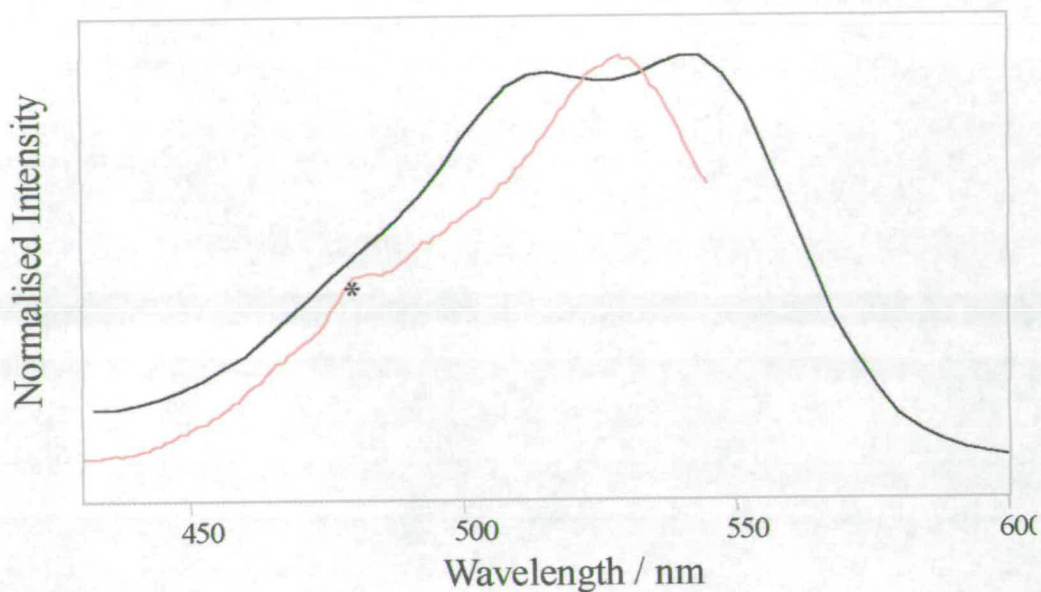
Figure 7.27 – Comparison of absorption spectrum-black, and fluorescence excitation spectrum of the monomer at emission wavelength of 560nm-red, of a 10-5M sample of trioxa~1 at room temperature. The * represents a solvent Raman peak.
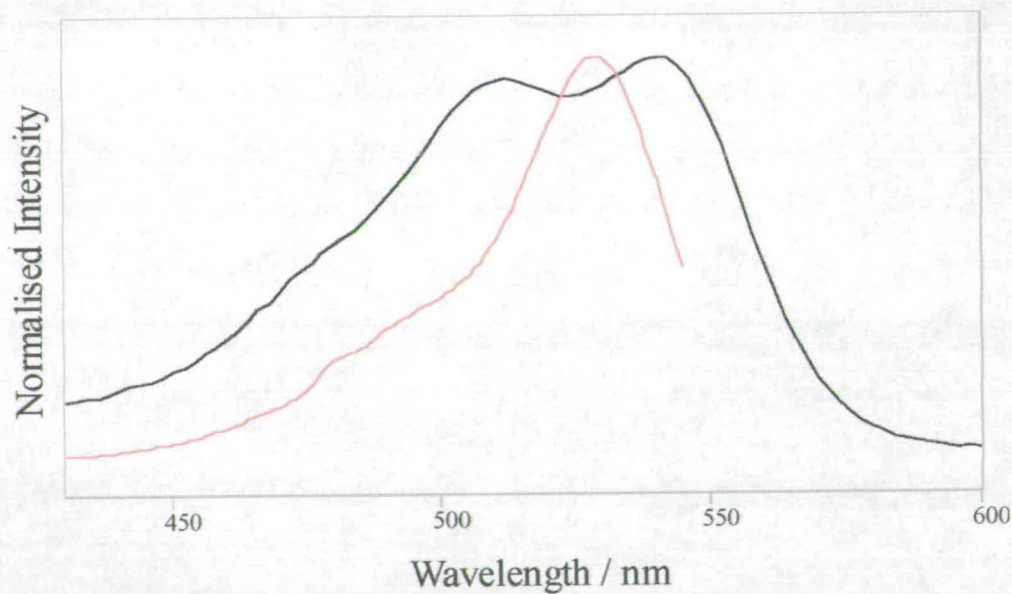
Figure 7.28 – Comparison of the absorption profile and fluorescence excitation spectrum resulting from emission wavelength of 560nm, of a 10^{-5} M sample of red~1 in ethanol.

Base~1 appears to aggregate in solution more than red~2 and trioxa~1. This has been attributed to the lack of extended structure through the triazinyl group that would cause a steric boundary to aggregation. The behaviour of trioxa~1 is more similar to red~1 than red~2. This is attributed to the possibility of the bis-chromophore system of trioxa~1 having the chromophores separated spatially to a greater extent than red~2. The separation comes through the linker groups, the trioxa linker group of trioxa~1 is longer than the linker group in red~2. Thus the bis-chromophore system of trioxa~1 behaves more like the mono-chromophore system of red~1 because of the distance between the two chromophores. The trioxa linker also allows for far more flexibility than the linker in red~2, this flexibility accounts for the possibility of less spatial correlation between the two chromophores in trioxa~1. Hence, taking both possibilities into account, the behaviour of red~1 being more like trioxa~1 than red~2.

7.4 – Conclusions

In ethanol base~1 shows no change in the UV-Vis profile over the concentration range 10^{-7} M to 10^{-4} M, but deviation from Beer's law indicates that in ethanol base~1 aggregates. The dye fluoresces and the emission broadens to the red with increased excitation wavelength, this red shifted emission is aggregate fluorescence. The single maxima broad absorption profile of base~1 is different to the other *o*-hydroxyazo dyes that have the characteristic double maxima. The presence of a higher concentration of higher aggregates could lead to the braodening of the spectrum. Base~1 appears to aggregate more than the other *o*-hydroxyazo dyes.

Although there is no change in the profile of the double maxima absorption spectrum of red~2 in water, the deviation from Beer's law allows the conclusion that red~2 aggregates in water. The fluorescence excitation and emission spectra of monomer and aggregate are detected. The extent of aggregation increased with the increase in concentration and decrease in temperature. Increasing the ionic strength through the

addition of salt increased the amount of aggregation. Similarly to turquoise~1 in chapter 5, at high salt concentration an isosbestic point indicated the presence of two absorbing species monomer and dimer. The salt containing system allows the absorption profile to be varied to an appreciable extent, this is the only dramatic variation of the absorption profile observed for any of the o-hydroxyazo dyes studied. Compared with red~1 the monomer excitation spectrum of red~2 is positioned under the absorption envelope while for red~1 it is positioned to the red of the double maxima on the red edge of the absorption envelope. There is qualitative evidence that on a cotton substrate red~2 aggregates to a greater extent than in solution, this is seen through the comparison of emission spectra that indicate the emission from the dye on the fabric significantly red shifted.

The absorption spectrum of trioxa~1 in ethanol also has the familiar double maxima, there is no change in the absorption profile over the concentration range of 10^{-7} M to 10^{-4} M. The spectroscopic properties of trioxa~1, a bis-chromophore system, appear to be more similar to the mono-chromophoric red~1 than the bis-chromophoric red~2.

CHAPTER 8 – LASER-INDUCED FADING

8.1 – Introduction

The photostability or light fastness of commercial dyestuffs is of paramount importance in the dyestuffs industry. The pursuit of dyes that have improved light fastness properties is of major interest as far as research objectives are concerned. The current techniques used for light fastness testing are of course improvements on the original method, that involved leaving dyed fabric samples on top of a mountain in India for days and months upon end. The current methods involve the usage of instruments such as fadometers; this involves exposing dyed fabric samples to an output from a Xe lamp in an enclosed dome shaped vessel, where the temperature and humidity are controlled. The output from the Xe lamp is passed through a filter in order to produce the required spectrum, so the dyed fibre is exposed to a simulation of sunlight. The disadvantage of the current test methods lies in the time taken to obtain results. Currently the experiments take too long to complete; they can last for a number of days or weeks. This chapter of work is a preliminary study to explore the feasibility of laser-induced fading of dyed textiles, in order to provide a rapid method of light fastness testing. The un-dyed, plain cotton and wool equivalents of those dyed fabrics investigated in this chapter were irradiated with identical peak power densities and times of irradiation referred to in each specific section with no effect to the fabric samples.

8.2 – Blue Wool Scales

The blue wool scales are a universal standard for assigning light fastness ratings to various dyes, as described in section 3.5. With laser output of 532nm the initial investigation, with experimental set-up as in section 4.5, involved observation of fading of the blue wool scale samples. This was to ascertain if laser irradiation would fade the fabric without damage, and if the times to fade the samples would go

in accordance to their light fastness ratings. That is, the higher light fastness rated samples taking longer to fade. The scale is geometric, that is each successive standard takes twice as long to fade, 1 is low light fastness and 8 is high light fastness. The standard with a light fastness of 1 is referred to as band one, relative light fastness of 1, while band 3 has a relative light fastness of 4. This nomenclature continues with the other bands.

Tables 8.1 to 8.4 show the relationship between the relative light fastness of a sample and the time taken to fade it. The values for time taken to fade are averaged values. For each relative light fastness the time to fade was measured ten times and then averaged. Each sample on the blue wool scale was irradiated with different peak power densities, expressed in Wmm^{-2}. The data in table 8.1 show that with a peak power density of 2.49×10^6 Wmm^{-2} that the blue wool scales did indeed fade without damage to the fabric itself. Also, the fading of the various bands of blue wool was in line with the actual light fastness of the sample. The greater the band number and relative light fastness then the greater the time taken to fade. The peak power density is calculated by dividing the power of the laser by the pulse length. This is then multiplied by the area of irradiation on the fibre.

Band	1	2	3	4	5	6
Relative Light Fastness	1	2	4	8	16	32
Time to Fade/minutes	2.0	3.1	18.3	24.0	32.8	120.2

Table 8.1 – Data for fading of blue wool scales with power output of 2.49 x 10^6 Wmm^{-2} from a 532nm laser output.
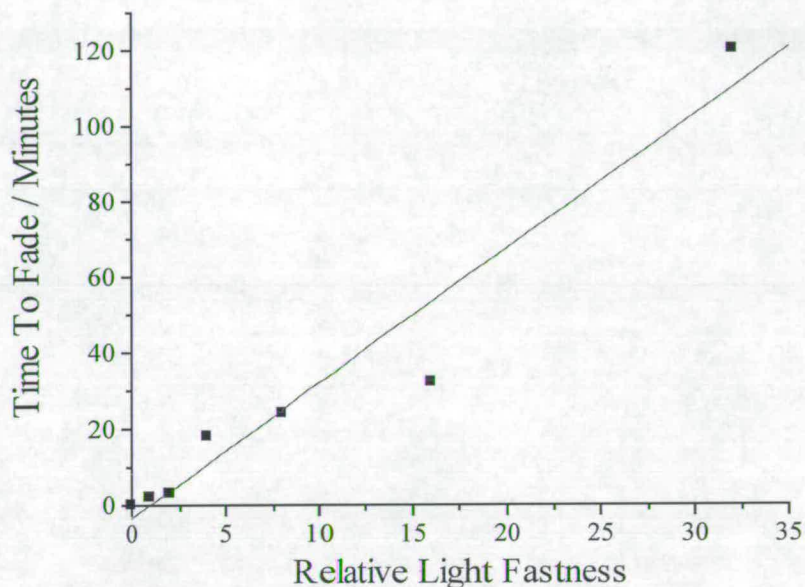
Figure 8.1 – Plot of time to fade in minutes versus the relative light fastness for fading of blue wool scales at peak power output of 2.49 x 10^6 Wmm^{-2} from a 532nm laser output.

In order to reduce the time taken to fade the samples the power density was increased, this was done gradually so as not to cause the fabric to be damaged. The results from the increased power output are shown in tables 8.2 to 8.4.

Band	1	2	3	4	5	6
Relative Light Fastness	1	2	4	8	16	32
Time to Fade/minutes	0.5	0.75	6.0	10.4	20.1	30.2

Table 8.2 - Data for fading of blue wool scales with power output of 4.5 x 10^6 Wmm^{-2} from a 532nm laser output.
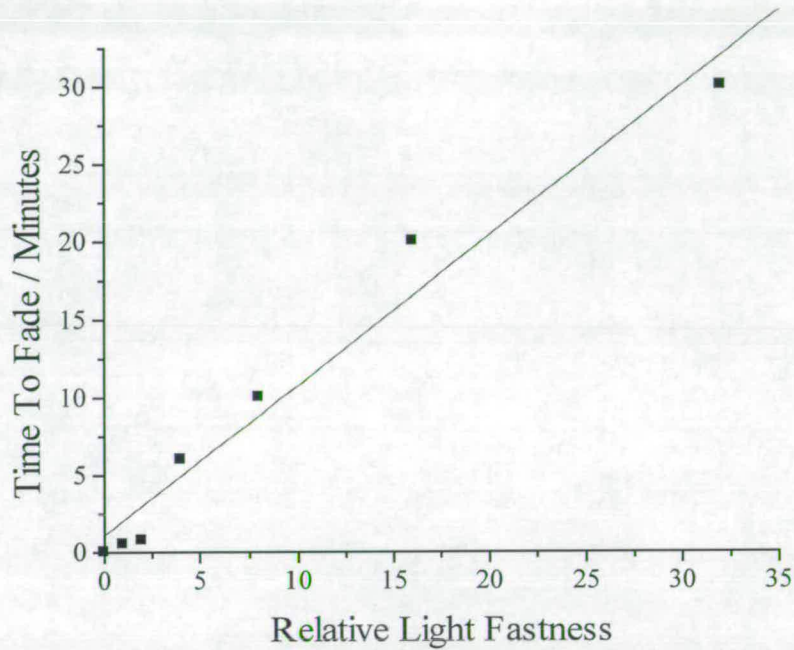
Figure 8.2 – Plot of time to fade in minutes versus the relative light fastness for fading of blue wool scales at peak power output of 4.5 x 10^6 Wmm^{-2} from a 532nm laser output.

Band	1	2	3	4	5	6
Relative Light Fastness	1	2	4	8	16	32
Time to Fade/seconds	8	15	40	44	50	55

Table 8.3 - Data for fading of blue wool scales with power output of 6 x 10^6 Wmm^{-2} from a 532nm laser output.
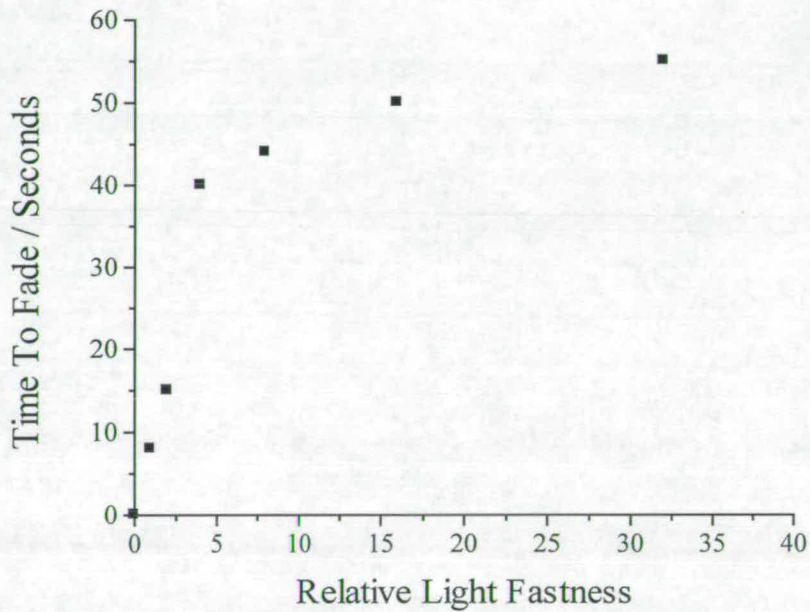
Figure 8.3 – Plot of time to fade in seconds versus the relative light fastness for fading of blue wool scales at peak power output of 6 x 10^6 Wmm^{-2} from a 532nm laser output.

Band	1	2	3	4	5	6
Relative Light Fastness	1	2	4	8	16	32
Time to Fade/seconds	4	9	10	15	18	22

Table 8.4 - Data for fading of blue wool scales with power output of 12×10^6 Wmm^{-2} from a 532nm laser output.
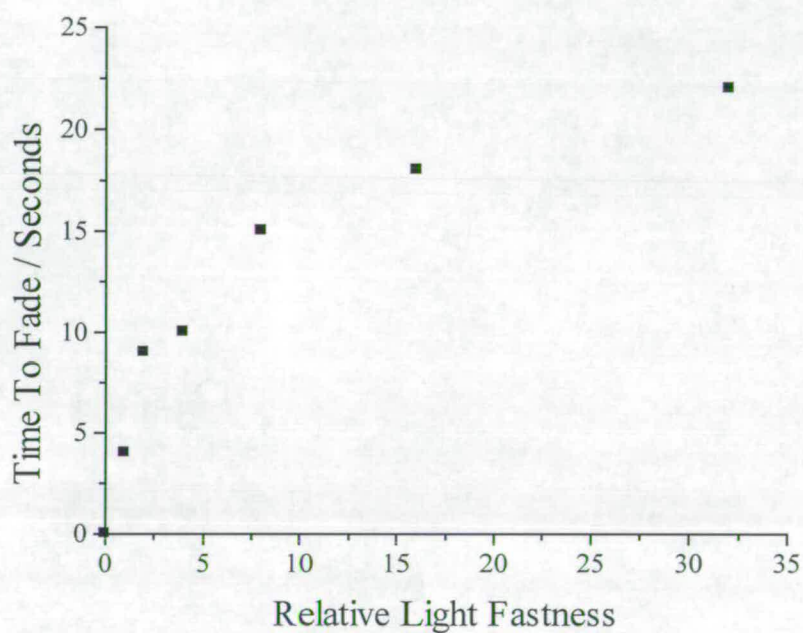
Figure 8.4 – Plot of time to fade in seconds versus the relative light fastness for fading of blue wool scales at peak power output of 12×10^6 Wmm^{-2} from a 532nm laser output.

The plots at peak powers of 2.49 x 10^6 and 4.5 x 10^6 Wmm^{-2}, figures 8.1 and 8.2, show a linear relationship between the relative light fastness and the time to fade. At the higher peak powers of 6 x 10^6 and 12 x 10^6, figures 8.3 and 8.4, the plots exhibit different behaviour. There is a linear relationship at greater times to fade, at shorter times to fade the plots begin to decay from linearity. These shorter fading times are of the order of seconds, thus the accuracy of the data points would be questioned due to the possibility of error in the judging the time taken to fade. Also, the pulse to pulse variation in the laser output may be significant for these short irradiation times, due to the small number of laser shots. This results in the power density effectively being higher for those samples, leading to anomalously short fading times. Monochromatic light at 532nm was used, it is likely that the different blue wool scale dyes have different absorption at this wavelength. This leads to the problem of comparing fading times obtained with the possibility of each dye absorbing differing amounts of energy at 532nm.

As is clear from the data, table 8.1 - 8.4, the fading times for the various bands of blue wool start to decrease as the power density is increased. The relationship between the peak power density and the time to fade as illustrated in figure 8.5 for relative light fastness 4, band 3, is clearly not linear. Rather, the time to fade decays as the power density increases through an exponential decay. The time to fade the highest light fast band, band 6 relative light fastness 32, goes from 120 minutes to only 22 seconds; this involves the power density increasing from 24.9 x 10^5 to 12 x 10^6. The time to fade the lowest light fast band goes from 2 minutes to 4 seconds, again this is accompanied by the power density increasing from 24.9 x 10^5 to 12 x 10^6.
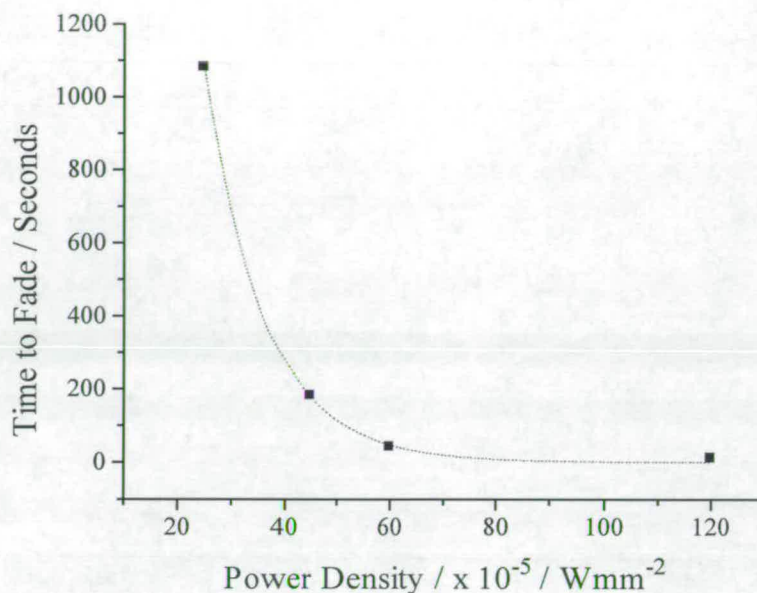
Figure 8.5 – Plot of time to fade versus power density for fading of blue wool scale band 3, relative light fastness 4.

8.3 – Dyed Cotton Samples

Given the ability to use laser irradiation to fade blue wool the fading of dyed cotton samples with a 532nm laser output was then investigated. The experimental set-up is defined in section 4.5.

8.3.1 – Red~2 on Cotton

It was found that the cotton dyed with red~2, an o-hydroxyazo dye, could be irradiated without damage at a peak power density of 4.5×10^6 Wmm^{-2} and wavelength of 532nm. The absorption of red~2 at 532nm is large in magnitude. The UV-Vis maximum for red~2 is 535nm, so the laser output of 532nm is almost at the maximum of the dye's absorbance. A sample of red~2 on cotton was irradiated with

a peak power density of 4.5×10^6 Wmm^{-2} for a total of 50 seconds, until the irradiated area faded. This is noted through the appearance of a dark brown colour. Having established that red~2 can be caused to fade on cotton with exposure to laser irradiation at 532nm, the effect that the loading of dye, or dyeing strength, has on the times to fade was investigated. The time to fade refers to the time taken for the dark brown colour to be established to a sufficient level as to be clearly visible. The greater the dye loading, or dye strength, the stronger and deeper the colour. Dye strength can be defined as the percentage mass applied to the cotton. A 2% dye strength involves application of 2g of dye for each 100g of cotton. The data in table 8.5 shows the dependence of the time taken to fade the sample on dye strength.

DYE STRENGTH / %	TIME / SECONDS
0.1	50
0.2	105
1	150
2	220
9	270

Table 8.5 – Data showing the relationship between the dye strength of red~2 on cotton and the time to fade it with laser output 532nm and power density 3 x 10^6 Wmm^{-2}.
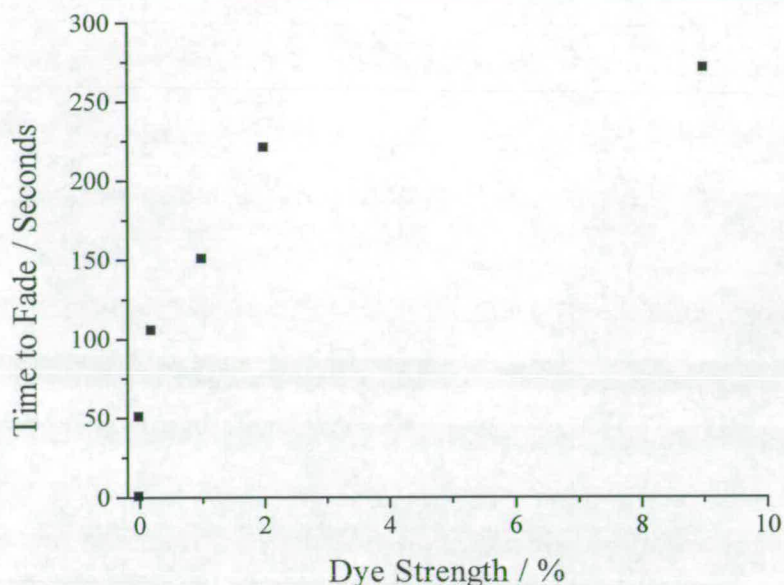
Figure 8.6 – Plot of time to fade versus dye strength for a sample of red~2 on cotton with laser output of 532nm and power density of 3 x 10^6 Wmm^{-2}. Plot is based on data in table 8.6.

The aggregation of a dye affects the value of the absorption co-efficient and the absorption co-efficient is a measure of the colour strength of the dye per mole. The colour strength is related to the dye strength. It is clear then, that the dye strength is an important property in dye technology. The need for a longer time to allow fading to occur on the greater dye strength samples is linked through the fact that the greater dye strength samples have more dye on the cotton. If a sample contains more dye then more photochemical product must be produced in order to give the same visual effect of fading, and thus a greater time is needed. Figure 8.6 illustrates qualitatively that the time to fade the sample does not increase linearly with dye strength. It is the case though that the plot appears to be linear at low fading times, this linearity does not persist at greater fading times, the perceived linearity is represented on figure 8.6. The deviation from linearity at higher dye strengths represents the approach towards exhaustive dyeing of the cotton and hence the approach to the maximum time of irradiation needed for fading to be achieved. The fading observed was fading of the upper layers of the dye, this gave the visual effect of fading. On the reverse side of

the fabric, in the area of faded dye on the front side, no fading was observed. Fading of a sample is not defined as being through all levels of the dye on the fibre, merely until a visual effect is observed. The results obtained from the use of a fadometer are in line with the results presented here. The general trend of greater times to fade as the shade, or dye strength, increases is seen with results from fadometers.

8.4 – Conclusions

The results in this chapter illustrate that with an appropriate peak power density, it is possible to irradiate a dyed textile sample and not cause any degradation of the fabric. The important outcome of this is that it is possible to use laser irradiation to cause photochemical change, that is, cause the dye to fade on the fabric. The advantage of the laser irradiation technique is the time scale that the experiments are completed in. The dyed fabrics that were investigated herein were all tested within minutes, exploratory testing took up to 2 hours but a higher peak power density reduced these times dramatically. The blue wool scales show fading times that increase with relative light fastness in a linear relationship. As the peak power densities are increased the relationship between relative light fastness and time to fade becomes curved. The times to fade the various light fast samples with a particular peak power density followed the pattern seen with fadometers, the greater the light fastness the greater the time to fade the sample. Exposure to laser irradiation causes red~2 on cotton to fade. The effect of dye strength has on the time to fade was investigated. The initial relationship between the dye strength and time to fade was linear but this linearity did not persist at greater dye strengths. These greater dye strengths represent the approach towards exhaustive dyeing of the cotton and hence the maximum time needed to cause photochemical change. If a sample contains more dye then more photochemical product must be produced in order to give the same visual effect of fading, and thus a greater time is needed. Further work is required to assess the practicality of the laser-induced fading experimental procedure, including variation of wavelength of laser output, applicability to other substrates - such as

polyesters, and other dye species. Development of a method to quantify the extent of fading would be highly desirable.

8.5 – Bibliography

1   P. F. Gordon & P. Gregory, *Organic Chemistry in Colour*, Springer-Verlag, **1987.**

CHAPTER 9 - CONCLUSIONS

The use of absorption spectroscopy alone to investigate dye aggregation is common practice. The results that have been presented in this thesis demonstrate the value of fluorescence spectroscopy as a sensitive probe in the detection and confirmation of aggregation, and show that the use of qualitative absorption spectroscopy alone may fail to detect aggregation. The commercially available reactive dyes that were studied all aggregated in aqueous and ethanolic solution, even at concentrations as low as 10^{-7} M. Both the monomer and dimer (aggregate) species of the dyes fluoresced; this was of particular interest in the case of turquoise~1, the copper phthalocyanine dye, since the observation of fluorescence from a phthalocyanine dimer is very rare.

The present work appears to be the first extensive application of fluorescence spectroscopy to investigate the aggregation of o-hydroxyazo dyes. There is a large amount of overlap between the absorption spectra of the monomer and dimer (aggregate) species; fluorescence spectroscopy has allowed the spectra of the two different species to be resolved. There is a domination of the dimer absorption spectrum over a wide concentration range; this leads to a lack of dependence of spectral profile on concentration. Aggregation is revealed through the deviation from Beer's law and not from the changing profile of the absorption spectrum.

The fact that the dyes studied aggregate is of interest to the dyestuffs industry, as discussed in chapter one. The effect of conditions in the dyebath on the state of aggregation of the dye prior to dyeing is of particular significance. Typically, the dye bath temperature is 80°C and salt is present at a concentration of about is $70gL^{-1}$ (1.2M) to aid the fixation process. In the present work it was shown that increasing the temperature of the dye solution decreases the extent of aggregation. Non-aqueous solvents, such as ethanol and DMSO, were also found to decrease the extent of aggregation in comparison to the aqueous environment. The variable that appears to induce the greatest change in the state of aggregation is the ionic strength. Indeed, the increase in dimerisation produced by the addition of salt to solutions of red~2 afforded the only significant change in the absorption envelope of an o-hydroxyazo

dye that was observed throughout this study. The outcome of theoretical modelling of the concentration dependence of the extinction coefficient of the phthalocyanine dye, turquoise~1, was particularly interesting. The model indicated that the formation of trimers and higher aggregates is suppressed at high salt concentration (>0.01M). This is contrary to the commonly held belief that the addition of salt increases the degree of aggregation. Further work is required to see if the effect of high salt concentration is common to other dyes.

The present work has shown that under typical dye bath conditions the dyes studied will be aggregated. Further work of interest would involve investigating the state of aggregation of dyes as they go from solution to being chemically bonded to the fabric. Fluorescence might provide a way of probing this and a preliminary experiment showed that it was possible to detect fluorescence from red~2 on cotton. The emission spectrum of red~2 on cotton suggested that the dye was aggregated to a greater extent than when in solution. It would be of interest to affix a cellulose unit chemically to the dye to investigate the effect of the cellulosic environment on the fluorescence spectrum, in order to assess whether the spectral effect observed on cotton is, in fact, an indicator of aggregation.

In an exploratory study of laser-induced fading, it was shown that, using an appropriate peak power density, it is possible to irradiate a dyed textile sample and cause photochemical change (fading) without degradation of the fabric. The main advantage of the laser irradiation technique, over the current fadometer test method, is the short measurement time. The dyed fabrics that were investigated were all tested within minutes. The fading occurs in line with standards set by the international dyestuffs industry, greater times taken to fade for higher light fastness and dye strength.

Further work is required to fully assess the practicality of the laser-induced fading technique, including variation of wavelength of laser output, applicability to other substrates - such as polyesters, and other dye species. Development of a method to quantify the extent of fading would be highly desirable. The initial results suggest that laser-induced fading shows potential.

PUBLICATIONS

[1] Observation of a Fluorescent Dimer of a Sulphonated Phthalocyanine, N. M. Speirs, W. J. Ebenezer and A. C. Jones, *PhotoChem. And PhotoBiol.*, 76(3), **2002**, 247-251.

[2] Aggregation of copper (II) tetrasulphonated phthalocyanine in aqueous salt solutions, P. J Camp, A. C. Jones, N. K. Neely and N. M. Speirs, *J. Phys. Chem. A*, 106, **2002**, 10725-10732.

[3] A Spectroscopic Study of the Aggregation of *o*-hydroxyazo Reactive Dyes, N. M. Speirs, W. J. Ebenezer and A. C. Jones, manuscript in preparation.

Observation of a Fluorescent Dimer of a Sulfonated Phthalocyanine[¶]

Neil M. Speirs[1], Warren J. Ebenezer[2] and Anita C. Jones*[1]

[1]Department of Chemistry, The University of Edinburgh, Edinburgh, UK and
[2]Dystar UK Ltd, Cheadle Hulme, Cheshire, UK

ABSTRACT

With very few exceptions, phthalocyanine dimers are found to be nonfluorescent. We report here the observation of a fluorescent dimer of a tetrasulfonated copper phthalocyanine in ethanol and water. Fluorescence excitation and emission spectra at room temperature and at 77 K are presented. These are consistent with the conventional model of exciton coupling in a cofacial dimer.

INTRODUCTION

Sulfonated phthalocyanines are well known to dimerize in aqueous solution. The influence of dimerization or aggregation on the photochemical properties of these molecules has important consequences in their traditional application as textile dyes and in their more recent use as photosensitizers in photodynamic therapy. In dyeing, aggregation is believed to enhance light fastness, which is a beneficial effect, but may also unfavorably affect the color quality of the dye. In photodynamic therapy, phthalocyanine dimers appear to be much less active as sensitizers than do monomers.

The dimerization of phthalocyanines (and the closely related porphyrins) and its effects on the UV–Vis absorption spectrum are well documented in the literature (1–10). Dimerization results in a significant blueshift in the Q band region together with some band broadening. That is, the absorption band of the dimer species lies at higher energy than does that of the monomer. This can be explained in terms of exciton coupling between the two monomer chromophores (4,5,11). For an eclipsed cofacial phthalocyanine dimer with overall D_{4h} symmetry (*i.e.* a centrosymmetric dimer with the two rings lying parallel), the Q (^1E_u) state of the monomer is split into two states, an upper state (E$_+$) of ^1E_u symmetry and a lower state (E$_-$) of ^1E_g symmetry. The pure electronic transition from the dimer ground state to the E$_-$ state is strictly forbidden. The observed transition to the E$_+$ state lies at higher energy than does the corresponding monomer transition. As illustrated in Fig. 1, the excitation energy of the two excitonic components of the electronic origin of a dimer (M$_2$) is given by

$$E_{\pm} = E_M + \Delta I \pm X \qquad (1)$$

where E_M is the excitation energy of the isolated monomer, ΔI the change in intermolecular interaction energy on excitation of M in the dimer (I′ − I″ in Fig. 1) and X the half-exciton splitting caused by the excitation exchange interaction between the two identical chromophores in the dimer (12–14).

Phthalocyanine dimers are found generally to be nonfluorescent (11,15–21). This is explained to some extent by exciton splitting because the fluorescence transition from the lower E$_-$ state to the ground state is formally forbidden for D_{4h} dimers. But the transition may gain intensity, giving rise to fluorescence, if the equilibrium geometry is distorted from a centrosymmetric structure by tilting or twisting of the monomer units. The transition may also be induced by vibronic coupling. Each vibrational level of the monomer gives rise to two vibrational levels in the dimer, the plus and minus combinations of the monomer states, v$_+$ and v$_-$, although the splitting between these levels is usually too small to be resolved. Vibronically allowed transitions can occur from the E$_-$ exciton state to the v$_-$ levels in the ground state.

In covalently bridged cofacial μ-oxo porphyrin dimers, both absorption and fluorescence of the lower exciton state have been observed (22–24), and this has been attributed to the tilting of the porphyrin planes from coplanarity. But a similar covalently bridged face-to-face stacking phthalocyanine dimer, bis(phthalocyanato)tin (IV), which showed relatively intense absorption to the E$_-$ state, was found to be nonfluorescent (11). Absorption to the lower exciton state has also been observed in nonfluorescent dimers of sulfonated phthalocyanines (17,21). Thus, in phthalocyanine dimers there appears to be an effective nonradiative decay channel, which inhibits fluorescence even when the E$_-$ state has a significant transition moment. A facile pathway for internal conversion in the dimer would account for both the absence of fluorescence and the reduction in photodynamic activity, the latter as a consequence of the decreased triplet quantum yield. It has been proposed that a low-lying dipole-forbidden charge-resonance state facilitates the rapid radiationless decay. This state has been theoretically predicted to lie at lower energy than does the lowest excited singlet state in nonfluorescent bis(phthalocyanato)tin (IV) but at higher energy in fluorescent μ-oxo bridged porphyrin dimers (11,24).

Neil M. Speirs *et al.*

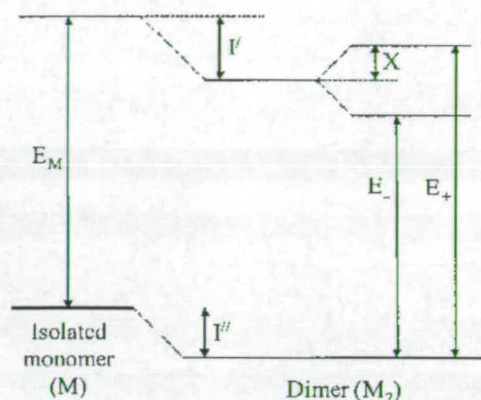**Figure 1.** Energy level diagram illustrating the relationship between monomer and dimer excitation energies.

Figure 2. The structure of $CuPcS_4$. One (as shown) or two of the sulfonate substituents carry monochlorotriazine groups.

Fluorescence from phthalocyanine dimers is not completely unknown. Oddos-Marcel *et al.* reported weak fluorescence from an oxygen-bridged silicon phthalocyanine dimer (25). The absorption bands of both lower and upper exciton states were observed, lying bathochromic and hypsochromic to the monomer band, respectively, with an exciton splitting of ~3800 cm^{-1}. The emission spectrum of the lower exciton state was in the range 8000–12000 cm^{-1}, with its short-wavelength tail overlapping the long-wavelength edge of the absorption spectrum. The fluorescence quantum yield of the dimer was ~10^{-3} that of the monomer. Similar absorption spectra and weak near-infrared emission were reported for Si–O–Ge and Si–O–Sn dimers (26).

There have been two previous reports of fluorescence from noncovalent dimers of sulfonated phthalocyanines, which have been refuted by subsequent studies. Yoon *et al.* (27) reported fluorescence from a dimer of chloroaluminium (III) phthalocyanine tetrasulfonate. In aqueous ethanolic solution they observed concentration-dependent absorption and fluorescence bands, both redshifted relative to the monomer spectra, which they attributed to a dimer. But all emission spectra presented were excited at the wavelength of the monomer Q band. The dimer absorption band was not directly excited, and the excitation spectrum of the alleged dimer emission was not reported. This work was subsequently challenged by Dhami *et al.* (17), who demonstrated that the concentration dependence of the fluorescence spectrum could be accounted for by reabsorption effects. Dhami found that the excitation of the redshifted dimer absorption band yielded no detectable emission. In a later study Kaneko *et al.* (28) observed redshifted absorption and emission bands in solutions of zinc(II) tetrasuphonatophthalocyanine in aqueous acetonitrile, which they attributed to a fluorescent dimer. The fluorescence excitation spectrum of the alleged dimer was shown to coincide with the redshifted absorption band. The Stokes shift between the dimer absorption and the emission spectra was very small, as for the monomer. In pure water a 'normal' dimer was observed, nonfluorescent, with a blueshifted absorption band and was assumed to have an eclipsed cofacial geometry. The formation of a fluorescent dimer in aqueous acetonitrile was attributed to a solvent-induced change in geometry to a slipped or tilted conformation. But subsequent work by Beeby *et al.* (29) has
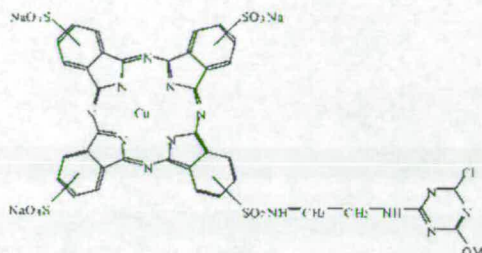
shown that the redshifted absorption and emission bands observed by Kaneko *et al.* are caused by protonation of the phthalocyanine monomer and not by the formation of a fluorescent dimer.

Recently, the formation of fluorescent aggregates by a tetra-solketal–substituted zinc phthalocyanine has been reported by Farren *et al.* (30). At low temperature (<175 K) this compound shows very strong aggregation. The growth of the characteristic blueshifted dimer absorption band with decreasing temperature is accompanied by the appearance of a new redshifted emission peak, which is attributed to a fluorescent dimer. The excitation spectrum of the redshifted emission correlates well with the dimer absorption band.

We report here the formation of a fluorescent cofacial dimer by a tetrasulfonated copper phthalocyanine ($CuPcS_4$) dye. This is a commercial dye in which one or two of the sulfonate groups carry a monochlorotriazine substituent, as shown in Fig. 2. The sample consists of approximately equimolar quantities of mono- and di-substituted compounds, both being a mixture of isomers (with different positions of sulfonation).

MATERIALS AND METHODS

Absorption spectra were recorded on a Unicam model UV-200 spectrometer, using fused silica cuvettes with a 1 cm path length. Fluorescence spectra were recorded on a Jobin Yvon Fluoromax spectrofluorimeter: a photon-counting spectrometer with a high-pressure xenon lamp as excitation source and a red-extended photomultiplier tube (Hamamatsu R928) as detector. Excitation and emission monochromator slits were set at a bandwidth of 5 nm. The response of the photomultiplier falls off steeply above 830 nm, and spectra were not recorded above this wavelength. Spectra were processed using the Jobin Yvon Datamax (Grams 386-based) software package. Excitation spectra were corrected for the spectral profile of the xenon lamp, and emission spectra were corrected for the spectral response of the photomultiplier tube.

For room temperature fluorescence measurements, samples were contained in disposable poly(methyl methacrylate) cuvettes with a 1 cm path length. These cuvettes have 100% transmission at wavelengths greater than 280 nm. For measurements at 77 K the samples were contained in fused silica tubes and cooled in liquid nitrogen in a fused silica dewar.

The sample of $CuPcS_4$ was synthesized in the research laboratory of DyStar UK Ltd and analyzed using comparative thin-layer chromatography, UV–Vis spectroscopy and mass spectrometry. Millipore deionized water and ethanol (Acros spectrophotometric grade) were used as solvents and were checked to insure that they were nonfluorescent in the region of interest before use. To record fluorescence spectra at 77 K, ethanol was used as solvent in preference to water because it freezes to form a high-quality transparent glass. When dissolved in ethanol the $CuPcS_4$ molecules are expected to carry the water of hydration associated with the sulfonate salt groups into the ethanolic solution.
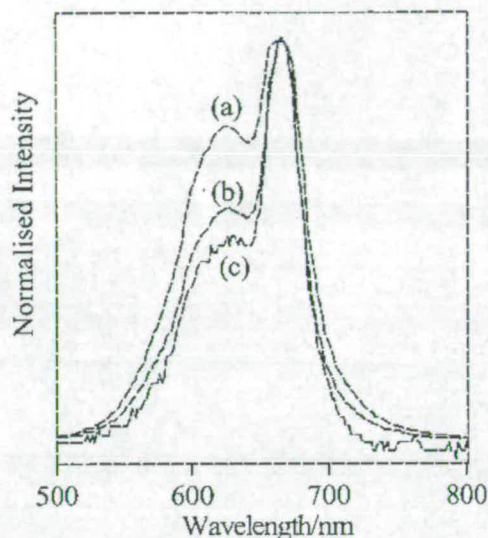
Figure 3. Absorption spectra of CuPcS$_4$ in aqueous solution at room temperature at concentrations of 10^{-4} M (a), 10^{-5} M (b) and 10^{-6} M (c).

Figure 4. Fluorescence emission spectra of a 10^{-5} M solution of CuPcS$_4$ in ethanol at room temperature at excitation wavelengths of 600 nm (a), 620 nm (b) and 650 nm (c).

RESULTS

The Q band region of the electronic absorption spectrum of CuPcS$_4$ in aqueous solution is shown in Fig. 3 for concentrations from 10^{-6} M to 10^{-4} M. At 10^{-6} M concentration the narrow Q band of the monomer at 665 nm is distinct. As the concentration increases, the spectrum broadens, and the band on the short wavelength side of the Q band, peaking at ~625 nm, increases in intensity. These observations are typical of the well-known spectral effects of dimerization of phthalocyanines and porphyrins. The hypsochromically shifted absorption band indicates the presence of dimers of CuPcS$_4$. Similar absorption spectra are observed in ethanol.

The fluorescence of CuPcS$_4$ is not intense but is easily detectable. The fluorescence spectra of a 10^{-5} M solution in ethanol, at various excitation wavelengths, are shown in Fig. 4. It can be seen that excitation of the monomer Q band at 650 nm gives a spectrum with a clearly defined Q band emission peak at 680 nm. As the excitation wavelength is decreased, giving preferential excitation of dimer over monomer species, the emission spectrum broadens slightly to the blue and more noticeably to the red. Measurement of the excitation spectrum as a function of emission wavelength (Fig. 5) confirms the observation of dimer fluorescence. As the emission wavelength is increased, the intensity of the monomer Q band decreases and the blueshifted dimer excitation band predominates. Comparison of Figs. 3 and 5 shows that the excitation spectrum of the redshifted dimer fluorescence coincides with the characteristic blueshifted dimer absorption band. Analogous fluorescence behavior was observed for aqueous solutions of CuPcS$_4$. The results for ethanol solutions are presented here because there is a greater Stokes shift, enabling better spectra of the monomer Q band to be obtained, and because ethanol was used for measurements at 77 K.

The dependence of the emission spectrum on excitation wavelength in ethanol glass at 77 K is shown in Fig. 6.
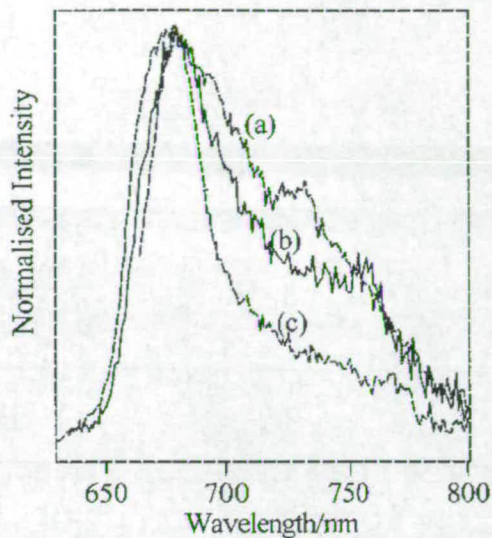
Excitation at 640 nm gives the fluorescence spectrum of the monomer, with a characteristic intense, narrow 0–0 band at 673 nm and two relatively weak vibronic bands with a vibronic interval of ~700 cm^{-1}. When the excitation wavelength is decreased to 600 nm, a shoulder appears to the blue of the monomer 0–0 and another to the red. Exciting at 580 nm, these shoulders become clearly defined bands at 658 and 688 nm, with another weaker band apparent at about 720 nm. These new bands constitute the spectrum of the dimer, with the 0–0 transition at 658 nm shifted ~300 cm^{-1} to the blue of the monomer 0–0.
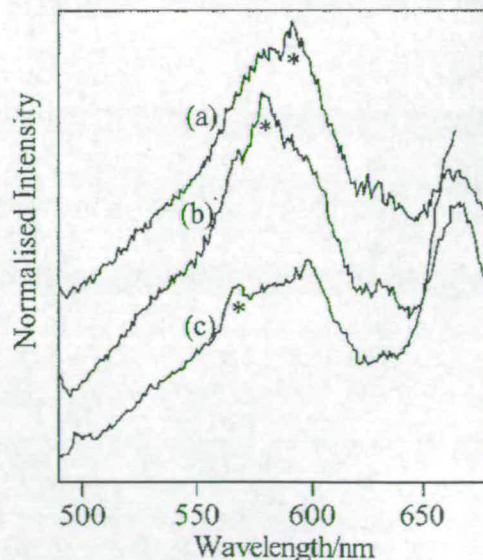
Figure 5. Fluorescence excitation spectra of a 10^{-5} M solution of CuPcS$_4$ in ethanol at room temperature at emission wavelengths of 720 nm (a), 700 nm (b) and 680 nm (c). "*" Indicates a solvent Raman band.

Neil M. Speirs *et al.*
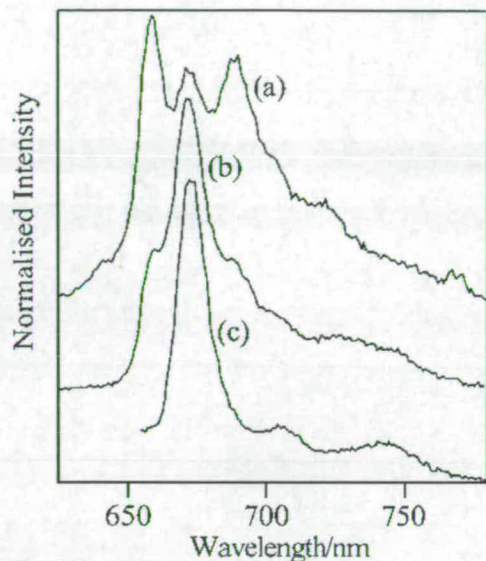
Figure 6. Fluorescence emission spectra of a 10^{-5} *M* solution of CuPcS$_4$ in ethanol at 77 K at excitation wavelengths of 580 nm (a), 600 nm (b) and 640 nm (c).

Figure 7. Fluorescence excitation spectra of a 10^{-5} *M* solution of CuPcS$_4$ in ethanol at 77 K at emission wavelengths of 720 nm (a), 687 nm (b) and 680 nm (c).

The excitation spectrum detected at 680 nm shown in Fig. 7c is characteristic of the monomer. Detection at 687 and 720 nm, corresponding to the dimer vibronic bands, gives a broad excitation band to the blue of the monomer 0–0 (Fig. 7a,b), which is very similar to the dimer excitation spectrum seen at room temperature.

DISCUSSION

The large shift between the dimer excitation and the emission spectra is consistent with the conventional model of exciton coupling in a cofacial phthalocyanine dimer in which the monomer transition moments are parallel, *i.e.* an upper allowed exciton state and a lower forbidden state. The observation of this large shift in frozen ethanol at 77 K rules out the possibility that this is because of solvent relaxation about the initially excited state or rearrangement of the structure of the Franck–Condon excited state. Although fluorescence from the lower exciton state is observed, there is no evidence of an absorption transition to this state, indicating that the transition moment remains small compared with that of the upper exciton state. Therefore, the observation of fluorescence appears to be primarily the result of an increase in fluorescence quantum yield in the emitting dimer species. This may be associated with the E$_-$ state becoming lower in energy than a low-lying charge-resonance state. The most obvious difference between CuPcS$_4$ and previously studied nonfluorescent sulfonated phthalocyanines is the presence of the monochlorotriazine substituents, which may perturb the electronic structure of the dimer. It is interesting that the recently reported fluorescent zinc phthalocyanine dimer (30) also has sizeable peripheral substituents, which Farren *et al.* suggest may influence the conformation of the dimer, perhaps producing a clamshell geometry.

The splitting between the upper and lower exciton states can be estimated from the shift between the dimer absorption
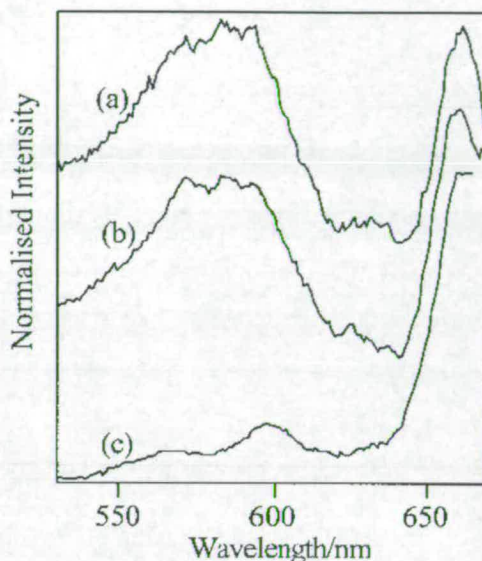
and emission spectra. Taking the separation between the rising edge of the excitation band and the emission 0–0 band to be ∼1300 cm^{-1}, and assuming that the Stokes shift of the dimer fluorescence is the same as that of the monomer (250 cm^{-1}), the exciton splitting (2X in Eq. 1) is estimated to be at least 1000 cm^{-1}. The lower exciton level lies 300 cm^{-1} above the monomer S$_1$ state, indicating a decrease in binding energy of the dimer on excitation of at least 800 cm^{-1}.

There is a noticeable difference between the intensity of vibronic bands in the dimer and monomer fluorescence spectra at 77 K (Fig. 6), demonstrating the contribution of vibronic coupling to the dimer spectrum. The high relative intensity of vibronically induced transitions, to v$_-$ levels of the ground state, in the dimer spectrum contrasts with the very low Franck–Condon intensity of vibronic transitions in the monomer spectrum.

The narrow vibronic structure of the dimer emission spectrum at 77 K indicates that the fluorescence arises from a single dimer structure or a small distribution of similar structures. But the dimer excitation spectrum at 77 K is broad, resembling that at room temperature, indicating absorption by a variety of dimer species in which the monomer experiences different intermolecular interactions and exciton splitting. The existence of several dimer species is not surprising given the presence of monosubstituted and disubstituted monomers plus isomers with different positions of sulfonation of the phthalocyanine nucleus. There must be efficient energy transfer from the various excited dimer species to the single emitting species, implying that the different species exist in close proximity as constituents of larger aggregates. Comparison of the dimer excitation and absorption spectra shows that most of the intensity in the excitation spectrum is caused by species that absorb in the short-wavelength tail of the absorption spectrum and contribute relatively little to the total absorption intensity. The fluorescence arises from excitation of the minority of the dimers, with the majority being nonfluorescent

themselves and unable to transfer their excitation energy to the higher energy–emitting species.

There are significant similarities between the dimer fluorescence observed here and that reported recently by Farren *et al.* (30) for tetra-solketal–substituted zinc phthalocyanine. In both cases the excitation spectrum of the dimer fluorescence correlates well with the characteristic blueshifted dimer absorption band, and there is a large Stokes shift between the dimer emission and the blueshifted absorption band. These features are indicative of absorption to the upper exciton state and emission from the lower exciton state in a dimer species and are quite distinct from the fluorescence properties of phthalocyanine monomers, which exhibit an extremely small Stokes shift between absorption and emission bands. In contrast, the redshifted absorption and emission bands attributed by Kaneko *et al.* (28) to a tetrasulfonated zinc phthalocyanine dimer were monomer-like in appearance with a very small Stokes shift and, indeed, were subsequently shown to be caused by the protonated monomer (29).

CONCLUSIONS

$CuPcS_4$ forms a fluorescent dimer in both ethanol and water. The emission spectrum of the dimer shows a large shift from its excitation spectrum, which is blueshifted relative to the monomer. This is consistent with the conventional model of exciton coupling in a cofacial dimer, *i.e.* excitations to the upper exciton state and emission from the formally forbidden lower exciton state. The absence of an appreciable absorption transition to the lower exciton state indicates that the fluorescent dimer shows little deviation from an eclipsed cofacial structure. There is a distribution of dimer species present in solution, but most of these are nonfluorescent. The emission of fluorescence appears to be restricted to a particular species in which a usually dominant nonradiative decay channel is absent. The observation at 77 K of energy transfer from multiple-absorbing dimer species to a single-emitting species suggests that the dimers are constituents of larger aggregates.

REFERENCES

1. Leznoff, C. C. and A. B. P. Lever (1989) *Phthalocyanines Properties and Applications.* VCH Publishers.
2. Gouterman, M. (1978) Optical spectra and electronic structure of porphyrins and related rings. In *The Porphyrins*, Vol. III (Edited by D. Dolphin), pp. 1–156. Academic Press, San Diego.
3. Sheppard, S. E. and A. L. Geddes (1944) Effects of solvents on the absorption spectra of dyes. IV. Water as solvent: a common pattern. *J. Am. Chem. Soc.* **66**, 1995–2002.
4. Gouterman, M., D. Holten and E. Lieberman (1977) Porphyrins XXXV. Exciton coupling in μ-oxo scandium dimers. *Chem. Phys.* **25**, 139–153.
5. Dodsworth, E. S., A. B. P. Lever, P. Seymour and C. C. Leznoff (1985) Intramolecular coupling in metal-free binuclear phthalocyanines. *J. Phys. Chem.* **89**, 5698–5705.
6. Monahan, A. R., J. A. Brado and A. F. DeLuca (1972) The dimerization of a copper(II)-phthalocyanine dye in carbon tetrachloride and benzene. *J. Phys. Chem.* **76**, 446–449.
7. Yang, Y. C., J. R. Ward and R. P. Seiders (1985) Dimerization of cobalt(II) tetrasulfonated phthalocyanine in water and aqueous alcoholic solutions. *Inorg. Chem.* **24**, 1765–1769.
8. Kobayashi, N., Y. Nishiyama, T. Ohya and M. Sato (1987)

9. Gasyna, Z., N. Kobayashi and M. J. Stillman (1989) Optical absorption and magnetic circular dichroism studies of hydrogen, copper(II), zinc(II), nickel(II) and cobalt(II) crown ether-substituted monomeric and dimeric phthalocyanines. *J. Chem. Soc., Dalton Trans.* 2397–2405.
10. Hush, N. S. and I. S. Woolsey (1971) The electronic absorption spectra of phthalocyanine monomers and dimers. *Mol. Phys.* **21**, 465–474.
11. Ohno, O., N. Ishikawa, H. Matsuzawa, Y. Kaizu and H. Kobayashi (1989) Exciton coupling in bis(phthalocyanoto)tin(IV). *J. Phys. Chem.* **93**, 1713–1718.
12. Craig, D. P. and S. H. Walmsley (1968) *Excitons in Molecular Crystals.* Benjamin, New York.
13. McClure, D. S. (1958) Energy transfer in molecular crystals and in double molecules. *Can. J. Chem.* **36**, 59–71.
14. Murrell, J. N. and J. Tanaka (1964) The theory of the electronic spectra of aromatic hydrocarbon dimers. *Mol. Phys.* **7**, 363–380.
15. Spikes, J. D. and J. C. Bommer (1986) Zinc tetrasulphophthalocyanine as a photodynamic sensitizer for biomolecules. *Int. J. Radiat. Biol.* **50**, 41–47.
16. Negri, R. M., A. Zalts, E. A. San Roman, P. F. Aramendia and S. E. Braslavsky (1991) Carboxylated zinc phthalocyanine, influence of dimerization on the spectroscopic properties—an absorption, emission and thermal lensing study. *Photochem. Photobiol.* **53**, 317–322.
17. Dhami, S., A. J. de Mello, G. Rumbles, S. M. Bishop, D. Phillips and A. Beeby (1995) Phthalocyanine fluorescence at high concentration: dimers or reabsorption effect? *Photochem. Photobiol.* **61**, 341–346.
18. Fernandez, D. A., J. Awruch and L. E. Dicelio (1996) Photophysical and aggregation studies of *t*-butyl substituted Zn phthalocyanines. *Photochem. Photobiol.* **63**, 784–792.
19. Lagorio, M. G., L. E. Dicelio and E. San Roman (1993) Visible and near-IR spectroscpic and photochemical study of substituted metallophthalocyanines. *J. Photochem Photobiol.* **72**, 153–161.
20. Ferencz, A., D. Neher, M. Schulze, G. Wegner, L. Viane and F. C. De Schryver (1995) Synthesis and spectroscopic properties of phthalocyanine dimers in solution. *Chem. Phys. Lett.* **245**, 23–29.
21. Ostler, R. B., A. D. Scully, A. G. Taylor, I. R. Gould, T. A. Smith, A. Waite and D. Phillips (2000) The effect of pH on the photophysics and photochemistry of di-sulphonated aluminium phthalocyanine. *Photochem. Photobiol.* **71**, 397–404.
22. Gouterman, M., D. Holten and E. Lieberman (1977) Porphyrins XXXV. Exciton coupling in μ-oxo scandium dimers. *Chem. Phys.* **25**, 139–153.
23. Kaizu, Y., N. Misu, K. Tsuji, Y. Kaneko and H. Kobayashi (1985) Electronic spectra of the aluminium (III) complexes of 5,10,15,20-tetraphenylporphin and 2,3,7,8,12,13,17,18-octaethylporphin. *Bull. Chem. Soc. Jpn.* **58**, 103–108.
24. Ohno, O., Y. Kaizu and H. Kobayashi (1985) Luminescence of some metalloporphyrins including the complexes of the IIb metal group. *J. Chem. Phys.* **84**, 1779.
25. Oddos-Marcel, L., F. Madeore, A. Bock, D. Neher, A. Ferencz, H. Rengel, G. Wegner, C. Kryschi and H. P. Trommsdorf (1996) Electronic states and relaxation dynamics of silicon phthalocyanine dimers. *J. Phys. Chem.* **100**, 11850–11856.
26. Pelliccioli, A. P., K. Henbest, G. Kwag, T. R. Carvagno, M. E. Kenney and M. A. J. Rodgers (2001) Synthesis and excited state dynamics of μ-oxo group IV metal phthalocyanine dimers: a laser photoexcitation study. *J. Phys. Chem. A* **105**, 1757–1766.
27. Yoon, M., Y. Cheon and D. Kim (1993) Absorption and fluorescence spectroscopic studies on dimerization of chloroaluminum (III) phthalocyanine tetrasulfonate in aqueous alcoholic solutions. *Photochem. Photobiol.* **58**, 31–36.
28. Kaneko, Y., T. Arai, K. Tokamaru, D. Matsunaga and H. Sakuragi (1996) Observation of a novel fluorescent dimer of zinc tetrasulphonatphthalocyanine. *Chem. Lett.* 345–346.
29. Beeby, A., S. Fitzgerald and C. F. Stanley (2001) Protonation of tetrasulfonated zinc phthalocyanine in aqueous acetonitrile solution. *Photochem. Photobiol.* **74**, 566–569.
30. Farren, C., S. Fitzgerald, A. Beeby and M. R. Bryce (2002) The first genuine observation of fluorescent mononuclear phthalocyanine aggregates. *Chem. Commun.* 572–573.

Aggregation of Copper(II) Tetrasulfonated Phthalocyanine in Aqueous Salt Solutions

Philip J. Camp,* Anita C. Jones, Robert K. Neely, and Neil M. Speirs

School of Chemistry, University of Edinburgh, West Mains Road, Edinburgh EH9 3JJ, United Kingdom

Received: July 17, 2002; In Final Form: September 2, 2002

The aggregation of a copper(II) tetrasulfonated phthalocyanine ($CuPcS_4$) dye in aqueous sodium chloride solution has been studied using UV–vis spectroscopy and statistical mechanics. The concentration dependences of the molar absorption coefficients at 626 and 665 nm have been measured for $CuPcS_4$ solutions with concentrations in the range 10^{-7} to 10^{-3} M and salt concentrations between 0 and 2 M. It is commonly believed that such results can be fitted adequately by assuming that a monomer–dimer equilibrium operates in the solution, but it is shown that this model has serious deficiencies, particularly at low salt concentrations. The experimental results have been analyzed using new expressions derived using statistical mechanics, taking into account the formation of trimers and higher aggregates. The model is based on the fact that π–π interactions between the essentially planar phthalocyanine molecules favor the formation of columnar aggregates. Therefore, cluster partition functions can be approximated in terms of two parameters corresponding to molecules with one and two nearest neighbors within the stack. The resulting theoretical expressions are shown to provide excellent fits to the experimental results over the entire range of dye and salt concentrations considered. The fitted equilibrium constants using the monomer–dimer equilibrium indicate an increase in aggregation with increasing salt concentration. In contrast, the fitted equilibrium constants from the new theory indicate that aggregation is suppressed at high salt concentrations.

1. Introduction

The aggregation of phthalocyanine (Pc), and related dye molecules, has been the subject of intensive study over many decades.[1] Water-soluble Pcs are used widely as textile dyes, and aggregation has significant effects on the light fastness and color quality of the dyestuff. In recent years, interest in Pc aggregation has been stimulated by the adoption of Pcs as photosensitizers in photodynamic cancer therapy and the observation that aggregates are much less active than monomers. Pcs are usually quite strongly aggregating because the planar molecular geometry admits significant π–π interactions between molecules, hence stabilizing columnar aggregates. Spectroscopic techniques can often be employed to analyze the nature and degree of aggregation. In Pcs, the UV–vis absorption spectrum is dominated by the Q-band arising from π–π^* transitions. Usually, one can assign individual peaks within the Q-band to either free molecules or molecules contained within aggregates, and hence the degree of aggregation within the solution can be inferred from the respective peak intensities. In general, the aggregate peak is blue-shifted with respect to the monomer peak because of the cooperative interaction between transition dipole moments on molecules within an aggregate. Quantitative predictions for the shift can be obtained using the molecular exciton approximation.[2] In Pc aggregates, this approximation is compromised by the presence of the strong π–π interactions, but the general trends remain valid.[3]

One of the earliest systematic studies of Pc aggregation was carried out by Gruen.[4] In this work, the aggregation in two different copper phthalocyanine reactive dyes was investigated by measuring the absorption spectra in various solvents. Spectra measured in aqueous solutions with dye concentrations in the range 2.0×10^{-6} to 2.0×10^{-4} kg L^{-1} showed relatively little variation, which was interpreted as indicating a very high equilibrium constant, such that the dye was almost entirely associated over this concentration range. Spectra measured at fixed solute concentration (2.0×10^{-6} kg L^{-1}) in different solvents, or at different ionic strengths, were observed to intersect at isosbestic points, suggesting that a simple monomer–dimer equilibrium operates in these systems. On the basis of the relative monomer and aggregate peak heights, it was concluded that aggregation increases with increasing solvent polarity and with increasing salt concentration. These results were explained on the basis of ionic and dielectric screening of the repulsions between like charges on the solvated Pc molecules.

There have been many subsequent studies of aggregation in solutions of phthalocyanine compounds (e.g., refs 3, 5, and 6). In ref 5, Yang et al. studied the monomer–dimer equilibrium in cobalt tetrasulfonated phthalocyanines in water and aqueous alcoholic solutions with solute concentrations up to 2×10^{-5} M. Equilibrium constants extracted from absorption measurements indicated nontrivial solvent effects that were probably due to the interplay between solute–solvent and water–alcohol interactions.

In ref 6, Martin et al. investigated the effects of pH and ionic strength on the dimerization of aluminum and zinc sulfonated phthalocyanines in aqueous solution, with solute concentrations up to 10^{-5} M. It was concluded that an increase in pH or ionic strength leads to an increase in the monomer–dimer equilibrium constant.

In ref 3, Schutte et al. investigated the aggregation of a metal-free octasubstituted Pc in dodecane solution over Pc concentrations in the range 10^{-7} to 10^{-2} M. UV–vis absorption spectra at different Pc concentrations were analyzed on the assumption that each spectrum is a superposition of individual monomer and aggregate spectra, weighted by the respective mole fractions. Results over the entire concentration were analyzed on the basis of a monomer–dimer equilibrium and over a restricted range up to 5×10^{-4} M assuming a monomer–dimer–trimer equilibrium. The monomer–dimer equilibrium constant was found to be on the order of 10^6, whereas that for the dimer–

trimer equilibrium was around 2 orders of magnitude smaller. Discrepancies between the fitted spectra and the experimental results became significant at only the highest concentrations and were attributed not only to the presence of tetramers and higher aggregates but also to the onset of discotic liquid-crystalline ordering of the aggregates.[7-9] This occurs at quite low Pc concentrations because the octasubstituted Pc is so bulky, which increases the entropic driving force for the development of orientational order. In ref 3, Schutte et al. observed that the aggregation of octasubstituted Pc is pronounced in low-polarity solvents such as dodecane, which has a dielectric constant of $\epsilon = 2.0$. This was attributed to the screening of the intermolecular interactions responsible for aggregation being minimized in such media. On this basis, an increase in solvent polarity should be accompanied by a decrease in solute aggregation, in contradiction with the claims of ref 4.

Studies of dye aggregation have not been limited to phthalocyanine compounds. Recently, Neumann and co-workers studied the aggregation of an azo dye, Acid Red 266, in aqueous solution by means of UV–vis spectroscopy, nuclear magnetic resonance spectroscopy, and static light scattering.[10,11] In these studies, dye concentrations were less than 5×10^{-6} M, and in ref 10, it was shown that a simple monomer–dimer equilibrium is sufficient to describe the observed concentration dependence of the absorption spectra. The effects of adding salt to the dye solution were also investigated in this study, the conclusion being that equilibrium constants increase with increasing salt concentration, in agreement with the general trends observed in refs 4 and 6. In ref 11, an equilibrium model that includes the contribution of higher aggregates was also tested. In this model, it is assumed that all of the relevant equilibrium constants are equal, which, if anything, should lead to an overestimation of the concentrations of trimers and higher aggregates. As we will show below, the predictions of a theory that contains only one distinct equilibrium constant will not be qualitatively very different from those based on the simple monomer–dimer equilibrium.

The consensus appears to be that the aggregation of phthalocyanine and azo dyes is well described by a simple monomer–dimer equilibrium and that an increase in ionic strength or solvent polarity increases the corresponding equilibrium constant. Perhaps the only counterevidence put forward to date is that presented by Schutte et al.[3] This work is distinguished by the wide range of dye concentrations considered and by the fact that the formation of trimers was shown to be significant even at quite low concentrations ($c > 10^{-4}$ M).

To investigate the high solute-concentration regime further, we have studied a copper(II) tetrasulfonated phthalocyanine (CuPcS$_4$) dye in aqueous solutions, with and without added salt, using UV–vis spectroscopy. The CuPcS$_4$ studied is an example of a commercial reactive textile dye and carries a monochlorotriazine substituent that is the reactive group that binds the dye to the textile fiber. The CuPcS$_4$ concentrations considered in this work are in the range $10^{-7} \leq c \leq 10^{-3}$ M. As in previous studies, the nature and extent of aggregation was inferred by monitoring molar absorption coefficients as functions of dye concentration. We will show that the simple monomer–dimer equilibrium and an unlimited-aggregation theory similar to that proposed in ref 11 provide poor descriptions of the aggregation in CuPcS$_4$ solutions with little or no added salt by virtue of having only one fitted equilibrium constant. It would therefore appear that aggregation may not be limited to the formation of dimers or trimers and that proper account should be taken of the presence of higher aggregates. It is likely that the clusters

consist of columns of the roughly planar CuPcS$_4$ molecules, and a theory has been developed for the full equilibrium distribution of clusters formed by such stacks of molecules, ranging from monomers to stacks with infinite extent. The predicted equilibrium cluster distribution is characterized by two parameters. In molecular terms, these parameters reflect the different degrees of confinement experienced by molecules at the ends of a cluster, having one nearest neighbor, and those in the middle of the cluster, having two nearest neighbors. Fits of these new expressions to the experimental results show excellent agreement.

In accord with earlier studies,[4,10] a naïve analysis of our experimental results using the monomer–dimer equilibrium suggests that the equilibrium constant increases with salt concentration. By contrast, an analysis using the new and quantitatively correct model shows that at low salt concentrations (~0.01 M) aggregation is enhanced slightly with respect to the pure-water solution, whereas at higher salt concentrations, aggregation is actually suppressed. At the highest salt concentrations (0.1 and 2 M), the new theory and the theories containing only one equilibrium constant converge, indicating that the mole fractions of molecules in trimers and higher aggregates can be safely ignored.

This paper is organized as follows. In section 2, we summarize the experimental methods employed in this work. Expressions for the equilibrium cluster distribution are derived in section 3. The results are presented in section 4, and section 5 concludes the paper.

2. Experimental Section

The CuPcS$_4$ was a gift from DyStar UK Ltd. The supplier estimated that the material consists of >95% tetrasulfonated phthalocyanine species, with the sulfonate groups located predominantly at the 4 (β) positions, as opposed to the 3 (α) positions. Sample solutions were prepared by dilution from a stock solution of 1.0×10^{-3} M CuPcS$_4$ in deionized water using an Eppendorf "Reference" micropipet (100–1000 μL) and volumetric flasks. To minimize cumulative dilution errors, no more than two successive dilutions were used to prepare any one solution. Absorbance measurements were made on a Unicam model UV-2 double-beam UV–vis spectrometer using a spectral band-pass of 2 nm and a signal integration time of 2 s. Matched pairs of glass cuvettes with the following path lengths, l, were used: 100 mm for 1.0×10^{-7} M $\leq c \leq 5.0 \times 10^{-6}$ M; 10 mm for 1.0×10^{-5} M $\leq c \leq 5.0 \times 10^{-5}$ M; and 1 mm for 1.0×10^{-4} M $\leq c \leq 1.0 \times 10^{-3}$ M. The absorbance, A, was measured at two wavelengths, 626 and 665 nm, taking the average of five measurements for each sample at each wavelength. From measurements on multiple samples prepared at the same concentration, it was estimated that the relative statistical uncertainties in the measured values of the absorbance were less than 1.5%. Results are reported in terms of the molar absorption coefficient, $\epsilon = A/cl$.

3. Theory

3.1. Equilibrium Distribution of Aggregates. In this section, we derive expressions for the equilibrium distribution of stack-like clusters, using statistical mechanics. We shall see that the results are equivalent to those that would be obtained from thermodynamics alone by assuming a priori only two distinct equilibrium constants—one for the monomer–dimer equilibrium and the other for successive inclusions of additional monomers. The statistical mechanics approach, however, yields a clear interpretation of the relative magnitudes of the two constants.

Copper(II) Tetrasulfonated Phthalocyanine

J. Phys. Chem. A, Vol. 106, No. 44, 2002 **10727**

The derivation below is along similar lines to that used by van Roij in studies of aggregation and phase transitions in strongly interacting dipolar fluids.[12,13]

Consider a solution containing N solute molecules in a volume V and at a temperature T. At equilibrium, there are N_1 free monomers, N_2 dimers, and in general N_n n-mers. The corresponding concentration of n-mers is given by $c_n = N_n/V$. The total concentration of monomers, $c = N/V$, is related to the values of c_n by

$$c = \sum_{n=1}^{\infty} n c_n \tag{1}$$

The conditions for thermodynamic equilibrium are

$$\mu_n = n\mu_1 \qquad (n \geq 1) \tag{2}$$

where μ_n is the chemical potential of n-mers. The cluster concentrations considered in this work are sufficiently low ($c \leq 10^{-3}$ M) that interactions between the clusters can be ignored, and so the solution is considered ideal. In a solution of noninteracting clusters, the partition function for the solution (ignoring the solvent degrees of freedom) is

$$Q = \prod_{n=1}^{\infty} \frac{q_n^{N_n}}{N_n!} \tag{3}$$

where q_n is the partition function of an n-mer. In eq 3, we have assumed that aggregates of a particular size are indistinguishable (i.e., there are no stereoisomers). We shall further assume that an n-mer ($n \geq 2$) is formed from a "stack" of monomers and thus contains two "external" molecules with one nearest neighbor and ($n - 2$) "internal" molecules with two nearest neighbors. From these considerations, we write q_n in the form

$$q_1 = \frac{V}{\Lambda^3} \tag{4}$$

$$q_n = \frac{V v_{ex} v_{in}^{n-2}}{\Lambda^{3n}} \qquad (n \geq 2) \tag{5}$$

where Λ is the de Broglie thermal wavelength of a single molecule, V is the volume accessible to the first external molecule in the stack, and v_{ex} and v_{in} are single-molecule parameters, with units of volume, that reflect how rigidly an external or internal molecule is constrained by its neighbor(s). We anticipate that $v_{ex} > v_{in}$ because an external molecule with only one nearest neighbor should be less strongly constrained than an internal molecule, which has two nearest neighbors. Roughly speaking, v_{ex} and v_{in} will also contain factors proportional to $\exp(-E/k_BT)$, where k_B is Boltzmann's constant and E is the energy "per bond". The partition function (eq 3) is related to the Helmholtz free energy, F, and the chemical potentials, μ_n, by the fundamental equations $F = -k_BT \ln Q$ and $\mu_n = (\partial F/\partial N_n)$, from which we obtain

$$\mu_1 = k_BT \ln(c_1 \Lambda^3) \tag{6}$$

$$\mu_n = k_BT \ln\left(\frac{c_n \Lambda^{3n}}{v_{ex} v_{in}^{n-2}}\right) \tag{7}$$

By inserting eqs 6 and 7 into eq 2, we arrive at the following relation between c_1 and c_n ($n \geq 2$):

$$c_n = v_{ex} v_{in}^{n-2} c_1^n \tag{8}$$

Using eq 8, it is easy to show that the equilibrium constant governing the equilibrium (monomer + monomer $\rightleftharpoons$ dimer) is equal to v_{ex} and that the equilibrium constant governing the equilibrium (n-mer + monomer $\rightleftharpoons$ {$n + 1$}-mer ($n \geq 2$)) is equal to v_{in}. It is important to recognize that, in general, all such equilibria can have distinct equilibrium constants. In the present case, where molecules can stack up to form columns, it is reasonable to expect that simply distinguishing v_{ex} from v_{in} will provide an adequate description.

Strictly speaking, eqs 6 and 7 and all subsequent relations should contain activity coefficients that take into account solute–solute and solute–solvent interactions. The dominant interactions are likely be Coulombic in nature, particularly in the presence of added salt. However, we do not yet know the oxidation states of the free molecules or the clusters in solution, so it is hard to estimate the activity coefficients even at the Debye–Hückel level. Nonetheless, general trends in the relative stabilities of monomers and clusters should be evident in the values of v_{ex} and v_{in} obtained by assuming an ideal solution.

Inserting eq 8 for c_n into eq 1 and summing the resulting geometric series leads to the following equation for c_1:

$$c = c_1 + \frac{v_{ex} c_1^2 (2 - v_{in} c_1)}{(1 - v_{in} c_1)^2} \tag{9}$$

To analyze the effective molar absorption coefficients measured experimentally requires predictions for the mole fractions of molecules in different environments, $x_1 = c_1/c$, etc. Using the fact that there are two external molecules per cluster and making use of eq 8 for c_n, we arrive at the following results for x_1, x_{ex}, and x_{in}:

$$1 = x_1 + \frac{v_{ex} c x_1^2 (2 - v_{in} c x_1)}{(1 - v_{in} c x_1)^2} \tag{10}$$

$$x_{ex} = 2 \sum_{n=2}^{\infty} \frac{c_n}{c} = \frac{2 v_{ex} c x_1^2}{(1 - v_{in} c x_1)} \tag{11}$$

$$x_{in} = 1 - x_1 - x_{ex} > 0 \tag{12}$$

This model will be referred to as UA1 (unlimited aggregation, model 1). To extract an explicit expression for x_1 from eq 10 requires solving a cubic equation; for reference, this is detailed in the Appendix.

We note two limiting cases of model UA1. When $v_{in} = v_{ex}$, there is just one equilibrium constant governing all equilibria of the type monomer + n-mer $\rightleftharpoons$ {$n + 1$}-mer, including the monomer–dimer equilibrium. The composition of the solution is then given by

$$x_1 = \frac{1}{v_{ex} c} + \frac{(1 - \sqrt{1 + 4 v_{ex} c})}{2(v_{ex} c)^2} \tag{13}$$

$$x_{ex} = \frac{2 v_{ex} c x_1^2}{(1 - v_{ex} c x_1)} \tag{14}$$

$$x_{in} = 1 - x_1 - x_{ex} > 0 \tag{15}$$

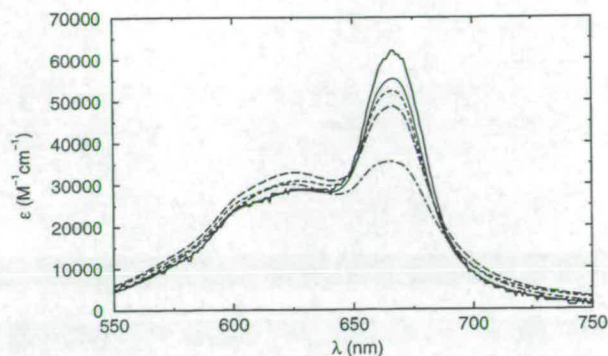We will refer to this model as UA2 (unlimited aggregation, model 2).

Figure 1. Molar absorption coefficients for CuPcS$_4$ solutions in pure water: $c = 1 \times 10^{-7}$ M (—), $c = 1 \times 10^{-6}$ M (···), $c = 1 \times 10^{-5}$ M (- - -), $c = 1 \times 10^{-4}$ M (— — —), $c = 1 \times 10^{-3}$ M (· — ·).

When $\nu_{in} = 0$, solving eqs 10–12 yields the explicit relations

$$x_1 = \frac{-1 + \sqrt{1 + 8\nu_{ex}c}}{4\nu_{ex}c} \tag{16}$$

$$x_{ex} = 2\nu_{ex}cx_1^2 \tag{17}$$

$$x_{in} = 1 - x_1 - x_{ex} = 0 \tag{18}$$

which correspond to the familiar results for a monomer–dimer equilibrium, with the equilibrium constant proportional to ν_{ex}. We will denote this model by MD (monomer–dimer model).

Finally, in an examination of the equilibrium cluster distribution, it is useful to define a cluster fraction, X_n, that is equal to the fraction of clusters that are n-mers:

$$X_1 = \frac{c_1}{\sum\limits_{n=1}^{\infty} c_n} = \frac{x_1}{x_1 + \frac{1}{2}x_{ex}} \tag{19}$$

$$X_n = \frac{c_n}{\sum\limits_{n=1}^{\infty} c_n} = \frac{x_1^n(\nu_{ex}c)(\nu_{in}c)^{n-2}}{x_1 + \frac{1}{2}x_{ex}} \quad (n \geq 2) \tag{20}$$

3.2. Molar Absorption Coefficients. In analyzing experimental results, it is assumed that we can assign distinct molar absorption coefficients to single molecules, external molecules, and internal molecules, denoted by $\epsilon_1(\lambda)$, $\epsilon_{ex}(\lambda)$, and $\epsilon_{in}(\lambda)$, respectively. The apparent molar absorption coefficient, $\epsilon(\lambda)$, at a particular wavelength, λ, is therefore equal to

$$\epsilon(\lambda) = x_1\epsilon_1(\lambda) + x_{ex}\epsilon_{ex}(\lambda) + x_{in}\epsilon_{in}(\lambda) \tag{21}$$

The concentration dependence of $\epsilon(\lambda)$ is contained in the variation of x_1, x_{ex}, and x_{in}, as predicted by models UA1, UA2, and MD.

4. Results

In Figure 1 we show absorption spectra in the range 550 nm $\leq \lambda \leq$ 750 nm for pure-water solutions of CuPcS$_4$ with concentrations in the range 10^{-7} to 10^{-3} M. The spectra are typical of those observed for Pc compounds: the narrow longer-wavelength band (at 665 nm) corresponds to the monomer 0–0 transition; the broader band at lower wavelength (626 nm) is
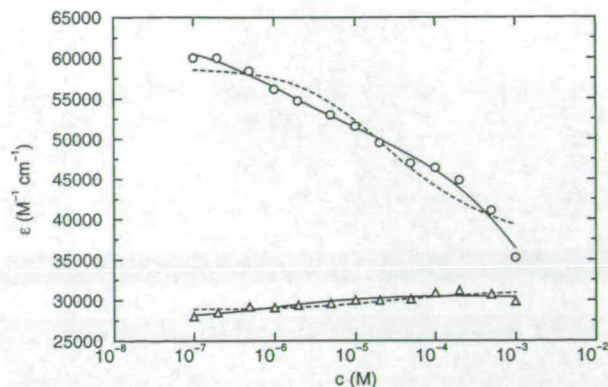

Figure 2. Molar absorption coefficients, ϵ, at $\lambda = 626$ ($\triangle$) and 665 nm (O) as functions of CuPcS$_4$ concentration in pure water. The curves are fits using models introduced in the text: UA1 (—), and MD (- - -). Note the logarithmic scale on the x axis.

attributed to those molecules within aggregates. This is on the basis that the transition dipole moment of a cluster should be greater than that of a monomer, and hence the excitation energy is blue-shifted. Note that the molar absorption coefficient at 665 nm decreases with increasing concentration, signaling an increase in aggregation. The absorption coefficient of the aggregate band is less sensitive to changes in concentration, but roughly speaking, it first rises with increasing dye concentration and then falls at a dye concentration of 10^{-3} M. Note the absence of any isosbestic points, which suggests that the aggregation is not of the simple monomer–dimer type.

In Figure 2, we show the molar absorption coefficients at 626 and 665 nm as functions of CuPcS$_4$ concentration in pure-water solutions. At 665 nm, there appears to be a point of inflection at $c \simeq 1.0 \times 10^{-6}$ M and a sharp decrease at $c > 10^{-4}$ M. The occurrence of such well-separated features suggests that two types of equilibria are operating in the solution—one at low concentrations, $c \simeq 10^{-6}$ M, and one at higher concentrations, $c \simeq 10^{-4}$ M.

The experimental results were fitted using models UA1, UA2, and MD. In all cases, the parameters ν_{ex} and ν_{in} were determined by fitting to the results at 665 nm because the concentration dependence of ϵ was most pronounced at this wavelength. In this way, the quality of the fit is not compromised by those sections of the molar absorption spectrum that show a very weak concentration dependence. Molar absorption coefficients at wavelengths in the range 550 nm $\leq \lambda \leq$ 750 nm were then fitted using the values of ν_{ex} and ν_{in} determined from the results at 665 nm.

The molar absorption coefficients at 626 and 665 nm of CuPcS$_4$ in pure-water solutions as fitted by models UA1 and MD are shown in Figure 2. The fits using model UA2 are omitted for clarity because on the scale of the Figure they are indistinguishable from those using model MD, although the fit parameters are different. The Figure clearly shows the poor qualitative description provided by model MD (and by extension, model UA2). At 665 nm, model UA1 is clearly superior to models UA2 and MD in that it captures the features at $c > 10^{-4}$ M as well as at the asymptotic low-concentration limit in which $\epsilon \rightarrow \epsilon_1$. The models are comparable at 626 nm because ϵ_1, ϵ_{ex}, and ϵ_{in} are all very similar at this wavelength (see Table 1). We note that even though model UA2 takes into account the possibility of unlimited aggregation the fact that there is only one fitted equilibrium constant restricts the shape of the curve to be almost coincident with the best-fit curve obtained using model MD.

TABLE 1: Fit Parameters from Models UA1, UA2, and MD[a]

solvent (M)	model	ν_{ex}	ν_{in}	$\epsilon_1(626)$	$\epsilon_{ex}(626)$	$\epsilon_{in}(626)$	$\epsilon_1(665)$	$\epsilon_{ex}(665)$	$\epsilon_{in}(665)$
		(M⁻¹)				(10⁴ M⁻¹ cm⁻¹)			
water	UA1	6.3×10^5	2.4×10^4	2.79(3)	3.09(3)	2.9(2)	6.2(1)	5.0(1)	~0
	UA2	9.1×10^4	9.1×10^4	2.85(2)	3.13(6)	3.03(4)	5.9(1)	5.1(1)	3.6(3)
	MD	2.8×10^4		2.89(2)	3.12(3)		5.9(1)	3.7(2)	
0.01 M NaCl(aq)	UA1	9.4×10^5	2.6×10^4	2.68(5)	2.98(4)	3.0(3)	5.7(2)	4.5(1)	~0
	UA2	1.5×10^5	1.5×10^5	2.74(4)	3.01(8)	2.95(5)	5.39(1)	4.7(1)	3.4(2)
	MD	4.7×10^4		2.79(3)	3.02(4)		5.4(1)	3.5(1)	
0.1 M NaCl(aq)	UA1	1.5×10^5	7.3×10^3	2.71(5)	3.03(8)	1.7(7)	5.09(6)	3.6(1)	~0
	UA2	1.6×10^5	1.6×10^5	2.68(5)	3.1(1)	2.76(7)	5.01(9)	4.3(1)	3.0(1)
	MD	5.1×10^4		2.77(5)	2.90(6)		5.01(7)	3.00(9)	
2 M NaCl(aq)	UA1	7.8×10^4	1.0×10^2	2.25(9)	2.6(3)	~0	3.73(6)	2.4(6)	~0
	UA2	1.1×10^5	1.1×10^5	2.16(7)	3.0(2)	1.9(3)	3.72(6)	2.8(9)	2.4(4)
	MD	7.8×10^4		2.25(7)	2.6(1)		3.73(4)	2.3(1)	

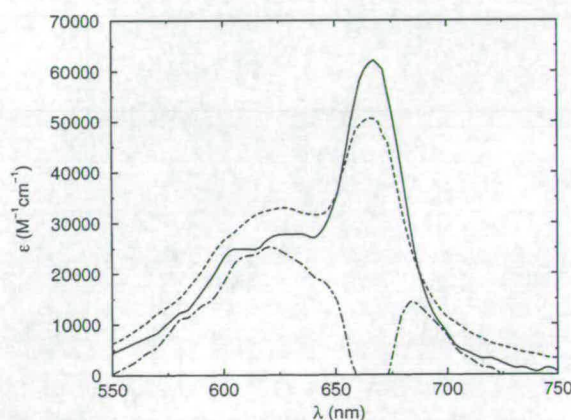[a] Figures in parentheses are the estimated statistical uncertainties in the last digits.

Figure 3. Fitted molar absorption coefficients of monomer, internal, and external molecules of CuPcS$_4$ in pure water using model UA1: $\epsilon_1(\lambda)$ (—), $\epsilon_{ex}(\lambda)$ (- - -), and $\epsilon_{in}(\lambda)$ (· — ·).

Figure 4. Fractions of molecules of different types as functions of the CuPcS$_4$ concentration in pure water from model UA1: fraction of monomer molecules, x_1 (—); fraction of external molecules, x_{ex} (- - -); and fraction of internal molecules, x_{in} (· — ·). Note the logarithmic scale on the x axis.

The fitted equilibrium constants for all models are presented in Table 1 along with the corresponding individual molar absorption coefficients at 626 and 665 nm. Statistical uncertainties are given for ϵ_1, ϵ_{ex}, and ϵ_{in}, and for the most part, the relative errors are less than 10%. Statistical errors in the fit parameters for model UA2 are larger than those for models UA1 and MD largely because of the constraint imposed by having equal values of ν_{ex} and ν_{in} in the former. The relative errors in all estimates of ν_{ex} and ν_{in} are very large, on the order of 100%. This is due to the insensitivity of the various expressions for x_1, x_{ex}, and x_{in} on ν_{ex} and ν_{in}. For this reason, statistical errors for ν_{ex} and ν_{in} have been omitted from Table 1, as it proved impossible to obtain meaningful and reliable estimates. The orders of magnitude should be reliable, however. The UA1 fit parameters for the pure-water solutions indicate that $\nu_{ex} \simeq 10^6$ M⁻¹ and $\nu_{in} \simeq 10^4$ M⁻¹. These figures are in broad agreement with those for the dimer and trimer equilibrium constants obtained by Schutte et al. for an octasubstituted Pc.[3] The MD model gives values of ν_{ex} over an order a magnitude smaller than does model UA1, and model UA2 yields values somewhere in between.

Figure 3 shows the fitted molar absorption coefficients $\epsilon_1(\lambda)$, $\epsilon_{ex}(\lambda)$, and $\epsilon_{in}(\lambda)$ in the range 550 nm $\leq \lambda \leq$ 750 nm using model UA1 with the values of ν_{ex} and ν_{in} determined at 665 nm. The monomer spectrum, $\epsilon_1(\lambda)$, and external-molecule spectrum, $\epsilon_{ex}(\lambda)$, exhibit strong peaks in the region of 665 nm; there seems to be a very slight blue-shifting of this principal peak in $\epsilon_{ex}(\lambda)$ with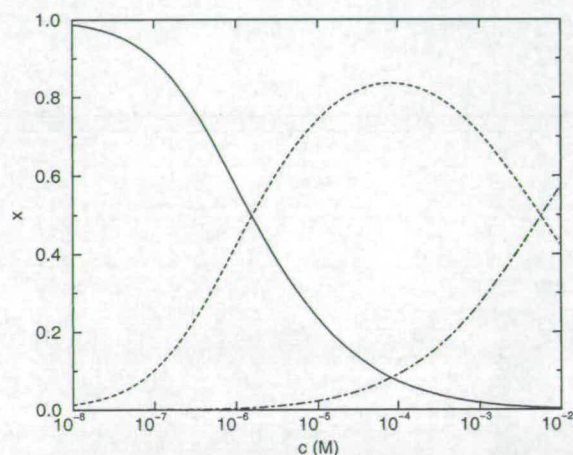 respect to that in $\epsilon_1(\lambda)$. All three spectra possess broad features at around 626 nm. At first sight, the fitted internal-molecule spectrum, $\epsilon_{in}(\lambda)$, appears very unusual. This can be explained by considering the high-concentration dependence of the molar absorption coefficient in the region of 665 nm. We would expect that at very high CuPcS$_4$ concentrations $\epsilon(\lambda)$ should approach a finite value equal to $\epsilon_{in}(\lambda)$. In Figure 2, however, we see that at the highest concentration accessible in our experiments ($c = 10^{-3}$ M) $\epsilon(665)$ has yet to level off, and hence our ability to fit $\epsilon_{in}(\lambda)$ in the region of 665 nm is severely limited. Nonetheless, it is clear that $\epsilon_{ex}(\lambda)$ and $\epsilon_{in}(\lambda)$ must be considerably different, as shown in Figure 3, particularly at wavelengths in the region of 665 nm.

The variations of the equilibrium cluster distributions with CuPcS$_4$ concentration in pure-water solutions according to model UA1 are illustrated in Figures 4 and 5. Figure 4 shows the mole fraction of molecules in each of the free-monomer, external, and internal environments (eqs 10–12). At low concentrations ($c \simeq 10^{-7}$ M), the molecules are largely unclustered, and hence x_1 is close to unity. At the higher concentrations ($c \simeq 10^{-3}$ M), large clusters are present, and hence a sizable percentage (~30%) of molecules will be accommodated within the bodies of the aggregates. At intermediate concentrations ($c \simeq 10^{-4}$ M), the fraction of external molecules reaches a maximum due to a majority of dimers. This is borne out in Figure 5, which shows the mole fraction of
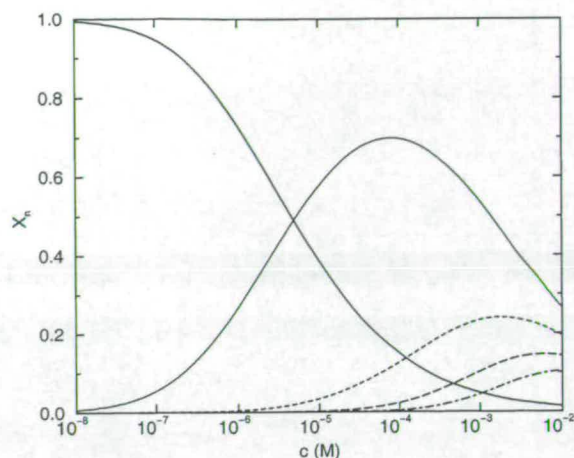
10730   *J. Phys. Chem. A, Vol. 106, No. 44, 2002*

Camp et al.

Figure 5. Fractions of aggregates containing n molecules as functions of CuPcS$_4$ concentration in pure water from model UA1: X_1 (—), X_2 (···), X_3 (- - -), X_4 (— — —), and X_5 (· — ·). Note the logarithmic scale on the x axis.
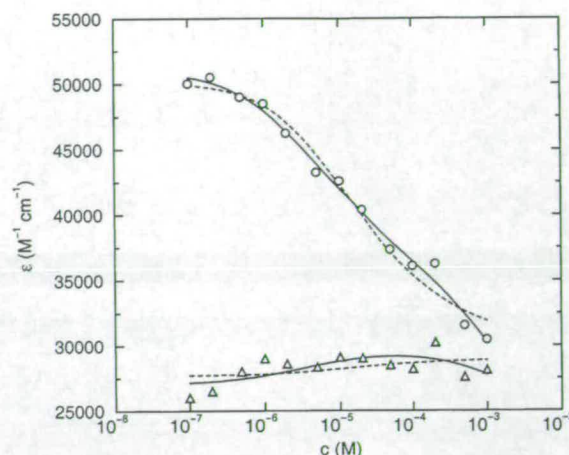

Figure 7. Molar absorption coefficients, ϵ, at $\lambda = 626$ ($\triangle$) and 665 nm (O) as functions of CuPcS$_4$ concentration in 0.1 M NaCl solution. The curves are fits using models introduced in the text: UA1 (—) and MD (- - -). Note the logarithmic scale on the x axis.

Figure 6. Molar absorption coefficients, ϵ, at $\lambda = 626$ ($\triangle$) and 665 nm (O) as functions of CuPcS$_4$ concentration in 0.01 M NaCl solution. The curves are fits using models introduced in the text: UA1 (—) and MD (- - -). Note the logarithmic scale on the x axis.
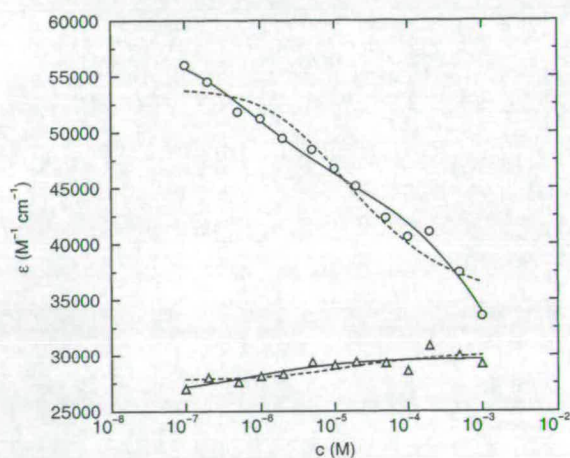
n-mers, X_n, as a function of CuPcS$_4$ concentration (eqs 19–21). In accord with the results in Figure 4, the dimer fraction, X_2, reaches a maximum at $c \simeq 10^{-4}$ M. The mole fractions of the higher clusters exhibit maxima at successively higher concentrations.

The molar absorption coefficients of CuPcS$_4$ at 626 and 665 nm in 0.01 M NaCl solutions are shown in Figure 6. The equilibrium constants were obtained by fitting the concentration dependence of the molar absorption coefficient at 665 nm. The fits using model UA2 are omitted for clarity because on the scale of the Figure they are indistinguishable from those using model MD, although the fit parameters are different. At 665 nm, the fits provided by model UA1 are superior to those provided by model MD, once again illustrating the significance of trimers and higher aggregates. As for the pure-water solution, the three models provide similar-quality fits at 626 nm. The corresponding fit parameters are presented in Table 1. All three models yield increased values for the equilibrium constants up to about 70% larger than the corresponding values in pure-water solution. It should be remembered that the relative statistical uncertainties in ν_{ex} and ν_{in} are likely to be on the order of 100%, so it is unclear whether these deviations are statistically

significant. However, the fitted values for all three models have increased, which suggests a systematic increase in the degree of aggregation with increasing salt concentration, so far in accord with earlier studies.[4,6,10]

The molar absorption coefficients of CuPcS$_4$ at 626 and 665 nm in 0.1 M NaCl solutions are shown in Figure 7. The equilibrium constants were obtained by fitting the concentration dependence of the molar absorption coefficient at 665 nm. The fits using model UA2 are omitted for clarity because on the scale of the Figure they are indistinguishable from those using model MD, although the fit parameters are different. Interestingly, the fits using model UA1 are quite close to those using the MD model. There is no longer a pronounced high-concentration feature in $\epsilon(665)$, and the fact that the MD model provides a fit that is at least qualitatively acceptable indicates that the contributions of trimers and higher aggregates are less significant in 0.1 M NaCl solution than they are at lower salt concentrations. The implication, therefore, is that the degree of aggregation is suppressed relative to that in the absence of salt. Quantitative evidence for the suppression of aggregation can be found in the fit parameters presented in Table 1. Using model UA1, the values of both ν_{ex} and ν_{in} are significantly smaller than those found in the absence of salt. By contrast, the MD model predicts an increased equilibrium constant, in keeping with earlier studies.[4,6,10]

Molar absorption coefficients of CuPcS$_4$ at 626 and 665 nm in a 2 M NaCl solution are shown in Figure 8. The equilibrium constants were obtained by fitting the concentration dependence of the molar absorption coefficient at 665 nm. The fits using model UA2 are omitted for clarity because on the scale of the Figure they are indistinguishable from those using model MD, although the fit parameters are different. At this very high salt concentration, the three models have provided fits that collapse onto a single curve, indicating that the contribution of trimers and higher aggregates is completely insignificant over the range of CuPcS$_4$ concentrations considered. The fit parameters in Table 1 confirm that the fitted values of ν_{ex}, ϵ_1, ϵ_{ex}, and ϵ_{in} using models UA1 and MD agree very closely. The fitted value of ν_{in} using model UA1 is only ~10 M^{-1}, which is insignificant over the range of CuPcS$_4$ concentrations considered in this work. The value of ν_{ex} from model UA2 is at odds with those from models UA1 and MD because of the inclusion of trimers of higher aggregates.
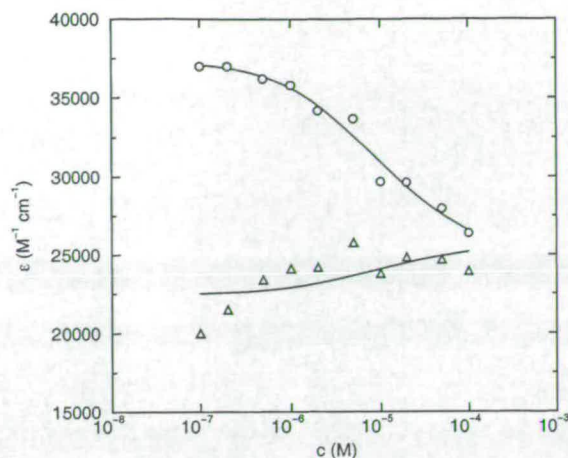
Copper(II) Tetrasulfonated Phthalocyanine

J. Phys. Chem. A, Vol. 106, No. 44, 2002 **10731**

Figure 8. Molar absorption coefficients, ϵ, at $\lambda = 626$ ($\triangle$) and 665 nm ($\bigcirc$) as functions of CuPcS$_4$ concentration in 2 M NaCl solution. The curves are fits using models introduced in the text: UA1 (—) and MD (- - -). Note the logarithmic scale on the x axis and that the UA1 and MD curves are coincident.

The fitted molar absorption coefficients at both 626 and 665 nm from all of the models show a downward trend as the salt concentration is increased. This can be understood by appealing to the theory of Myers and Birge.[14] By considering the effect of the coupling between the transition dipole moments on solute and solvent molecules, one may predict the oscillator strength, f, of a solute molecule in a solvent with refractive index n to be proportional to

$$f \propto 1 - 3G\left(\frac{n^2 - 1}{n^2 + 2}\right) \tag{22}$$

where the factor G depends on the geometry of the molecule and on the orientation of the transition dipole moment with respect to the molecular axes. For cylindrical molecules of radius r and half-height l, the following expressions apply to transition moments parallel ($\parallel$) and perpendicular ($\perp$) to the cylinder symmetry axis, respectively:

$$G^{\parallel} = \frac{l}{\sqrt{l^2 + r^2}} - \frac{2}{3} \tag{23}$$

$$G^{\perp} = \frac{1}{2}\left[\frac{2}{3} - \frac{l}{\sqrt{l^2 + r^2}}\right] \tag{24}$$

CuPcS$_4$ is a disk-shaped molecule for which $r/l \gg 1$, and the $\pi-\pi^*$ transition moment is perpendicular to the "cylinder axis".[15] Hence, the relevant factor in eq 22 is $G^{\perp}$, which is positive for $r/l \gg 1$. Generally speaking, the (frequency-dependent) dielectric constant and refractive index of the solvent will increase upon the addition of salt, which according to eq 22 should lead to a reduction in the oscillator strength of the molecule, in agreement with our experimental results. It should be noted that any interactions involving permanent electric dipoles on the solute or the solvent are ignored in the theory, but experimental results presented in ref 14 indicate that these interactions do not alter the general trends predicted by eq 22.

In summary, model UA1 provides excellent fits to the experimental results over the full range of dye and salt concentrations considered. The MD model provides a poor fit to the experimental results for the pure-water solution but improves as salt is added. The equilibrium constants obtained

by fitting model UA1 indicate a decrease in aggregation with increasing salt concentration, whereas the MD results show an increase in aggregation. It is notable that the fitted values of the parameter ν_{ex} from model UA2 are at variance with those from models UA1 and MD despite the curves for UA2 and MD being almost indistinguishable. This is due to the constraint that all equilibrium constants are equal (i.e., $\nu_{ex} = \nu_{in}$), probably leading to an underestimation of the dimer concentration and an overestimation of the higher-aggregate concentrations.

5. Conclusions

In this paper, we have investigated the aggregation properties of CuPcS$_4$ in aqueous salt solutions using UV–vis spectroscopy and equilibrium statistical mechanics. By exploiting the sensitivity of the peak intensities at the absorption maxima, we have been able to extract the CuPcS$_4$ concentration dependence of the equilibrium cluster distribution. We have shown that the monomer–dimer model (MD) is unable to describe the qualitative behavior of the molar absorption coefficients at CuPcS$_4$ concentrations above 10^{-4} M. We have put forward an alternative model (UA1) that takes into account the formation of trimers and all higher aggregates. It has been demonstrated that the new model provides excellent fits to the experimental results over the entire range of CuPcS$_4$ concentrations considered. A third model (UA2) has also been examined, which describes the formation of trimers and higher aggregates according to an equilibrium constant equal to that for the monomer–dimer equilibrium. In each case considered in this work, model UA2 produces a fit indistinguishable from that provided by the simple monomer–dimer equilibrium, albeit with different fit parameters.

We have also investigated the variation of the equilibrium constants with increasing salt concentration. This is of practical concern in the dye industry because the dyeing process is carried out in the presence of salt and the optical properties of the dye are clearly sensitive to the degree of aggregation. The effects of ionic strength may also be significant in the aggregation of Pcs in intracellular media; this is of great relevance to photodynamic therapy. A typical cellular environment may have an ionic strength of ~ 0.1 M, which we have shown is high enough to affect strongly the aggregation of Pc molecules. It appears that the choice of model is crucial when assessing the degree of aggregation in the presence of added salt. In previous studies,[4,6,10] it was claimed that aggregation is enhanced upon the addition of salt. We have confirmed for CuPcS$_4$ in aqueous NaCl solutions that a naïve analysis using the monomer–dimer equilibrium does indeed lead to this conclusion. The rationale traditionally put forward is that the ionic screening provided by the salt reduces the repulsions between like charges on the solute molecules. This is unlikely because even in a typical room-temperature aqueous solution of a univalent electrolyte with an ionic strength of, say, 0.1 M, the Debye–Hückel estimate of the screening length is around 3 nm (i.e., at least as large as molecular dimensions). At lower salt concentrations, the screening length will be even longer, and hence the short-range behavior of the interaction potential responsible for aggregation should be quite insensitive to the ionic strength. This is in contrast to colloidal dispersions in which the "solute" colloid particles have diameters on the order of 10^{-6} m; in this case, the solute size is at least as large as typical screening lengths.

As mentioned above, model UA1 proposed in this work is quantitatively more reliable than models UA2 and MD. Equilibrium constants obtained with model UA1 indicate that

10732 *J. Phys. Chem. A, Vol. 106, No. 44, 2002*

Camp et al.

aggregation is suppressed when the salt concentration is raised above 0.01 M. One possible explanation is as follows. Regardless of the salt concentration, the formation of clusters from an initial pure-monomer state is accompanied by a decrease in $\pi-\pi$ interaction energy, $\Delta U_{\pi\pi} < 0$, and a decrease in entropy, $\Delta S < 0$, because of the confinement within each cluster. The total Gibbs free energy change is then $\Delta G \simeq \Delta U_{\pi\pi} - T\Delta S$ (ignoring the $P\Delta V$ term, which is likely to be insignificant). In the presence of salt, there will be an additional contribution to the interaction energy from Coulombic interactions between solute and electrolyte, U_C. The Coulombic energy contribution (per molecule) should be more negative for free molecules than for aggregated molecules because in the latter case the solvent and electrolyte would be excluded from the region of each solute–solute "bond". Hence, $\Delta U_C > 0$, and so the total Gibbs free energy change, $\Delta G \simeq \Delta U_{\pi\pi} + \Delta U_C - T\Delta S$, will increase with increasing salt concentration, leading to an overall reduction in the degree of aggregation. In effect, the addition of salt might energetically stabilize free molecules with respect to the aggregates. It is also likely that solute–solvent and solvent–solvent interactions play an important role in stabilizing or destabilizing aggregates.[16]

Finally, we have observed that the fitted molar absorption coefficients for monomers, external molecules, and internal molecules all decrease with increasing salt concentration, regardless of the model used. We have confirmed that this trend is in agreement with the theoretical predictions of Myers and Birge,[14] which correlate changes in the oscillator strength with the molecular geometry and the refractive index of the solvent.

Appendix A: Solution of the Cubic Equation

The solution of eq 10 to yield the monomer fraction, x_1, is obtained as follows (see, for example, ref 17). First, rewrite it in the form

$$z^3 + a_2 z^2 + a_1 z + a_0 = 0 \tag{25}$$

where z is written in place of x_1 and the coefficients are given by

$$a_2 = \frac{2v_{ex}c - 2v_{in}c - (v_{in}c)^2}{(v_{in}c)^2 - v_{ex}v_{in}c^2} \tag{26}$$

$$a_1 = \frac{1 + 2v_{in}c}{(v_{in}c)^2 - v_{ex}v_{in}c^2} \tag{27}$$

$$a_0 = \frac{-1}{(v_{in}c)^2 - v_{ex}v_{in}c^2} \tag{28}$$

Define the following combinations:

$$Q = \frac{3a_1 - a_2^2}{9} \tag{29}$$

$$R = \frac{9a_1 a_2 - 27a_0 - 2a_2^3}{54} \tag{30}$$

$$D = Q^3 + R^2 \tag{31}$$

With typical values of v_{ex}, v_{in}, and c, $D < 0$, which implies that all three solutions of eq 25 are real. Defining the quantity

$$\theta = \arccos\left(\frac{R}{\sqrt{-Q^3}}\right) \tag{32}$$

the solutions of eq 25 are given by

$$z_1 = 2\sqrt{-Q}\,\cos\left(\frac{\theta}{3}\right) - \frac{1}{3}a_2 \tag{33}$$

$$z_2 = 2\sqrt{-Q}\,\cos\left(\frac{\theta + 2\pi}{3}\right) - \frac{1}{3}a_2 \tag{34}$$

$$z_3 = 2\sqrt{-Q}\,\cos\left(\frac{\theta + 4\pi}{3}\right) - \frac{1}{3}a_2 \tag{35}$$

With physically relevant parameters, the required solution of eq 10 is $x_1 = z_3$.

References and Notes

(1) *Phthalocyanines: Properties and Applications*; Leznoff, C. C., Lever, A. B. P., Eds.; VCH: New York, 1989.

(2) Kasha, M.; Rawls, H. R.; El-Bayoumi, M. S. *Pure Appl. Chem.* **1965**, *11*, 371.

(3) Schutte, W. J.; Sluyters-Rehbach, M.; Sluyters, J. H. *J. Phys. Chem.* **1993**, *97*, 6069.

(4) Gruen, L. C. *Aust. J. Chem.* **1972**, *25*, 1661.

(5) Yang, Y.-C.; Ward, J. R.; Seiders, R. P. *Inorg. Chem.* **1985**, *24*, 1765.

(6) Martin, P. C.; Gouterman, M.; Pepich, B. V.; Renzoni, G. E.; Schindele, D. C. *Inorg. Chem.* **1991**, *30*, 3305.

(7) Piechocki, C.; Simon, J.; Skoulios, A.; Guillon, D.; Weber, P. *J. Am. Chem. Soc.* **1982**, *104*, 5425.

(8) Mausurel, D.; Sirlin, C.; Simon, J. *New J. Chem.* **1987**, *11*, 455.

(9) Schouten, P. G.; van der Pol, J. F.; Zwikker, J. W.; Drenth, W.; Picken, S. J. *Mol. Cryst. Liq. Cryst.* **1991**, *195*, 291.

(10) Neumann, B. *Langmuir* **2001**, *17*, 2675.

(11) Neumann, B.; Huber, K.; Pollmann, P. *Phys. Chem. Chem. Phys.* **2000**, *2*, 3687.

(12) van Roij, R. *Phys. Rev. Lett.* **1996**, *76*, 3348.

(13) van Roij, R. *Simple Theories of Complex Fluids.* Thesis, University of Utrecht, Utrecht, The Netherlands, 1996.

(14) Myers, A. B.; Birge, R. R. *J. Chem. Phys.* **1980**, *73*, 5314.

(15) Stillman, M. J.; Nyokong, T. In *Phthalocyanines: Properties and Applications*; Leznoff, C. C., Lever, A. B. P., Eds.; VCH: New York, 1989; Chapter 3, p 133.

(16) van der Pol, J. F.; Neeleman, E.; Zwikker, J. W.; Nolte, R. J. M.; Drenth, W.; Aerts, J.; Visser, R.; Picken, S. J. *Liq. Cryst.* **1989**, *6*, 577.

(17) Abramowitz, M.; Stegun, I. A. *Handbook of Mathematical Functions*; Dover Publications: New York, 1965.